AN X-RAY DIFFRACTION STUDY OF CHROMITE SPINELS

A THESIS SUBMITTED FOR THE DEGREE OF DOCTOR OF PHILOSOPHY IN THE UNIVERSITY OF ASTON IN BIRMINGHAM

RONALD JAMES HILLEARD, B. Sc.,

Physics Department

June 1973.

ABSTRACT

An X-ray diffraction study of eight members from the spinel series $MgAl_{2-x}Cr_xO_4$ with $0 \leqslant x \leqslant 2$ is presented. Experimental results from these samples showed the line profiles to be broadened to an extent which depended upon the chromium concentration, the maximum broadening occurring in the specimen in which $x = 0.5$, coinciding with the anomalous optical behaviour of chromium doped spinels reported by Poole (1964).

Refinement of the crystal structure according to Fd3m symmetry indicates negligible change in oxygen position parameter u which was found to be 0.387 ± 0.001 in each case. However the Debye-Waller temperature factor B appeared to increase uniformly with increasing chromium concentration. This was attributed to displacements of certain ions from their conventional positions in agreement with earlier results from optical and magnetic measurements which had indicated that the symmetry of the site occupied by Cr^{3+} was C_{3v} rather than D_{3d} expected for consistency with the space group Fd3m.

Following a suggestion by Grimes (1971) a further refinement of the structure parameters of $MgCr_2O_4$, based on $F\bar{4}3m$ symmetry has been performed in which O^{2-} displacements together with very small displacements of Cr^{3+} were made to give a structure consistent with local C_{3v} symmetry. The temperature factor was then found to be comparable with that previously estimated from infra-red measurements.

Lattice parameters have been determined by the centroid method whilst line breadths were investigated by both integral breadth and variance methods. It is established that diffraction line broadening exhibited by the compounds of mixed composition arises from some effect other than particle size or strain, the most probable source being thought to be a form of anti-phase domain structure.

Experiments on specimens quenched from 900°C and 1100°C suggest that the small amount of line broadening in $MgAl_2O_4$ arises from stacking faults similar to those observed in face centred cubic metals.

INDEX

CHAPTER 1

THE SPINEL STRUCTURE AND FACTORS INFLUENCING ITS MODIFICATION

1.1 The spinel structure.

Spinel is a collective name given to a range of compounds which have a crystal structure related to that of the mineral spinel, $MgAl_2O_4$. The first attempts to describe the structure were made by Bragg (1915) and Nishikawa (1915) who independently proposed an atomic arrangement based on a cubic close packing of the relatively large oxygen ions with the metal ions occupying interstitial sites in this close packed structure.

According to this scheme, each unit cell contained 8 molecular units organised so that the Mg^{2+} ions occupied 8 of the 64 available interstitial holes with four-fold co-ordination, since called the tetrahedral or A sites, while the Al^{3+} ions occupied 16 of the 32 available interstitial holes with six-fold co-ordination, these being the octahedral or B sites.

This description of the spinel structure was later refined by reference to the space group $Fd\bar{3}m$ when the metal ions were allocated the special positions

Mg^{2} in 8a : $0, 0, 0; \frac{1}{4}, \frac{1}{4}, \frac{1}{4}$;

plus f.c.c. translations

Al^{3} in 16c : $\frac{5}{8}, \frac{5}{8}, \frac{5}{8}; \frac{5}{8}, \frac{7}{8}, \frac{7}{8}; \frac{7}{8}, \frac{5}{8}, \frac{7}{8}; \frac{7}{8}, \frac{7}{8}, \frac{5}{8}$;

plus f.c.c. translations

and the oxygen ions being placed in

32c : $u, u, u; \frac{1}{4}-u, \frac{1}{4}-u, \frac{1}{4}-u;$

$u, \bar{u}, \bar{u}; \frac{1}{4}-u, \frac{1}{4}+u, \frac{1}{4}+u;$

$\bar{u}, u, \bar{u}; \frac{1}{4}+u, \frac{1}{4}-u, \frac{1}{4}+u;$

$\bar{u}, \bar{u}, u; \frac{1}{4}+u, \frac{1}{4}+u, \frac{1}{4}-u;$

plus f.c.c. translations.

where the unknown position parameter 'u' may be determined by a comparison of measured and calculated diffraction intensities.

The u parameter is a measure of the disturbance to the ideal close packing of the oxygen ions by the insertion of the metal ions into the holes within this structure. Perfect close packing of these oxygen ions corresponds to u = 0.375 while experimental data for $MgAl_2O_4$ and related compounds, is fitted most closely by assuming values somewhat greater than this (Wyckoff 1951). The increase in u is realised structurally as an increase in bond length between the tetrahedrally co-ordinated metal ion and its neighbouring oxygen ions, the latter being moved outwards along the line of the bond, a [111] direction, by an amount

$$a\sqrt{3} \cdot \delta$$

where a = unit cell size

and $\delta = u - 0.375$.

This displacement is indicated by the arrow in figure 1.1 which shows a tetrahedrally co-ordinated ion (shaded), its nearest and next nearest neighbours in the lattice.

It should be emphasised that the structural modifications introduced by $u < 0.375$ leave the symmetry of the tetrahedral site completely unaffected. This is not true however for the situation of the octahedral site. The latter suffers a change of local symmetry as the u parameter is increased above 0.375 from cubic O_h to trigonal D_{3d} as well as a reduction in bond length to nearest oxygen ions.

1.2 Alternative forms of cubic spinel structure.

The structure described above in which the divalent cations occupy A sites and the trivalent cations occupy B sites, is known as the NORMAL SPINEL STRUCTURE and it was thought for many years to be common to all compounds isomorphous with $MgAl_2O_4$. However, in 1931, Barth and Posnjak

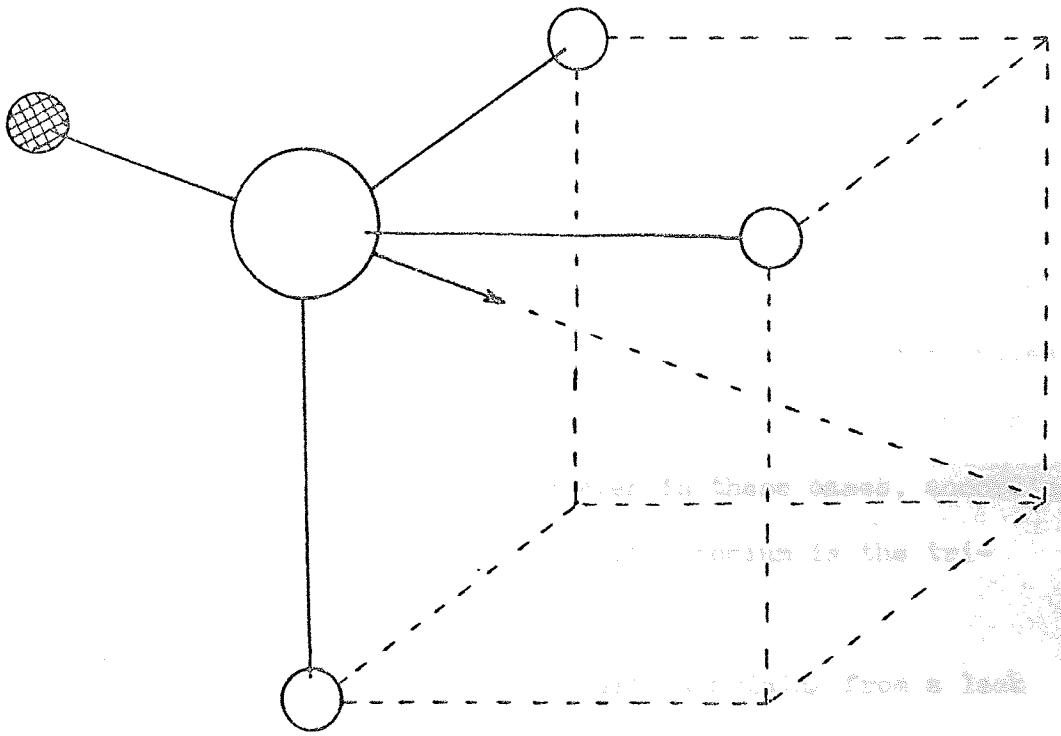

fig.1.1. Displacement of oxygen ions arising from the insertion of a metal ion into a tetrahedral site.

were able to prove that this was not always the case. They found for example, that the intensity pattern of X-rays diffracted by $MgGa_2O_4$ could not be accounted for in terms of a normal structure. The experimental data could be fitted if it were postulated that the 8 A sites were occupied by Ga^{3+} ions and the 16 B sites shared randomly between the remaining Ga^{3+} ions and the Mg^{2+} ions.

Such an arrangement is now commonly known as the INVERSE SPINEL STRUCTURE and may be indicated by writing the formula for the corresponding compounds as

$$Me^{3+} (Me^{2+} Me^{3+}) O_4$$

where the parentheses indicate the ions occupying the octahedral or B sites.

Following this work, Barth and Posnjak (1932) were able to identify a number of inverse spinels but showed that spinels in which the trivalent ion was Al^{3+} or Cr^{3+} appeared to be normal. Spinels also occur in which the oxygen has been replaced by sulphur and even in these cases, according to Hahn (1951), the result is a normal spinel if chromium is the trivalent cation.

In some cases, however, there were ambiguities arising from a lack of X-ray scattering contrast between the metal ions occupying the cation sites. For example, the situation in $MgAl_2O_4$ remained uncertain until the development of neutron diffraction techniques when it was found that the cation distribution in this material was close to normal with possibly a slight tendency to inverseness (Bacon, 1952). Later investigations by Stoll, Fischer, Halg and Maier (1964) suggested that there may be 10 - 15% inversion.

It is interesting to observe that Verwey and Heilmann (1947) were able to distinguish between normal and inverse spinels through studies on differences in lattice parameters of spinel series. Their results indicated that most trivalent ions prefer to occupy octahedral sites

but that some, for instance, Fe^{3+}, In^{3+} and Ga^{3+} prefer to occupy the tetrahedral site, i.e. they tend to form inverse spinels.

Subsequent work in this field has shown that a completely normal or a completely inverse structure represents extreme cases for the system and a more general representation of spinel is

$$Me^{2+}_{\delta}\ Me^{3+}_{1-\delta}\ (\ Me^{2+}_{1-\delta}\ Me^{3+}_{1+\delta}\ )\ O_4$$

where the ions before the brackets occupy A sites, those inside occupy B sites and δ is a measure of the degree of inversion. Thus for a normal spinel $\delta = 1$, for inverse $\delta = 0$ and for a completely random distribution of cations over both types of site, $\delta = \frac{1}{3}$. In some systems the value of δ depends upon the method of preparation. For example in a given sample of $MgFe_2O_4$ the cation distribution can be influenced by its thermal history. Thus Bacon and Roberts (1953) and Corliss and Hastings (1953) found $\delta \simeq 0.1$ with annealed $MgFe_2O_4$ while other studies, especially magnetic measurements, indicate much higher values in quenched specimens (Smit and Wijn, 1959).

1.3 Factors influencing the degree of inversion of spinels.

The discovery that in spinels the metal ions may be distributed in more than one way among the available interstitial sites provided by the anions, has led to considerable effort to investigate the factors which determine the degree of inversion in any given sample. At the present time, three factors are thought to be particularly important, namely, ionic size relative to the interstitial site radius, the problem of minimising Coulomb energy and the electronic configuration of the metal ions concerned.

1.3.1 Effect of ionic radius.

In the spinel lattice with a close packed cubic configuration of oxygen ions, the tetrahedral site is smaller than the octahedral site.

However, when the structure of a real spinel referred to the space group Fd3m, is considered, the size of the interstitial holes provided by the anions becomes a simple function of the lattice constant 'a' and the anion 'u' parameter. Thus the nearest neighbour distances are

$$p = a\sqrt{\left(\frac{1}{16} - \frac{1}{2}\delta + 3\delta^2\right)}$$

and

$$q = a\left(\frac{1}{8} + \delta\right)\sqrt{3}.$$

for the octahedral and tetrahedral holes respectively where $\delta = u - 0.375$ (Gorter, 1954). When $\delta = 0.0125$, i.e. where $u = 0.3875$, the holes are equal in size and therefore $q > p$ if u is larger and $q < p$ if u is smaller than this value.

The ionic radii of metal ions on the other hand, tend to get smaller as the valency increases (see for example Shannon and Prewitt, 1969). Thus apart from co-ordination effects, ionic radius alone would tend to favour the inverse spinel structure when the u parameter is low and the normal structure when u is high.

1.3.2 Electronic effects in the spinel lattice.

If we regard the bonds in the spinel lattice as ionic, the lattice energy consists of a Coulomb term which is attractive and the Born repulsive energy. This energy depends on the lattice parameter and the charge distribution amongst the lattice sites of the ions. So far it has been implicitly assumed that the u parameter and metal ion radius to be independent, however the real situation is more complicated. For instance the ionic radius forms one factor in the Born repulsive energy term. Also, due to the differences of valency of ions on the A and B sites, the intermediate O^{2-} ions become polarised, which has the effect of lowering the total energy of the system. It is more effective to have a lower valency on the A site and a higher valency ion on the B site, thus polarisation effects favour a normal arrangement of cations.

The final cation distribution therefore arises from an optimisation of the total lattice energy, and this can include ordering within one type of site. Thus for example, in Fe_3O_4, Fe^{2+} and Fe^{3+} are ordered on the octahedral sites below 119 K leading to a distortion of the crystal to orthorhombic symmetry (Verwey and Haaymann, 1941, Verwey, Haaymann and Romeijn, 1947).

Calculations of the Madelung energy by Verwey, de Boer and van Santen (1948) showed that the structure is more stable for low average charge on the tetrahedral site with large u value or high average charge on the tetrahedral site with low u value.

The degree of inversion of spinels has been related to the value of u using electrostatic considerations and it has been shown that normal spinels are most stable if

$$u > 0.379$$

whereas an inverse spinel is stable if

$$u < 0.379$$

(Verwey et al, 1947, de Boer, van Santen and Verwey, 1948 and 1950).

In general it is found that electrostatic considerations alone are not sufficient to account for the observed cation distributions and it is necessary to consider other factors which can influence the distribution.

1.3.3 Effect of electronic configuration.

The site preferences indicated in the previous paragraphs may be over-ridden by the electronic configuration of the ions concerned. For instance Zn^{2+} and Cd^{2+} show a preference for the A site due to their forming covalent bonds with O^{2-} and these bonds orientate towards the corners of a tetrahedron. Thus these ions often appear in spinels in the normal structure even when the trivalent ion is Fe^{3+}. However, it is known that the method of preparation of $ZnFe_2O_4$ affects the structure of the spinel and in certain circumstances it can become partially inverse

as indicated by magnetic (Lotgering, 1966) and specific heat measurements (Westrum and Grimes, 1957 and 1958).

Similarly Ni^{2+} and Cr^{3+} have a preference for the B site and this has been explained as being due to the favourable fit of the charge distribution in the crystal field of the octahedral configuration (McClure, 1957).

Investigations by Verwey and Heilmann (1947) into the cation distribution of $MgCr_2O_4$ definitely pointed to a normal distribution. Later, Romeijn (1953) suggested that Cr^{3+}, more than any other transition metal ion has a greater tendency to occupy octahedral sites. This was later supported by evidence provided through crystal field theory (Dunitz and Orgel, 1957a) and McClure (1957) produced a table of octahedral site preference energies which predicted that of all spinels, those containing Cr^{3+} were most likely to be normal. It was suggested that although the energies involved were small, they may be large enough to determine whether a given spinel is normal or inverse and in fact experiment shows that all spinels of the type

$$Me^{2+}\ Me_2^{3+}\ O_4,$$

where the trivalent ion is Cr^{3+}, have been found to be normal (Bragg and Claringball, 1965).

Any ion when placed in a crystal comes under the influence of a crystal field which may cause a splitting of the energy levels. These effects are particularly important in the case of transition ions because these have electronic ground states which are non-spherically symmetrical. The extent of the splitting depends on the distance r between the ions in the site, the dependence, in the case of the point charge approximation, being

$$\Delta \propto \frac{1}{r^5} \quad \text{(McClure, 1963)}$$

In practice, however, when the cation under investigation is Cr^{3+} the

dependence has been found to vary from compound to compound. McClure's relation given above does indeed hold for a ruby series treated at various pressures (Poole and Itzell, 1963) but appears to be incorrect when different parameters are varied. Poole (1964) showed that in a similar ruby series at different temperatures

$$\Delta \propto \frac{1}{r^9}$$

whereas if the chromium content of this ruby series is altered

$$\Delta \propto \frac{1}{r^2}$$

Poole suggested that if a Cr^{3+} ion is placed in a site, it causes a uniform expansion of the site in all directions, the only effect being a change in the u parameter leaving the dependence of Δ with r unchanged. On the other hand his experiments showed that in spinels the dependence became

$$\Delta \propto \frac{1}{r}$$

while in other systems containing Cr^{3+} ions, the dependence was different again. The conclusion reached by Poole was that different treatments of Cr^{3+} containing compounds produced different lattice distortions about the Cr^{3+} ion and that structure refinements were necessary to account for these differences.

1.4 Tetragonal and other distorted spinels.

In the description of spinel so far, the structure has been assumed to be face centred cubic. However, many spinels can take up a tetragonal structure depending upon the metal ions present in the material. These ions, on insertion into the cubic lattice, are thought to cause distortions which ultimately convert the structure to tetragonal symmetry. Unfortunately it is conventional to consider the tetragonal structure according to body centred symmetry whereas comparison with the cubic structure requires an alternative choice of axes.

Figure 1.2 in which two body centred tetragonal unit cells are shown, indicates the relationship between the equivalent face centred and body centred tetragonal structures. The lattice positions are indicated by black circles. The shaded planes form part of a face centred system of atoms which becomes cubic if the axis AD equals the tetragonal face diagonal AB.

When a face centred cubic spinel is tetragonally distorted it takes up a structure related to Hausmannite (Mn_3O_4) the atoms in the unit cell having been allocated the following special positions in the space group D_{4h}^{19} I_4/amd

4 Mn ions in positions (a)

$0,0,0;\quad 0,\frac{1}{2},\frac{1}{4};$

plus body centred translations

8 Mn ions in positions (d)

$0,\frac{1}{4},\frac{1}{8};\ 0,\frac{3}{4},\frac{5}{8};\ \frac{1}{4},0,\frac{3}{8};\ \frac{3}{4},0,\frac{3}{8};$

plus body centred translations

16 O ions in positions (h)

$0,u,v;\quad 0,\bar{u},v;\quad u,0,\bar{v};\quad \bar{u},0,\bar{v};$

$0,u+\frac{1}{2},\frac{1}{4}-v;\quad 0,\frac{1}{2}-u,\frac{1}{4}-v;$

$u,\frac{1}{2},v+\frac{1}{4};\quad \bar{u},\frac{1}{2},v+\frac{1}{4};$

plus body centred translations.

where $u \simeq \frac{1}{4}$ and $v \simeq \frac{3}{8}$ (Wyckoff, 1951).

The face diagonals of the square ends of four neighbouring unit cells make a face centred square which when c equals the length of the side of this square, form the face centred cubic spinel structure.

If the tetragonal atomic positions are transformed to this face centred unit cell, the metal ion positions correspond to those expected for the cubic spinel; however, when the other positions are compared it is found that in the transformation from cubic to tetragonal, the oxygen ions are displaced from their face centred positions. Figure 1.3

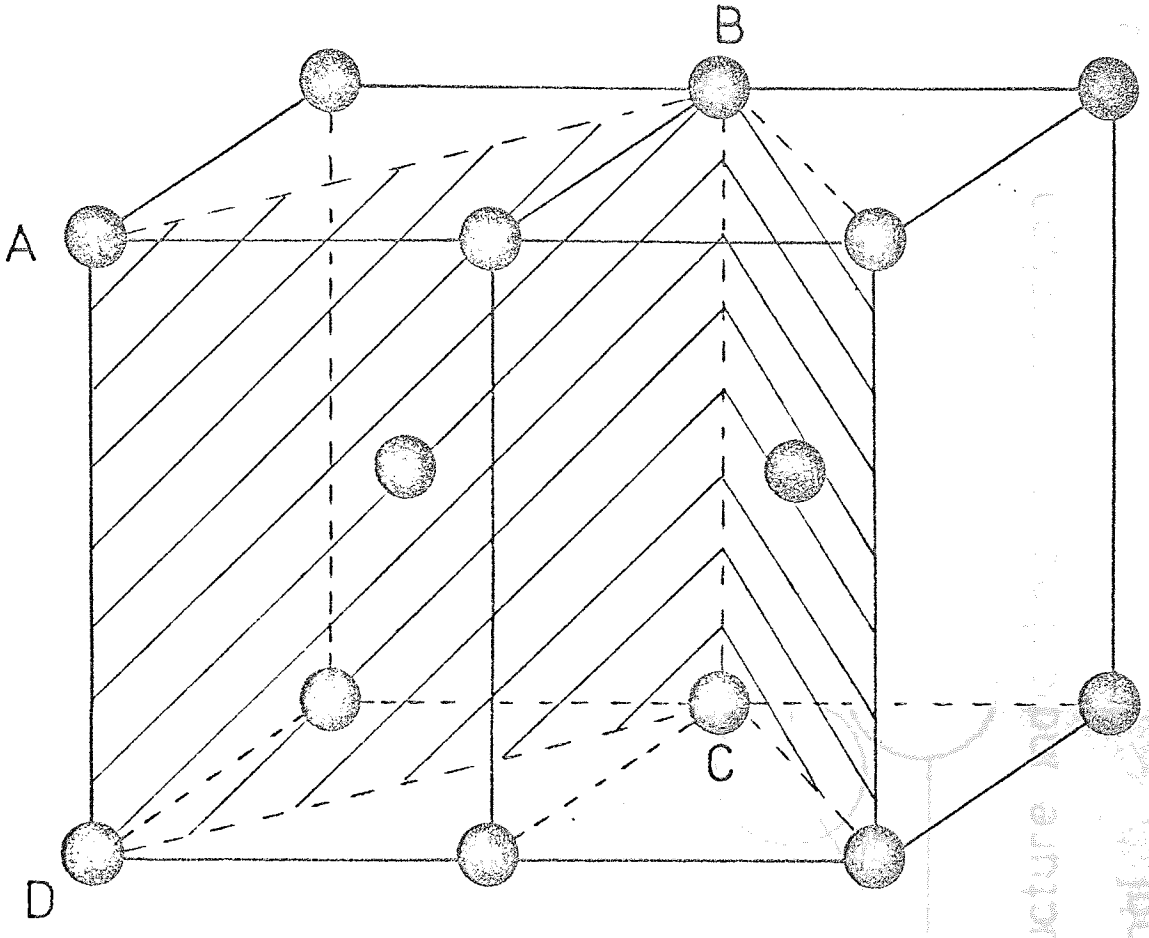

fig. 1.2. The relationship between f.c.c. and b.c. tetragonal structures.

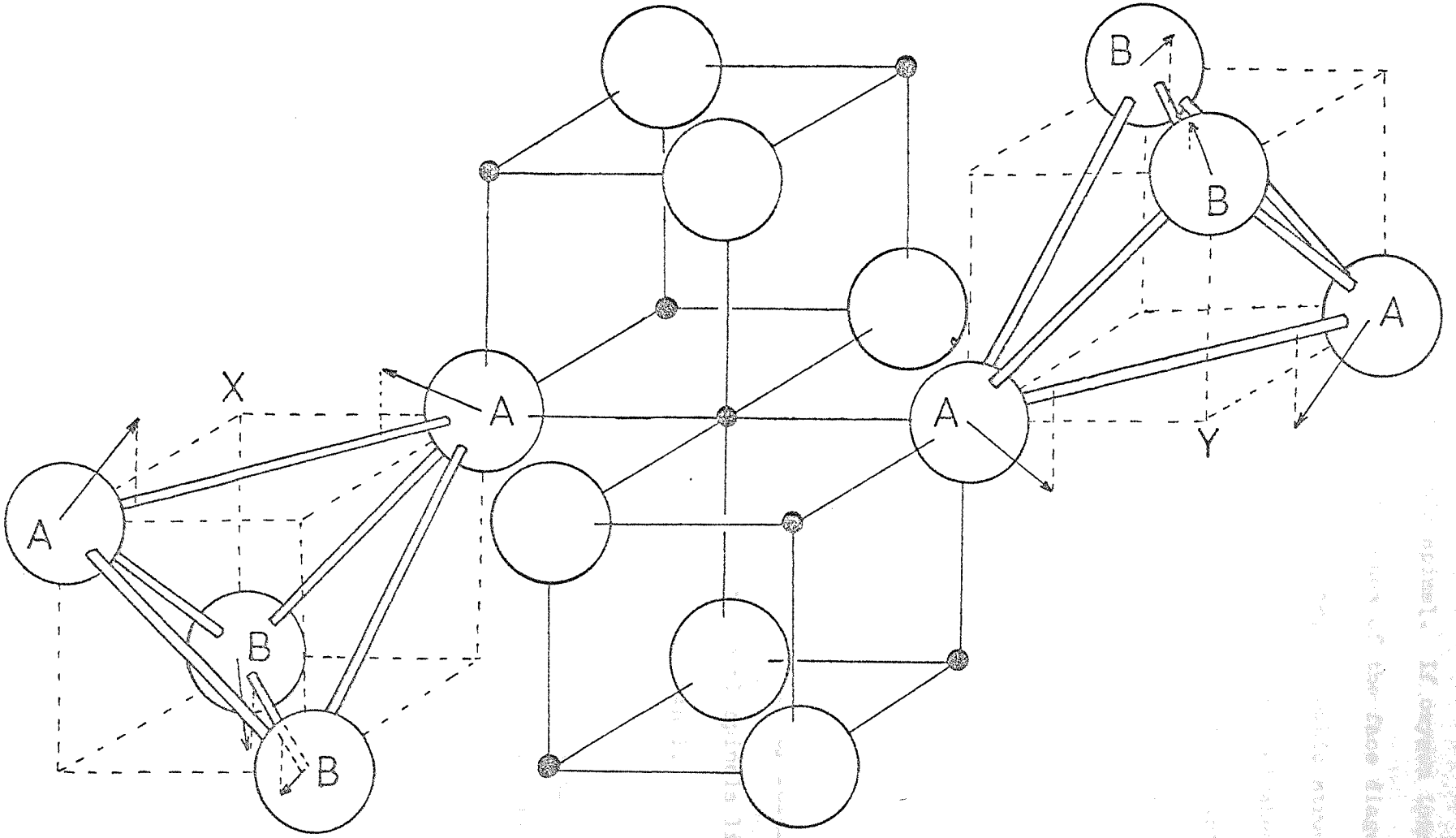

fig.1.3. Part of the spinel structure indicating the distortion from cubic to tetragonal.

is a diagramatic representation of part of the cubic unit cell in which are shown two A site tetrahedral and two neighbouring B sites cubes, the open circles representing oxygen ions. The length XY in figure 1.3 equals the lattice parameter of the cubic spinel. If oxygen ions are displaced in directions which are in the planes of the face diagonals of the elementary cubes indicated in the diagram, the cubic structure becomes distorted to tetragonal. When the A site oxygen tetrahedra are only considered, this displacement may be described by a distortion of the tetrahedra such that the distances AA and BB in the diagram are shortened, the directions of the oxygen ion displacements are indicated by arrows.

The oxygen ions of the B site cubes are also corners of neighbouring tetrahedra, thus these are displaced in a similar way, the actual directions of the displacements depending on the orientation of the tetrahedron to which each is part.

The displacements involved are small as can be seen by reference to table 1.1 in which values of c/a for the tetragonal spinels listed there are found to be marginally greater or smaller than 1.

1.4.1 The Jahn-Teller Effect and its application to spinels.

The distortion of an interstice in cubic spinels leading to tetragonal symmetry has been thought to arise from the presence of certain transition ions which exhibit the Jahn-Teller Effect (Dunitz and Orgel, 1957). The ions concerned are those with orbital degeneracy, two classic examples being Cu^{2+} and Mn^{3+} (Goodenough, 1963).

Dunitz and Orgel explain the phenomenon as being due to the anisotropy of the electron density distribution in the incompletely filled sub-shells. The presence of Jahn - Teller ions, in the spinel lattice when occupying more than a critical fraction of the B sites produces distortions from cubic to tetragonal symmetry according to Goodenough (1963) who cites numerous examples. Table 1.1 shows a selection of spinels containing

various Jahn-Teller ions.

Table 1.1 A Selection of Spinels containing Jahn-Teller ions.

Compound	Jahn-Teller ion	Structure	c/a	Reference
$CuFe_2O_4$	Cu^{2+}	tetragonal	1.06	Dunitz and Orgel(1957)
Mn_3O_4	Mn^{3+}	"	1.16	Sinha et al (1957)
$ZnMn_2O_4$	Mn^{3+}	"	1.14	Sinha et al (1957)
$FeCr_2O_4$	Fe^{2+}	"	0.97	Francombe (1957)
$NiCr_2O_4$	Ni^{2+}	"	1.025	Lotgering(1956)
$CuCr_2O_4$	Cu^{2+}	"	<1	Dunitz and Orgel(1957)

Buerger (1936) has suggested that Mn^{3+} ions in octahedral sites show tetrahedral distortions of the sites and Satomi (1961) measured the oxygen parameters of Mn_3O_4 to indicate directly that the octahedral site is distorted while the tetrahedral site remains unaffected. More recent investigations by Cervinka, Vogel and Hosemann (1970) on this ion (Mn^{3+}) have been carried out using X-ray intensity measurements and they quote displacements of ions corresponding to such distortions.

No detailed explanation of these tetragonal distortions was offered until recently when Kataoka and Kanamori (1972) developed the Jahn-Teller theory to include the elastic properties of the crystal and they suggest there is a coupling between electronic states and certain elastic waves which could cause the distortions. Experimental evidence supplied by Terauchi, Mori and Yamada (1972) and Kino, Lüthi and Mullen (1972) supports some aspects of this theory.

1.4.2 Phase transition in spinels containing Jahn-Teller ions.

The distortions discussed above can arise from Jahn-Teller ions

in either type of site. For instance Mn^{3+} ions occupying B sites will cause a distortion to tetragonal structure whereas a similar distortion occurs when Cu^{2+} occupies A sites. Two examples of A site distorted tetragonal spinels are $NiCr_2O_4$, with $c/a = 1.04$ (Delorme, 1955) and $CuCr_2O_4$, with $c/a = 0.91$ (Bertaut and Delorme, 1954 and Miyahara and Ohnishi, 1956). Prince (1957 and 1961) using neutron diffraction techniques, has shown the distortions in the latter materials to be in fact due to deformation of the A sites, he also suggests that the octahedral co-ordination around the Cr^{3+} ion in these compounds to be better than in most cubic spinels.

The concentration of Jahn-Teller ions in the lattice to produce a cubic to tetragonal transition is critical and Wickham and Croft (1958) have shown that in several oxides containing Mn^{3+} ions when the fraction of B sites occupied by Mn^{3+} ions lies in the range $0.6 < f < 0.65$ the transition occurs - the change over being quite abrupt - and in most materials exhibiting the transition, if $f > 0.5$ tetragonal symmetry occurs although there have been reported some cases in which the transition occurs if $f < 0.5$. A similar critical fraction of A site occupancy for tetragonal symmetry has been observed in $Zn_yCu_{1-y}Fe_2O_4$ when $y < 0.1$ (Goodenough, 1963). Above this fraction the spinel is cubic and it is thought to be due to the large size of the Zn^{2+} ion which when entering the lattice increases the u parameter so that the Madelung energy is altered to accommodate large numbers of Cu^{2+} ions on A sites without the occurrence of distortions.

The above description neglects the effects of temperature, for almost all the tetragonal spinels become cubic at sufficiently high temperatures (Finch, Sinha and Sinha 1957). At higher temperatures the larger thermal energies of the ions in the lattice overcome the effect of the energies involved in the formation of distorted sites due to the Jahn-Teller effect. The transition temperature can in fact range from quite low temperatures, of the order of 160 K for instance for some

spinels of the series $CuCr_xFe_{2-x}O_4$ to 900 K for other members of the same series depending on the value of x.(Ohnishi and Teranishi, 1961).

Above the transition temperature however distortions can still occur and Baltzer and Wojtowicz (1959) have suggested that this could happen in the case of Cr^{3+} which is spin quenched at high temperatures and in this condition the ion may be Jahn-Teller and that a dynamic Jahn-Teller effect may cause the ion to take up low spin states.

In investigations of the spinels $FeCr_2O_4$ and FeV_2O_4 using measurements on the Mossbauer effect, it has been suggested that there are structural distortions in the cubic phase, these distortions being shared between 3 axes so the overall cubic symmetry is maintained. These observations were made at 30 -40 K above the transition temperature for the cubic to tetragonal phase change.(Tanaka, Tokoro and Aiyama, 1966).

The presence of tetragonal distortions in an apparently cubic structure has also been observed by Brabers (1969) in manganese ferrites. His infra-red measurements indicate the presence of tetrahedrally distorted $Mn^{3+}O_6^{2-}$ octahedra in this material. The magnitude of the ion displacements in the manganese ferrite spinel lattice has also been reported by Cervinka (1965) having been calculated from temperature factor determinations using X-ray intensities.

1.5 Chromite spinels.

From the evidence outlined above it may be seen that among oxide spinels relatively simple behaviour is expected of chromite spinels. For instance all chromites are normal because of the high octahedral site preference energy (section 1.3.3). The chromium ion is not expected to be Jahn-Teller since in high spin state there is no orbital degeneracy thus no distortions are expected in the Cr_6^{3+} octahedra.

At the time when the present work was commenced all these considerations indicated that the chromite spinels were well understood; yet there were indications that suggested the presence of Cr^{3+} in the lattice

was accompanied by effects which could not be explained in terms of the accepted structure of chromite spinels. For instance, Stahl-Brada and Low (1959) studied the electron spin resonance spectrum of the Cr^{3+} ion in single crystals of natural spinels and found indications that the local environment of the ion in the crystal was trigonally distorted. According to their evidence the distortions observed were exceptionally strong and had one or other of the possible [111] directions as an axis of symmetry. The optical spectra of similar materials have been studied by Ford and Hill (1960) and their results were also consistent with the [111] trigonal distortions reported by Stahl-Brada and Low.

In an investigation into the optical properties and colour of chromium containing compounds, Poole (1964) shows the effect that chromium concentration has on the splitting of energy levels in a Cr^{3+} ion when it enters the octahedral site. He shows an anomaly in the optical properties of spinels with about 18% Cr^{3+} occupation of the available octahedral sites which is not seen in other chromium compounds. The optical data indicates that when the Cr^{3+} content changes there is a distortion in the octahedron surrounding the Cr^{3+} ion, the type of distortion depending on the nature of the crystal under investigation. Poole suggested that the actual positions of the cations must be determined before these optical anomalies can be explained. Figure 1.4 shows the data for spinels extracted from Poole's work showing the variation of the Racah parameter (R) against the ligand field parameter Δ . R is a function of the differences in wave numbers of the optical transitions observed when a Cr^{3+} ion is in a strong octahedral electric field and Δ is the wave number of the smallest optical transition of such a Cr^{3+} ion.

Theory suggests that R is invariant with Cr^{3+} concentration but spinel shows an anomalous behaviour at low chromium concentration. Poole's data for spinels (figure 1.4) shows a discontinuity at a concentration similar to that in $Mg(Al_{1.8125}Cr_{0.1875})O_4$ - one of the samples used in

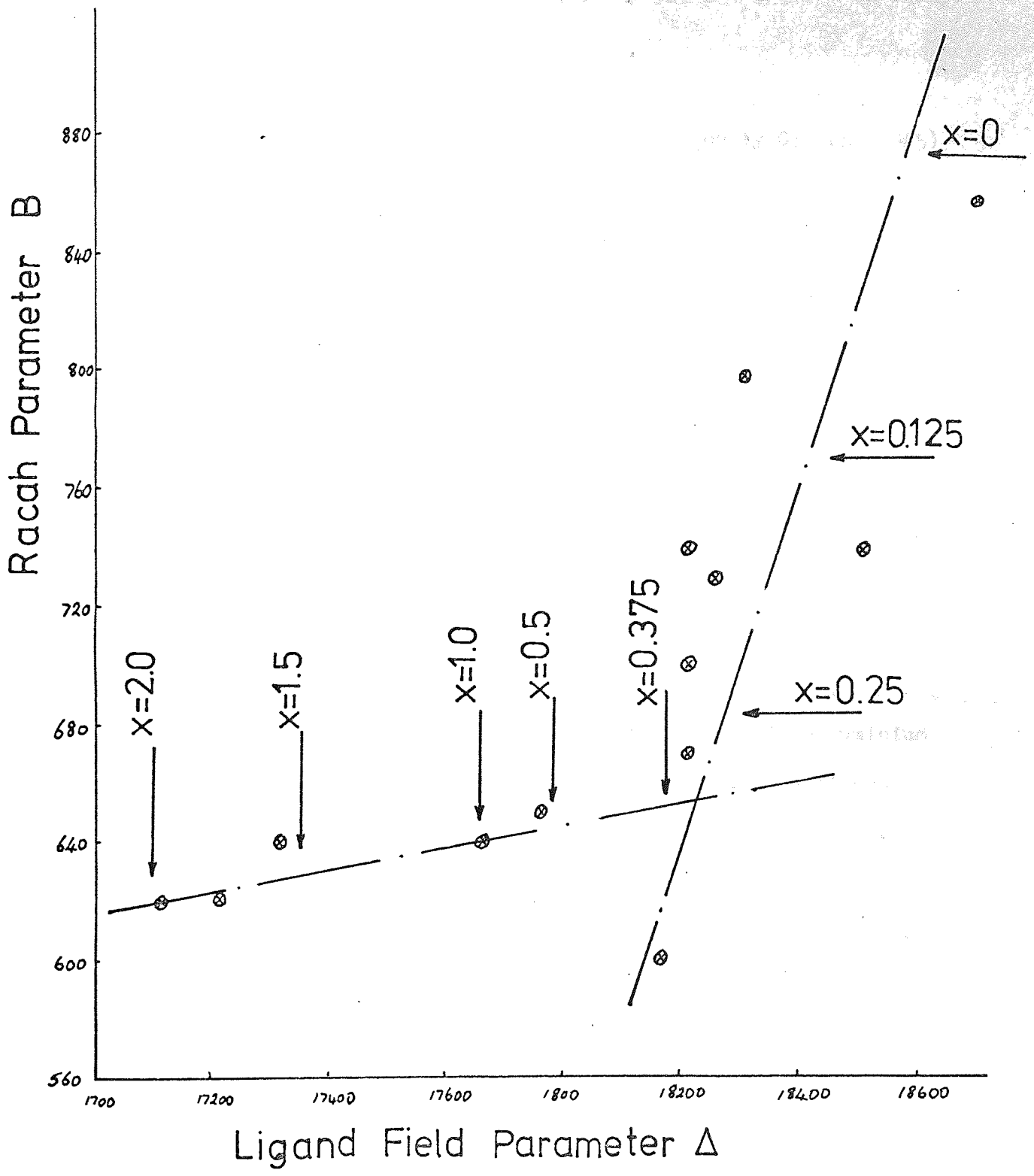

fig.1.4. Optical data for spinel specimens similar to those used in this study (after Poole, 1964)

this study. Also indicated in figure 1.4 are the chromium doped spinels similar in composition to the remaining specimens prepared for this study.

1.6 The scope of the present work.

The work described here arose from the observation by Grimes (1965) that X-ray diffraction photographs taken of the series of spinels $MgAl_{2-x}Cr_xO_4$ showed that when x approached the value 0.5, the diffraction lines became very broad. This roughly corresponds to the anomaly observed in the optical phenomena (Poole, 1964) and also with the anomaly reported by Thilo and Saur (1955) in the variation of the lattice parameter with chromium concentration.

The experimental results to be described were obtained from a fresh batch of eight specimens prepared by the author, using A.R. quality chemicals.

The X-ray line profiles for $MgAl_2O_4$ and $MgCr_2O_4$ were confirmed as sharp, in fact those of $MgCr_2O_4$ were almost as well defined as a well annealed metal.

On the other hand , with all specimens of mixed chromium-aluminium content, the profiles were broadened to various extents. The effect is best shown by comparison of the (533) profiles for all specimens. This line has a fairly high intensity at large diffraction angle, and in the two pure substances the $\alpha_1 - \alpha_2$ doublet is well defined. Thus this line serves as a good indicator of broadening throughout the range of specimens. Figure 1.5 illustrates the profiles drawn with the angular displacement shown correctly and with the same intensity scale for each.

It can be seen that the resolution of the $\alpha_1 - \alpha_2$ doublet deteriorates as x increases from zero until at 0.5 the two peaks are indistinguishable. There-after the separate peaks begin to appear and the resolution improves steadily, becoming most marked at x = 2.

Other points of interest to be noted from figure 1.5 are

(i) The regular way in which the integrated intensity increases through the range

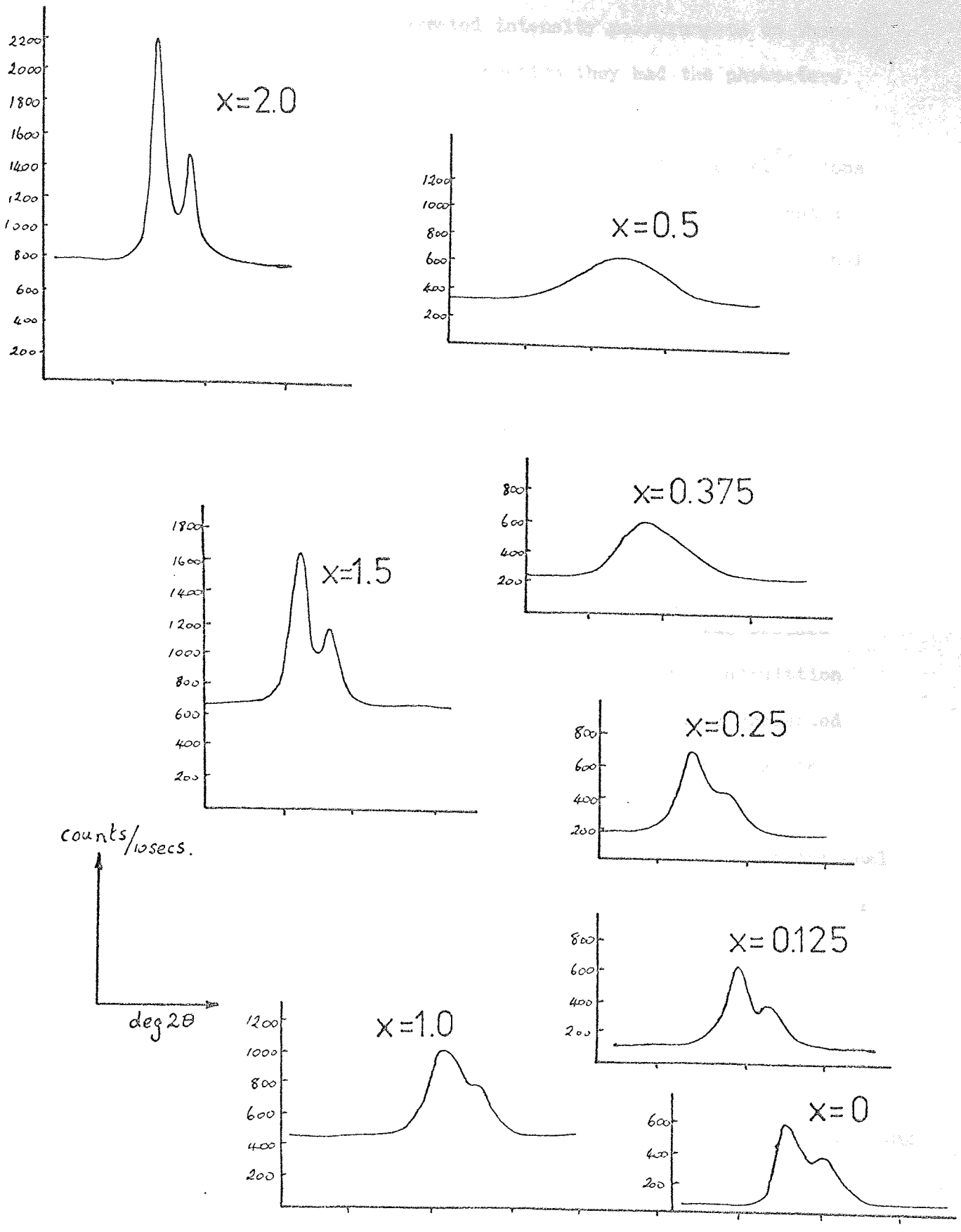

fig.1.5. Variation of line shape with Cr^{3+} content; (533) profile.

(ii) the regular way in which the general background level increases with increasing chromium content.

It was decided to make integrated intensity measurements on these samples to check the structure and to confirm they had the parameters already reported in the literature.

Successive substitution of larger Cr^{3+} ions in place of Al^{3+} ions causes an increase in the unit cell edge (a_o). It has been suggested (e.g. by Nicks, 1951) that the increase in a_o is directly proportional to the percentage impurity - a behaviour analogous to that described by Vegard's law in the theory of alloys and which appears to hold for many mixed systems. Vegard's law, the expected linear variation of lattice parameter with impurity holds for some metals provided a single phase is produced by the substitution, it has also been found to hold in a number of ionic salts and some spinels.

Most previous lattice parameter determinations had been performed using peak positions of line profiles. In this study it was decided to use the centroid position of the line profiles for the calculation of a_o for these specimens as the centroid can be rigorously corrected for all the various instrumental effects (Wilson, 1963a) and can be very accurately determined.

These spinels with $0 \leqslant x \leqslant 2$ are structures in which substitutional ions are inserted in increasing concentration into the lattice. Wilson (1963) has developed a theory for the analysis of X-ray line profiles. This involves the use of the variance of the profile as a measure of the breadth which can be expressed in terms of the various properties of the crystal and its structure, i.e. particle size, strain, mistakes, etc. This theory has been used in an attempt to identify the cause of broadening observed in this series of spinels.

The slight broadening of the $MgAl_2O_4$ (533) profile compared with $MgCr_2O_4$ was also of some interest in view of the suggestions by Bacon(1952) and Stoll et al (1964) that $MgAl_2O_4$ might be partially inverse.

A partially inverse spinel contains a mixture of trivalent and divalent cations on both octahedral and tetrahedral sites, and it was thought that this might be associated with the cause of broadening in the $MgAl_2O_4$ sample.

Having seen the effect of increasing the chromium concentration on the profiles of Cr^{3+} doped spinels, it was decided to attempt to change the system in some other way and perform a further analysis to ascertain any changes that may have occurred.

Selected examples were suspended in a nickel basket in a vertical tubular furnace and heated at various temperatures ranging from 900°C to 1100°C for 6 - 8 hours. They were quenched by dropping them into liquid nitrogen.

Diffraction profiles were taken from these samples as before and analysed in a similar manner to the unquenched samples.

CHAPTER 2

ANALYSIS OF DIFFRACTION LINE PROFILES

2.1 Origins of the breadth of diffraction line profiles.

2.1.1 Instrumental effects.

Traditionally Bragg's equation

$$2 d \sin\theta = n\lambda \qquad \ldots\ldots\ldots\ldots 2.1$$

is interpreted as though the wavelength λ was single valued and subject to diffraction by a crystal with unique spacing d. This implies that diffraction maxima would be observed with negligible width at an angle 2θ with respect to the direction of the primary beam. In practice, diffraction line profiles are observed to spread over a range of angles in the neighbourhood of the angle 2θ, chiefly because of the finite width of the characteristic emission lines. However, numerous other contributions can be significant, arising from both instrumental and diffraction sources.

Firstly, the output from an X-ray tube consists of two components, the continuous or 'white' spectrum and the characteristic radiation consisting of fairly discrete intense lines, the most important being the K_α and K_β radiation. Use of filters removes all but a small fraction of the K_β radiation, allowing the K_{α_1}, K_{α_2} and the K_α satellite lines, all of different wavelengths, to emerge from the filter. These lines each have a certain wavelength spread, the K_{α_2} peak being wider than the K_{α_1} peak. Thus this range of wavelength values exists even with an ideal instrument and a perfect crystal i.e. one with a single value of lattice spacing throughout, it would mean that the detector would record a composite line profile with an intrinsic breadth.

In addition the instrument itself causes broadening of the line. The source, specimen and detector entrance slit all have finite size

which means that there will be radiation received by the detector over a further range (Wilson, 1963a). To decrease this effect, the size of the slit or source could be reduced, but the effect of this remedy would be to reduce the intensity to be detected, thus a compromise has to be made. The overall effect is that there is a variation of intensity across a finite range of θ (equation 2.1) even with diffraction from perfect crystals.

2.1.2 Specimen effects.

In addition to instrumental contributions to the line breadth, there may be a greater or lesser contribution from the specimen which further increases the breadth. These contributions due to the specimen are those which contain information about the structure or condition of the specimen and it is necessary to separate these from the instrumental effects. The evaluation of this residual breadth due to specimen properties has been a problem which has given rise to various methods of analysis of line profiles.

2.2 Measures of diffraction line breadths.

2.2.1 The Scherrer breadth.

Scherrer (1918) was the first to study broadening of diffraction line profiles, his work dealing with the effect of crystallite size. He derived the following expression :

$$B = \frac{K\lambda}{L\cos\theta} \qquad \ldots\ldots\ldots\ldots\ldots 2.2$$

where K is the Scherrer constant

L is the average length of crystals

λ and θ have the usual meaning and

B is the half-breadth of the diffraction line.

The half-breadth is defined as the angular distance between two points

$2\theta_1$ and $2\theta_2$ where the intensity of the diffraction profile above background falls to half the peak value,

i.e. $B = (2\theta_2 - 2\theta_1)$

This is an apparently easy measurement to make experimentally although only of moderate accuracy. However aberrations on the half-width are present and theoretically the effect of these aberrations are almost impossible to calculate (Wilson 1963a). Thus the separation of instrumental and diffraction effects is extremely difficult to perform.

An accurate determination of the experimental half-width depends on the facility with which the background levels can be chosen; this is subject to statistical fluctuations due to the method of collection of the original intensity data, and it may be affected by neighbouring diffraction profiles whose 'tails' overlap the line under investigation. Theoretically the tail of a profile extends to infinity for most broadening effects and experimentally it is extremely difficult to determine where the tail of the line becomes indistinguishable from the background level.

Another problem arises from the presence of the doublet structure to the K_α line. To use this measure of width, the two components of the doublet must be separated so the larger, $K_{\alpha 1}$, may be used in the equation 2.2 above.

Rachinger (1948) suggested a method of performing this separation but his method makes assumptions about the shape of the profile which introduces further uncertainty into the final breadth measurements.

2.2.2 The Integral breadth.

The theoretical and practical limitations of the Scherrer breadth were recognised and a more theoretically sound measure was seen to be required. A new measure to be used in the Scherrer equation (2.2) was described by von Laue in 1926. His definition was:

$$\beta = \frac{1}{I_p} \int I(2\theta) \cdot d(2\theta).$$

i.e. the integrated intensity divided by the peak height. The use of the total intensity under the profile in this measure, as opposed to just one value, the peak value , of the Scherrer approach means that the integral breadth is less dependent upon the choice of background.

Laue derived an expression for β which was of the same form as the Scherrer equation, however, the constant was different and Jones (1938) and Wilson (1963) show that the value of K in equation 2.2 depends upon the assumptions made about the crystals. Laue also assumed, in an attempt to remove instrumental broadening effects from the measured profile, that the total breadth of the diffraction profile was given by the sum of the breadth due to instrumental effects plus the breadth due to the state of the crystal.

$$\text{i.e. } B_{total} = B_{inst.} + B_{crystal} \quad \ldots\ldots\ldots\ldots 2.3$$

Thus if a reference sample is used, with no broadening of its profiles except for instrumental effects, which gives a line close to the line given by the sample under investigation, the difference between the integral breadths would give the breadth due to crystal defects.

However, the relation of equation 2.3 is only true if the profiles are Cauchy curves. If the profile is Gaussian then the relation becomes

$$B^2_{total} = B^2_{inst.} + B^2_{crystal} \quad \text{(Warren and Biscoe 1938)}$$

This assumes also that the profile has been corrected for the presence of the $\alpha_1 - \alpha_2$ doublet. However most experimental curves lie between Cauchy and Gaussian and Wagner and Aqua (1964) used the empirical relation given below:

$$B_{total} = B_{crystal} + B^2_{crystal} / B_{total}$$

2.2.3 Fourier Analysis of line breadth.

Fourier analysis offers a means of determining the breadth which overcomes the problem of separating instrumental effects from crystal defect effects.

The breadth of a profile from a sample under investigation is due to a combination of the instrumental effects and defect effects within the crystal and an expression for the intensity of the line profile has been derived (see for example Rooksby Peiser and Wilson 1955) If the intensity of the line broadened by diffraction effects is $F(x)$ at a distance x from the peak, then the intensity associated with the element lying between x and $x + dx$ is $F(x).dx$. The intensity due to the instrumental effects is $g(x).dx$. If both effects occur, then the diffraction broadening will be spread further by the instrumental broadening to give an intensity $F(x).dx.g(x')$, x' being the distance further than x from the peak. If the distance from the peak is $q = x + x'$, then the intensity at q is

$$F(x).g(q - x).dx$$

The total intensity at this distance from the peak will be given by

$$h(q) = \sum_{x=-\infty}^{\infty} F(x).g(q - x).\Delta x \qquad \ldots\ldots\ldots\ldots 2.4$$

By taking intensity measurements on a broadened line, the experimental data for $h(q)$ can be obtained by comparing it with a reference specimen which gives sharp diffraction lines - i.e. with breadth due to instrumental effects only, thus $g(x)$ can be found.

Application of Fourier transform methods to equation 2.4 to separate the two effects was first demonstrated by Stokes (1948) who analysed line profiles from cold worked copper and annealed copper; the transform due to cold working being given by

$$\text{Transform of } \underset{\text{(cold work)}}{\text{(hkl) profile}} = \frac{\text{Transform of broadened (hkl) profile}}{\text{Transform of (hkl) profile } \underset{\text{(annealed Cu)}}{}}$$

In this way a measure of broadening due to the cold working was found.

This method of analysis has been successfully used in the separatim of particle size and strain effects which often occur simultaneously (Warren and Averbach, 1950). Warren (1959) for example has used Stoke's method to separate the contribution of particle size to the breadth from that due to strain in his sample. No assumption about the shapes of the lines, i.e. whether Cauchy or Gaussian, is required although very accurate line profile data are essential to obtain satisfactory results.

2.2.4 Variance as a measure of breadth of diffraction profiles.

The breadth of a profile which is subject to different aberrations is some combination of the breadth due to each effect, i.e. if the profile is Gaussian, the relation between breadths is

$$B^2_{total} = B^2_{inst.} + B^2_{diffraction} \quad \ldots\ldots\ldots\ldots 2.5$$

where B is either the half-width or the integral breadth.

If the profile is Cauchy, the relation becomes

$$B_{total} = B_{inst.} + B_{diffraction} \quad \ldots\ldots\ldots\ldots 2.6$$

Experimental profiles can be mixtures of both types of curves. For instance both crystal size distribution effects (Jones, 1938, Alexander, 1950) and instrumental effects (Alexander, 1948) can give an intensity distribution which differs from the Gaussian form. Thus profiles from these examples are a mixture of distributions for which neither of the two equations 2.5 and 2.6 above would hold.

However, there is a measure of dispersion which can be used and is unaffected by the types of distributions present in the measured profile. This measure is the standard deviation (σ) or variance (W) of the profile ($W = 4\sigma^2$). The property of the variance is that in any distribution consisting of a number of distributions, the total variance is the sum of the variances of the constituent distributions.

$$\text{i. e.} \quad W_{total} = W_{inst.} + W_{diffraction}$$

also

$$\sigma^2_{\text{total}} = \sigma^2_{\text{inst.}} + \sigma^2_{\text{diffraction}}$$

The variance of an X-ray line profile was recognised as a possible measure of dispersion as early as 1931 (Spencer, 1931) but there was a practical problem in as much as the distribution theoretically stretches to infinity so that the variance of such a distribution is consequently infinite. However, Pitts and Willets (1961) used standard deviations of profiles instead of integrated breadths to calculate crystallite size and lattice distortions using the Scherrer equation, but these were truncated profiles and truncation necessarily causes the elimination of a large contribution to the variance from the tails of the profile (Ladell, Parrish and Taylor, 1959).

Tournarie (1956) criticised the use of half-widths and integral breadths because they gave undue weight to a few points on the profile. He suggested that use could be made of the fact that the variance of a truncated distribution is directly proportional to the range over which the variance is calculated, this gives all points on the distribution equal weight. Wilson (1961, 1962, 1963) followed this suggestion by developing a theory which expresses the slope and intercept of the type of graph described by Tournarie in terms of the various physical properties of the material under investigation, e.g. particle size, strain and mistakes in crystals.

Use has been made of this theory mainly in the investigation of particle size and strain in metals, for instance by Langford and Wilson (1963) and Langford (1968), in studies of aluminium and nickel; Langford compared the results from variance analysis with those obtained from observations with the electron microscope and found good agreement. A comparison of various measures of breadth, namely variance, Fourier analysis and integral breadths has been made on aluminium, the results showing that all techniques gave very similar values (Aqua, 1966).

The technique has also been used in an attempt to account for mistakes in non-metallic materials (Grimes, Hilleard, Waters and Yerkess, 1968).

An advantage of the variance technique is that instrumental effects can easily be evaluated by using a standard material as a reference. If this reference sample is a pure sample with a particle size around 10^{-5}m, then the profile variance is due entirely to instrumental effects, thus if a profile from a defect sample is taken under the same experimental conditions, the variance of this profile is the sum of the variance due to instrumental effects and the variances due to each type of defect i.e.

$$W_{total} = W_{instrument} + \sum W_{defects}$$

Thus the difference between the variances of the reference and defect samples gives $\sum W_{defects}$.

Provided the distributions decay as the inverse square of the distance from the peak, then it is relatively simple to show that the variance of a profile is

$$W = A\sigma + B$$

where σ is the range over which the variance is calculated and A and B are constants which depend on the form of the distribution (Wilson, 1962a). Wilson (1961,1962 and 1963) has developed expressions for A and B, the slope and intercept of the variance-range plot, which describe the diffraction due to various crystal defects.

Another advantage of the variance technique of analysis is that it has an automatic 'correct' background selection procedure. In any analysis of a line profile, the background has to be estimated and subtracted from the line intensity before analysis can be commenced. The most popular, is to assume a linear variation of background between the tails of the profile and the slope of this variation calculated from visually estimated values of intensity levels at large ranges either side of the peak. This approach is very subjective and is

considered to be unsatisfactory when extensive broadening is present. Langford and Wilson (1963) describe a method of estimation in which the variance of a line profile is calculated with an assumed background level subtracted from the intensity data. If the background is correctly chosen, the variance-range plot of the corrected profile is linear for large ranges. However, if the background is chosen incorrectly, the variance expression includes a cubic term in $\Delta 2\theta$ as shown below:

$$W_{2\theta} = S.\Delta 2\theta + I + D(\Delta 2\theta)^3$$

(here S and I are the expected slope and intercept of the linear portion).

$$D = \text{background error} / 12x(\text{Integrated intensity})$$

Thus the variance-range characteristic will curve upwards if the chosen background is too low and downwards if it is too high (see figure 2.1).

2.3 Contributions to line breadth due to crystal defects.

Having considered methods to separate instrumental from the crystal diffraction effects in measured line profiles it will be useful to consider the various factors which can increase the breadth of the line.

2.3.1 Particle size effects.

A diffractometer powder sample consists of many crystallites usually randomly orientated. The size of these particles has an important effect upon the breadth of the diffraction lines.

According to Bragg's Law, a beam of X-rays and the reflecting planes within the crystal must meet at one of a set of precisely defined angles in order to obtain a maximum of diffracted intensity. If the diffracting crystal is large then there is a very large number of parallel 'reflecting' planes and this condition produces very sharp diffraction maxima as it must be satisfied exactly. Reducing the size

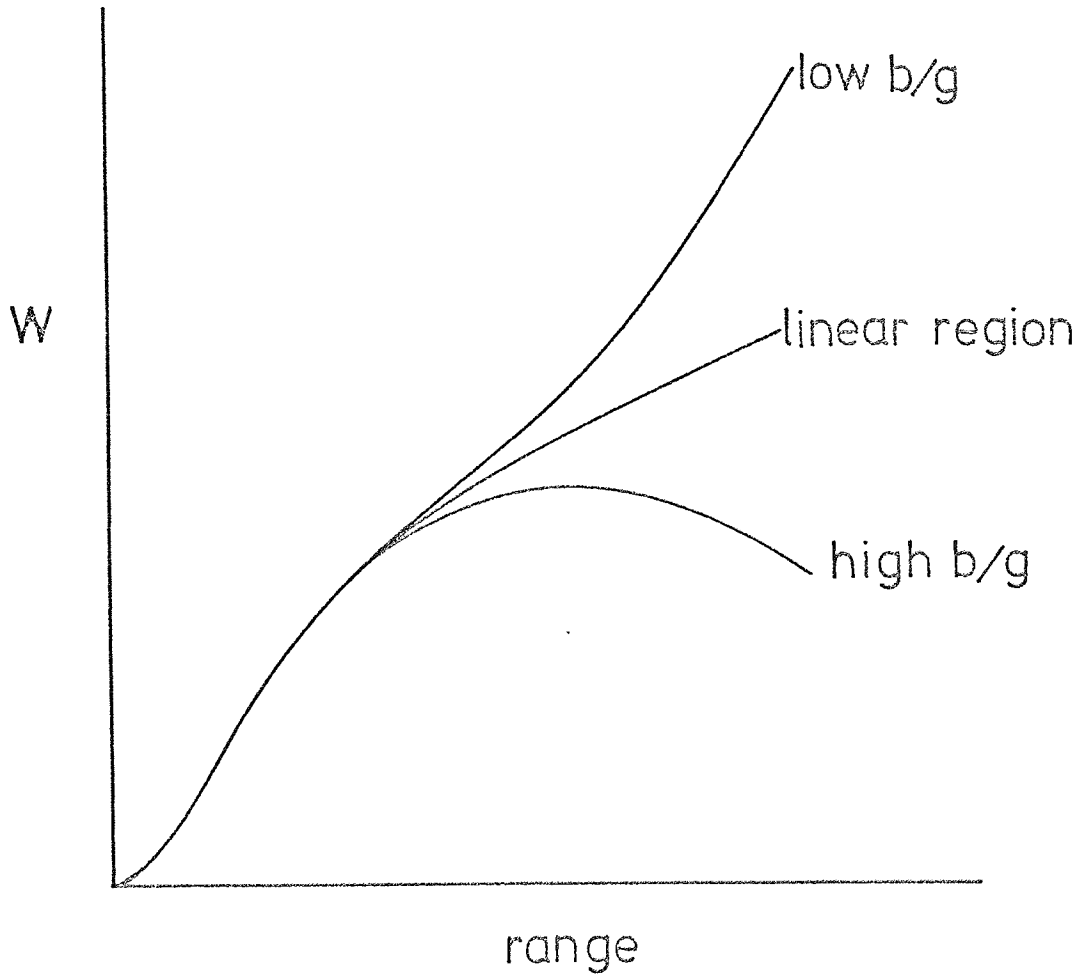

fig.2.1. Effect of background on the variance-range characteristic.

of the diffracting crystal reduces the number of diffracting planes and the precision of the condition is relaxed and the diffraction lines become broader. As the crystal size decreases the normally sharp diffraction maxima become broader, with a corresponding reduction in maximum intensity to keep constant the total intensity of the line, which is related to the content of each unit cell. With very small crystallites, the line is so broad that it becomes lost in the background radiation which is encountered in all methods of detection.

Very small crystallites, average diameter 10^{-8}m and less, produce no discernable diffraction maxima corresponding to normal line profiles. There is however, usually a diffraction halo at a low angle of diffraction which is entirely due to the X-rays being diffracted by the small particles, this is comparable with diffraction halos seen when visible radiation is viewed through a suitably finely divided medium. The dimensions of these low angle 'reflections' can give information about the size of the specimen particles, for instance colloid particle sizes may be estimated in this way.

Small crystals, up to 2×10^{-7}m diameter, produce diffraction profiles in the expected regions according to Bragg's Law, but these are broadened. Again this broadening can be studied to obtain the size of the particles in the sample, but the instrumental effects must be eliminated as discussed above in section 2.2.2.

Particle sizes up to 10^{-5}m produce sharp diffraction maxima, the breadths of these lines being due entirely to instrumental effects. Specimens with particles of this size are consequently ideal for use as reference samples to remove instrumental effects from profiles from specimens giving broad lines.

Larger crystallites, up to 10^{-4}m, are approaching the size at which they can be considered as single crystals and these produce diffraction spectra of spots - the effect on a powder photograph is to produce spots superimposed on the expected diffraction powder rings.

Particle size effects have a specified effect on the results obtained from variance analysis. Wilson (1962) has derived the following expression for the variance of a diffraction line due to particle size:

$$W_{2\theta} = \frac{K\lambda\Delta 2\theta}{2\pi^2 p \cos\theta} - \frac{L\lambda^2}{4\pi^2 p^2 \cos^2\theta}$$

where λ and θ have the usual meaning,

Δ 2θ is the range over which $W_{2\theta}$ is calculated,

K is the variance Scherrer constant - analogous to the constant derived by Scherrer in 1918 using half-widths,

L is the taper parameter.

Values of K and L are also listed by Wilson for various particle shapes.

$W_{2\theta}$ is the residual variance in $(\Delta 2\theta)^2$ after the profile variance has been corrected for instrumental effects.

Values of K are shown to be positive, L is also shown to be positive but for some crystal shapes and directions can take the value zero. Thus the residual variance due to particle size gives a result in which the slope of the variance-range plot is positive and the intercept generally negative, but in very few instances zero for crystallites with shapes other than spherical. However in the few cases of zero residual intercept, other profiles from the same sample would give a negative intercept contribution to particle size variance. For spherical crystals, K and L take values of a positive constant and zero respectively so that all profiles of such a sample would give zero residual intercept for particle size.

2.3.2 Preferred orientation effects.

In the above discussion it has been assumed that all crystallites in the sample are randomly orientated, thus giving equal chance of diffraction from a particular type of plane to occur in any direction.

However in some samples the shape of the crystallites could cause them to become aligned in approximately the same direction. For instance the drawing of a wire tends to align crystallites in a particular direction: the effect of this alignment is to produce a larger choice of reflections in particular directions, i.e. with a needle shaped crystal there is a greater chance of reflection in the equatorial plane than others, thus the powder diffraction rings show greater intensity at particular positions on the rings at the expense of the rest. This could be a difficulty in the use of a powder diffractometer in the analysis of such a sample as this enhanced intensity may or may not be observed by the detector as the diffractometer only scans a small fraction of the diffraction ring.

2.3.3 Effects due to specimen imperfections.

When discussing the breadth due to instrumental effects above, the diffraction by perfect crystals was considered. However all samples investigated are not perfect crystals. A crystal is an arrangement of atoms in a three-dimensional periodic array and is one extreme of the construction of a solid whereas a glass, which is a random collection of atoms with no such long range order, may be considered as another extreme. Usually X-ray diffraction samples fall some way between these two extremes, i.e. there is some departure from the perfect crystallinity defined above. This departure has an effect on the diffraction profile which may be analysed to give information about the effect.

2.3.3.1 Strain effects in crystals.

In the production of a sample, it may undergo the effects of external influences such as heat and pressure. These cause the deformation of the crystal lattice i.e. the crystal may be stretched or compressed to various degrees throughout the structure. This produces a system in which the lattice spacing (d) varies from place

to place, thus the Bragg condition changes slightly at different positions in the crystal and instead of a sharp diffraction line corresponding to one d value, a broadened profile appears reflecting the range of d values now present in the sample due to strain effects, i.e. the sample behaves as a group of crystallites with varying lattice parameter (Patterson, 1939).

The contribution to the variance, due to strain in crystals, of a profile has been derived by Wilson (1963) to be

$$W_{2\theta} = 4 \tan^2\theta \cdot \langle e^2 \rangle$$

where $\langle e^2 \rangle$ is the variance of the strain.

Thus a sample with only strain present would give a result in which the slope of the variance-range plot is unchanged compared to that of a reference specimen but elevated by some value. The value of this intercept varies as $\tan^2\theta$ as can be seen from the above equation so that strain effects are more pronounced at high Bragg angles.

2.3.3.2 Deviation from perfect stacking of atoms in crystals.

In close packed structures i.e. hexagonal close-packed and face centred cubic, the crystals consist of densely populated planes of atoms stacked together in prescribed ways perpendicular to these planes, the difference between these two structures being the number of planes necessary to be stacked in order to complete the translation period. Under certain conditions it is possible to obtain a mixture of these stacking sequences - giving rise to discontinuities in the structure- these are called stacking faults. The effect of these faults is to cause a broadening on the high angle side of the profile and to cause a shift of the lines in some cases (Azaroff and Buerger, 1958) although Patterson (1952) has reported that deformation stacking faults on (111) planes of face centred cubic metals cause symmetrical broadening of the lines, this being accompanied by line shifts. He also reports that twin stacking faults cause asymmetric broadening

with negligible line shift.

The effect of stacking faults on the diffraction pattern is similar to that of small particle size except that the effect varies in an irregular way with the plane of reflection (Wagner, 1966, Warren, 1969).

The discussion above refers to the observations seen in metals, however stacking faults can also occur in non-metals. For instance $MgAl_2O_4$ can accomodate large ranges of non-stochiometry without loss of the spinel structure (Roy,Roy and Osborne, 1953) being due to vacancies occurring on some sites normally occupied by the Al^{3+} ions (Jagodzinski and Saalfeld, 1958).

In an investigation of the defect structure of Spinel, Lewis (1966) formulated models for the structure to account for observations that the O^{2-} ion lattice was undisturbed by the observed faults but was characterised by a fault in the cation stacking - this type of fault is called an anti-phase boundary and their appearance can be explained in terms of nucleation of different domains in the crystal during crystal growth. Figure 2.2a illustrates the formation of an anti-phase boundary by projecting two layers of ions parallel to the (100) planes and perpendicular to the anti-phase boundary. Cations are distributed in alternately filled rows and a displacement of a portion of crystal by a distance R in the diagram produces an anti-phase boundary with no disturbance of the O^{2-} lattice. Figure 2.2 b shows the introduction of an anti-phase boundary by the formation of a dislocation.

Anti-phase boundaries have been reported to occur in lithium ferrite (Cheary, 1971). His results indicate that the growth of anti-phase domains is impeded by the presence of Cr^{3+} ions in the crystal, and he suggests that a large fraction of the Cr^{3+} ions migrate to the vicinity of the anti-phase boundaries and occupy B sites there. Due to its stability in this site (McClure, 1957) migration of Li^{+} ions on B sites, which is necessary if one domain is to grow at the

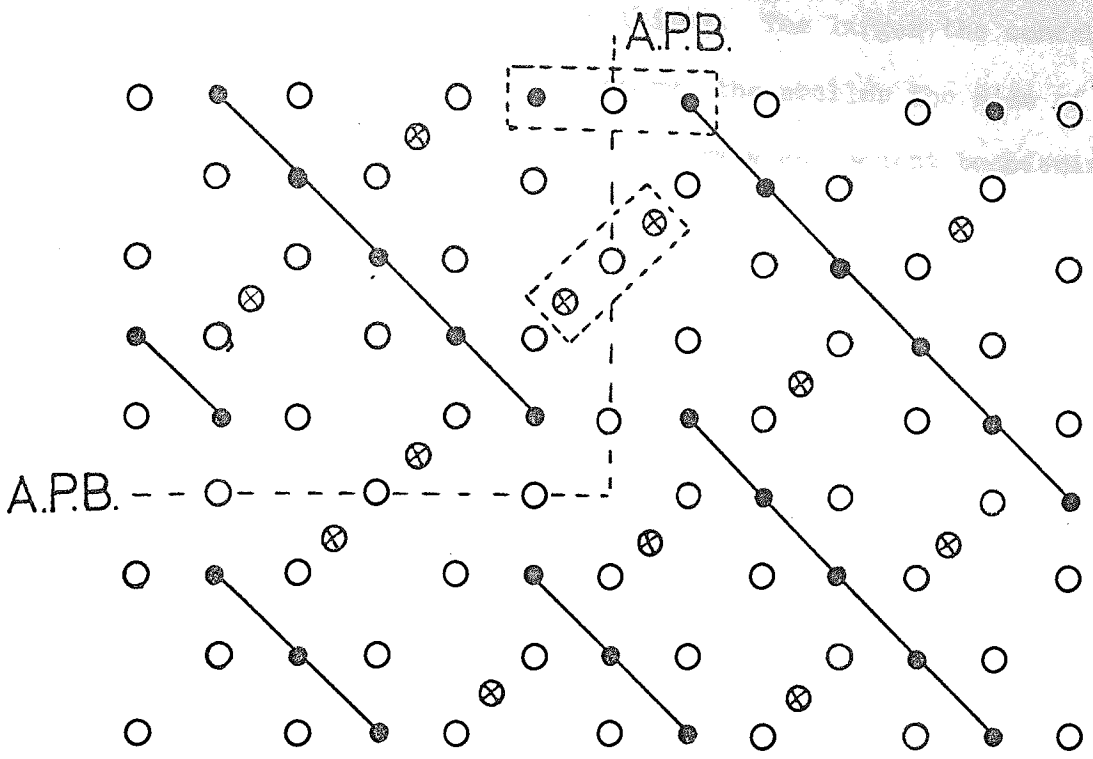

○-O^{2-} at layer 1. ⊗-Mg^{2+} at layer 2.

●-Al^{3+} at layer 1.

a. Displacement of lattice by vector R.

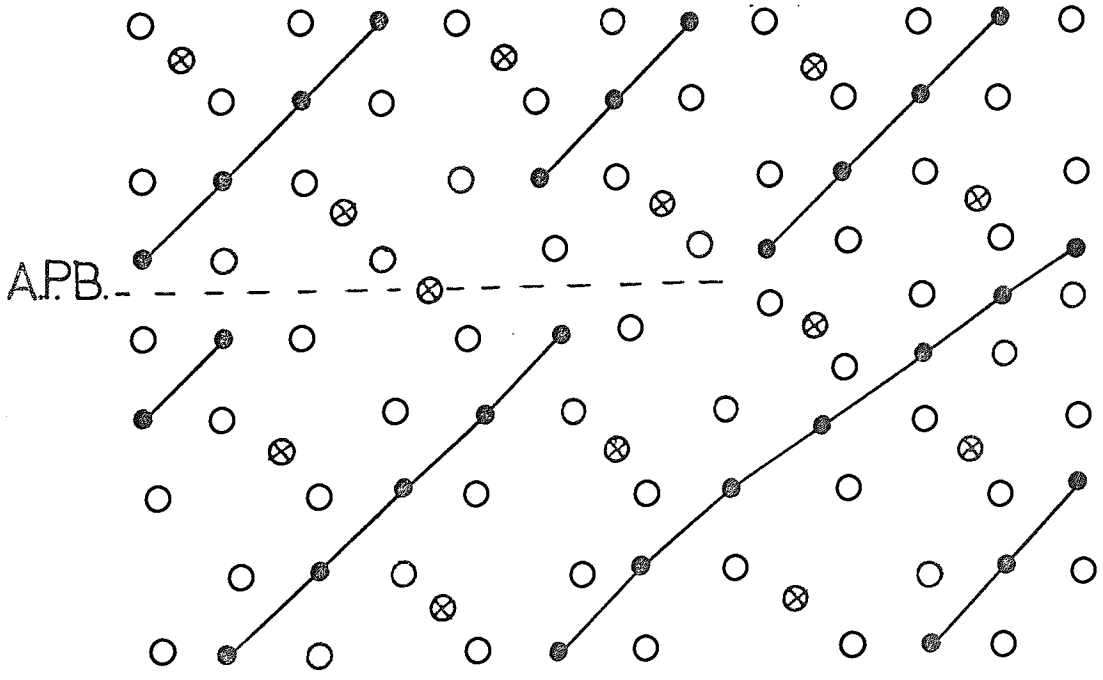

b. Introduction of dislocation.

fig. 2.2. Occurrence of anti-phase boundaries in the spinel lattice.(Lewis 1966)

expense of its neighbour, is inhibited. The larger the concentration of Cr^{3+}, up to levels used by Cheary, the smaller the size of anti-phase domain, this being accompanied by a consequent broadening of the diffraction profiles.

2.3.3.3 Disordered crystals.

If in a crystal consisting of more than one type of atom, each atom occupying a particular position in the unit cell throughout the crystal is an ordered crystal. However, it is possible for some atoms in the structure to occupy different positions in the unit cell from place to place in the crystal - this is a disordered crystal -the system being periodic only in a statistical sense. Disorder such as this occurs in alloys, a well documented example being Cu_3Au (see for instance Jones and Sykes, 1938, Wilson, 1943).

In a sample of Cu_3Au with a random distribution of atoms throughout the crystal, the statistical structure is face centred cubic in which the atoms can be regarded as composite atoms - 3 parts copper, 1 part gold - on the lattice positions. The diffraction lines for this structure are well defined and form the typical face centred cubic metal pattern.

By annealing the metal at elevated temperatures it is possible to cause a redistribution of the gold and copper atoms in the lattice. Annealing causes the atoms to take up specific positions in the lattice and the face centred cubic diffraction pattern is augmented by a number of extra diffraction lines called superlattice lines. The longer the annealing process below a certain critical temperature, the more ordering occurs in the crystal and the more intense are the extra diffraction lines. In the ordered state of Cu_3Au, the gold atoms occupy the cube corners and the copper atoms the face centred position, figure 2.3(a) indicates the difference between the ordered and disordered structure. In the ordered state the structure is primitive cubic. The diffraction

lines which are common to both structures are sharp, the superlattice lines being broadened to an extent which depends on the size of the ordered parts of the crystal. If these are the same size as the crystals in which they are formed, the superlattice lines are as sharp as the original lines, if the ordered regions are smaller, the superlattice lines are broader - the original line breadths being unaffected (Lipson and Steeple, 1970). Figure 2.3(b) shows the difference in diffraction patterns of ordered and disordered Cu_3Au alloys, the presence of the superlattice lines being indicated in the case of the ordered alloy.

Ordering has also been observed in non-metallic materials with spinel structure in which ordering of ions can occur in a variety of ways:-

(i) 1:1 order on octahedral sites e.g. $Zn(LiNb)O_4$ in which Li^+ and Nb^{5+} ions take alternative positions in the (110) rows of octahedral sites (Blasse, 1964)

(ii) 1:3 order on octahedral sites: lithium ferrite being one of this type (Braun, 1952)

(iii) 1:5 Order on octahedral sites: γ Fe_2O_3 has a spinel structure in which vacancies occur on the normally occupied B sites with an order which results in a tetragonal lattice with $c = 3a$, a being the lattice parameter of the disordered type (Oosterhout and Rooymanns, 1958)

(iv) 1:1 order on tetrahedral sites: $LiFeCr_4O_8$ is an example of this type in which Li^+ ions occur at (000) - f.c.c. translations and Fe^{3+} occur at $(\frac{111}{444})$ - f.c.c. translations (Gorter, 1954)

(v) 1:2 order on tetrahedral sites: an example of this is β-In_2S_3 which has vacancies which become ordered on A sites below 420°C with a consequent change of lattice to tetragonal with $c = 3a$, a being the face diagonal of the

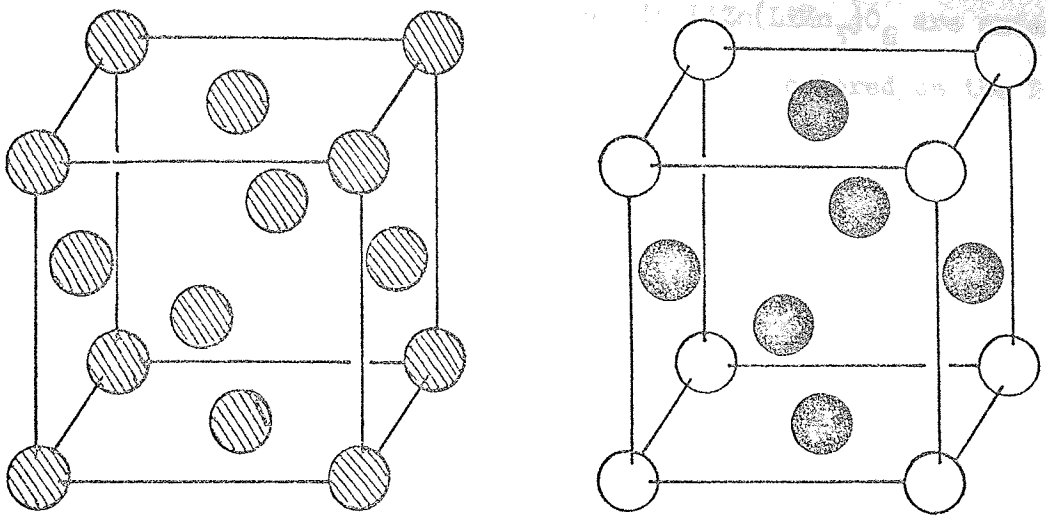

a. Ordered and disordered structures of Cu_3Au.
○-Au, ◎-Cu, ◍-$\frac{1}{4}$ Au $\frac{3}{4}$ Cu.

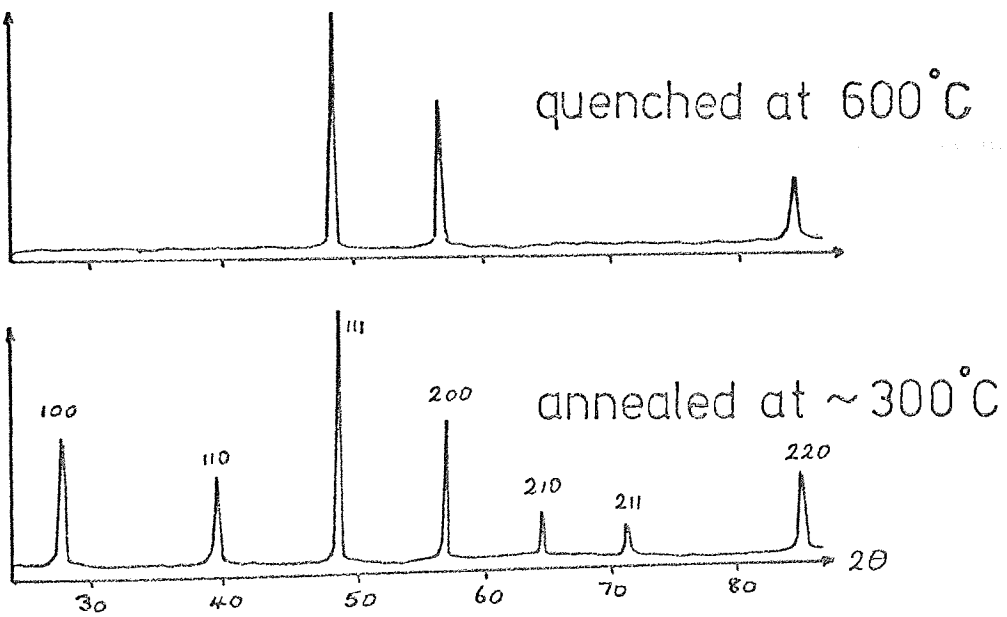

b. Diffraction patterns of powdered Cu_3Au using CuK_α radiation. (after Warren 1969).

fig. 2.3. Order-disorder in Cu_3Au.

disordered unit cell (King, 1962)

(vi) 1:1 order on A sites with 1:3 order on B sites; below 400°C the Li^+ and Zn^{2+} ions in $LiZn(LiMn_3)O_8$ are ordered on A sites and Li^+ and Mn^{3+} ions are ordered on the B sites (Blasse, 1963).

An important feature of ordering is that superlattice lines appear at the outset of this ordering. The breadths of the superlattice lines being a measure of the ordered domain size i.e. as is the case with Cu_3Au alloy, the larger the fraction of crystal which has order, the sharper the superlattice lines. If the variance analysis is used on this type of sample, the sharp lattice lines, i.e. those obtained from the disordered crystals may be used as reference lines to analyse the breadth of the superlattice lines. Cheary (1971) has investigated the ordering of Cr^{3+} ions in lithium ferrite using this technique and was able to report the clustering of Cr^{3+} ions at anti-phase boundaries.

Samples in which atomic distributions vary from place to place within a crystal can be termed mistake structures. Wilson (1963) has derived an expression for the variance contribution to a diffraction profile due to mistakes in a crystal, its form being similar to that for particle size effects in that it contributes both to the slope and intercept of the variance-range characteristic of the total profile variance. Wilson's expression is

$$W_{2\theta} = \frac{J_s - J_a}{TJ_s} \cdot \frac{\lambda \Delta 2\theta}{2\pi^2 \cos\theta} - \left[\frac{J_s - 2J_a + J_n}{TJ_s} Q'(0) + \frac{K_a}{TJ_s} \right] \frac{\lambda^2}{4\pi^2 \cos^2\theta}$$

where J_a is the mean value of FF^* for cells in the same domain i.e. the integrated intensity of the profile.

$(J_a - iK_a)$ is the mean value of FF^* for cells in adjacent domains,

T is the domain thickness,

J_n is the mean value of FF^* for cells in next but one domains,

$Q(x)dx$ is the fraction of domain thickness in the hkl direction lying in the range x to x + dx

the other symbols having their usual meaning.

The slope is always positive. The intercept value depends to some extent on the value of the slope i.e. if part of the intercept term is rewritten thus:

$$\frac{-J_s + 2J_a - J_n}{TJ_s} Q'(0) = \left[\frac{J_a - J_n}{TJ_s} - \frac{J_s - J_a}{TJ_s} \right] Q'(0)$$

it can be seen that the intercept could reflect the value of the slope, thus a variation of intercept with angle diffraction need not be a smooth variation as is found in the case of particle size broadening.

CHAPTER 3

EXPERIMENTAL DETAILS

3.1 Introduction.

The series of spinels used in this study contained two pure well documented materials, namely $MgCr_2O_4$ and $MgAl_2O_4$ for which crystallographic data have been published. These materials were used as checks, by making integrated intensity measurements on them to ensure that they were similar to those described in the published literature (e.g. Verwey et al 1947, Bacon, 1952).

3.2 The spinel series used in this study.

3.2.1 Factors influencing the choice of specimens.

The spinels chosen for this work were the series

$$Mg(Al_{2-x}Cr_x)O_4$$

with x taking values from 0 to 2. The choice of the particular values of x between these two extremes was governed partly by the structure properties of the spinel unit cell and partly by the approximate value of x at which the anomaly in the optical properties of Cr^{3+} containing spinels was observed by Poole (1964) in his work on Cr^{3+} doped crystals.

The ion which was substituted was the trivalent ion, i.e. that occupying the octahedral or B site. In the spinel unit cell there are sixteen occupied B sites and the intention was to replace the aluminium ions in $MgAl_2O_4$ successively by chromium ions. Table 3.1 gives the projected compositions and the number of chromium ions per unit cell in each specimen.

The first 5 samples listed in the table were chosen to 'bracket' the range of samples in Poole's data which show the anomaly in the optical properties, so that if possible X-ray analysis might lead to an explanation, through crystallographic properties, of this phenomenon.

Table 3.1 Projected compositions of the specimens used in this study

Formula	No. of Cr^{3+} ions per unit cell
$MgAl_2O_4$	0
$MgAl_{1.875}Cr_{0.125}O_4$	1
$MgAl_{1.75}Cr_{0.25}O_4$	2
$MgAl_{1.625}Cr_{0.375}O_4$	3
$MgAl_{1.5}Cr_{0.5}O_4$	4
$MgAlCrO_4$	8
$MgAl_{0.5}Cr_{1.5}O_4$	12
$MgCr_2O_4$	16

3.2.2 Possible methods of specimen preparation.

The choice of preparation of the samples lay between two relatively direct methods. These were

(i) the mixed oxide method described for instance by Verwey and Heilmann (1947) and

(ii) the mixed nitrate method described by Lotgering (1956).

It may be of interest to note here that an enormous amount of crystallographic and magnetic investigations has been carried out on spinels and ferrites manufactured by one or other of these methods (Gorter, 1954).

The mixed oxide method of preparation is the more convenient as it involves a single mixing process. Oxides of the metals to appear in the final spinel sample were taken in appropriate proportions and mixed thoroughly in a mechanical mixer, this mixing to continue for a long time. The mixed powders were then compressed into pellets

in a metallurgical press and sintered in an oxygen atmosphere at a high temperature for about 24 hours. They were then allowed to cool to room temperature, this taking about 30 hours.

X-ray powder photographs of these specimens were then taken and it was found that they were mainly spinels but also present was a certain amount of the oxide phases. It was attempted to remove these oxide phases by sintering at higher temperatures but the oxide phase was always present to some extent.

The mixed nitrate method involved weighing the nitrates of the metals to appear in the final specimens in the appropriate proportions. These were then dissolved in the least volume of distilled water necessary. The solution was evaporated to dryness, slowly to stop the loss of material carried off by too fast an evaporation. This left a mixture of metal nitrates. This mixture was then prefired at 600°C until all the nitrogen oxides had been driven off, leaving a residue of mixed metal oxides. After crushing this residue to powder form, it was compressed into pellets and sintered as described above at a high temperature in an oxygen atmosphere.

Powder photographs of these specimens were taken and it was found that in every case, the only phase present was spinel.

From the consideration of the presence of the oxide phase in the final specimen, it seems as though the main problem is in the thoroughness of the mixing process. It seems desirable to mix the constituents on a sufficiently fine scale to ensure that in the final pellet to be sintered, the occurrence of regions rich in a particular metal was avoided. The mixed oxide method, although the more convenient, was subject to this problem and the thoroughness of the mixing was limited by the size of the oxide particles. In the case of the nitrate method, mixing of solutions of these salts of the constituent metals meant that the ions were mixed on an atomic scale, this is probably the reason for the presence of the spinel phase only in the final product.

However a further problem occurs in weighing the appropriate amounts of raw material. The oxide method presents no trouble as compounds may be obtained in a very pure condition and it is a simple task to weigh the correct amounts to give a final specimen of the desired composition. In the case of the nitrate method, the water of crystallisation in the nitrate crystals introduces a possible source of error due to dehydration. This is most noticeable in the case of aluminium nitrate in which the water of crystallisation varies with time after its production so that the calculation of the necessary weight of this constituent may be in error..

3.2.3 Preparation of specimens.

It was decided to use the nitrate method of preparation for the specimens as the final products were shown, through X-ray powder photographs, to be spinel phase only indicating that the reaction between the constituent oxides during sintering had been complete.

The preheating stage of the oxide mixtures taken from the evaporation stage took place in a tubular furnace at 600°C for 2 - 3 hours until no more oxides of nitrogen were evolved. The resulting mixture was pressed into pellets in a hydraulic press under a pressure of 15 tons per square inch.

Pellets for all eight specimens, with values of x shown in table 3.1, were all loaded into a high temperature furnace in an oxygen atmosphere, the temperature was raised to 1550°C. The sintering process was spread over 4 days, the first period brought the furnace up to the sintering temperature, the specimens were sintered for 24 hours and then allowed to cool to room temperature over a period of 30 hours.

3.2.4 Treatment and analysis of the prepared specimens.

In the analysis of X-ray line profiles, a reference sample is required to eliminate instrumental and other unwanted contributions

to the breadths of the lines. In this study the choice of a reference is difficult in that it has to be similar to the materials under investigation and give diffraction lines close to those of these materials.

Visual inspection of the line profiles showed those of $MgCr_2O_4$ to be extremely well defined, so that it could be assumed their breadths to be due entirely to instrumental effects. Information was to be sought of the effect of introducing foreign atoms into Spinel and $MgCr_2O_4$ being similar in composition to Spinel and giving diffraction lines near to those under investigation seemed an ideal reference sample, this being coupled with the experimental evidence of its normality and high degree of structural order (Verwey et al 1947, McClure, 1957), against which results from the mixed spinels could be evaluated. An interesting feature noticed in the initial inspection of the powder photographs was the occurrence of extreme broadening of the diffraction lines in the same region as Poole's optical anomaly where $x = 0.5$ i.e. nominally 4 of the octahedral sites per unit cell being occupied by Cr^{3+} ions. It was at first thought that this broadening was due to the method of preparation but similar broadening was found to occur in all specimens where $x = 0.5$ no matter by which method they were prepared. Also from this initial inspection of the powder photographs the variation of lattice parameter was found to be approximately linear with chromium concentration which suggested the broadening to be due to some effect other particle size.

All eight specimens were sintered at the same time and in the same furnace to ensure, as near as possible, that physical conditions in all specimens, for instance particle size, strain, to be the same so that any differences which may show up could be attributed to differences in the crystallographic structure of the samples.

The actual chromium content in the final prepared specimens was determined by chemical analysis and was found to differ slightly from the expected values. Table 3.2 summarises these differences and indicates

the colours for all eight specimens.

Table 3.2 Cr^{3+} content of the sintered specimens.

Nominal x	Measured x	Δx	Specimen colour
0.0	0.0	0.0	white
0.125	0.124	0.001	pale pink
0.25	0.23	0.02	pink
0.375	0.354	0.021	deep pink
0.5	0.48	0.02	grey pink
1.0	0.984	0.016	red
1.5	1.442	0.008	red-green
2.0	2.0	0.0	green

The differences indicated in table 3.2 from the expected values of x may be due to the volatility of Cr_2O_3 at high temperatures.

After sintering, the specimens were carefully ground with pestle and mortar and sieved through 300 mesh, to ensure an upper limit of particle size in each of the diffractometer specimens which was the same for each. The sieved samples were formed into the usual flat diffractometer specimens using the aluminium formers provided for the purpose, taking care that the surfaces of each were level with the top of the former to minimise aberrations due to specimen unevenness which causes distortion of the diffraction lines at low angles (Klug and Alexander, 1954).

3.3 Collection of X-ray intensity data.

3.3.1 The X-ray equipment.

The apparatus used to obtain the X-ray intensity measurements was a Philips PW105 diffractometer, plate 3.1, used in conjunction with a Philips 1010 X-ray generator. The radiation chosen for the analysis

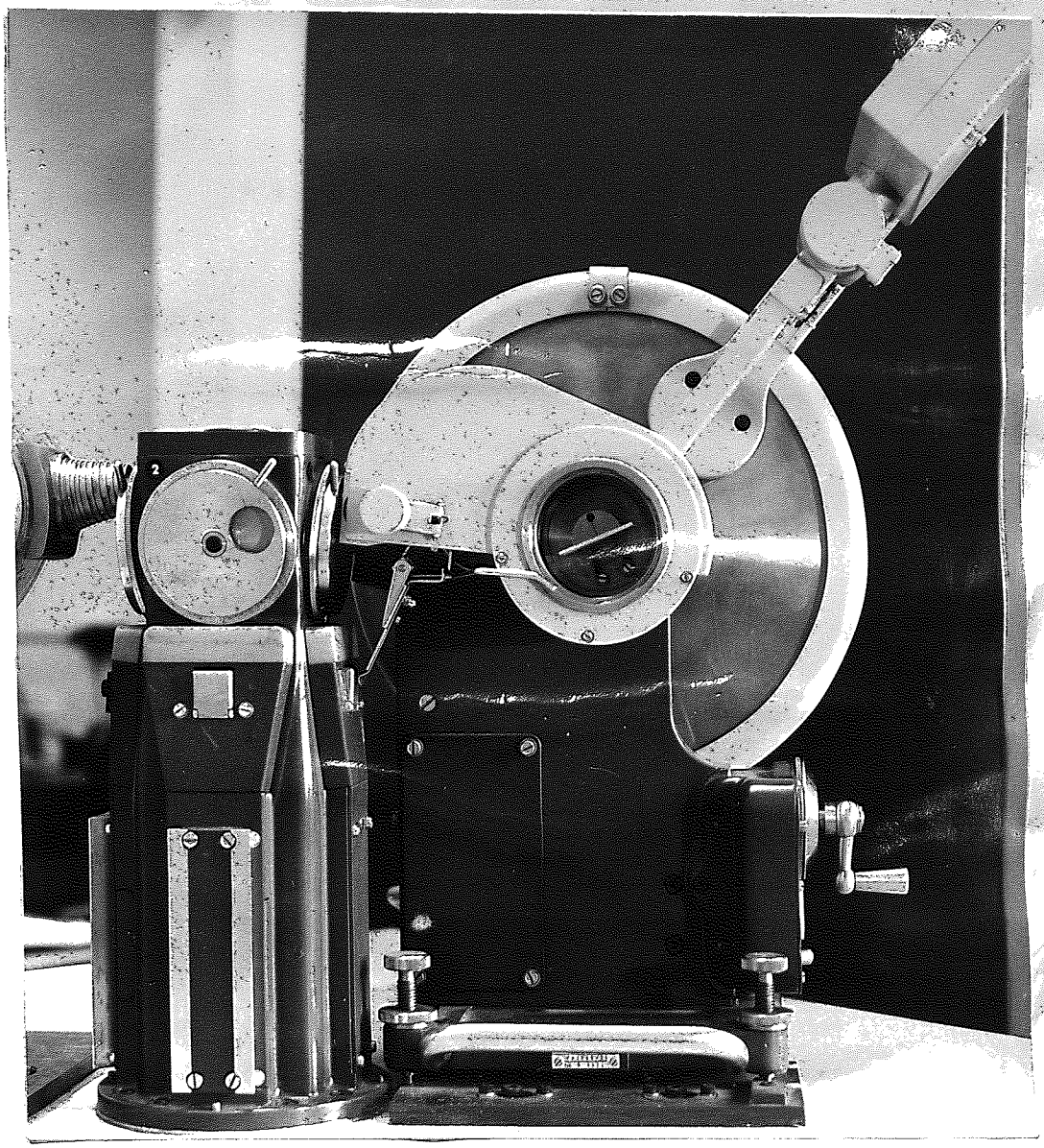

plate 3.1A Philips powder diffractometer (PW1050)

was CrK_{α} radiation which gave 12 well spaced diffraction lines common to each sample at angles ranging from $28^{\circ}2\theta$ to $140^{\circ}2\theta$. Radiation of shorter wavelength, e.g. CuK_{α}, gave more lines but in samples with chromium present fluorescence occurred and in those specimens with high chromium concentration, this fluorescence caused the background to swamp the diffraction lines, thus a comparison could not be carried out across the whole 'spectrum' of samples.

The facilities also available to use in conjunction with the diffractometer were:

(i) automatic step scanning capabilities which allowed the collection of data across the line profiles to be performed

(ii) standard counting equipment including pulse height analyser

(iii) a printer and 8 hole punch tape output to register measured intensity values.

The methods of accumulation of data available with this diffractometer were:

(i) at any angle setting 2θ, counts could be collected for a predetermined fixed time; this number of counts was punched on paper tape together with the angular setting. The goniometer stepped on automatically by a predetermined angle, and the counting procedure repeated at the new setting. In this instrument, step lengths available were $0.01^{\circ}2\theta$, $0.02^{\circ}2\theta$ or $0.05^{\circ}2\theta$.

(ii) at any angle 2θ, the time taken to accumulate a fixed number of counts is printed out as before and the goniometer stepped on by the preset angle and the process repeated.

The choice of step length depends to some extent on the width of the entrance slit and exit slit of counter and source (Langford, 1968),

these together with other experimental details for the experimental set up are given in table 3.3. The most suitable step length for the experimental conditions of those available was found to be $0.02^{\circ}2\theta$.

Using a silicon standard specimen, the diffractometer setting was calibrated. The standard silicon diffractometer peaks occur at precisely known values of 2θ; these were compared to the angles measured on the diffractometer goniometer over the whole range of interest in this study, this showed the diffractometer reading to be $0.02^{\circ}2\theta$ too high.

3.3.2 Intensity statistics.

In X-ray diffractometry, the accuracy of the intensity measured using a counter is subject to statistical errors. The error in the number of counts representing an intensity measurement can be expressed in terms of the standard deviation of error, which in the case of an intensity count of N counts is $\sqrt{N}$ and the probable error is $0.67\sqrt{N}$ (Arndt, 1955) . In the case where the time to accumulate a given number of counts is recorded, it can be seen that at each point across a profile, the error in the intensity recorded, i.e. line and background, will be a constant, the error in the time depending on the timer accuracy. In the case where the number of counts is recorded for a fixed time, the error in the intensity measurement will vary from point to point across the profile as the number of counts recorded varies from point to point. For a smaller number of counts accumulated, i.e. in the tails of the profiles, the percentage error will be larger than for intensities measured at the peak. For the purposes of this study it was decided to perform fixed count timing to give a constant accuracy across the profiles although Wilson (1967) has since analysed the effect of errors in intensity readings on various parameters of the line profile and he has suggested that the choice, whether to perform fixed count timing or fixed time counting, depends on the parameter of the line that is required.

Table 3.3 Experimental conditions of the diffractometer system (see Wilson (1963a) for a fuller description of terms).

Radiation	CrK_α -vanadium filter.
X-ray tube supply	30KV, 30mA.
Angle of take off	6°
Divergence slit	1°
X-ray source size	1.6mm x 12mm.
Sample size	2cm x 1cm x 0.2cm.
Aperture of Soller slits	2.25° .
Receiving slit	0.1mm.
Source to sample distance	17.3cm.
Anti-scatter slits	1°
X-ray counter	Xenon proportional counter.
Displacement of receiving slit from focussing circle	$<$ 1mm.
Inclination of specimen plane to goniometer axis	Unknown, but small .
Angular mis-setting of 2:1 ratio	Unknown, but small.
Displacement of goniometer outside focussing circle	0.025mm.
Angular mis-setting of receiving slit	Unknown, but small.
Angular mis-setting of centroid of X-ray beam	Small.

3.3.3 Collection of the intensity data.

The diffractometer specimens, described in section 3.2.4. were placed in turn in the diffractometer. At each profile, after the peak position had been found, the diffractometer goniometer was set about $1^{o}2\theta$ from the peak in the background region on the low angle side and allowed to step - scan through the peak to well into the background region on the far side of the peak. The results i.e. the angle in degrees 2θ, and the time taken to count 2000, or 4000 counts, depending on the sample under investigation, were printed out on paper tape. These times were converted, by means of a simple computer program to counts per ten seconds and these results could be plotted against 2θ to give the line profiles from which the various parameters were calculated. Figure 3.2 a to 3.2 k are typical profiles obtained in the mixed spinel, $x = 0.5$, compared to the reference sample profiles from $MgCr_2O_4$; broadening occurs in the other specimens to various but lesser extents. The number of profiles observed in this way and analysed, including those from the quenched samples, amounted to over 130.

It was found convenient to time for 4000 counts in the case of $MgCr_2O_4$ - which was used as the reference sample, but for the other specimens it was found more reasonable to time for 2000 counts as in the tails of the profiles from these samples, the intensity was such that the time for 4000 counts was too long for convenience.

3.3.4 Treatment of the intensity data.

From the intensity readings collected as described above, it was necessary to calculate the first and second moments, as functions of the range of calculation, for each of the diffraction line profiles. This involves an enormous amount of calculation. To facilitate the calculation a computer program was developed for the purpose. The calculation performed by the program follows closely the expression derived for the variance by Langford and Wilson (1963).

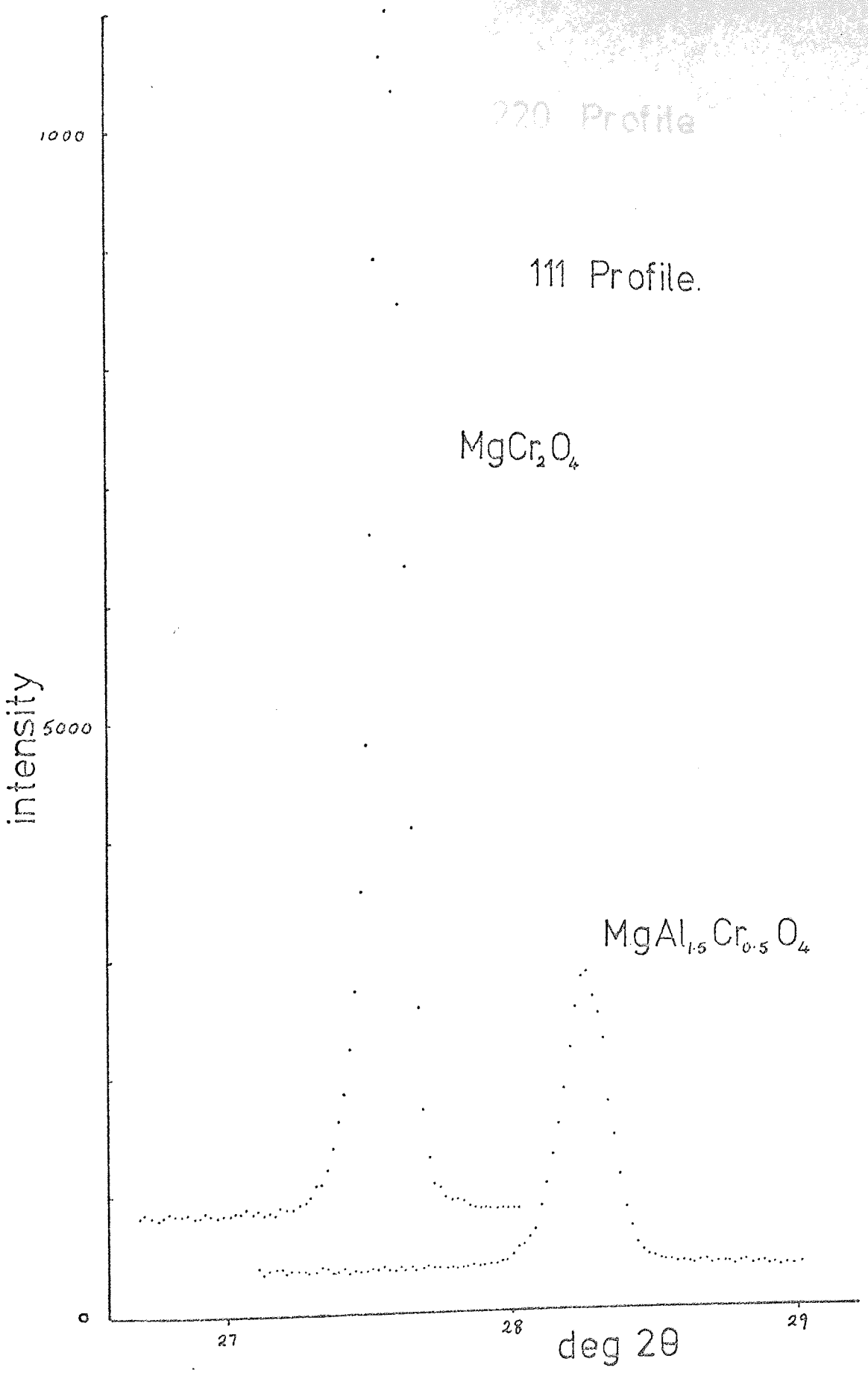

fig.3.2.a. Typical examples of observed profiles.

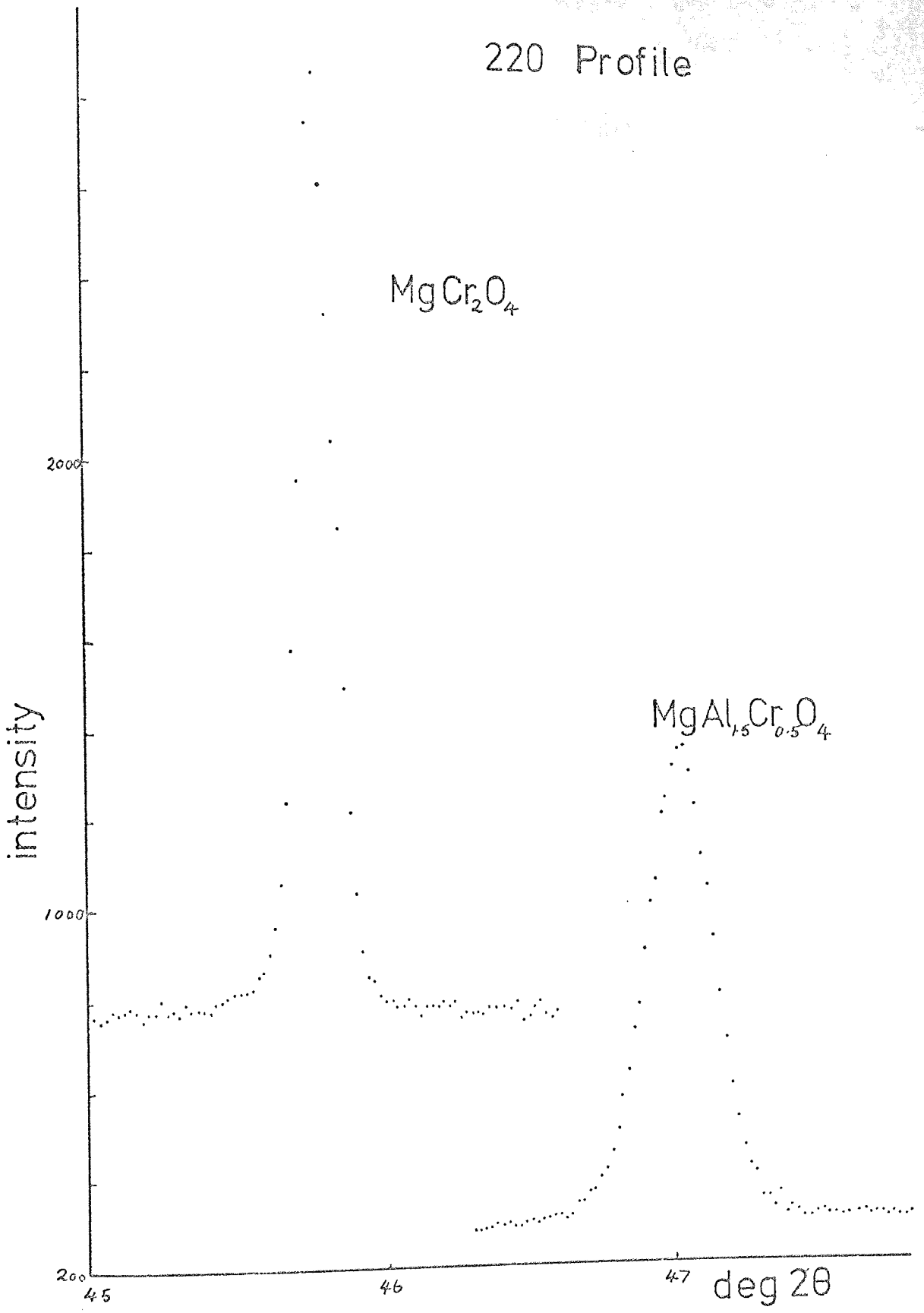

fig.3.2.b. Typical profiles.

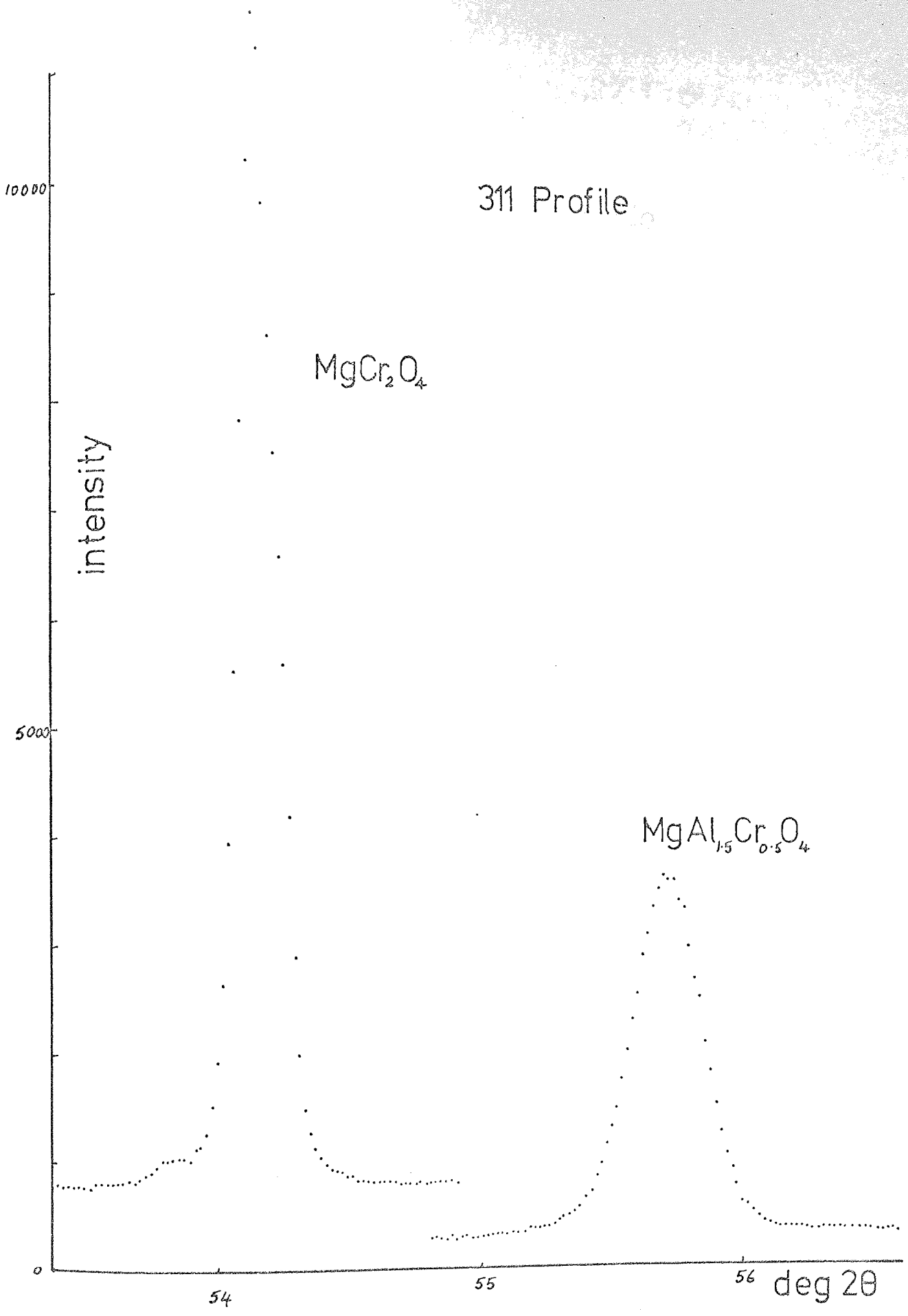

fig.3.2.c. Typical profiles.

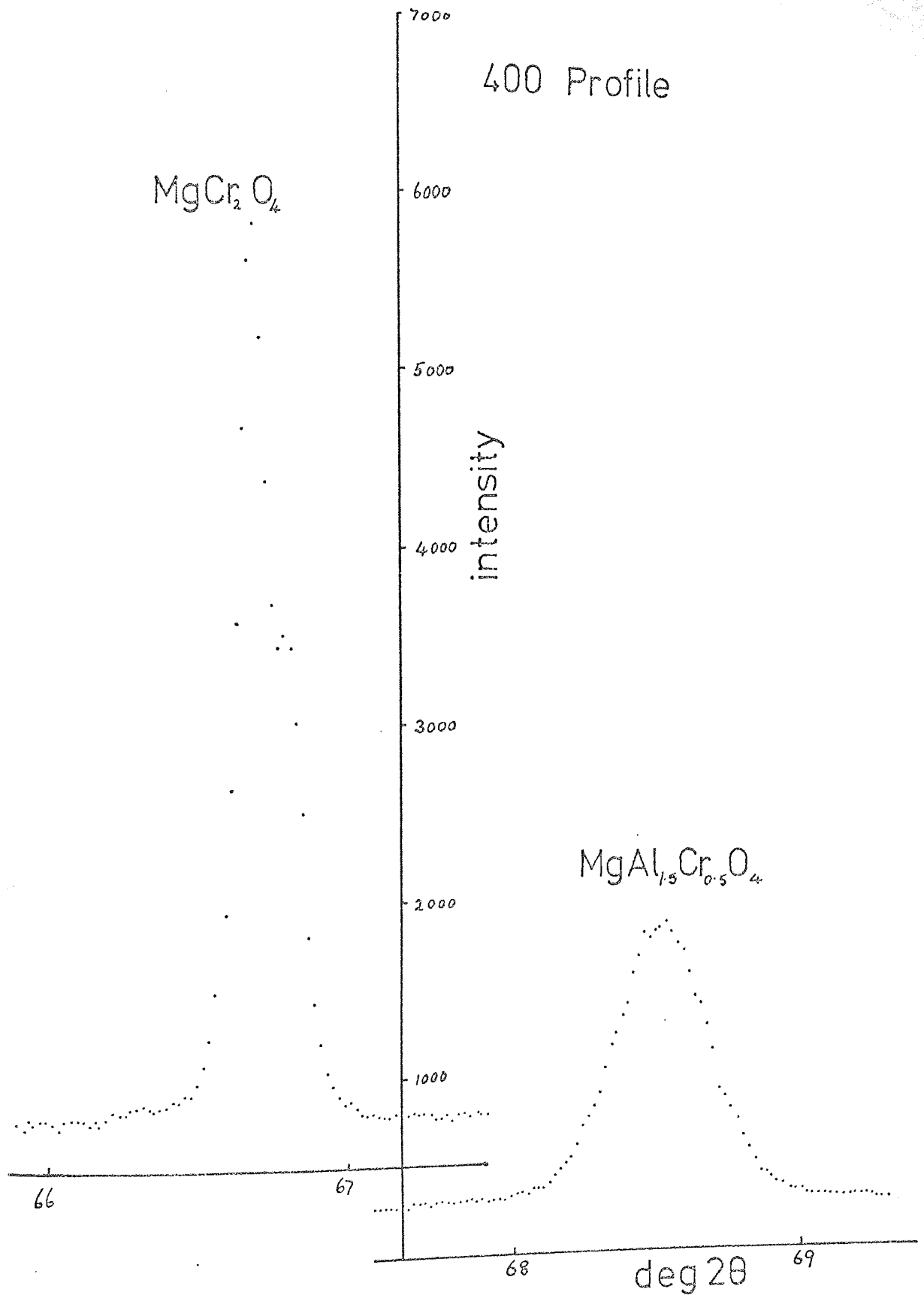

fig. 3.2.d. Typical profiles.

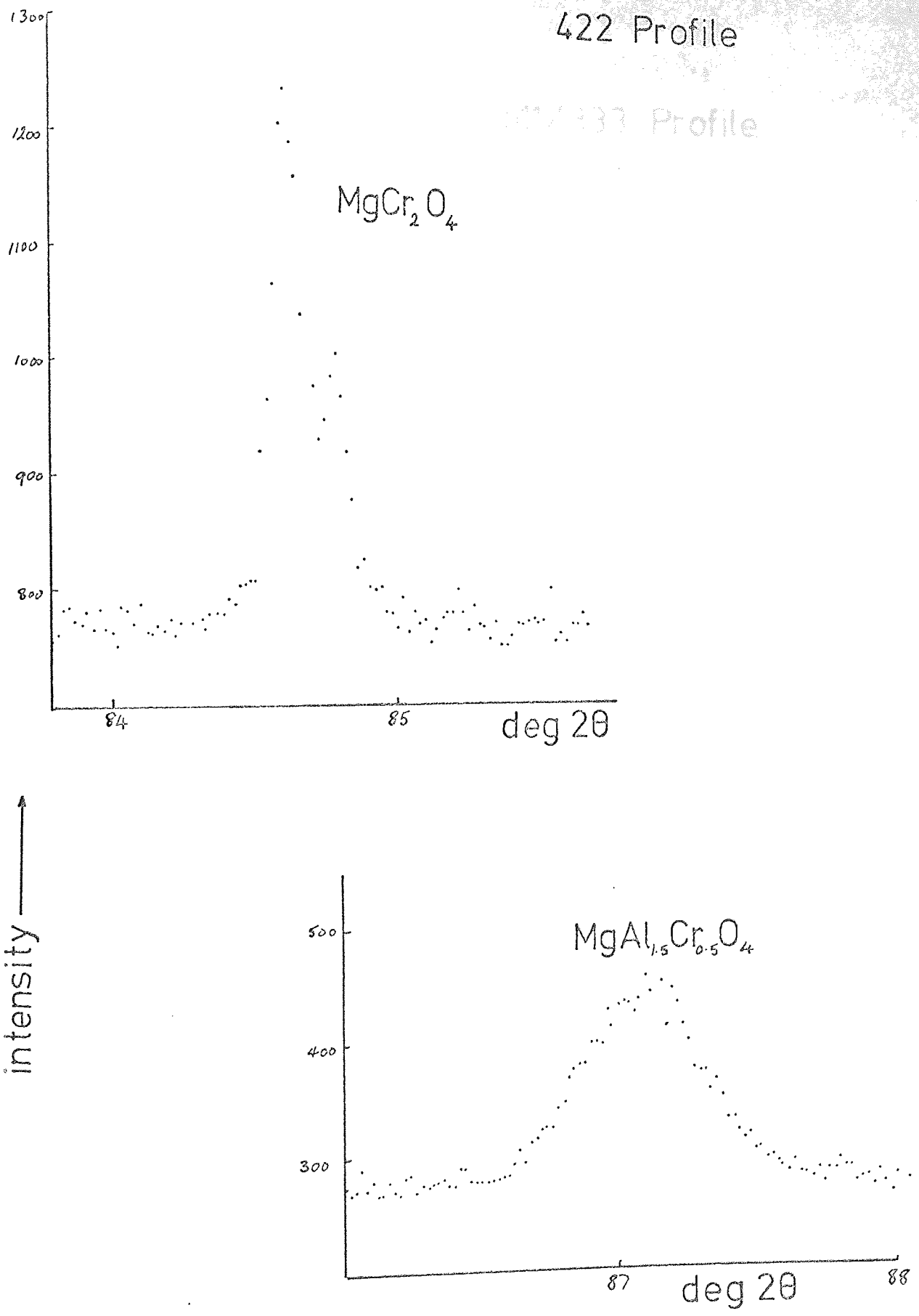

fig.3.2.e. Typical profiles.

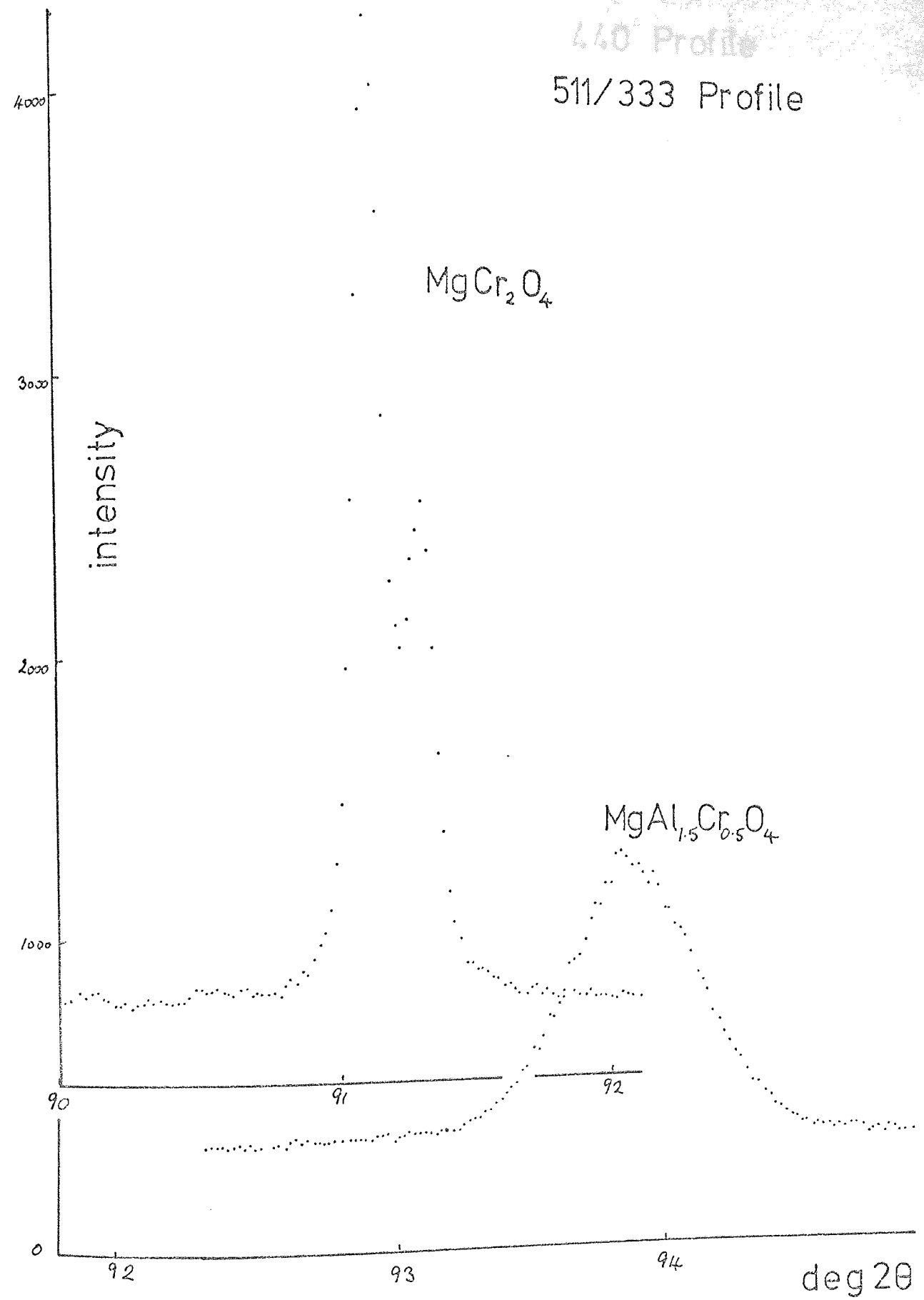

fig.3.2.f. Typical profiles.

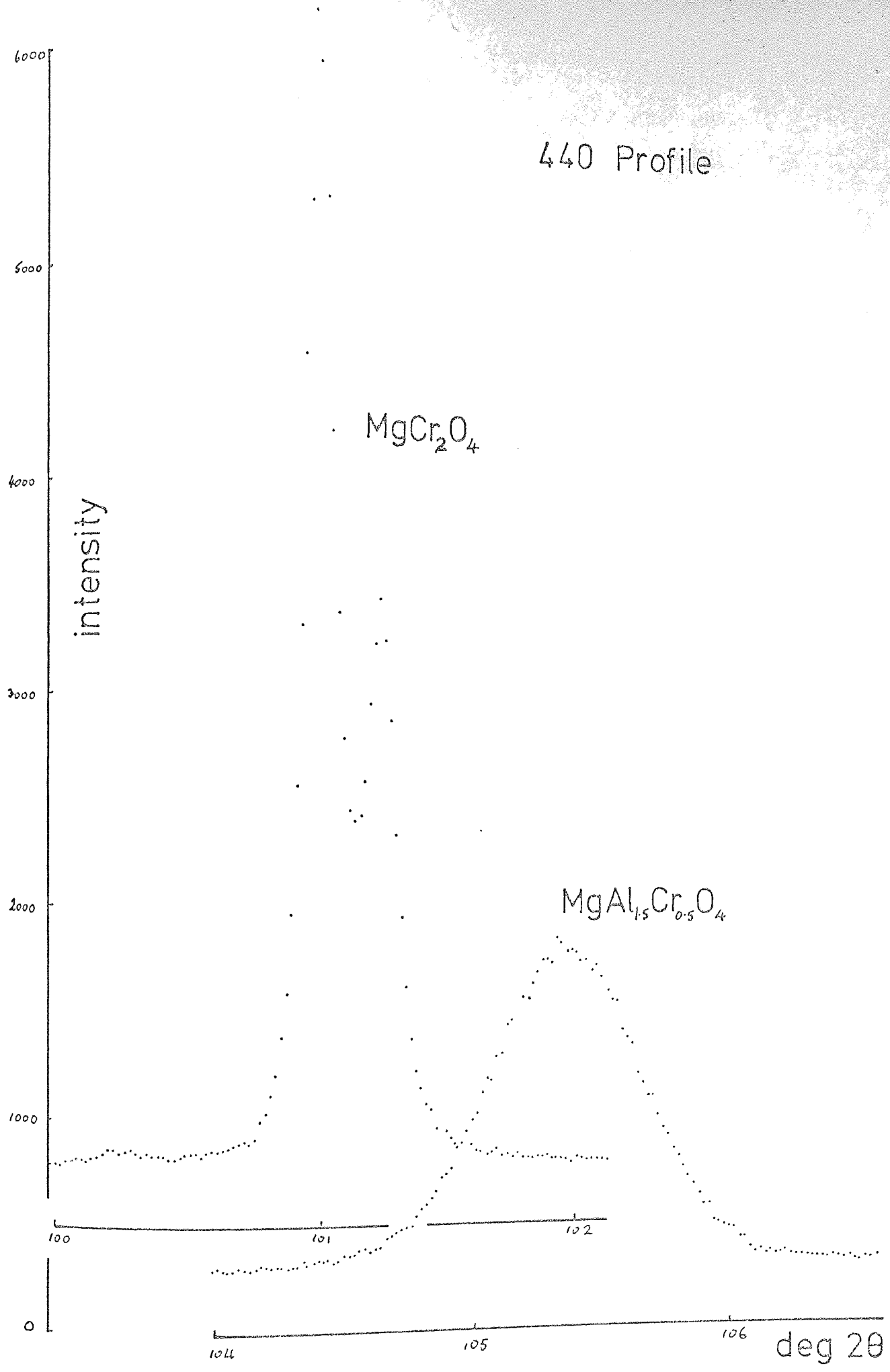

fig. 3.2.g. Typical profiles.

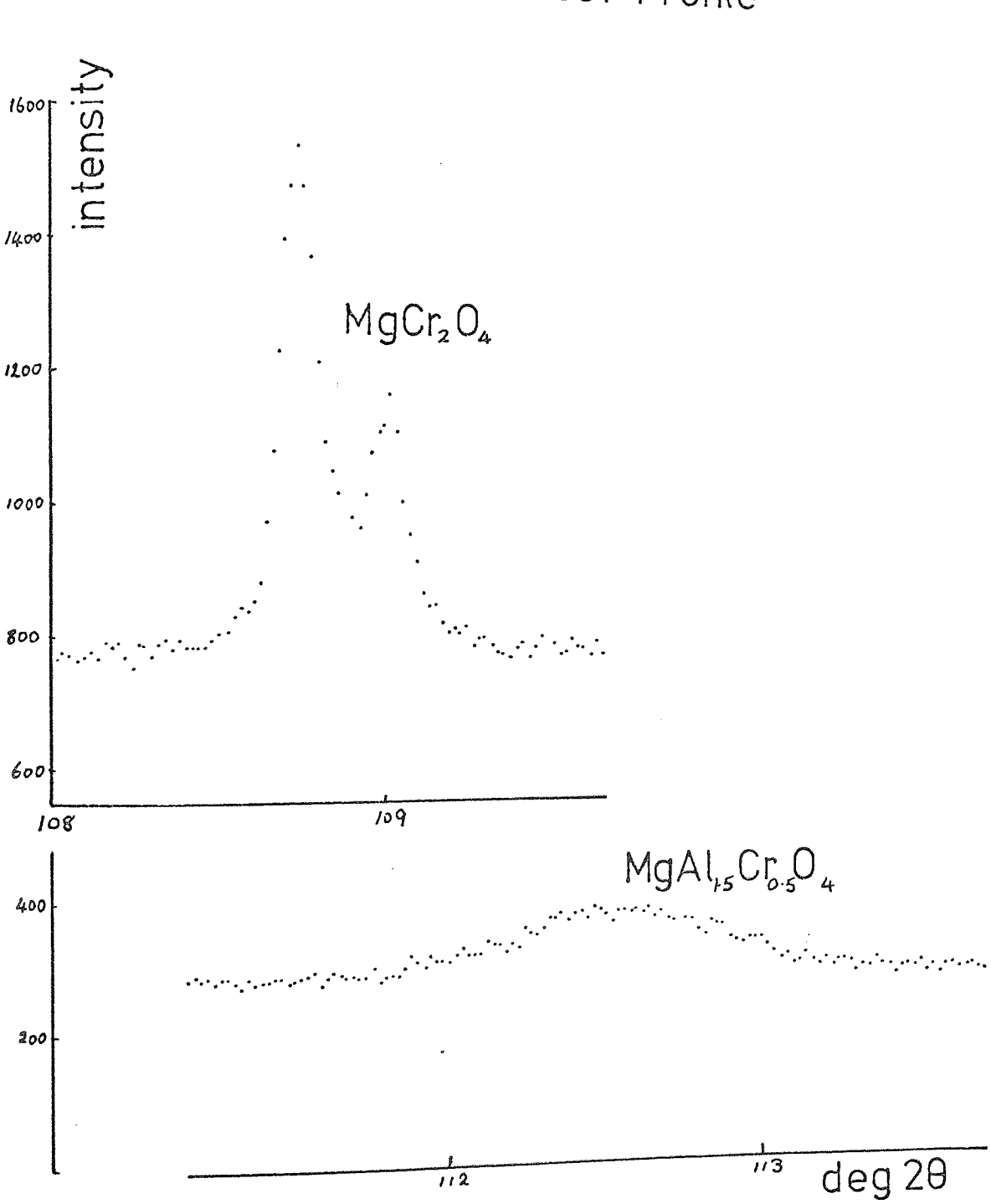

fig.3.2.h. Typical profiles.

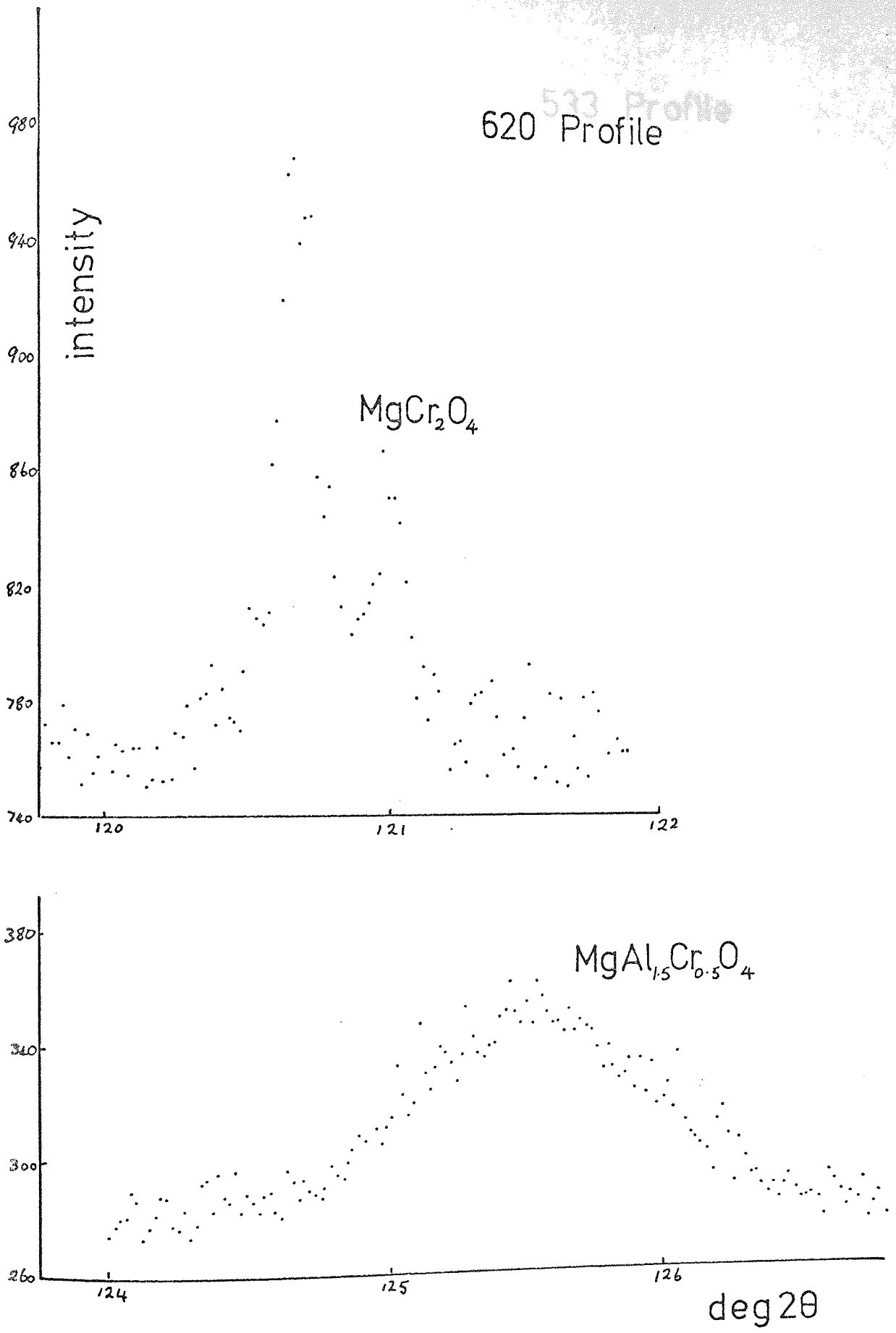

fig.3.2.i. Typical profiles.

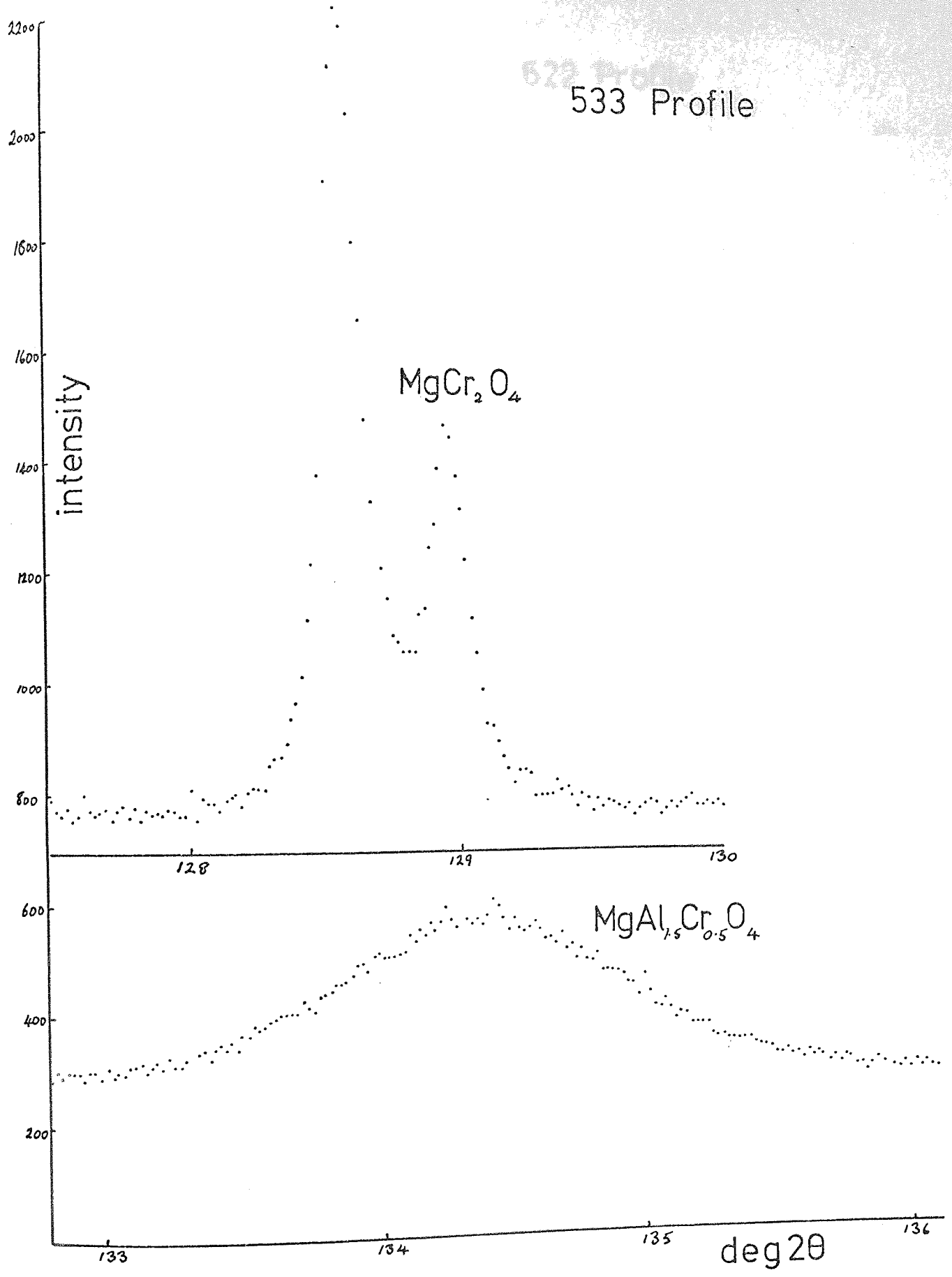

fig.3.2.j. Typical profiles.

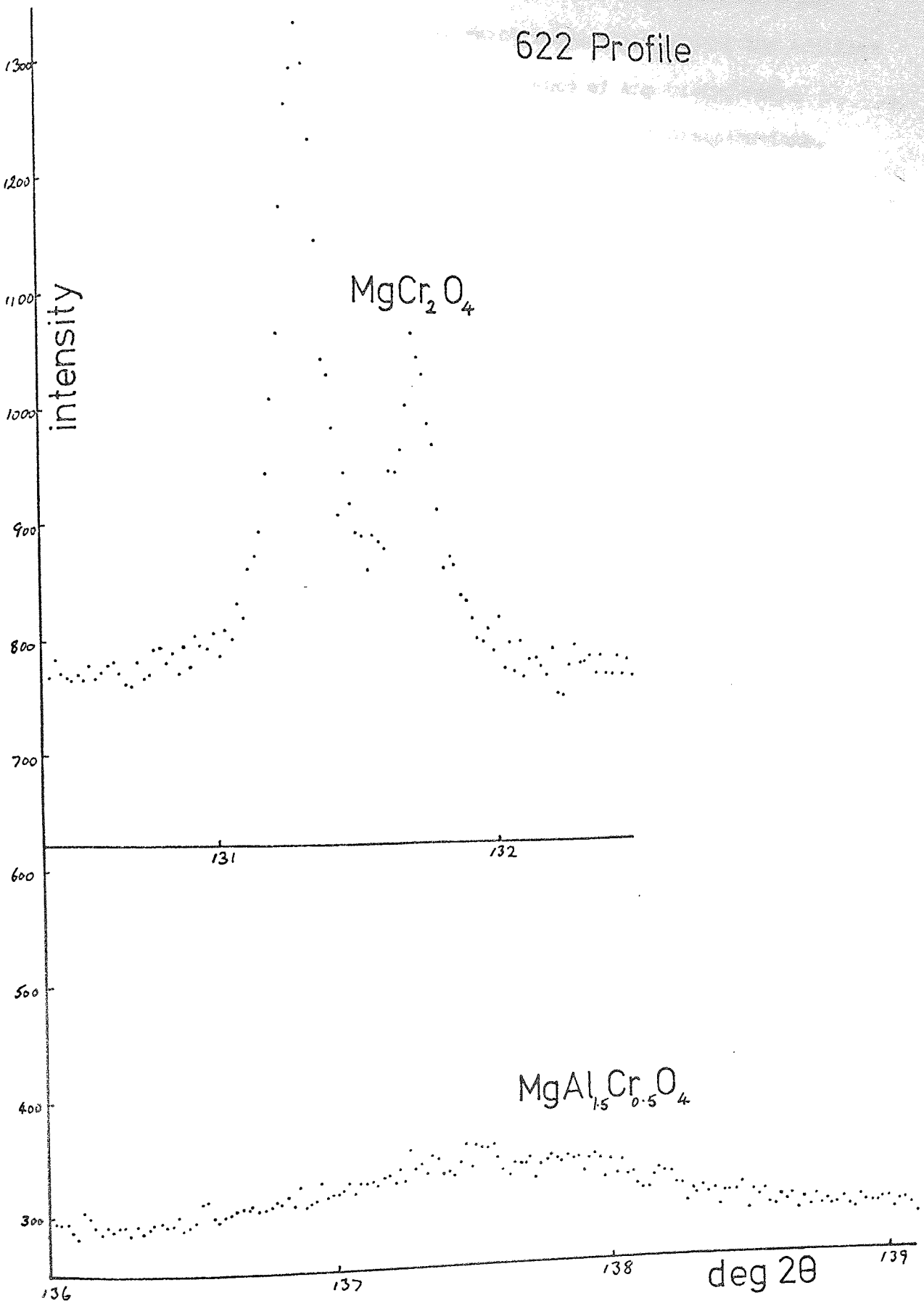

fig.3.2.k. Typical profiles.

The program evaluates the expression of the variance of the line profile given by Langford and Wilson, which takes into account the additive property of the variance, i.e. that the variance of any distribution is equal to the sum of the variances of the constituent distributions, in this case

$$W_{profile} = W_{(profile + background)} + W_{(background)} .$$

For each variance evaluated, the centroid of the profile over the same range is calculated using the expression given by Pike and Wilson (1959) equation 27, which is itself incorporated in the variance calculation.

The data were collected and fed into the computer as counts per ten seconds. The usual assumption that the background varied linearly across the profile was taken (see figure 3.3). From the intensity data the average background intensity was calculated as half the sum of the intensities at A and B where A and B were the extreme values of the profile data. To eliminate, to a certain extent the effect of statistical fluctuations in intensity values in the tails of the profile, the levels A and B were estimated by the following procedure. The first few recorded intensities were replaced by their average value, which meant that these first few punched intensities were identical. The mean value of the last 5 to 10 readings was calculated and punched onto the tape as the final reading B (figure 3.3). This involved a minor amount of editing of the data tape originally obtained as described in 3.2.4.

Using the data fed to it, the program calculated the centroid, total intensity for the line profile and background, and mean background from the values represented by A and B and printed them. The angular distance from the data at B to the calculated centroid was determined (EC = δ), and an equal distance from and beyond C gives A′, the data to the left of A′ being discarded.

The variance and centroid of the line, excluding the background was calculated (after Langford and Wilson) over the range A′B. These

were printed out together with the range DE. The range was subsequently decreased by Δ 2θ at each end to D$'$E$'$ and the calculation repeated, this whole process was repeated until the range of calculation had been reduced to zero. The background was then reduced by some preset value to FG and the variances and centroids calculated as before. The program produced variance and centroid range characteristics for 6 values of background. These background levels could be chosen to include the required linear variance range characteristic. The program has since been described fully by Hilleard and Webster (1969).

Figure 2.1 indicates the effect of background on the variance range characteristic. With too high an assumed background the characteristic curves downwards, when the background is too low the characteristic curves upwards, the reason for this having been discussed in 2.2.4. The linear portion was selected over a range which corresponded to the tails of the profile i.e. in the region where the intensity decreased inversely as the square of the distance along the axis.

3.3.5 Corrections to the variance calculations.

The emission spectrum from an X-ray source contains in addition to the K_{α_1}, K_{α_2} and K_β lines some satellite lines which appear in the tail of the main profile on the low angle side. The effect of these satellite lines on the variance range characteristic has been reported by Langford (1968) and it is an effect which causes a discontinuity in the linear portion of the characteristic (see figure 3.4). The portion AB in the figure is the effect due to the K_α radiation and CD is elevated due to the presence of the satellites. However Edwards and Toman (1970) have suggested two methods of eliminating this effect. The first method is to remove the satellites, by interpolation, from the profile before the analysis. For this, the contribution to the intensity of the satellites is required and its removal by this method is not always complete and in the case of extreme broadening is very difficult to perform.

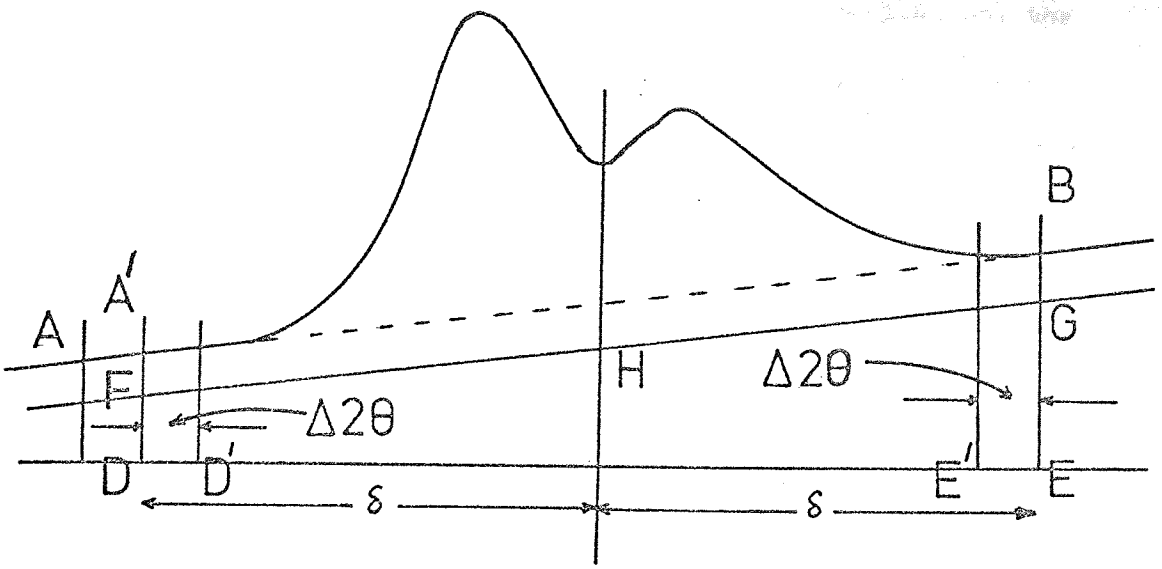

fig.3.3. The variance calculation.

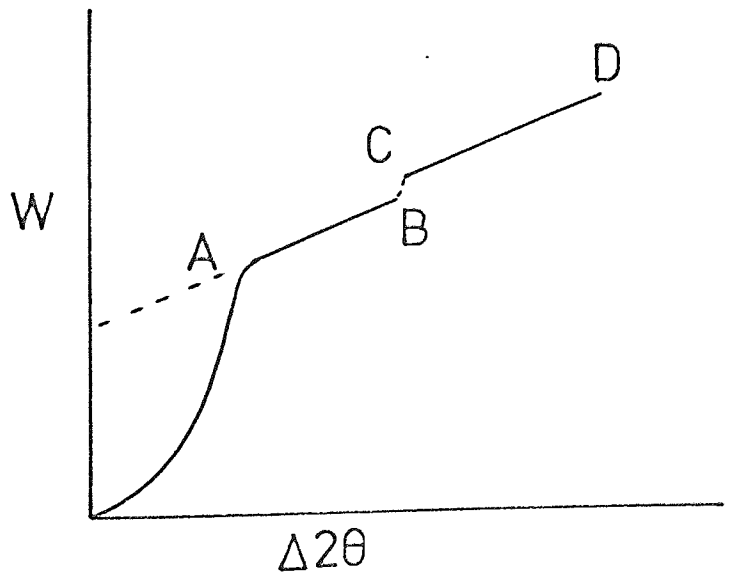

fig.3.4. Effect of satellite lines on the variance-range characteristic.

Figure 3.5 shows two simulated profiles (after Cheary, 1971): one (figure 3.5 a) shows a theoretical profile in which there is little or no broadening, in which the satellites are clearly defined and the method of removal suggested by Edwards and Toman may be useful in a profile of this type. However, figure 3.5 b shows a profile suffering extreme broadening and it can be seen that the above method would be very difficult to perform.

The second method of Edwards and Toman is to take the portion AB, figure 3.4, as the required line. However Cheary has noted the effect of truncation on the variance calculation and has devised a graphical method of correction for this truncation. He has shown that the expected slope is lower than the calculated one extracted from data taken from the truncated profile. Using simulated X-ray profiles with different degrees of broadening, a relation between the apparent slopes and intercepts, given by the dotted line in figure 3.6, and calculated slopes and intercepts (solid line AB) was found. Comparison of these simulated values with values taken from experimental curves gives a simple method of correction of the variance results.

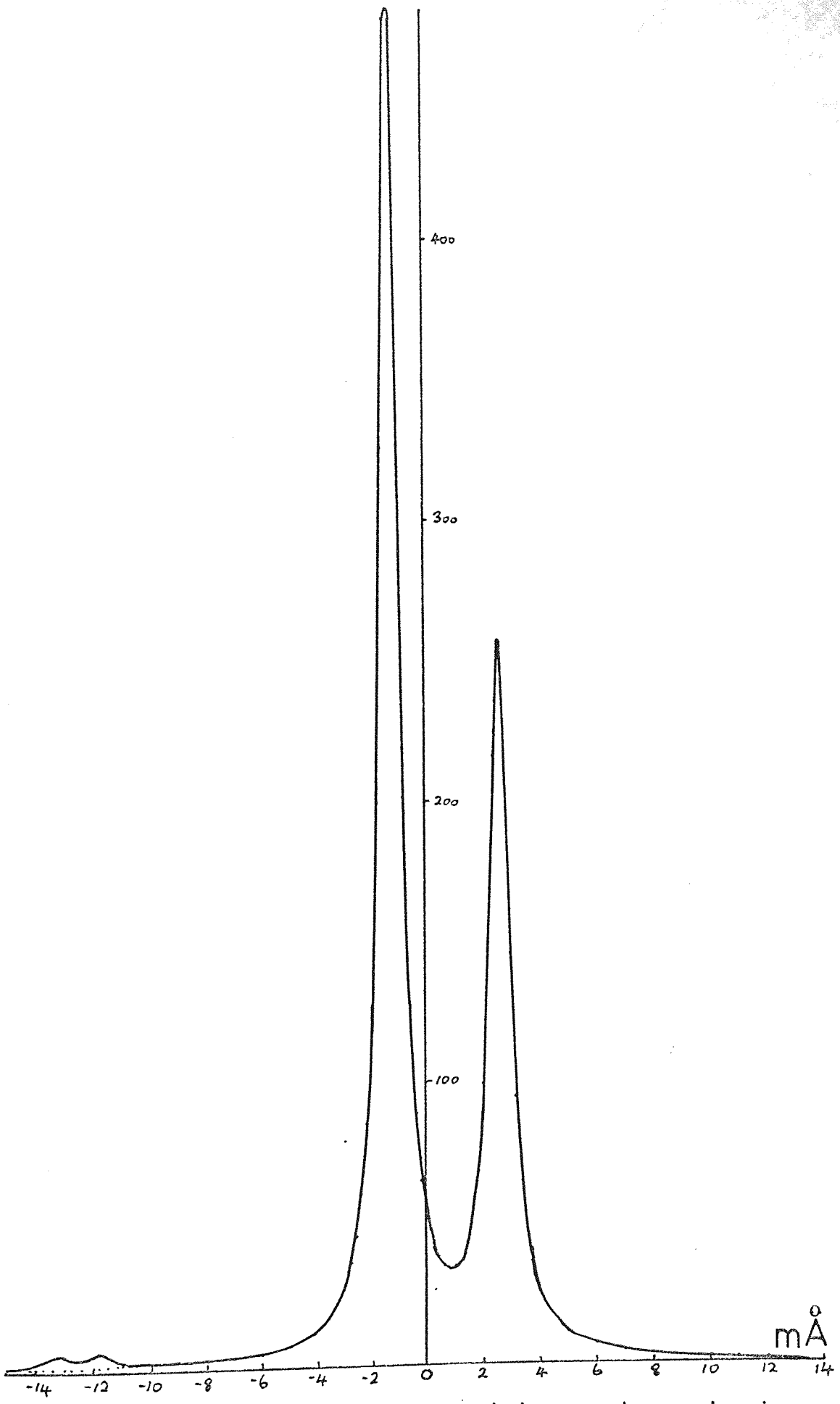

fig.3.5.a. Simulated profile-minimum broadening, satellites indicated.

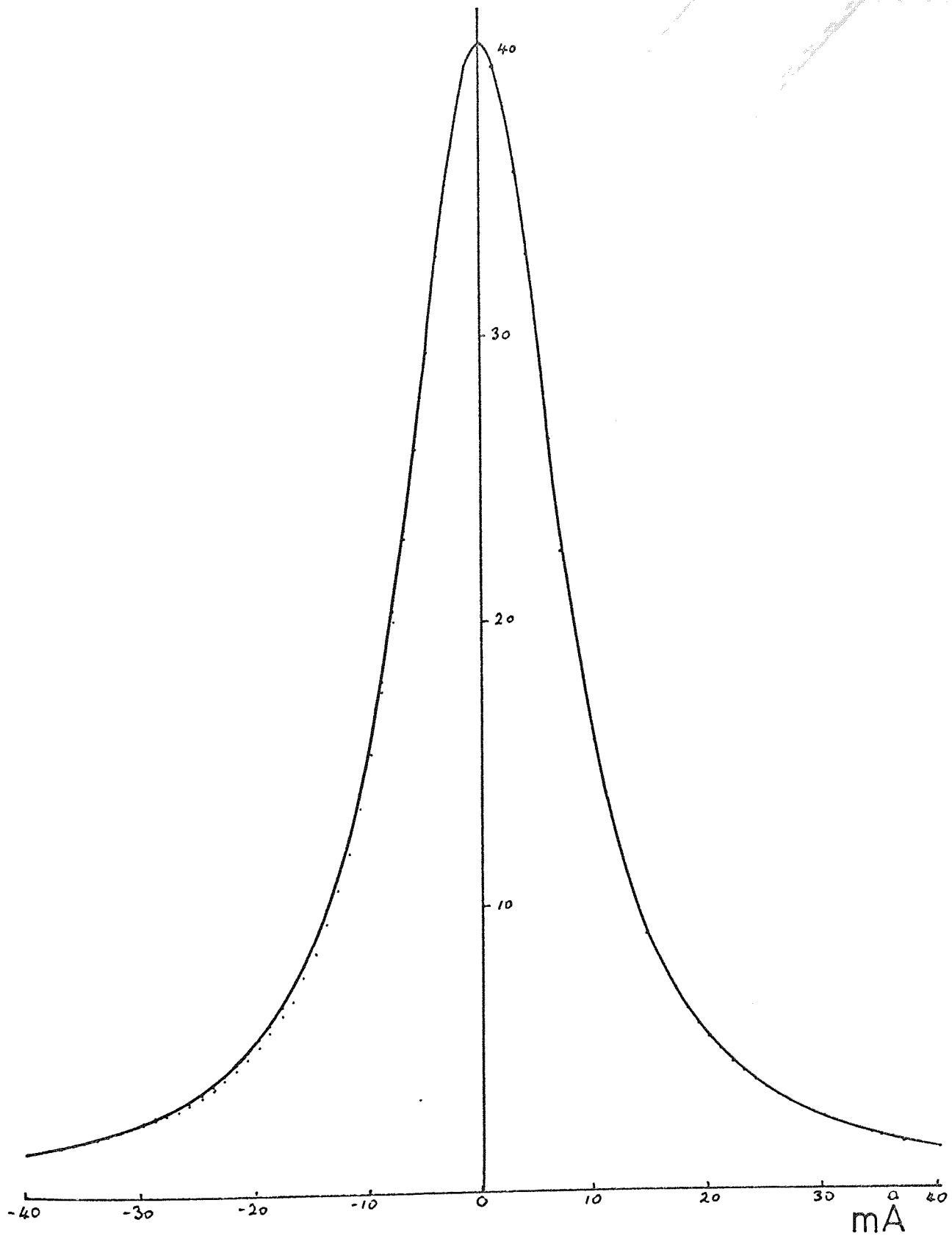

fig.3.5.b. Simulated profile-extreme broadening. (dotted line indicates the removal of satellites)

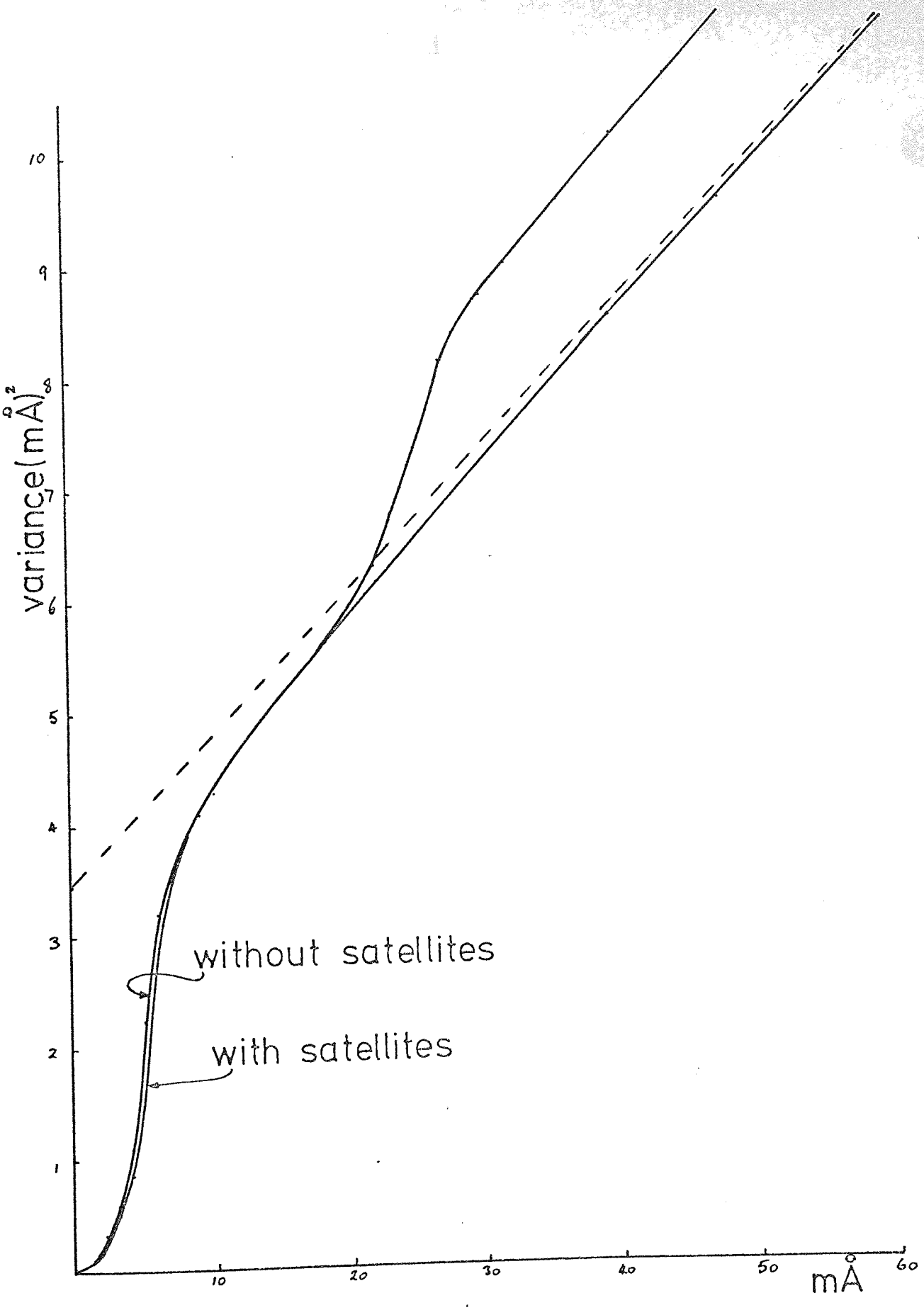

fig.3.6. Correction of the variance characteristic (after Cheary 1971)

CHAPTER 4

CRYSTAL STRUCTURE AND LATTICE SIZE

4.1 Introduction.

There have been many studies in which the variation of lattice parameter with composition of mixed oxide systems have been investigated (for instance see Villers, Lecerf and Raoult, 1965, Verwey and Heilmann, 1947, Thilo and Saur, 1955, Romeijn, 1953, Warshaw and Kieth, 1954, Nicks, 1951). Many of these studies show that the lattice parameter of mixed oxide systems bears a linear relationship to the composition, i.e. if a metal ion is replaced by a larger ion, the lattice parameter increases in proportion to the amount of substituted ion present, this is known as Vegard's Law (Vegard, 1921). Although this relationship holds for many systems, some have been reported with a deviation from this law. Thus Romeijn has reported deviations, both positive and negative, from Vegard's Law and examples are given in figure 4.1.

The system $MgAl_{2-x}Cr_xO_4$ $(0 \leqslant x \leqslant 2)$ has been studied by a number of workers with somewhat differing results for the lattice parameter-concentration variation. For instance, Warshaw and Kieth found a simple linear variation of lattice parameter with chromium concentration whereas Thilo and Saur suggest that there is a negative deviation from the law in the region $x = 0.25$. More recently, however, Lou and Ballentyne (1968), working with single crystal material, reported a positive deviation in the same region. Poole (1964), in his study of the optical properties of chromites, suggests that the lattice parameter should vary regularly with the chromium contration.

Now, it is almost certain that at least part of the cause of this controversy lies in the poor accuracy of many results. In some cases for example, lattice parameters were deduced from powder diff-raction photographs with little or no consideration for the aberrations

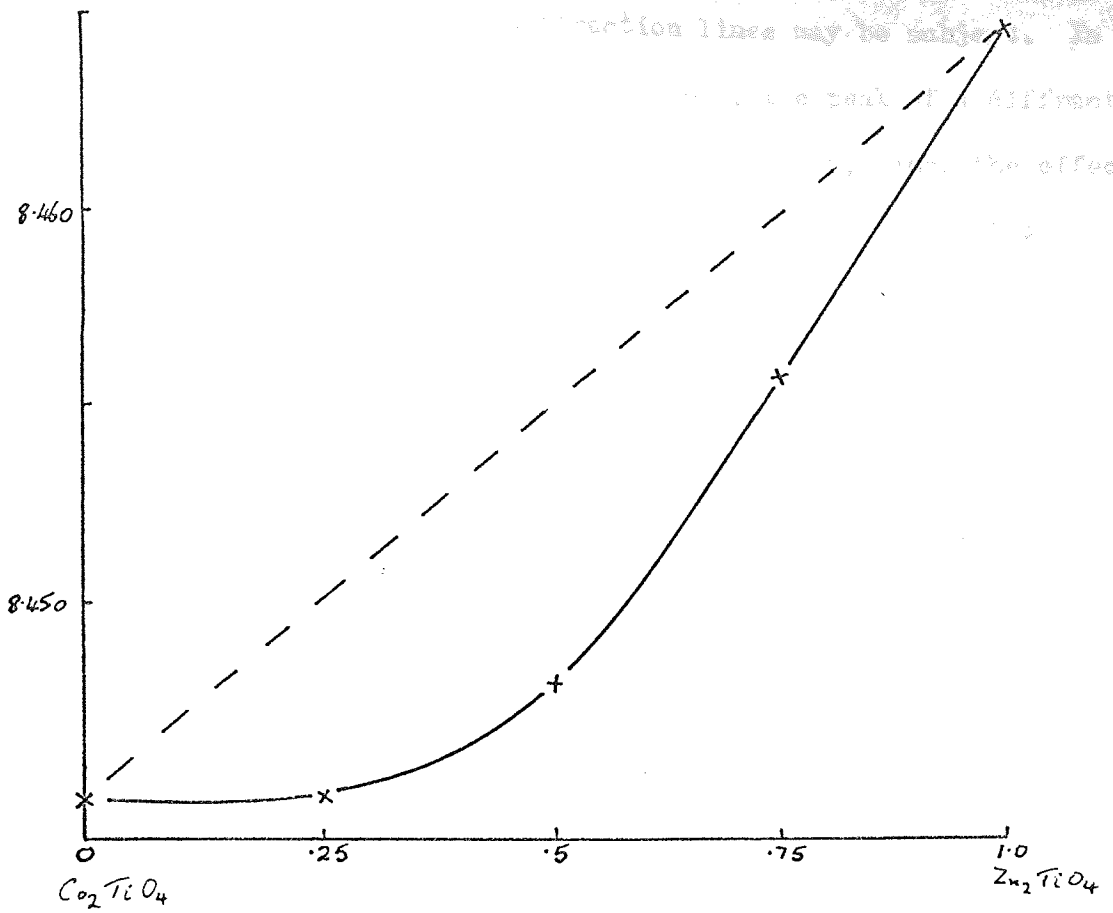

fig. 4.1.a. Negative deviation from Vegard's law.

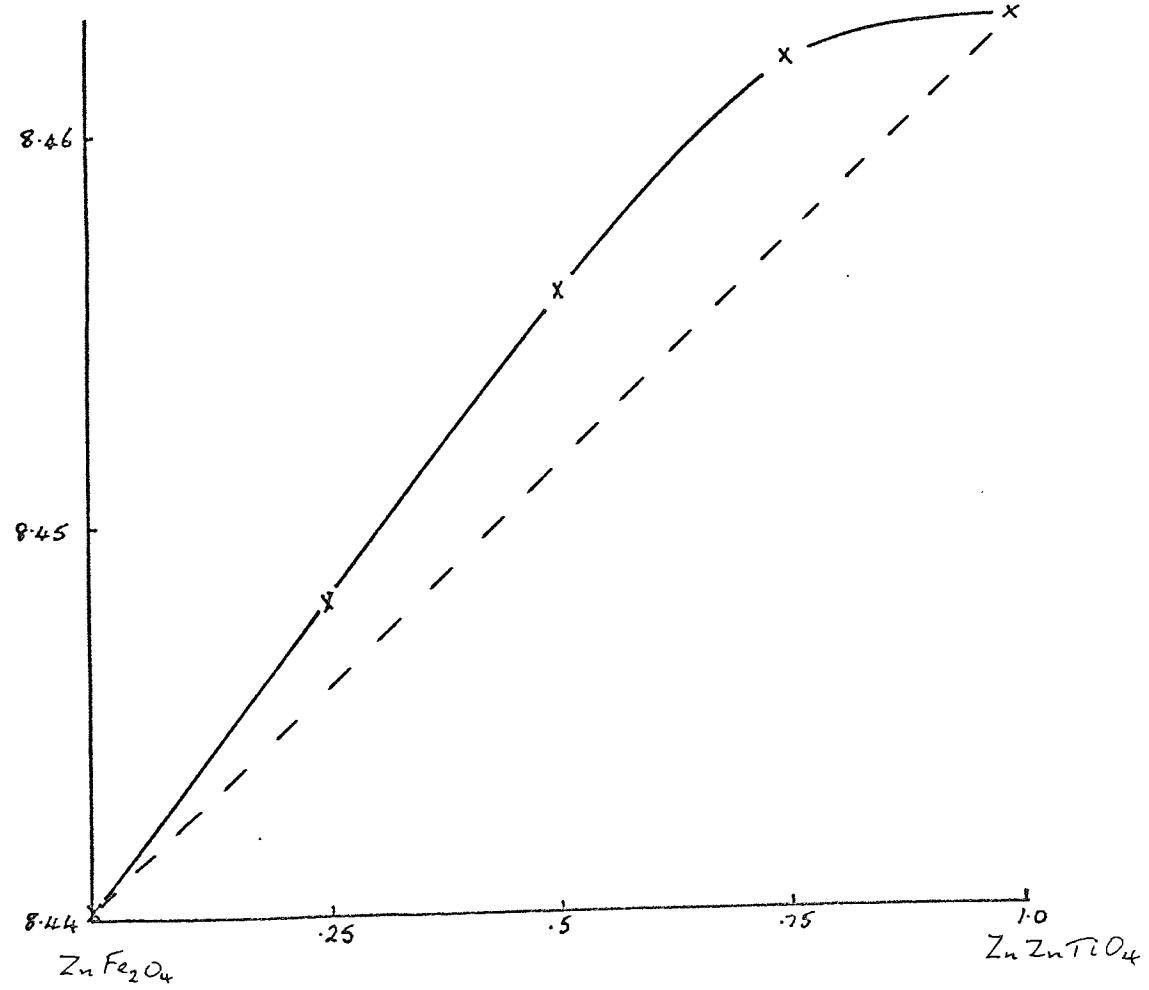

fig. 4.1.b. Positive deviation from Vegard's law.

to which the positions of the diffraction lines may be subject. In any event, as Wilson (1963a) has pointed out, the peak of a diffraction line is not a very satisfactory measure of position, since the effect of aberrations upon the peak position is difficult to correct with mathematical rigour. Wilson recommends the centroid of the line profile as a measure of position and has shown how this may be corrected for aberrations in a systematic way. The practical determination of centroids has been described by Pike and Wilson (1959) and was used in the present analysis. The centroids of the line profiles were of course required as a pre-requisite for the analysis of the line breadths by the variance technique (see Chapters 2 and 3).

Two of the materials investigated here, namely $MgAl_2O_4$ and $MgCr_2O_4$, have been the subjects of many studies with the result that the various parameters of these structures should be well established. Integrated intensity measurements were made on the specimens to confirm the similarity between these and those already reported.

Bacon (1952) and Stoll et al (1964), both using neutron diffraction techniques, have shown $MgAl_2O_4$ to be substantially normal, although the latter authors suggested it to be 10 to 15% inverse. The crystal structure of the material in both studies was referred to the space group Fd3m and the u parameter, the measure of displacement of the oxygen ion, was calculated as 0.387 ± 0.001 (Bacon) while the Debye-Waller or temperature factor was estimated to be $0.4 Å^2$ (Bacon). Fischer (1967) reports the values as $u = 0.387 \pm 0.001$ and $B = 0.56 Å^2$ and a lattice parameter $a_o = 8.0832 \pm 0.0005 Å$.

According to Verwey et al (1947), $MgCr_2O_4$ has $u = 0.385$ and $a_o = 8.312 Å$ but later work suggests that both these figures are too low. Thus the recent neutron diffraction measurements by Shaked, Hastings and Corliss (1970) gave refined parameters $u = 0.3868 \pm 0.0006$ and $a_o = 8.335 Å$, but in the present context it is interesting to note that no value was given for the Debye-Waller or temperature factor.

4.2 Lattice parameter determination.

4.2.1 Determination of line position.

It was decided to use the centroid as the measure for line position and to use the correction procedures for this measure as described by Wilson (1963a). The calculation of the centroid of a diffraction profile has been outlined by Pike and Wilson (1959) and is included in the profile variance calculation described by Langford and Wilson (1963). The computer program used in the analysis of the data in this study includes the calculation of the variation of profile centroid with range of calculation and Pike and Wilson have indicated that such a variation rises to some maximum at 3 to 5 times the $\alpha_1 - \alpha_2$ separation. Cheary and Grimes (1972) have shown the effect on the centroid-range plot of the presence of satellite lines. With satellites present, the plot drops from the maximum described by Pike and Wilson to some constant value at large range; with no satellites present, the plot reaches the maximum and continues at this value for all ranges above the critical value. Figure 4.2 illustrates this effect.

Figure 4.3 shows a typical plot, obtained experimentally for the (533) profile of $MgCr_2O_4$, of calculated centroid angle (2θ) against the range of calculation ($\Delta 2\theta$). Also indicated on the graph is the range ($\Delta 2\theta_p$) corresponding to the spread of wavelengths of the emission profile. This is calculated from the expression

$$2a_o \sin\theta = \sqrt{N}\ \lambda$$

where $N = h^2 + k^2 + l^2$

hence

$$2a_o \cos\theta\ d\theta = \sqrt{N}\ d\lambda$$

$d\lambda$ being 5 times the $\alpha_1 - \alpha_2$ separation,

θ is the estimated centroid position,

a_o is the lattice parameter.

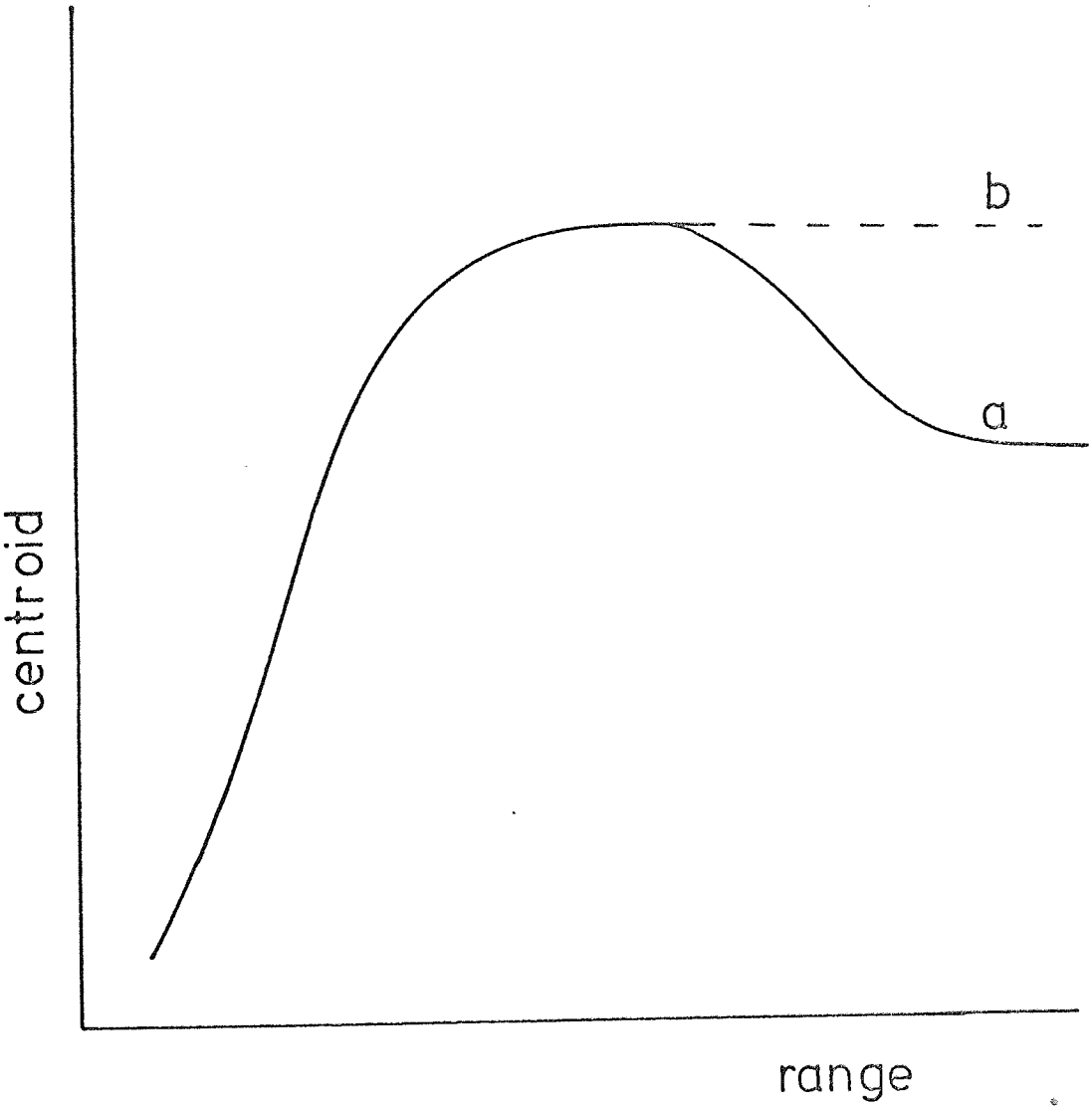

fig.4.2. Effect of satellite lines on the centroid of a diffraction line profile.

a. satellites present.

b. satellites removed.

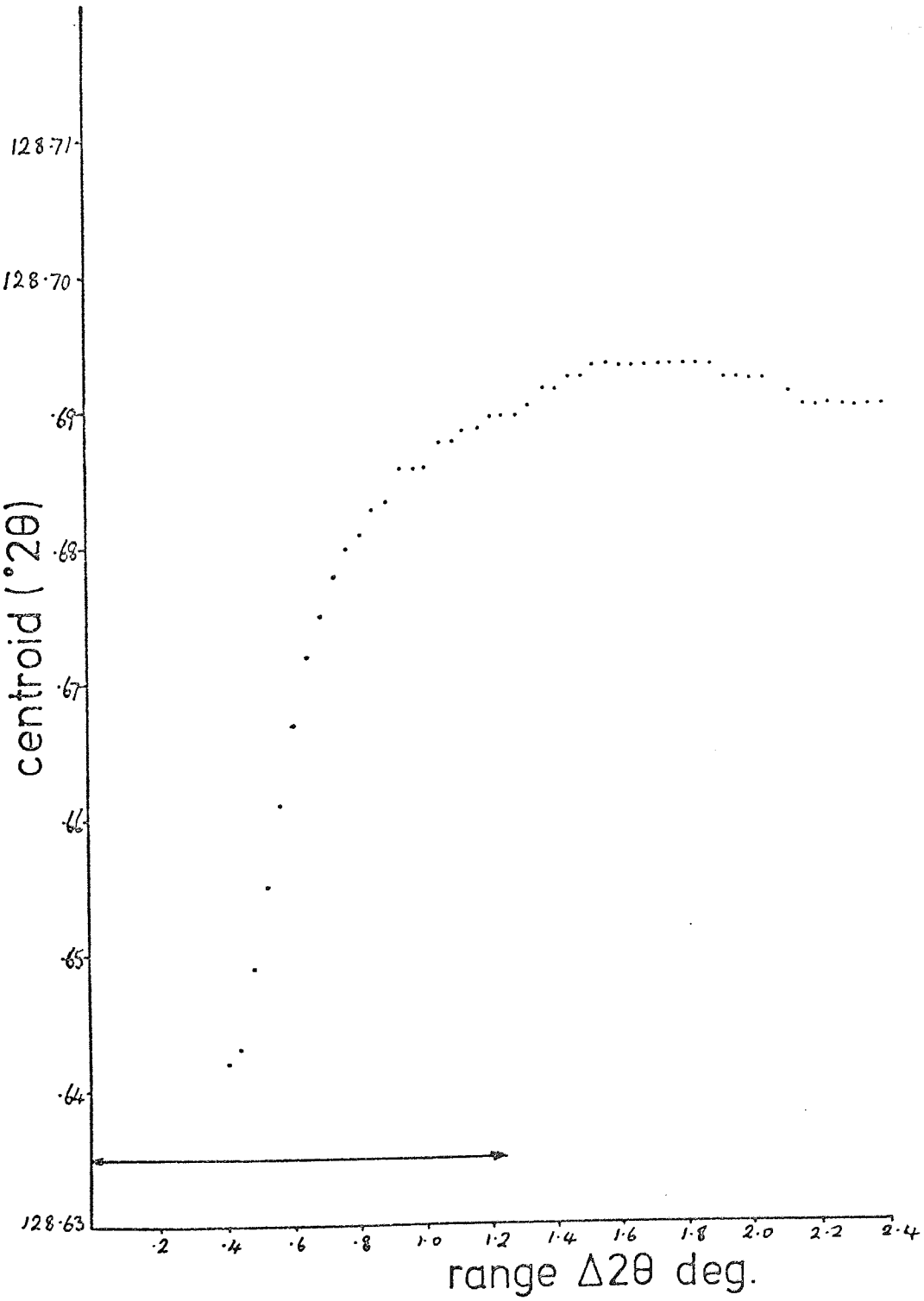

fig.4.3. Typical experimental centroid-range plot.
$MgCr_2O_4$-(533) profile.

Taking published values of lattice parameter for $MgAl_2O_4$ and $MgCr_2O_4$, the ranges $\Delta 2\theta_p$, for the twelve profiles common to each specimen at which to choose the actual centroid value, were calculated. For specimens containing mixtures of Al^{3+} and Cr^{3+} ions, interpolated values of lattice parameter, between these two extremes, were used. In every case the calculated range $\Delta 2\theta_p$ fell in the maximum on the centroid - range plot, these maxima being taken as the observed centroid positions.

Following Wilson (1963a), the experimentally determined line positions were corrected for the following aberrations:

(a) axial divergence,

(b) specimen transparency ,

(c) flat specimen error,

(d) refraction (wavelength effect),

(e) Lorentz-polarisation factor,

(f) differential wavelength absorption of the X-ray beam in its path from X-ray source to the counter,

(g) dispersion.

The correction to be applied in each case was calculated from the experimental conditions given in table 3.3 of Chapter 3. The variation of the angular dependent part of the total correction for $MgCr_2O_4$ is shown in figure 4.4. In the calculation of specimen transparency, the linear absorption coefficients of the specimens were required. Taking $MgCr_2O_4$ as an example, the linear coefficient was calculated as $290cm^{-1}$, this being the value expected for the solid material. However in this study powders were used and the coefficient must be corrected to allow for this. It was estimated that the value would be reduced to about a third of the calculated value, i.e. $100cm^{-1}$, this value being used in the transparency calculation. The coefficient for $MgAl_2O_4$ was calculated as $270cm^{-1}$ and in view of the drastic

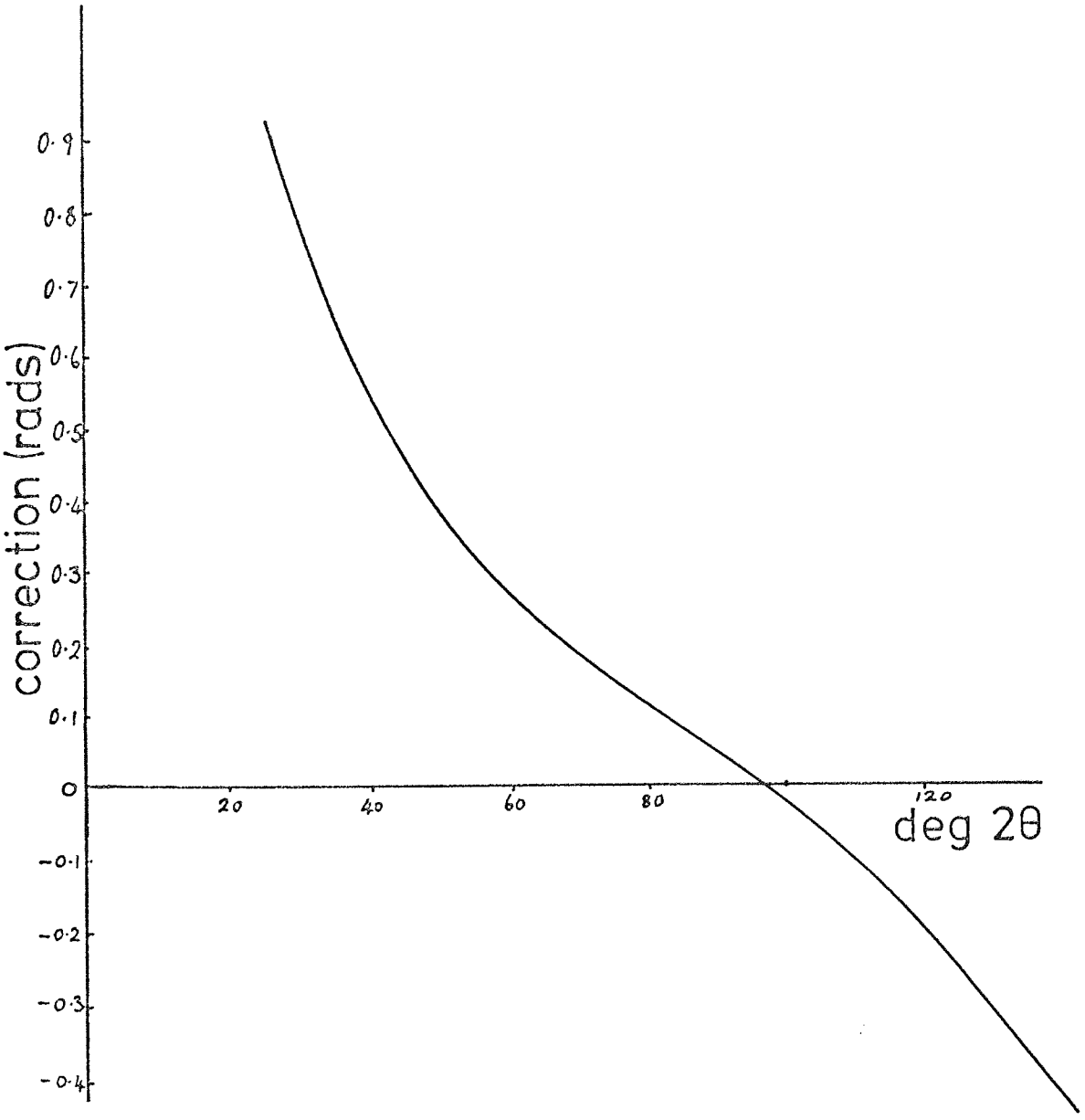

fig.4.4. Variation of centroid correction with centroid position.

reduction of this value due to the sample being a powder, it was considered that the value could be taken as a constant for all specimens thus figure 4.4 could be used as a source of correction for line shift due to aberrations listed above without too great a loss of accuracy. Table 4.1 indicates corrected centroids for all specimens of the series $MgAl_{2-x}Cr_xO_4$.

Table 4.1 Corrected centroids for all specimens, results quoted in deg2θ

x / hkl	0	0.125	0.25	0.375	0.5	1.0	1.5	2.0
111	28.476	28.427	28.332	28.325	28.296	28.033	27.870	27.609
220	47.344	47.213	47.069	47.002	47.045	46.518	46.195	45.789
311	56.156	55.931	55.838	55.732	55.726	55.136	54.742	54.265
222	58.891	58.702	58.588	-	-	-	57.395	56.892
400	69.143	68.914	68.765	68.593	68.533	67.836	67.318	66.720
422	88.011	87.685	82.502	87.251	87.073	86.204	85.501	84.670
511/333	94.926	94.568	94.348	94.061	93.875	92.905	92.073	91.169
440	106.665	106.278	105.964	105.618	105.364	104.194	103.150	102.085
531	114.035	113.564	113.234	112.829	112.567	111.225	110.061	108.840
620	127.442	126.876	126.384	125.933	125.516	123.821	122.308	120.808
533	136.771	136.070	135.475	134.836	134.358	132.340	130.479	128.683
622	140.254	139.485	138.834	138.115	137.558	135.423	133.454	131.510

4.2.2 Calculation of lattice parameters.

As the centroids of diffraction profiles were used as the measure of line position, it was also necessary to use the centroid wavelength of the emission profile of the radiation used. This was calculated using the expression:

$$\lambda_c = \frac{\lambda_{K\alpha_1} + c\,\lambda_{K\alpha_2}}{1 + c}$$ (Pike and Wilson, 1959)

where $\lambda_{K\alpha_1}$ and $\lambda_{K\alpha_2}$ are the wavelengths of the K lines for chromium radiation as reported by Bearden (1968). These values are given as $\lambda_{K\alpha_1} = 2.28970$ Å

$\lambda_{K\alpha_2} = 2.293606$ Å,

the factor C is the ratio of intensities of the $K\alpha_1$ and $K\alpha_2$ lines quoted in International Tables (1962) as 0.515.

The lattice parameter a_{hkl} was calculated for each line observed and plotted against $\cot^2\theta$. The resultant graph was then extrapolated to cot θ = 0 and the intercept from this extrapolation taken as the required value of the lattice parameter. This procedure follows closely that suggested by Wilson (1963a).

The lattice parameter for each profile was calculated in the usual manner for cubic materials using the expression

$$a_{hkl} = \frac{\lambda_c \sqrt{(h^2 + k^2 + l^2)}}{2\sin\theta_c}$$

λ_c being the centroid wavelength

θ_c being the profile centroid corrected for the various experimental aberrations.

The calculated values for all the lines analysed in all specimens are given in table 4.2 and inspection of these shows that they all increase with increasing θ and following Wilson, a plot of a_{hkl} against $\cot^2\theta$ was made for each specimen. Figure 4.5 summarises these results an inspection indicates that a_{hkl} is a linear function of $\cot^2\theta$. A least squares operation was therefore performed on each set of data to give the extrapolated value a_o in each case. Also calculated for each set of data was the correlation coefficient (r). This gave a measure of the scatter of points about the straight line calculated by the least squares operation, the closer r being

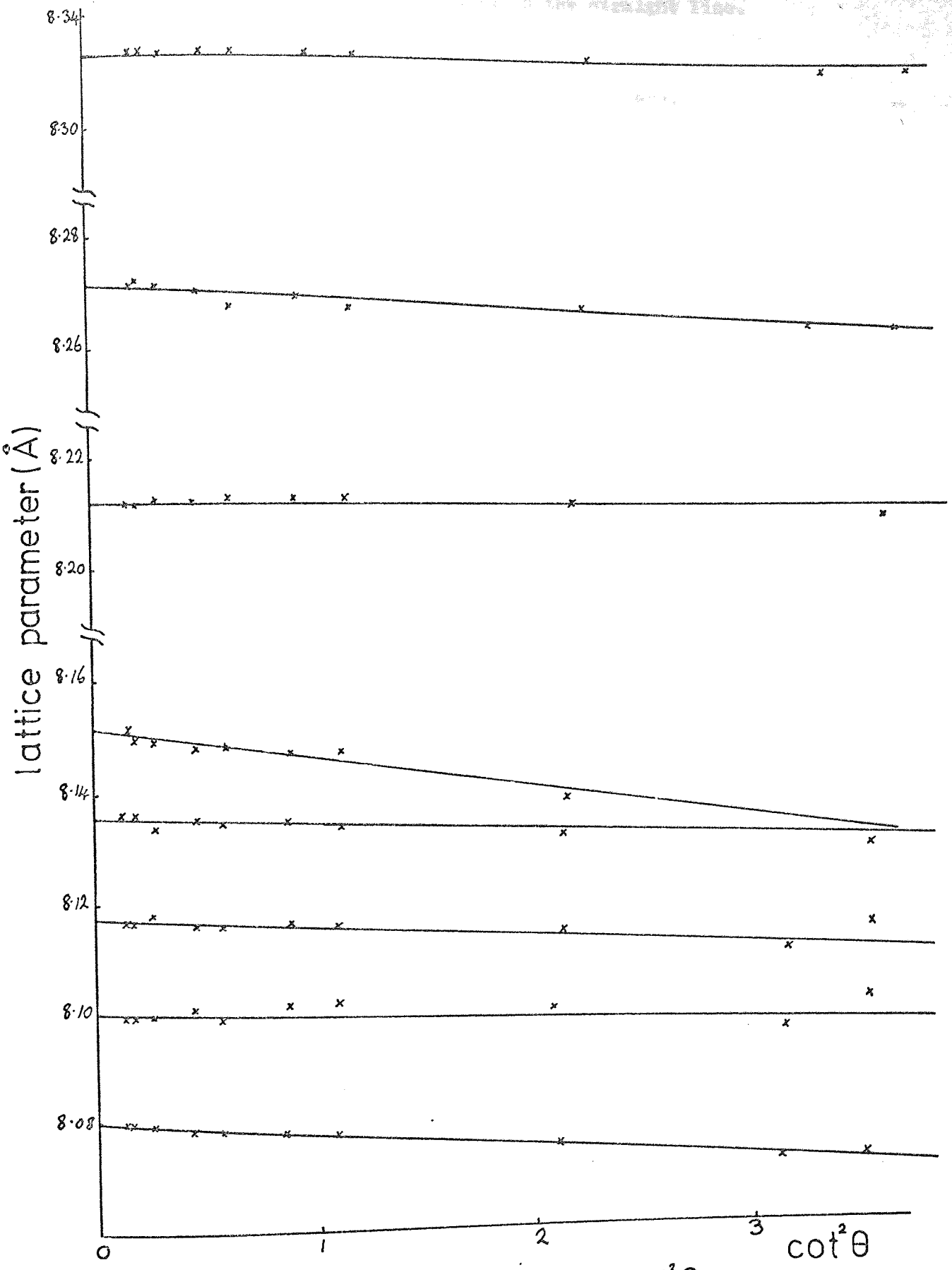

fig. 4.5. Variation of a_{hkl} against $\cot^2\theta$.

to unity the better the fit of the data to the straight line.

Table 4.2 Calculated values of a_{hkl} for all specimens.
(results quoted in Å)

x / hkl	0	0.125	0.25	0.375	0.5	1.0	1.5	2.0
111	8.053	8.081	8.109	8.109	8.117	8.192	8.235	8.315
220	8.070	8.091	8.114	8.125	8.118	8.205	8.259	8.328
311	8.072	8.102	8.114	8.128	8.129	8.214	8.264	8.331
222	8.072	8.096	8.110	-	-	-	8.264	8.331
400	8.075	8.099	8.114	8.132	8.138	8.211	8.271	8.333
422	8.078	8.102	8.115	8.134	8.147	8.213	8.267	8.333
511/333	8.078	8.101	8.116	8.135	8.147	8.212	8.268	8.333
440	8.078	8.099	8.116	8.134	8.148	8.212	8.271	8.333
531	8.078	8.101	8.116	8.135	8.147	8.212	8.270	8.333
620	8.080	8.100	8.117	8.134	8.149	8.212	8.271	8.333
533	8.080	8.100	8.117	8.135	8.150	8.212	8.272	8.334
622	8.080	8.100	8.117	8.136	8.151	8.212	8.272	8.334

Table 4.3 gives the extrapolated values of a_o together with the correlation coefficients. It should be noted that the value of r for $MgAl_2O_4$ and $MgCr_2O_4$ are remarkably high indicating a high degree of linearity for these plots. The values of r for the remainder of the specimens show a slight decrease in r, probably reflecting the varying breadthe of the lines involved in the calculations. The final aberration free values for a_o for the two pure samples, 8.080 Å and 8.333 Å, agree very well with those for the compounds listed in the ASTM index.

A plot of a_o against chromium concentration (figure 4.6) shows a departure from Vegard's Law with a maximum deviation at 18% Cr^{3+} concentration, the lattice parameter is larger than expected according

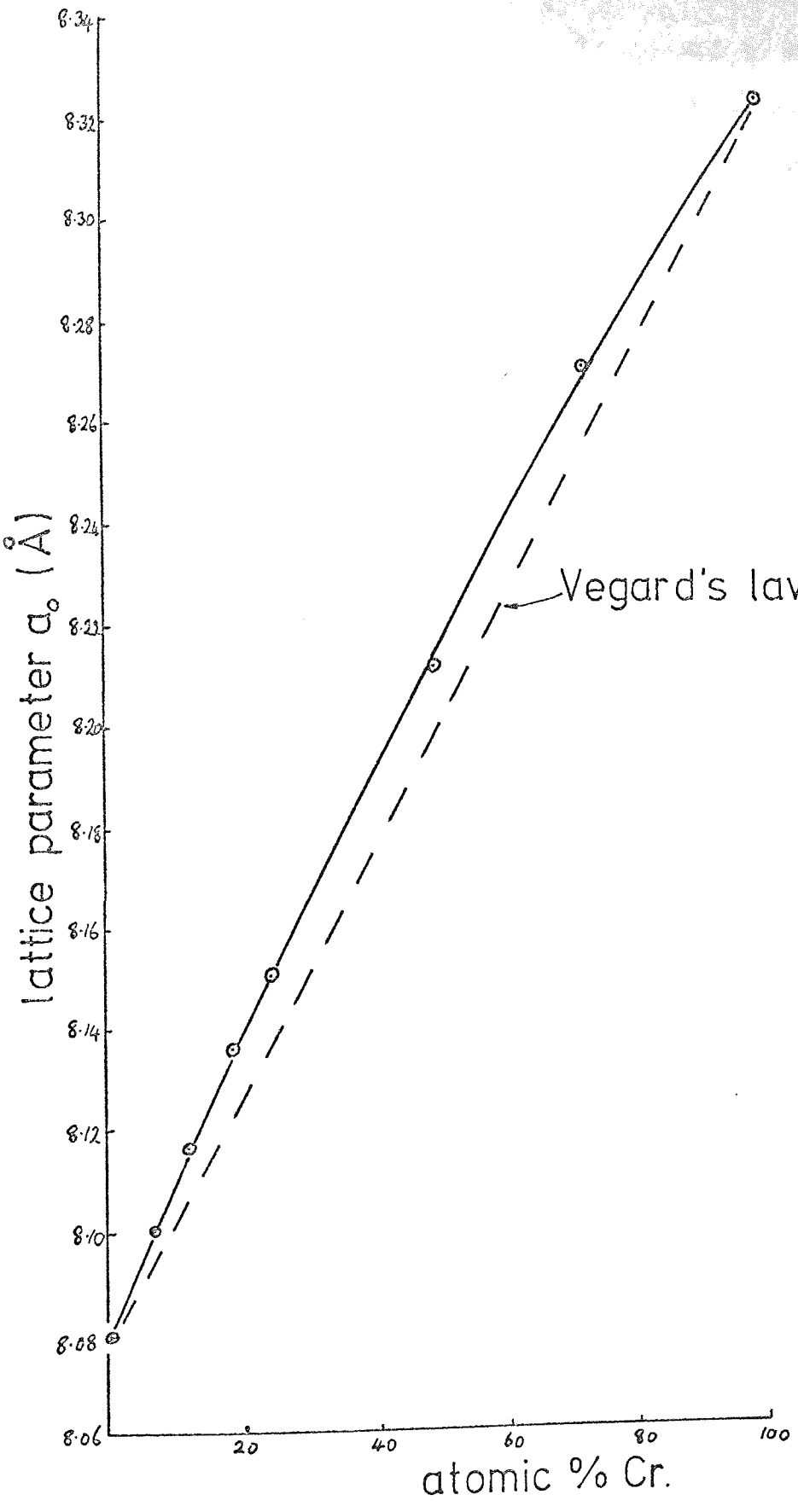

fig.4.6. Lattice parameter variation with Cr^{3+} concentration for the spinel series $Mg(Al_{2-x}Cr_x)O_4$

to the law, i.e. a positive deviation. The position of the maximum deviation is in agreement with that reported by Thilo and Saur (1955) and Lou and Ballentyne (1968) although the former authors reported a negative deviation.

Table 4.3 Aberration free values of lattice parameters for all specimens (Å).

x	a_o/Å	r
0	8.080	-0.99
0.125	8.101	-0.94
0.25	8.117	-0.96
0.375	8.136	-0.94
0.5	8.151	-0.95
1.0	8.212	-0.97
1.5	8.272	-0.92
2.0	8.333	-0.97

Romeijn (1953) has analysed the effect of replacement of ions in the spinel lattice and his conclusion was that Vegard's Law holds in the formation of solid solutions of spinels with the same type of ionic distribution. He explained that a positive deviation occurs when

(i) the tendency for complete solid solution is small, and

(ii) in the solid solution, the pattern of order is destroyed.

From the results described above, points (i) and (ii) should hold, but inspection of the diffraction pattern of each specimen showed there to be only the spinel phase present, i.e. solid solution was complete, thus (i) can be discounted. Comment on point (ii) can only be made after the analysis of the line shape has been described.

4.3 Crystal structure determination of $MgAl_{2-x}Cr_xO_4$

4.3.1 Discussion of experimental effects on the intensity measurements.

Initially the task of determining the structure of the specimens was considered as a confirmatory exercise as the two pure materials in the series, i.e. those in which x = 0 and x = 2, have been examined many times and the various structure parameters were considered to be extremely well established.

The u parameters of these two substances and their Debye-Waller temperature factors were calculated on the assumption that they had the Fd3m symmetry structure as is normally ascribed to cubic spinels; then the same parameter of each of the mixed specimens could be estimated.

The experimental integrated intensities for each line were determined in the usual manner. Figure 4.7 shows a sketch of a typical line profile. The integrated intensity is calculated as the difference between the areas ACBDE and ABDE. The line AB joins the measured background intensities well into the tails of the profile and the assumption made here is that the background varies linearly over the angular range ED.

Well established theory (see James 1965) shows that the intensity of a powder diffraction line is given by

$$I_{hkl} \propto \frac{1 + \cos^2\theta}{\sin^2\theta \cos\theta} \; p.A_p.|F|^2 \exp\frac{-2B\sin^2\theta}{\lambda^2} \qquad \ldots\ldots 4.1$$

where θ is the Bragg angle

p is the multiplicity factor which takes into account the number of reflections from the set of planes in the crystal which are superimposed to form the powder line,

A_p is the absorption factor for a powder,

F is the structure factor,

B is the Debye-Waller temperature factor,

λ is the wavelength used and

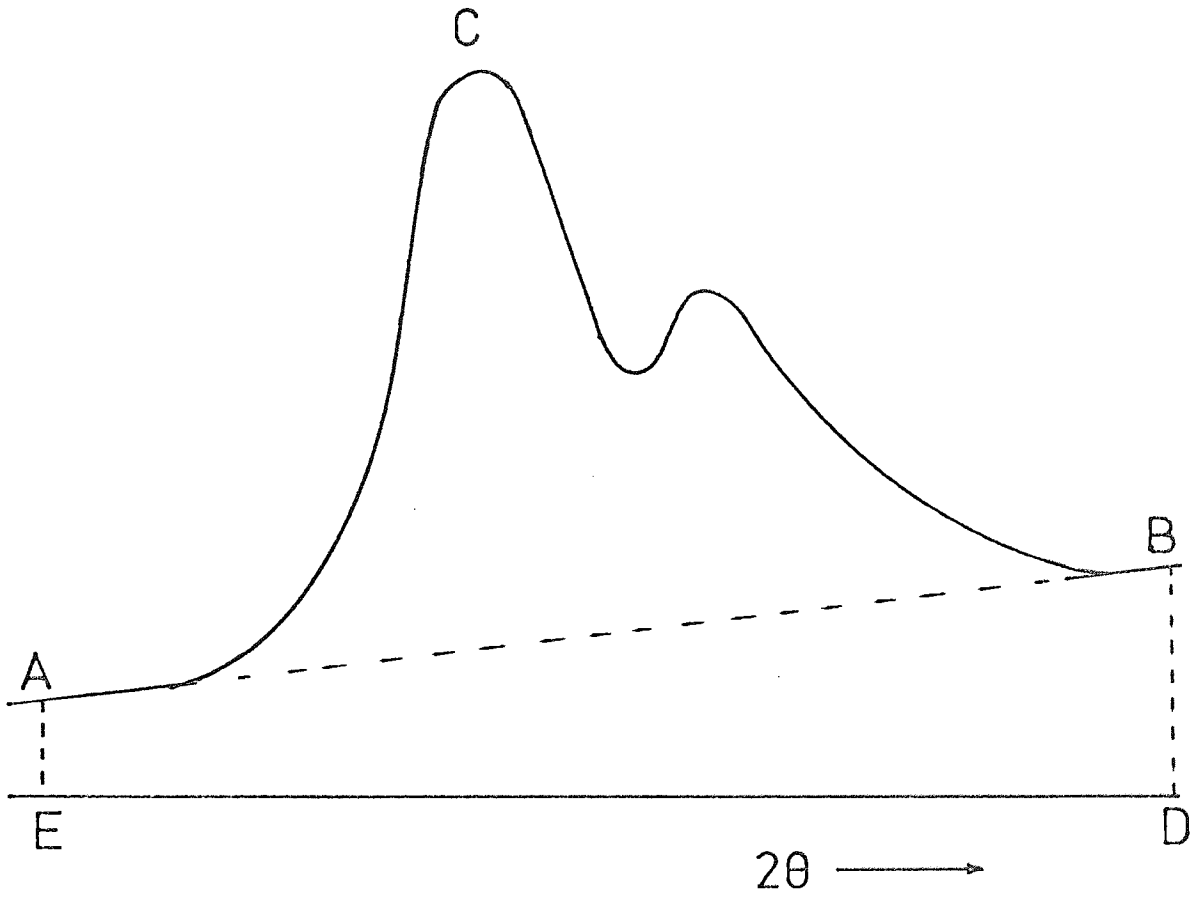

fig. 4.7 Calculation of integrated intensity.

the trigonometric function is the Lorentz-polarisation factor.

The range of angle over which the diffraction lines were observed was $28^{\circ}2\theta$ to $140^{\circ}2\theta$ and the absorption effect differs depending on the angle of the line. International Tables gives an expression for this angular dependence and calculation shows the absorption effect to vary only by a few percent over this range.

A description of the estimation of the absorption coefficients has already been given above in which it was thought that it was substantially constant for the 8 specimens as they were powders. These observations suggest that the absorption effect can be considered as a constant for all specimens over the whole range. Thus equation 4.1 may be rewritten as

$$I_{hkl} = K |F|^2 \exp \frac{-2B \sin^2 \theta}{\lambda^2} \qquad \ldots\ldots\ldots\ldots 4.2$$

where K is a constant which included all corrections to be made to the observed intensity including absorption effects.

Thermal diffuse scatter has not been accounted for in the above expression and calculations made on the contribution to the integrated intensity by this effect were made according to Chipman and Paskin (1959). The percentage contribution is given by

$$Q = \frac{B \sin 2\theta}{240 \lambda^2} \times \Delta 2\theta$$

where B is the temperature factor in $\mathring{A}^2$ and $\Delta 2\theta$ is the range in degrees over which the integrated intensity was measured. The effect is greatest at high angles and using $B = 0.5\mathring{A}^2$, a value close to that accepted for $MgAl_2O_4$, it was found that the percentage contribution was of the order of 1%. Thus as the effect was so small, no correction was made for it.

Expression 4.1 also ignores the effect of extinction. Primary extinction is only expected to effect the intensities from powders to a small extent (James, 1965). However secondary extinction is

still troublesome even in powders especially in the case of strong reflections (Brown, 1955) for which the observed intensity should be lower than that expected theoretically. This introduces a problem - present in all structure determinations - of how much smaller than expected are the observed intensities. For the specimens in this study the problem is probably largely confined to 2 lines in each, namely, the (400) and (440) profiles.

4.3.2 Structure parameters for $MgCr_2O_4$ and $MgAl_2O_4$

For the purpose of this exercise Spinel and picrochromite were initially assumed to have a structure based on Fd3m symmetry as is usually ascribed to the cubic spinels, and values of $|F|^2_{calc}$ were derived accordingly for each profile observed. A parameter of the structure which can have a large effect on the calculated integrated intensity is the oxygen u parameter and Bacon (1952) in his neutron diffraction study of Spinel has shown that the ratio of the intensity of the (440) line to the intensity of the composite (511)/(333) line is very sensitive to the value of u used in calculating the intensities. He used this ratio to obtain an estimate of the actual value of u possessed by the structure.

These two lines are adjacent in the cubic spinel diffraction pattern and having large intensities can be determined with good accuracy. For example, when CrK_α radiation is used, these lines appear at 91° and 104° 2θ (approximately) respectively. Inspection of the variation of the correction factors which are dependent on θ shows that in the region occupied by the two lines, these factors are substantially constant, thus the ratio of the intensities of the lines - corrected for multiplicity - would eliminate the effects dependent on θ thus the ratio is substantially independent of the value of B also.

The ratio of the measured intensities was taken and compared with the ratio of the theoretical intensities calculated from the accepted model of the spinel structure using various values of u.

In the spinel unit cell, there are 32 oxygen atoms present whose Fd3m positions are

$$u,u,u;\quad (\tfrac{1}{4}-u),\ (\tfrac{1}{4}-u),\ (\tfrac{1}{4}-u);$$
$$u,\bar{u},\bar{u};\quad (\tfrac{1}{4}-u),\ (\tfrac{1}{4}+u),\ (\tfrac{1}{4}+u);$$
$$\bar{u},u,\bar{u};\quad (\tfrac{1}{4}+u),\ (\tfrac{1}{4}-u),\ (\tfrac{1}{4}+u);$$
$$\bar{u},\bar{u},u;\quad (\tfrac{1}{4}+u),\ (\tfrac{1}{4}+u),\ (\tfrac{1}{4}-u);$$

plus f.c.c. translations,

thus the contribution of the oxygen ions to the calculated structure factor could have a marked effect depending on the value of u assumed.

The structures factors for (440), (511) and (333) reflections were calculated as $|F|^2_{440}$, $|F|^2_{511}$ and $|F|^2_{333}$ and the theoretical ratio of the integrated intensities, suggested by Bacon, as measured on the diffractometer would be

$$\frac{24\,|F|^2_{511} + 8\,|F|^2_{333}}{12\,|F|^2_{440}}$$

the numerical factors being the multiplicity factors for these reflections.

The ratio was calculated with values of u ranging from 0.375 to 0.400 and the results are shown graphically in figure 4.8 for both $MgAl_2O_4$ and $MgCr_2O_4$. The experimentally observed ratio for each are also indicated in the diagram.

The B factor for each specimen was initially estimated in a similar manner. The observed intensity for a profile (hkl) can be expressed as

$$I_{hkl} = K\,|F|^2_{calc}\ \exp\ \frac{-2B\sin^2\theta}{\lambda^2}$$

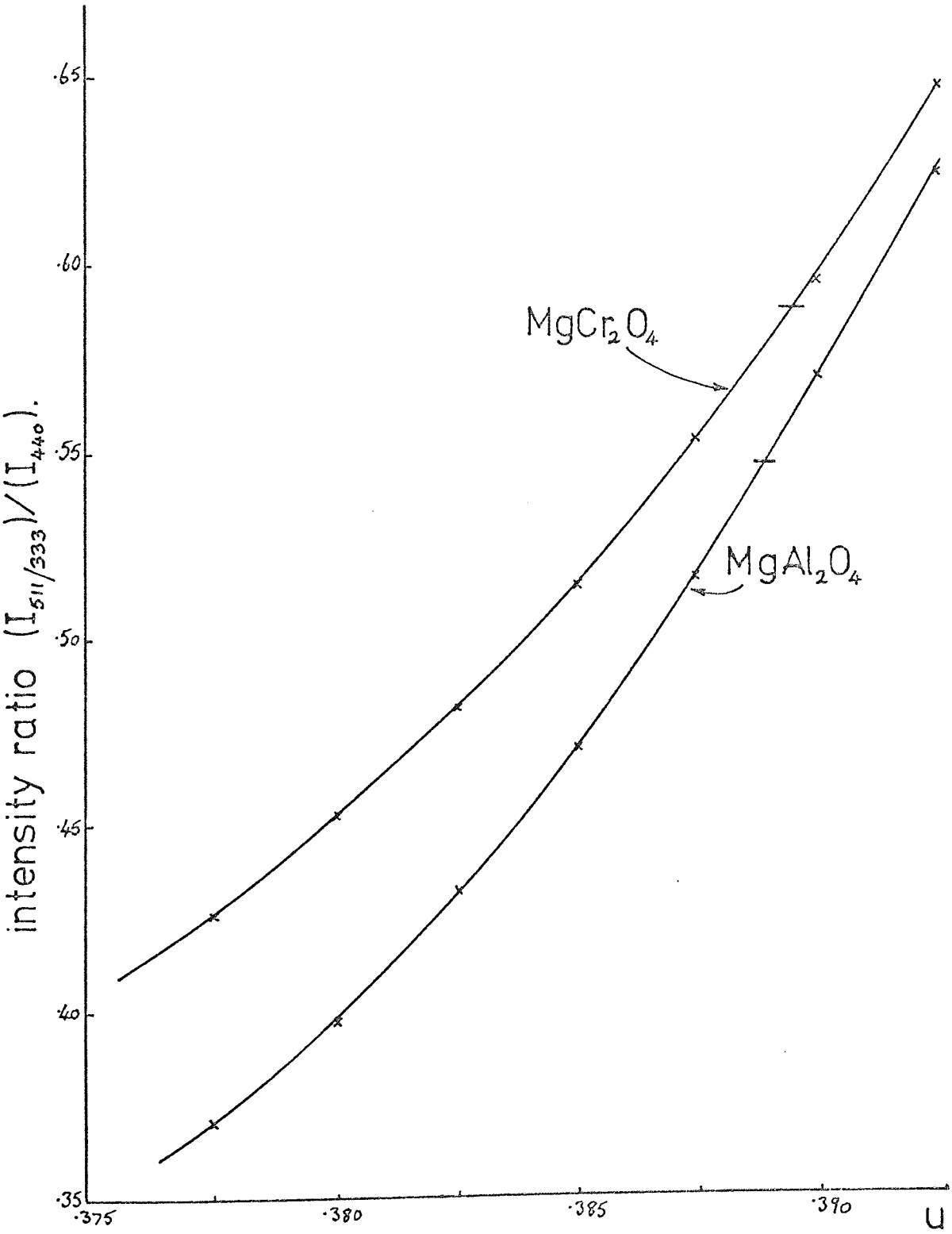

fig. 4.8. Variation of (511/333)-(440) intensity ratios with u parameter.

where I_{hkl} has been corrected for Lorentz - polarisation and multiplicity factors and K is the scale factor. The equation may be re-written as

$$\log_e \left[\frac{I_{hkl}}{|F|^2_{calc}} \right] = \log_e K - \frac{2B\sin^2\theta}{\lambda^2} \qquad \ldots\ldots\ldots 4.3$$

Using strong reflections fairly widely spaced, for instance the (311) and (440) profiles, values of K and B may be deduced by calculating $\log_e \left[\frac{I_{hkl}}{|F|^2_{calc}} \right]$ and $\frac{2B\sin^2\theta}{2}$ for each line. The provisional values for B, u and K upon which a later refinement was based are summarised in table 4.4.

Table 4.4 Preliminary values of B, u and K for specimens $MgAl_2O_4$ and $MgCr_2O_4$

Sample	u	B/Å^2	K
$MgAl_2O_4$	0.389	0.2	23
$MgCr_2O_4$	0.389	1.23	22

Adjustments to these values of u, B and K were made and the corresponding theoretical intensities were calculated. These calculated values were compared with the observed intensities. The combination of values of u, B and K which gave the best agreement were taken as the final results. The scale factor was thought to be substantially constant for all specimens as the results were all taken under similar experimental conditions.

The comparison of the calculated intensity with the observed intensity was made using the R factor (e.g. Rooksby, Peiser and Wilson, 1955).

$$\text{i.e.} \quad R = \frac{\sum |I_{obs} - I_{calc}|}{I_{calc}} \times 100\%,$$

the smallest value of R indicating best fit. Strictly the use of R should be reserved for use when there are a great many diffraction lines However, since in this case the structure refinement involves only three adjustable parameters, only one of which represents a structural change, it was considered that the use of R as a guide to the goodness of fit was admissable. Final values of the parameters found by this procedure are listed in table 4.5.

Table 4.5 Final values of B, u and K for $MgAl_2O_4$ and $MgCr_2O_4$.

Sample	u	$B/\AA^2$	K
$MgAl_2O_4$	0.387	0.4	22
$MgCr_2O_4$	0.387	1.1	22

4.3.3 Integrated intensities for the mixed spinels.

Table 4.5 above indicates the value u for both pure specimens to be the same. However, the B values are widely different. B refers to the displacement of lattice atoms about their mean position and is described by the expression

$$B = 8\pi^2 \overline{u^2} \qquad \text{.....4.4}$$

where $\overline{u^2}$ is the mean square displacement of the atom from its normal position. The value obtained for $MgCr_2O_4$ was surprisingly high and the increase in the B value was associated with the presence of Cr^{3+} ions. It was assumed that B varied linearly with Cr^{3+} concentration and interpolated values of B were used to correct the experimentally observed intensities for the mixed spinels. The results showed that R factors calculated from intensities calculated using these values of B and the observed intensities, were low, of the order of 4% which suggested the assumption taken for determining values of B for the

mixed spinels was reasonable.

In order to calculate intensities from the known structure of spinel for the mixed samples, it was assumed that the Cr^{3+} and Al^{3+} ions were distributed at random over the B sites. To do this the scattering factor of the equivalent trivalent ion was calculated as the weighted mean of the scattering factors of the ions assumed to be on the B sites in the unit cell, this mean value being used in the structure factor evaluation.

These results are summarised in table 4.6, which gives the fully corrected intensities for the eight specimens and the resultant R factor when compared with the calculated intensities given in table 4.7.

Table 4.6 Corrected experimental intensities for all specimens.

x / hkl	0	0.125	0.25	0.375	0.5	1.0	1.5	2.0
111	2900	3430	3800	4240	5000	7730	10600	14300
220	6450	6220	5830	6230	6240	6470	6400	6400
311	13650	14400	14600	16600	16950	20600	24700	28100
222	1050	630	330	190	-	50	1990	4390
400	52300	50500	53300	57900	62900	75400	87000	94700
422	4390	3150	3350	3520	3600	3600	3870	3840
440	79400	83600	83100	87700	93600	106600	118000	120200
531	960	1050	1310	1180	1550	2210	3070	4390
620	2330	2170	2010	2490	2150	2160	2470	2160
533	8000	8030	8770	9670	10000	11900	14650	15800
622	950	1130	1370	1250	1780	3200	4490	5960
R%	2.5	3.7	4.0	2.4	3.2	4.5	4.6	4.2

Table 4.7 Theoretical intensities calculated assuming u 0.387 and random distribution of trivalent ions on B sites.

hkl \ x	0	0.125	0.25	0.375	0.5	1.0	1.5	2.0
111	2900	3380	3870	4380	4920	7420	10500	14000
220	6550	6550	6550	6550	6550	6550	6550	6550
311	13650	14400	15200	16000	16900	20400	24100	28600
222	1600	1130	730	420	200	150	1350	4200
400	51200	53800	56500	59200	62000	73900	86900	101000
422	3460	3460	3460	3460	3460	3460	3460	3460
440	80100	82500	84900	87300	89800	100100	111000	122400
531	1100	1240	1380	1550	1720	2480	3380	4420
620	2010	2010	2010	2010	2010	2010	2010	2010
533	8170	8520	8870	9190	9550	11000	12600	14250
622	700	900	1140	1390	1670	3060	4860	7070

4.3.4 Discussion of intensity results.

Inspection of the table 4.6 above shows that the R factor tends to increase from x = 0 to x = 2.0 although all these values would suggest the structure model chosen to be quite reasonable.

The intensity values observed show a variation from $MgAl_2O_4$ to $MgCr_2O_4$ (i.e. x = 0 to x = 2.0) similar to that indicated by the random distribution model, however there are three lines which do not follow this pattern exactly, these are the (220), (422) and (620) line profiles, the intensities of which are all independent of the ion on the octahedral site (Grimes, 1968, table 1).

(i) The (220) Profile:

The intensity of this line should remain constant, apart from small effects due to the consequent increase in lattice parameter due to insertion of the larger Cr^{3+} ions on atomic scattering factors. However,

observed intensity results show that the intensity of this line decreases to a minimum value at $x = 0.25$ after which it increases and follows the random model intensities. Figure 4.9 shows this variation of intensity with chromium concentration. Note that the line is relatively strong with a high intensity so that measurements can be made with good accuracy (of the order of 2%). Thus the effect shown in figure 4.9 is believed to be real.

(ii) The (422) Profile:

This is a weak reflection and therefore relatively inaccurate. However the observed intensities indicate a similar effect to that of the (220) reflection.

(iii) Again an intensity anomaly appears to exist in the same region as for the (220) and (422) profiles, although the low intensity above background tends to mask the effect.

These observations suggest that Cr^{3+} ions may be substituted in the lattice in a non-random manner.

The difference in the values of B found for the two pure specimens in this study raises an interesting point. The B value for $MgAl_2O_4$ is approximately one third of that for $MgCr_2O_4$. Many spinels have been investigated and it has been found that a great many have B values around 0.4 Å^2, see table 4.8 for a selection of these spinels.

The values around 0.4 Å^2 are thought to give a measure of the thermal agitation of the atoms in the crystal at the temperature of measurement. Grimes (1972) has compared these values of B with those computed from values of Debye temperature found from infra-red spectral studies, by the expression

$$B = \frac{6h^2T}{km\theta^2}\left[\phi\left(\frac{\theta}{T}\right) + \frac{\theta}{4T}\right] \qquad \ldots\ldots\ldots 4.5$$

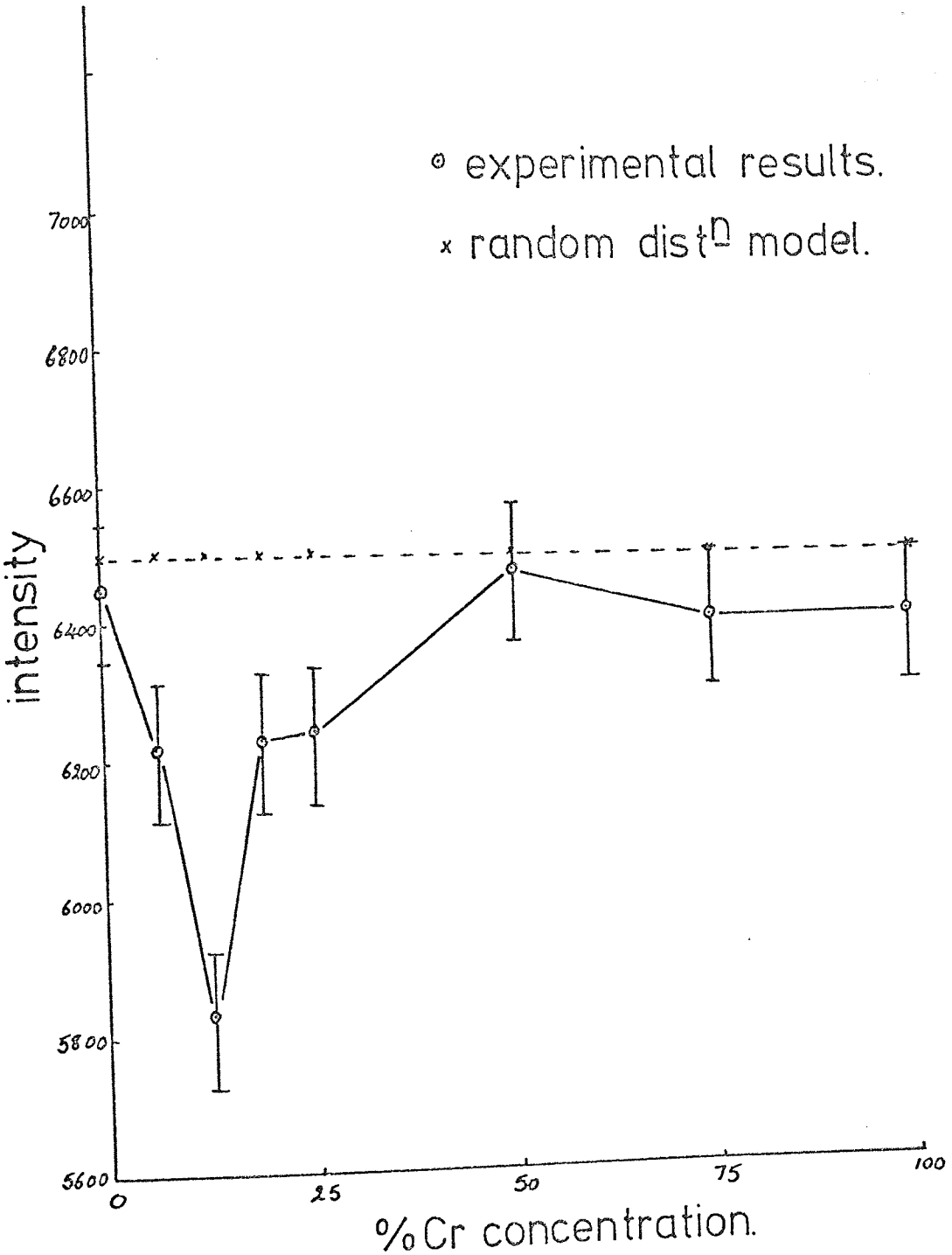

fig. 4.9. Variation of integrated intensity of the (220) profile with Cr^{3+} concentration.

θ is the Debye temperature as measured by infra-red techniques,

$\bar{m}$ is the mean atomic weight of atoms in the unit cell,

the remaining symbols having their usual meaning.

Table 4.8 Values of Debye-Waller temperature factors for a selection of spinels.

Compound	B/Å^2	Reference
$MgFe_2O_4$	0.5	Bacon and Roberts (1953)
$ZnAl_2O_4$	0.31	Fischer (1967)
$ZnCr_2O_4$	0.36	Raccah, Bouchard and Wold (1966)
$CdCr_2O_4$	0.33	
$ZnFe_2O_4$	0.49	Brockhouse, Corliss and Hastings, (1955)
$CaCo_2O_4$	0.40	Kanomata, Ido and Kaneko (1970)

These computed values of B give a true indication of the thermal displacements of atoms in the structure and for the compounds listed in table 4.8 and $MgAl_2O_4$, the infra-red B is approximately equal to the Debye-Waller B, although generally smaller in value. Thus from this evidence it would seem that this Debye-Waller B should be the value associated with thermal vibrations of the atoms within the crystal. Using equation 4.5 to calculate the infra-red B factor for $MgCr_2O_4$, Grimes shows it to be 0.30 Å^2 compared to his value for $MgAl_2O_4$ of 0.36 Å^2, i.e. the B factor should be slightly less for picrochromite. However, X-ray integrated intensity measurements give a value of B = 1.1 Å^2. Cervinka (1965) has reported a similar effect in manganites and he compared values for these compounds with the smaller values for other spinels and suggested that the extra size in B is due to the displacement of ions from their normal position in the lattice due to the

presence of Mn^{3+} ions; i.e. he suggested that equation 4.4 be rewritten

$$B = \frac{8}{3} \pi^2 \left(\overline{u_T^2} + \overline{u_D^2} \right)$$

where $\overline{u_T^2}$ is the mean square displacement due to thermal effects

and $\overline{u_D^2}$ is the mean square displacement of ions from their normal position due to distortions caused by the presence of Mn^{3+} ions in the lattice.

In the case of Cr^{3+} doped spinels, by analogy, the extra distortion indicated by the B factor could be due to the presence of slightly displaced Cr^{3+} ions causing distortions. The value of $\overline{u_T^2}$ can be estimated from the B value found for $MgAl_2O_4$ which may be assumed to be entirely due to thermal effects. The substitution of the larger chromium ions for aluminium into the spinel lattice would imply that the thermal vibrations of the ions at the same ambient temperature, if anything, be smaller than in pure Spinel provided one assumes that bond strengths are substantially unaltered by the substitution. This latter assumption is reasonable considering the similarity of the melting points of these materials. Thus the value of B for $MgCr_2O_4$ should be smaller than that for $MgAl_2O_4$. Grimes' infra-red measurements confirm this view and show that in fact there are slight changes in bond strength which tend to produce a smaller result for B.

Using this model of lattice distortions due to the presence of Cr^{3+} ions, the values of $\overline{u_D^2}$ were calculated and table 4.9 gives the interpolated values of B and corresponding values of $\left(\overline{u_D^2} \right)^{\frac{1}{2}}$, the mean displacement, for all eight samples.

The fact that there appears to be distortions present in picrochromite is surprising as all chromium containing spinels have been considered to be the most well behaved of the spinels. (see discussion on chromite spinels in Chapter 1.)

Table 4.9 Values of B and $(\overline{u_D^2})^{\frac{1}{2}}$ for the spinels series $MgAl_{2-x}Cr_xO_4$

x	0	0.125	0.25	0.375	0.5	1.0	1.5	2.0
B($\pm$ 0.1) / $Å^2$	0.4	0.5	0.55	0.6	0.65	0.8	0.95	1.1
$(\overline{u_D^2})^{\frac{1}{2}}$ / Å	0.0	0.061	0.076	0.087	0.097	0.123	0.144	0.163

4.4 Evidence for the departure of $MgCr_2O_4$ from Fd3m symmetry.

4.4.1 Introduction.

Distortions in spinels containing transition metal ions were thought to be well understood in terms of ions which exhibit the Jahn-Teller effect(Dunitz and Orgel, 1957a). However $MgAl_{2-x}Cr_xO_4$ in which the Cr^{3+} ions occupy the octahedral sites, is expected to be free of such distortions although Poole (1964) has indicated in his study of optical behaviour of chromites that his results suggest in fact that the effect of Cr^{3+} ions in the spinel structure is far from well understood; and the integrated intensity results from this study through the values of B described above supports this view.

Lotgering (1962) has made magnetic susceptibility measurements on $MgCr_2O_4$ and has found that it corresponds closely to the spin only value - this indicates that the Cr^{3+} ion in the lattice is in its normal ground state thus precluding the possibility of the ion exhibiting the Jahn-Teller effect and the consequent distortions. However Grimes (1971) suggests that this does not exclude the possibility of structural distortions in the lattice and Lotgering's results show a slight discrepancy which could be explained by the presence of a trigonal component of the local crystal field in the structure which is larger than expected in the conventional description.

This suggested explanation is supported by evidence supplied by

Stahl-Brada and Low (1959) through electron spin resonance measurements. Their results show that in low Cr^{3+} concentration samples of natural spinel, the Cr^{3+} spectrum indicated an exceptionally strong trigonal field with a [111] direction as an axis of symmetry. Lou and Ballentyne (1968) in their study of the optical spectra of synthetic single Spinel crystals reached a similar conclusion but further that the distortion increased in severity with increasing chromium content up to 10% by weight. Their optical results led to new selection rules which indicated C_{3v} local symmetry for the Cr^{3+} ion.

This description differs from the one expected for an ideally normal spinel which would be D_{3d}, and Grimes and Collett (1971) point out the difference between these symmetries in their analysis of the infra-red spectra of the same samples as were used in this study. They also noted that D_{3d} symmetry would become distorted to C_{3v} if the Cr^{3+} ion occupied a different position along the trigonal axis. Figure 4.10 shows the difference schematically between these two symmetries. The D_{3d} site has all cation - anion bond lengths equal whereas C_{3v} has the metal ion shifted to produce 3 equal shorter bonds and 3 equal longer bonds.

The latter configuration is incompatible with the space group Fd3m, i.e. that structure to which spinel is usually referred. Grimes and Collett suggest that this configuration would occur in the space group $F\bar{4}3m$ although this structure would imply the presence of extra lines to those usually found with cubic spinels. But inspection of the whole of the range of 2θ in the diffraction pattern of $MgCr_2O_4$ has revealed no such lines.

However the $F\bar{4}3m$ structure is one in which cations and anions can be displaced from their conventional positions and Grimes and Collett suggest that for some combinations of these displacements the extra lines may become very weak.

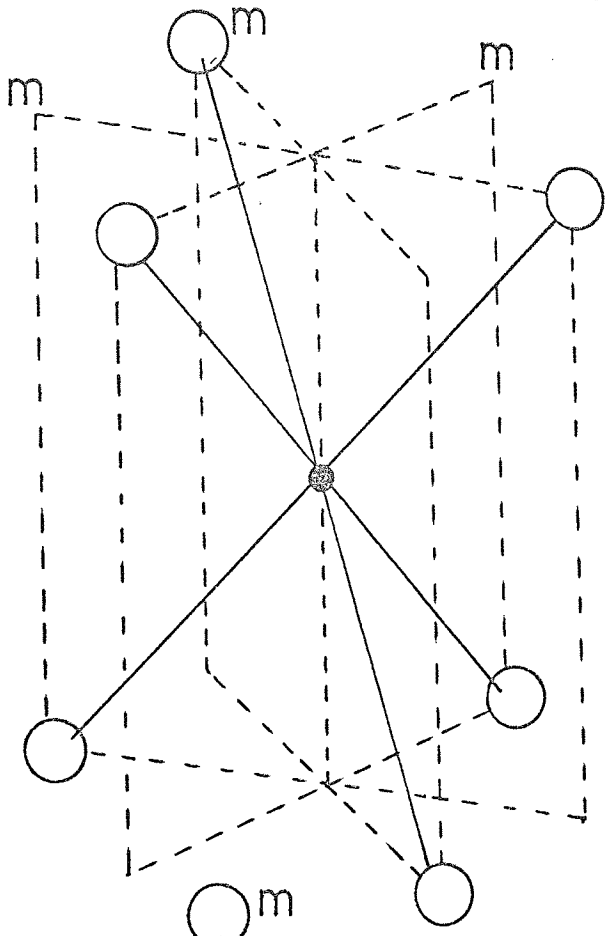

a.

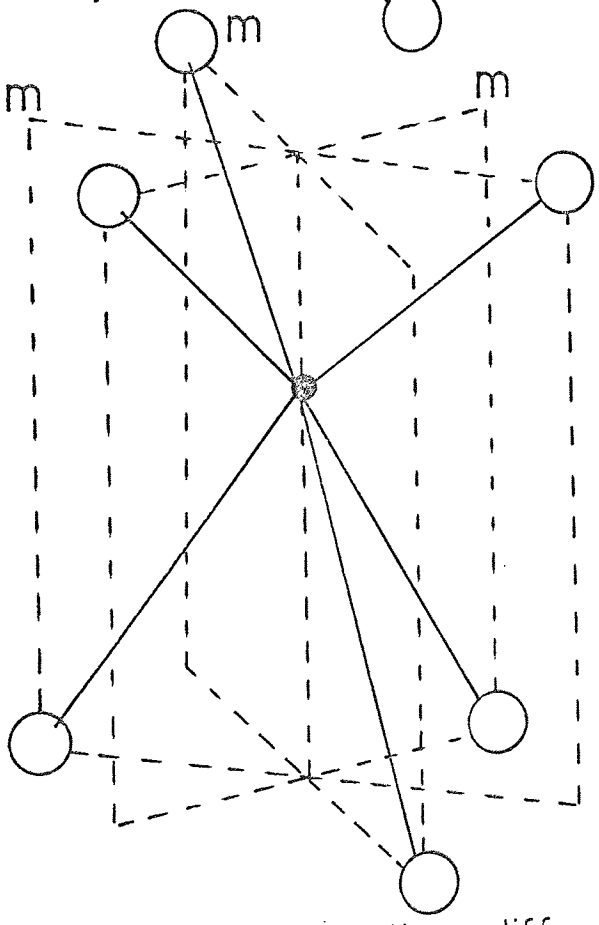

b.

fig.4.10. Illustration of the difference between a. D_{3d} and b. C_{3v} symmetries.

The $F\bar{4}\,3m$ structure has ions on the following positions within the unit cell:

Tetrahedral ions

$\frac{1}{4}, \frac{1}{4}, \frac{1}{4}$; 0, 0, 0;

plus f.c.c. translations

Oxygen and octahedral ions

u, u, u; u, $\bar{u}$, $\bar{u}$; $\bar{u}$, u, $\bar{u}$; $\bar{u}$, $\bar{u}$, u:

plus f.c.c. translations.

Two values u, say u_1 and u_2 may be assigned to describe the 32 oxygen ion positions and another value, say u_3, to describe the 16 octahedral ion positions.

It was decided to attempt a structure analysis of $MgCr_2O_4$ using this model by refining u_1, u_2 and u_3 from their optimum values according to Fd3m.

In this context, it is interesting that Roth (1964a) in his neutron study of $MnAl_2O_4$ has shown this material to give lines at low temperatures extra to those usually associated with the spinel structure and which correspond to those expected if the space group $F\bar{4}\,3m$ is considered. Roth suggested these lines to be due to a magnetic scattering effect. $CoCo_2O_4$ has also been shown to have similar structure at low temperatures (Roth, 1964b).

In electron diffraction studies of $MgFe_2O_4$, Walters and Wirtz (1972) have observed the presence of (200) and (420) lines, i.e. those forbidden in the Fd3m spinel structure; their explanation for this presence was that either ordering had occurred on the B sites or that they were due to double diffraction of the electron beam in the crystal. Similar studies by Hulsher, van der Berg and Lodder (1972) have shown the same reflections to occur in manganese ferrite. However these reflections can occur in the $F\bar{4}\,3m$ symmetry.

Inspection of equation 4.3 shows that in a structure analysis, if $\log_e (I_{calc} / I_{obs})$ is plotted against $\sin^2\theta / \lambda^2$, this should

result in points scattered about a straight line of slope 2B if the model chosen to calculate the values of I_{calc} is correct (e.g. Lipson and Cochran, 1966). Figure 4.11 shows this plot obtained for the intensities observed for the sample $MgAl_2O_4$, structure factors being calculated using u = 0.387; figure 4.12 gives a similar plot for $MgCr_2O_4$ (again u = 0.387). The B factor for $MgAl_2O_4$ was found to be 0.4 $Å^2$ and that for $MgCr_2O_4$ to be 1.1 $Å^2$. Figures 4.11 and 4.12 indicate that the points are scattered reasonably close to a straight line which suggests that the Fd3m structure is a reasonable model for these materials although the steep slope in figure 4.12 is a surprising result for a well crystalline material whose atom displacements were expected to be of thermal origin only.

Although $MgAl_2O_4$ has been assigned the structure Fd3m, Jagodinski and Saalfeld (1958) report that single crystals of this material did not strictly obey the symmetry rules of Fd3m. Stoll et al (1964) have reported a temperature independent contribution to the temperature factor in Spinel. Grimes (1972) in his discussion of 'off centre' ions suggests that the similarity of the size of the Mg^{2+} and Al^{3+} ions in Spinel make it difficult to identify off centre ion in the material through observations on the Debye-Waller temperature factor but Hwang, Heuer and Mitchell (1973) have observed the lines forbidden in the Fd3m symmetry in electron diffraction studies of $MgAl_2O_4$.

4.4.2 Structure calculations for $MgCr_2O_4$ using the $F\bar{4}3m$ model.

In the Fd3m structure, octahedral site ions are assigned positions

$$\frac{5}{8},\frac{5}{8},\frac{5}{8};\quad \frac{5}{8},\frac{7}{8},\frac{7}{8};\quad \frac{7}{8},\frac{5}{8},\frac{7}{8};\quad \frac{7}{8},\frac{7}{8},\frac{5}{8};$$

plus f.c.c. translations

and the oxygen positions are :

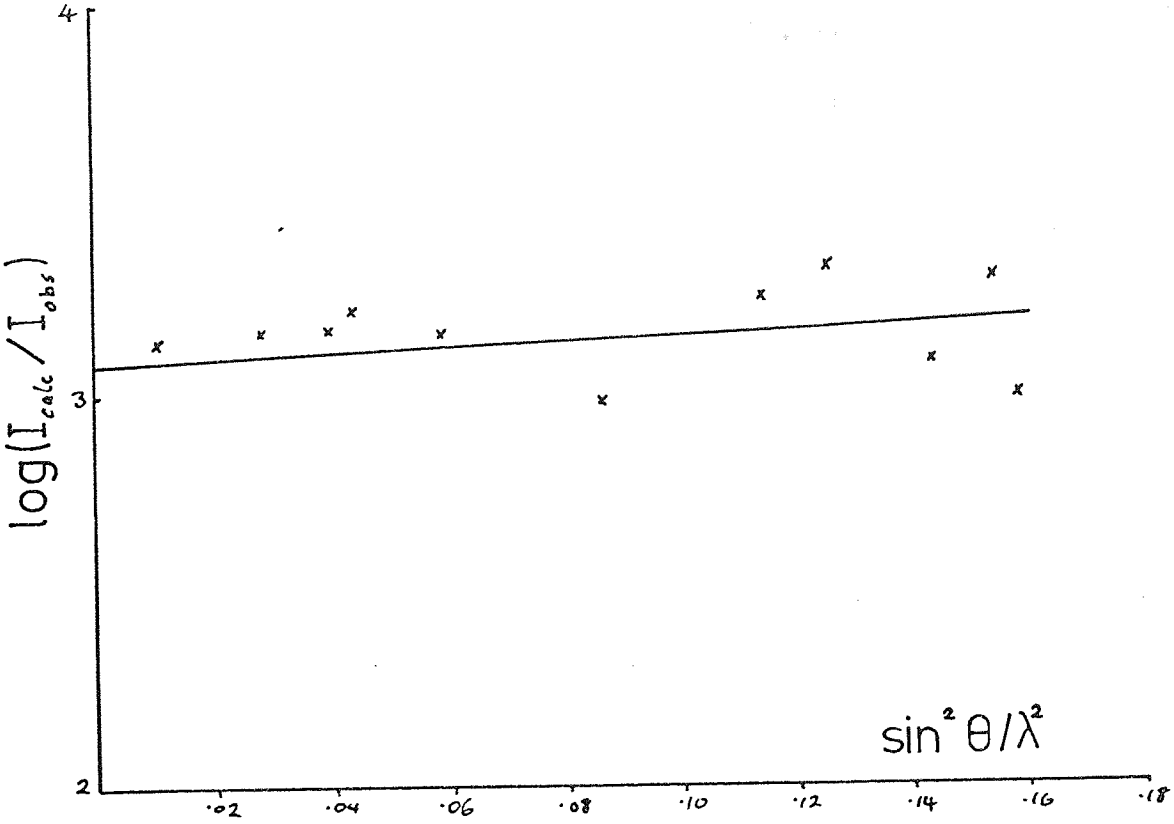

fig. 4.11. Log(I_{calc}/I_{obs}) vs $\sin^2\theta/\lambda^2$ for $MgAl_2O_4$, Fd3m structure, u=0.387.

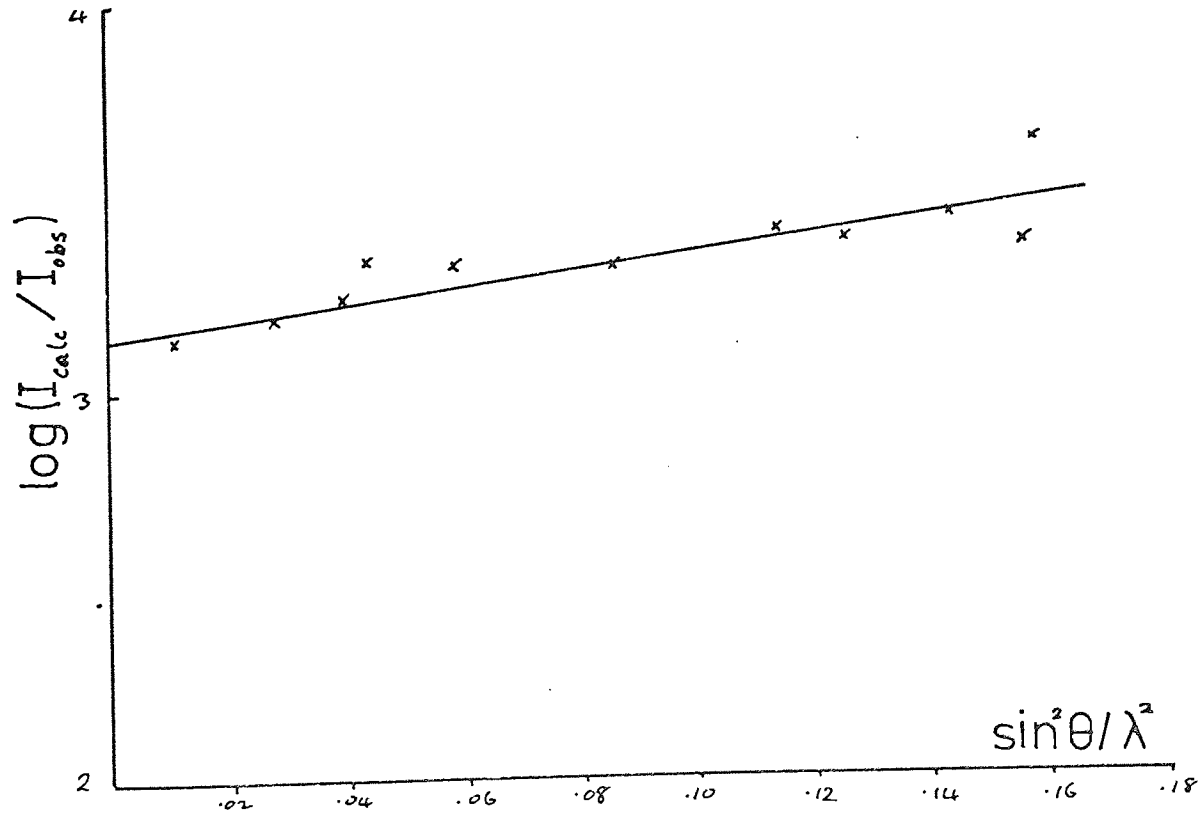

fig. 4.12. Log(I_{calc}/I_{obs}) vs $\sin^2\theta/\lambda^2$ for $MgCr_2O_4$, Fd3m structure, u=0.387.

$u,u,u;\quad u,\bar{u},\bar{u};\quad \bar{u},u,\bar{u};\quad \bar{u},\bar{u},u;$

$\frac{1}{4}-u,\ \frac{1}{4}-u,\ \frac{1}{4}-u;\quad \frac{1}{4}-u,\ \frac{1}{4}+u,\ \frac{1}{4}+u;$

$\frac{1}{4}+u,\ \frac{1}{4}-u,\ \frac{1}{4}+u;\quad \frac{1}{4}+u,\ \frac{1}{4}+u,\ \frac{1}{4}-u;$

plus f.c.c. translations.

In the ideal spinel lattice $u = \frac{3}{8}$ and substituting this value, all the oxygen positions in the unit cell may be found, these are listed in table 4.10 below.

Table 4.10 Oxygen positions in the Fd3m unit cell $u = 0.375$.

$\frac{3}{8},\frac{3}{8},\frac{3}{8};\ \frac{3}{8},\frac{5}{8},\frac{5}{8};\ \frac{5}{8},\frac{3}{8},\frac{5}{8};\ \frac{5}{8},\frac{5}{8},\frac{3}{8};$	A
$\frac{7}{8},\frac{7}{8},\frac{7}{8};\ \frac{7}{8},\frac{5}{8},\frac{5}{8};\ \frac{5}{8},\frac{7}{8},\frac{5}{8};\ \frac{5}{8},\frac{5}{8},\frac{7}{8};$	B
$\frac{7}{8},\frac{7}{8},\frac{3}{8};\ \frac{7}{8},\frac{1}{8},\frac{5}{8};\ \frac{1}{8},\frac{7}{8},\frac{5}{8};\ \frac{1}{8},\frac{1}{8},\frac{3}{8};$	A
$\frac{3}{8},\frac{3}{8},\frac{7}{8};\ \frac{3}{8},\frac{1}{8},\frac{5}{8};\ \frac{1}{8},\frac{3}{8},\frac{5}{8};\ \frac{1}{8},\frac{1}{8},\frac{7}{8};$	B
$\frac{3}{8},\frac{7}{8},\frac{7}{8};\ \frac{3}{8},\frac{1}{8},\frac{1}{8};\ \frac{5}{8},\frac{7}{8},\frac{1}{8};\ \frac{5}{8},\frac{1}{8},\frac{7}{8};$	A
$\frac{7}{8},\frac{3}{8},\frac{3}{8};\ \frac{7}{8},\frac{1}{8},\frac{1}{8};\ \frac{5}{8},\frac{3}{8},\frac{1}{8};\ \frac{5}{8},\frac{1}{8},\frac{3}{8};$	B
$\frac{7}{8},\frac{3}{8},\frac{7}{8};\ \frac{7}{8},\frac{5}{8},\frac{1}{8};\ \frac{1}{8},\frac{3}{8},\frac{1}{8};\ \frac{1}{8},\frac{5}{8},\frac{7}{8};$	A
$\frac{3}{8},\frac{7}{8},\frac{3}{8};\ \frac{3}{8},\frac{5}{8},\frac{1}{8};\ \frac{1}{8},\frac{7}{8},\frac{1}{8};\ \frac{1}{8},\frac{5}{8},\frac{3}{8};$	B

In the $F\bar{4}\,3m$ structure the oxygen and octahedral site positions are described by the parameters u_1, u_2 and u_3 as is discussed above in section 4.4.1. If we choose $u_1 = \frac{3}{8}$ and $u_2 = \frac{7}{8}$, the oxygen positions can be evaluated and it is found that those positions in table 4.10 labelled A correspond to positions in the $F\bar{4}\,3m$ structure with $u_1 = \frac{3}{8}$, those labelled B correspond to $u_2 = \frac{7}{8}$.

A similar analysis of the octahedral site positions in the Fd3m

structure correspond to $u_3 = \frac{5}{8}$ in the $F\bar{4}$ 3m structure, thus it seems reasonable to suggest that Fd3m is a particular case of the $F\bar{4}$ 3m structure. All three u values in the latter can deviate from these values given here in the same way that the oxygen parameter of spinels varies from compound to compound depending on ion sizes and normality.

Figure 4.13 shows two elementary cubes (side a_o / 4) in the unit cell of the Fd3m structure in which the octahedral ions are denoted as black circles. The oxygen ions (open circles) are labelled A or B depending on which group of oxygen positions they occupy (see table 4.10). Shifts of these ions along a [111] direction together with a small shift of the metal ion as shown by the arrows in the diagram will distort the figure to C_{3v} symmetry.

The position of the octahedral ion can be described in $F\bar{4}$ 3m by using $u = \frac{5}{8}$ and a displacement of this atom along a [111] direction will produce an 'off centre' ion as described by Grimes (1972).

Using this model and varying u_1, u_2 and u_3, u_1 and u_2 being constrained to displacements of similar size and u_3 displacements being small, values of I_{calc} can be calculated and compared to the observed values of integrated intensity.

A further constraint to the model is to keep those lines expected on the $F\bar{4}$ 3m model but absent in the Fd3m model, small, these lines being (200),(420) and (600), as they were found to be absent during the collection of the intensity data. If this model for picrochromite is true, then values of u_1, u_2 and u_3 should give intensities for these lines small enough to be lost in any background scatter which is always present when observing X-ray lines.

It was decided to give u_1 and u_2 displacements of similar magnitude to correspond to the oxygen parameter for $MgCr_2O_4$ found using the Fd3m symmetry model and small variations of u_3 around $\frac{5}{8}$ in the calculation of the expected intensities. Fairly coarse adjustments of

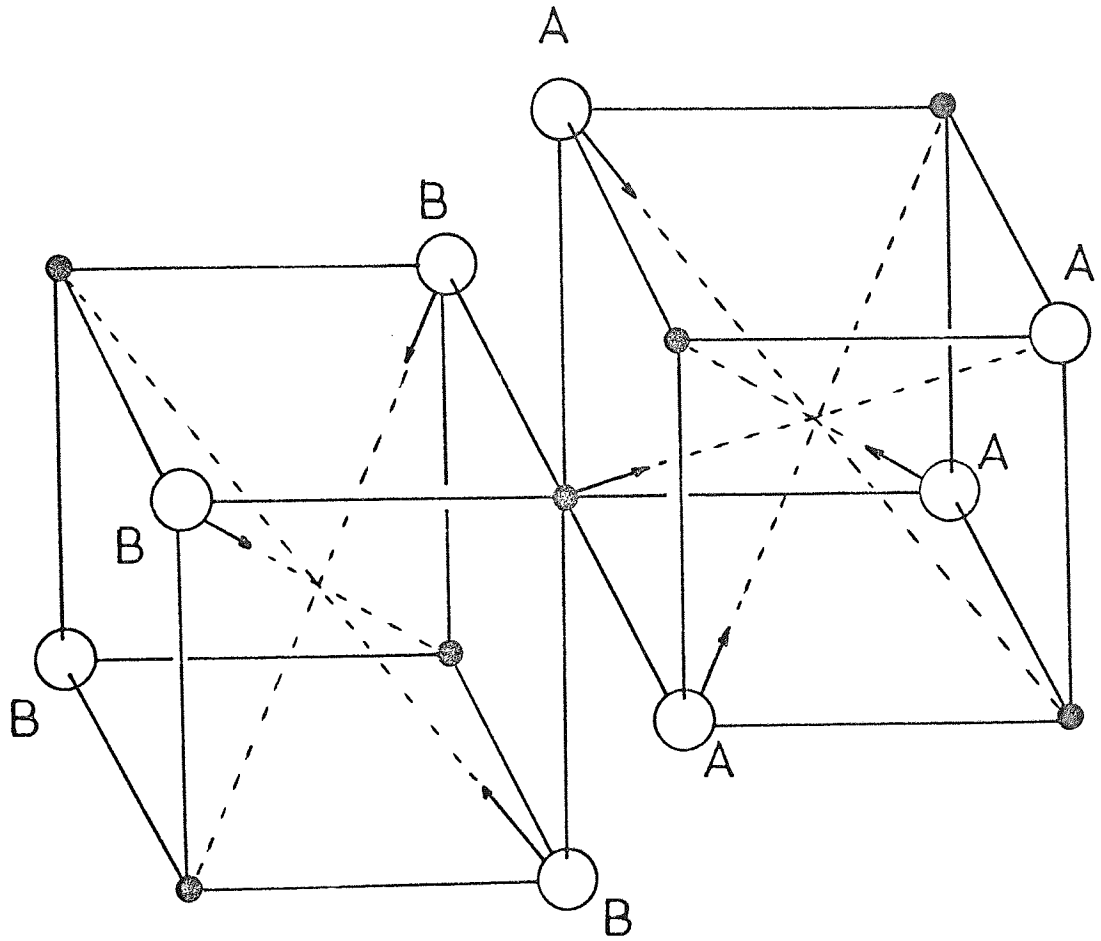

fig. 4.13. Displacements of ions around the octahedral site in the $F\bar{4}3m$ structure.

the values of u_1 and u_2 produced a result in which the B factor, taken from a plot of $\log_e(I_{calc} / I_{obs})$ against $\sin^2\theta / \lambda^2$, was found to be around 0.5 A^2 with R factors of the order of 6%. This suggested that the model chosen may be a better one to describe $MgCr_2O_4$ than Fd3m. Finer adjustments of u_1, u_2, and u_3 dropped the value of B to 0.4 A^2 and R = 3.1%.

Figure 4.14 shows a plot of the final result in this analysis which can be compared with figure 4.12 which is a similar plot calculated from Fd3m structure. It should be noted that the scatter of points about the line is as good as before indicating a reasonable fit of the observed data to the structure chosen.

Table 4.11 lists the final results with values of u_1, u_2 and u_3 to be compared to the observed intensities, the R factor also being included. Also in the table are the expected intensities of the lines (200), (420) and (600) - these are very weak and may easily be swamped by the background intensity, thus preventing them from being observed.

The experimental error in this analysis for B is estimated at $\pm$0.1 A^2. The error estimated by Grimes (1972) in his infra-red data determination of B is $\pm$0.05A^2, thus there is an agreement, within experimental error, between these two results which were obtained from the same sample.

From the value of u_3 in table 4.11 it may be seen that the Cr^{3+} ion in the B site has been shifted slightly from the position expected in the Fd3m structure in which the value of u_3 would be 0.625: u_1 lies close to the Fd3m u parameter which has been found to be 0.387.

Using these parameters, the values of the Cr-O distances were calculated and it was found that there were three bonds of length 1.97$\pm$ 0.01 A and three of length 1.94$\pm$0.01 A. These values for Cr-O bond lengths compare reasonably well with those found by Newnham and Dehaan (1962) in Cr_2O_3 (2.02 A and 1.97 A respectively).

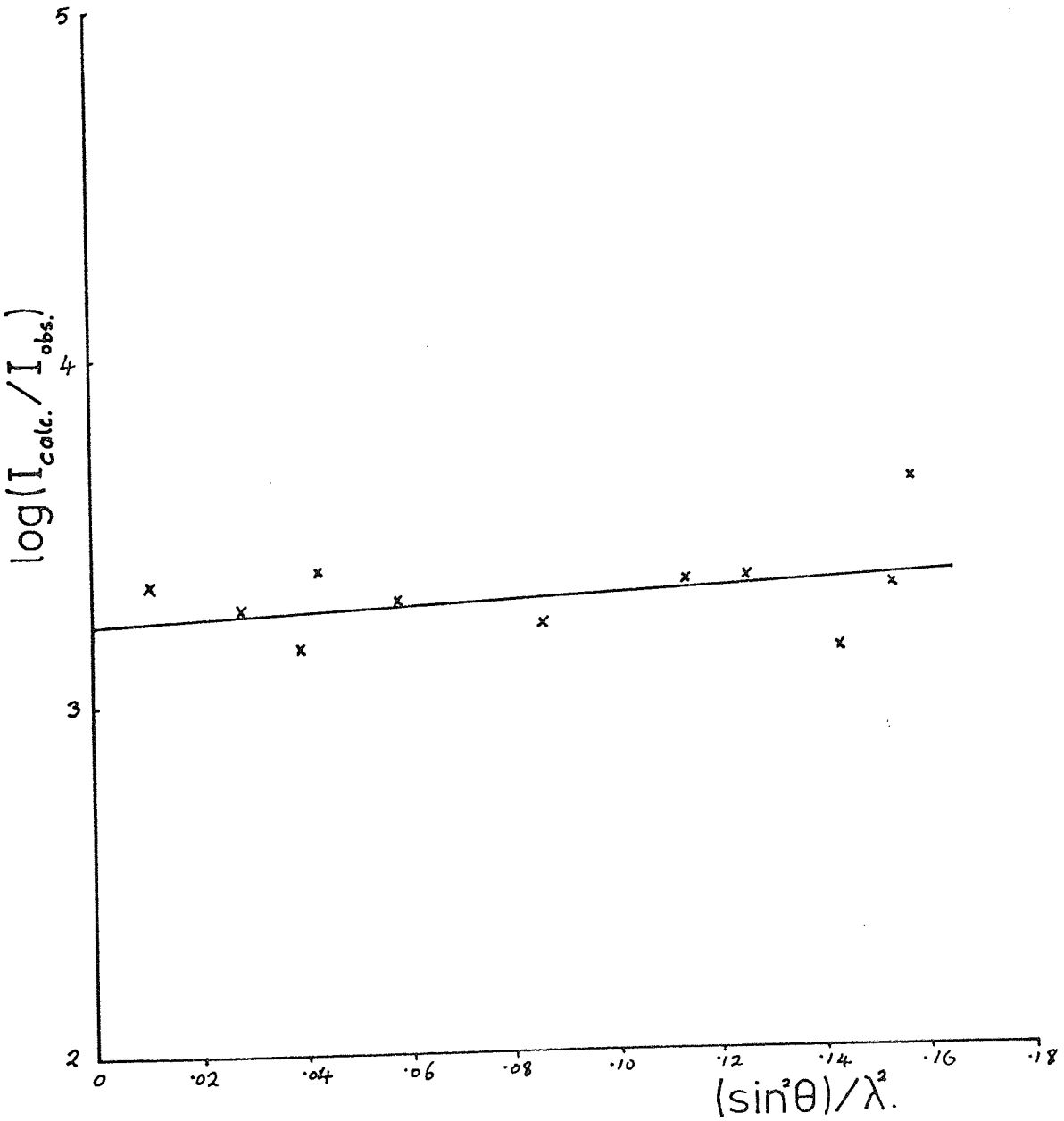

fig. 4.14. Log $(I_{calc.}/I_{obs.})$ vs $(\sin^2\theta)/\lambda^2$ plot for $MgCr_2O_4$-$F\bar{4}3m$ structure.

Table 4.11 Final theoretical and observed intensities for $MgCr_2O_4$ based on the $F\bar{4}3m$ structure.

hkl	Observed intensity	Theoretical intensity
111	15880	17230
220	7130	7150
311	30240	26650
222	4060	4510
400	100000	100000
422	3480	3170
440	116000	117000
531	4320	4390
620	1870	1510
533	14520	14000
622	5500	7170
200	-	10
420	-	10
600	-	40

$R = 3.1\%$

$u_1 = 0.392_5$ $\quad B = 0.4\ \text{Å}^2$

$u_2 = 0.857_5$

$u_3 = 0.625_9$

4.5 Conclusions.

In their analysis of X-ray results from this series of spinels Grimes and Hilleard (1970) compared their results for the anomalously high values of B with those of Cervinka (1965), who suggested that distortions in the series $Mn_xFe_{3-x}O_4$ due to the presence of Mn^{3+} ions,

was due to the Jahn-Teller effect. However, it was known that Cr^{3+} was not a Jahn-Teller ion in its ground state. The structure analysis described in section 4.4.2 represented an extention of the original analysis in an attempt to account for the large value of temperature factor observed in $MgCr_2O_4$.

As has been outlined in section 4.4.1, optical studies on chromium doped spinels (e.g. Poole, 1964, Ford and Hill, 1960, Lou and Ballentyne, 1968) have indicated that the site occupied by chromium ions was not that expected in the Fd3m symmetry.

Having performed the structure analysis on the integrated intensity results using refinements to the $F\bar{4}$ 3m symmetry, the principal conclusion from it is that the diffraction measurements strongly support the proposed changed of space group to describe the cubic spinel structure. It is significant that the refinement according to $F\bar{4}$ 3m symmetry not only provides a site for the Cr^{3+} ion consistent with C_{3v} symmetry as indicated by optical data, but also results in a temperature factor of a value usually attributed to thermal effects only and in agreement, within experimental error, of the value calculated through infra-red measurements.

The displacement of the Cr^{3+} ion from the centre of the octahedral site causes lines of the type (hk0) with $h + k = 4n + 2$ to become allowable reflections. However the small displacements from the centre, necessary in the refinement, gave theoretical intensities to those (hk0) lines which may have been observed under the conditions in these experiments, namely the (200), (420) and (600). These intensities were too small for the lines to be seen above the background radiation and in fact they were not observed.

The intensity anomalies described in section 4.3.4 in which the behaviour of the (220), (422) and (620) lines with chromium concentration is discussed, lead to an interesting conclusion if the departure from Vegard's Law of the lattice parameter-chromium concentration plot is

considered. The maximum deviation from Vegard's Law occurs around the same concentration as the intensity anomaly for these three lines. If the lattice parameter is larger than expected, then the octahedral site will be larger, thus the octahedral site ion has more space which would encourage any tendency that it may have to go off centre. In the Fd3m structure, (220), (422) and (620) are independent of the octahedral site ion, this assumes that there is D_{3d} symmetry at the site. However if the ion goes off centre, the contribution of the B site ions to the intensity becomes finite but small and its phase is in opposition to the additional contribution due to the oxygen ion displacement described in the $F\bar{4}$ 3m structure refinement above. This nett reduction of the contribution to the integrated intensity is probably the cause of the minimum observed in the intensity of the three lines cited above. With larger concentration of chromium the deviation from Vegard's Law becomes smaller, thus the effect described above probably occurs to a much lesser extent.

Grimes (1973) has noted that the consequent displacement from the centre of the site of the Cr^{3+} gives rise to antiferro-electric properties in spinels. The structure refinement of spinel described here indicates a displacement of the Cr^{3+} ion to be about 0.01 Å, a value which is within the range suggested by Grimes to account for these antiferro-electric properties.

CHAPTER 5

LINE PROFILE ANALYSIS

5.1 Introduction.

Before the analysis of the line breadths is described, observations on the behaviour of the diffraction lines of the spinel series $MgAl_{2-x}Cr_xO_4$ may be summarised as follows.

Firstly there is, as indicated in figure 1.5, a marked variation in line breadth with chromium content. It was observed that the line breadth increased with increasing chromium content and a maximum broadening occurred at $x = 0.5$. Thereafter the width of the lines decreased so that $MgCr_2O_4$ exhibited very sharp profiles, comparable with those from a well annealed metal under similar experimental circumstances. This variation was observed in all profiles from each specimen, figure 1.5 showing the variation seen in the (533) profile as a typical example, although the broadening behaviour was complicated to a certain extent by the change in integrated intensity from one sample to the next.

Similar variations in line breadths have been observed in metal alloys like Cu_3Au, the effect being described in Chapter 2; these alloys contain anti-phase domains which cause broadening in 'super-lattice' lines only. However in the case of the spinels used in this study, no super-lattice lines were observed and the diffraction profiles of the conventional spinel pattern were all broadened to varying degrees. Thus in this case it appears as though particle size or strain effects were present but in some way dependent on the chromium concentration.

The purpose of the quantitative analysis was to investigate the broadening further and to confirm if possible, the interpretation in terms of particle size or to find the true nature of the effect.

The investigation was initially carried out using an integral breadth analysis to indicate the nature of the effect observed and this was followed by a determination of more refined parameters using the variance technique described in Chapter 2.

5.2 Integral breadth analysis.

The purpose of this integral breadth analysis was to obtain some idea of the major contributions to the line breadth. Thus for example, Langford (1968a), after a suggestion by Mazur (1949), recommends a plot of $M\cos\theta$ against $\sin\theta$, where M represents a convenient measure of the breadth. The possible results of such an analysis are summarised in figure 5.1. The interpretation of the defect broadening may be described as follows:

(i) poirts lying close to a line of zero slope (symbol ⊙ in figure 5.1). The main source of broadening is due to particle size effects from spherical particles.

(ii) points with a large scatter about a line of zero slope (symbol x); particle size broadening by non-spherical particles.

(iii) points scattered about a line of zero slope with a few points on or near the $\sin\theta$ axis (symbol △); broadening due to stacking faults in a metal like Cobalt for instance in which lines of the type (001) remain sharp while others are broadened when faults occur in the stacking of layers in the close packed metal.

(iv) points lie on a straight line with non-zero slope through the origin (symbol ⊡); broadening due to lattice strain.

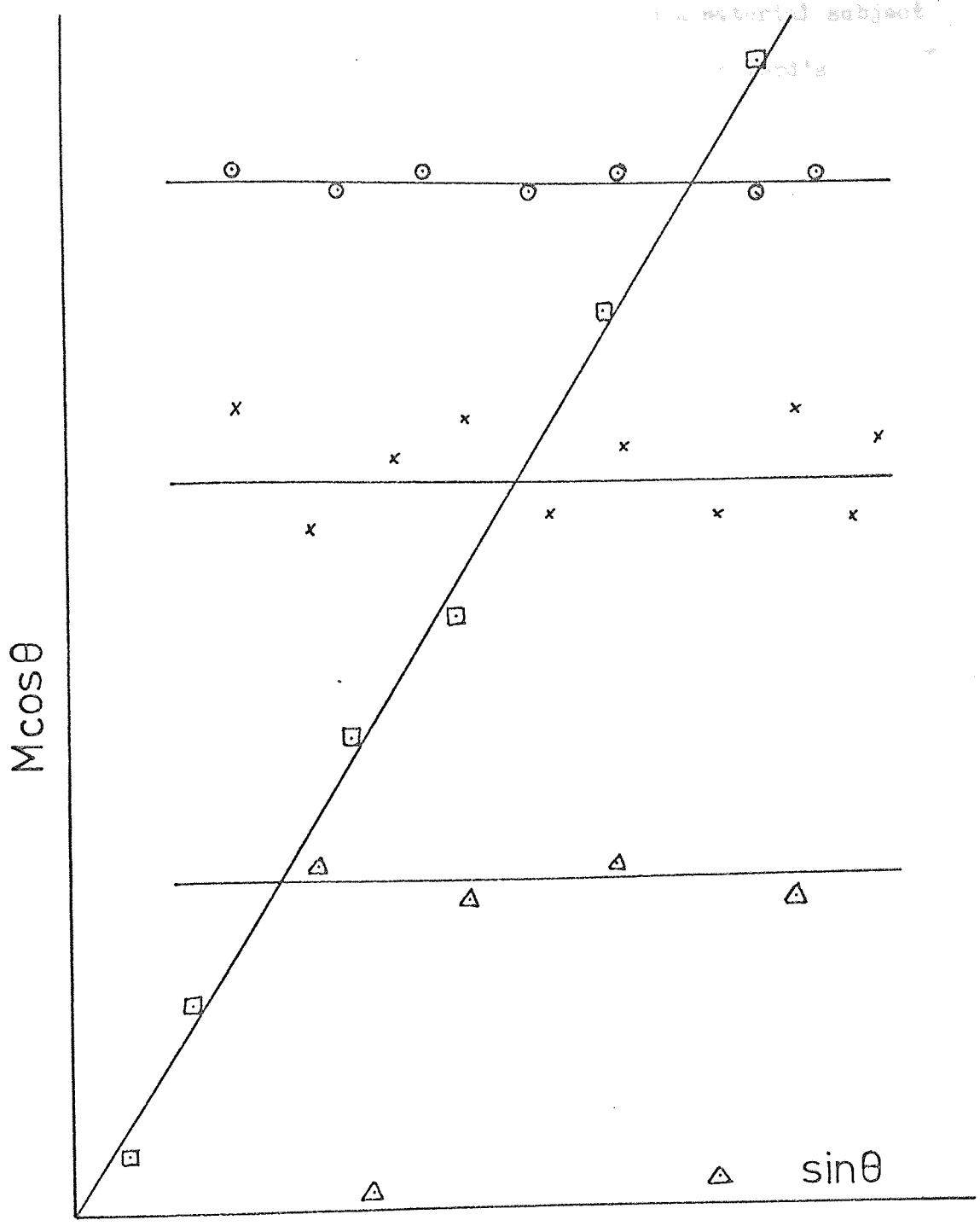

⊙ spherical particles
× non-spherical particles
△ stacking faults
⊡ strain

fig.5.1 Plot to indicate cause of line breadth (after Langford, 1968)

The case described by (iii) above is a mistake structure in one dimension; however the case of line broadening in a material subject to mistakes in three dimensions is not included in Langford's discussion.

Following this suggestion, the integral breadths of each line observed from each sample were calculated as outlined in Chapter 2. These have been tabulated in table 5.1 below.

Table 5.1 Integral breadth (M) for samples $MgAl_{2-x}Cr_xO_4$

$0 \leqslant x \leqslant 2$ (degrees 2θ)

hkl \ x	0	0.125	0.25	0.375	0.5	1.0	1.5	2.0
111	0.16	0.16	0.16	0.18	0.21	0.17	0.16	0.15
220	0.19	0.19	0.19	0.22	0.30	0.20	0.17	0.17
311	0.21	0.23	0.22	0.27	0.34	0.22	0.20	0.18
222	0.23	0.20	0.29	-	-	-	0.19	0.16
400	0.24	0.24	0.27	0.32	0.41	0.26	0.22	0.20
422	0.28	0.30	0.31	0.41	0.58	0.33	0.27	0.20
511/333	0.34	0.34	0.36	0.50	0.62	0.39	0.29	0.23
440	0.39	0.36	0.41	0.60	0.88	0.44	0.30	0.22
531	0.43	0.41	0.47	0.53	0.42	0.47	0.37	0.27
620	0.57	0.49	0.51	0.87	1.06	0.63	0.42	0.27
533	0.64	0.57	0.65	0.99	1.29	0.74	0.44	0.32
622	0.69	0.62	0.71	1.01	1.17	0.76	0.50	0.34

A graph of $M\cos\theta$ against $\sqrt{(h^2 + k^2 + l^2)}$, a similar plot to that described by Langford with no instrumental correction was made for $MgCr_2O_4$ and is given in figure 5.2. The result is a set of points scattered about a line parallel to the $\sqrt{(h^2 + k^2 + l^2)}$ axis. This is similar to the plot expected for a sample subject to particle size

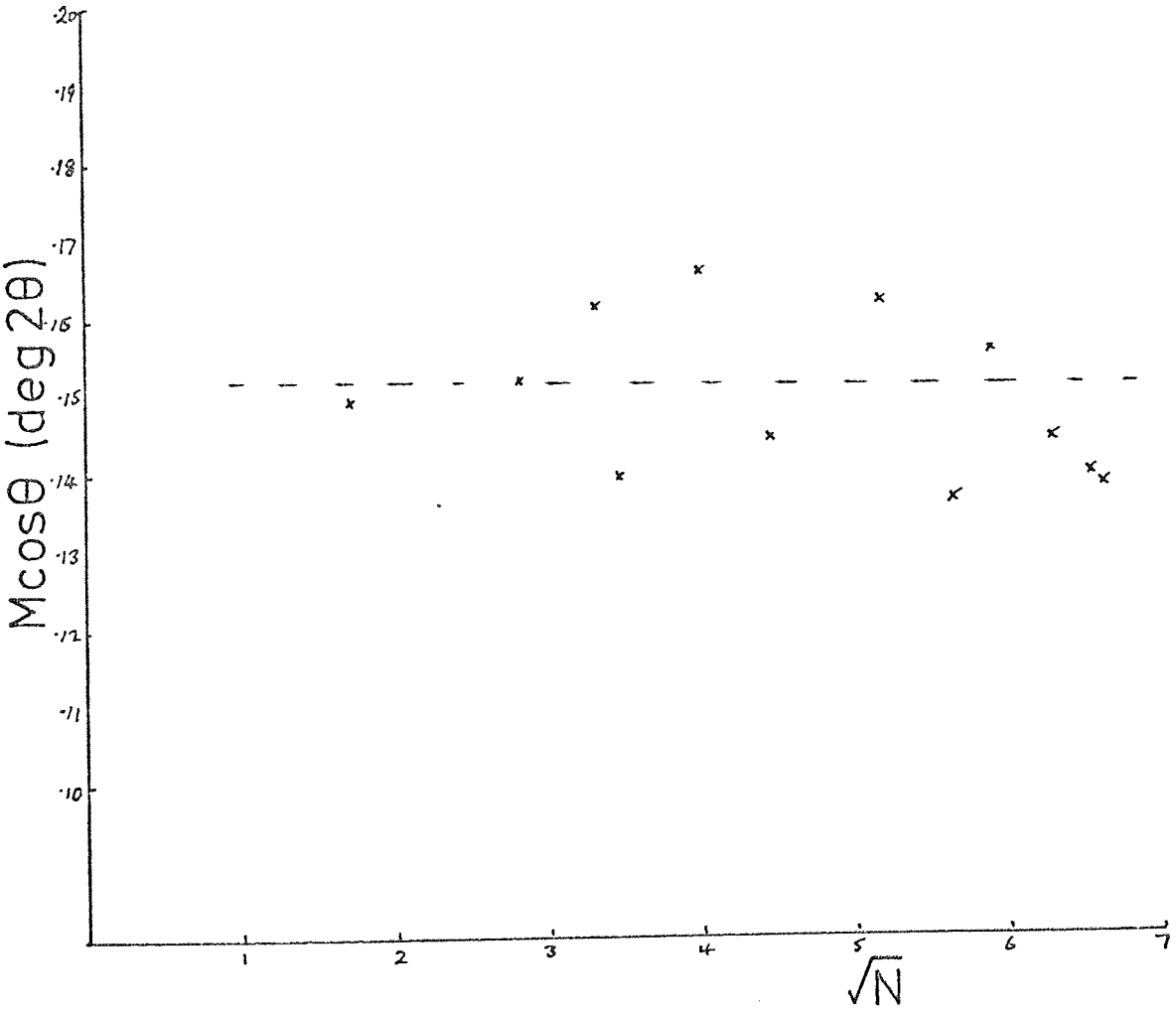

fig.5.2 Langford plot for $MgCr_2O_4$
(no instrumental correction)

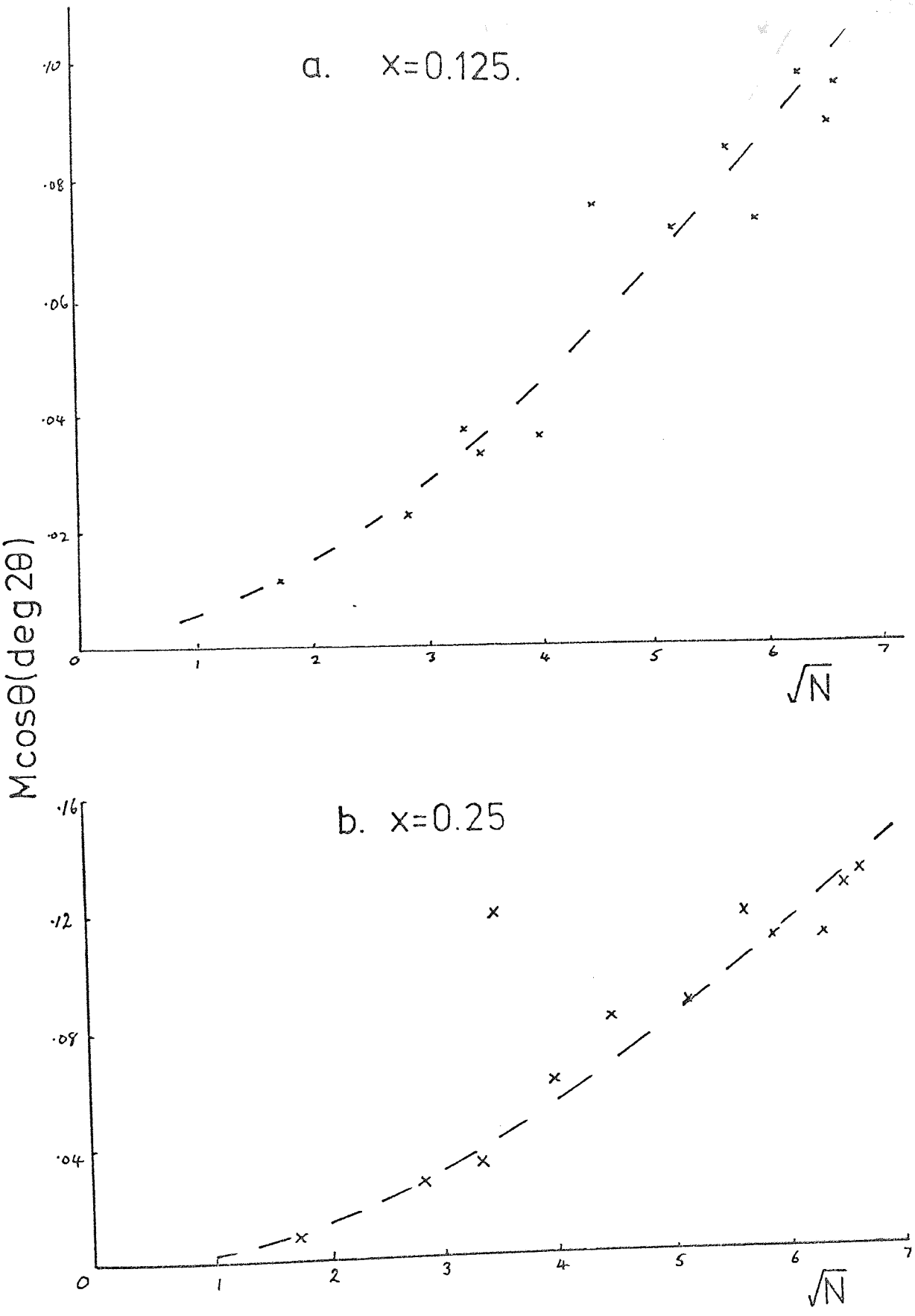

fig.5.3 Langford plot for $MgAl_{2-x}Cr_xO_4$

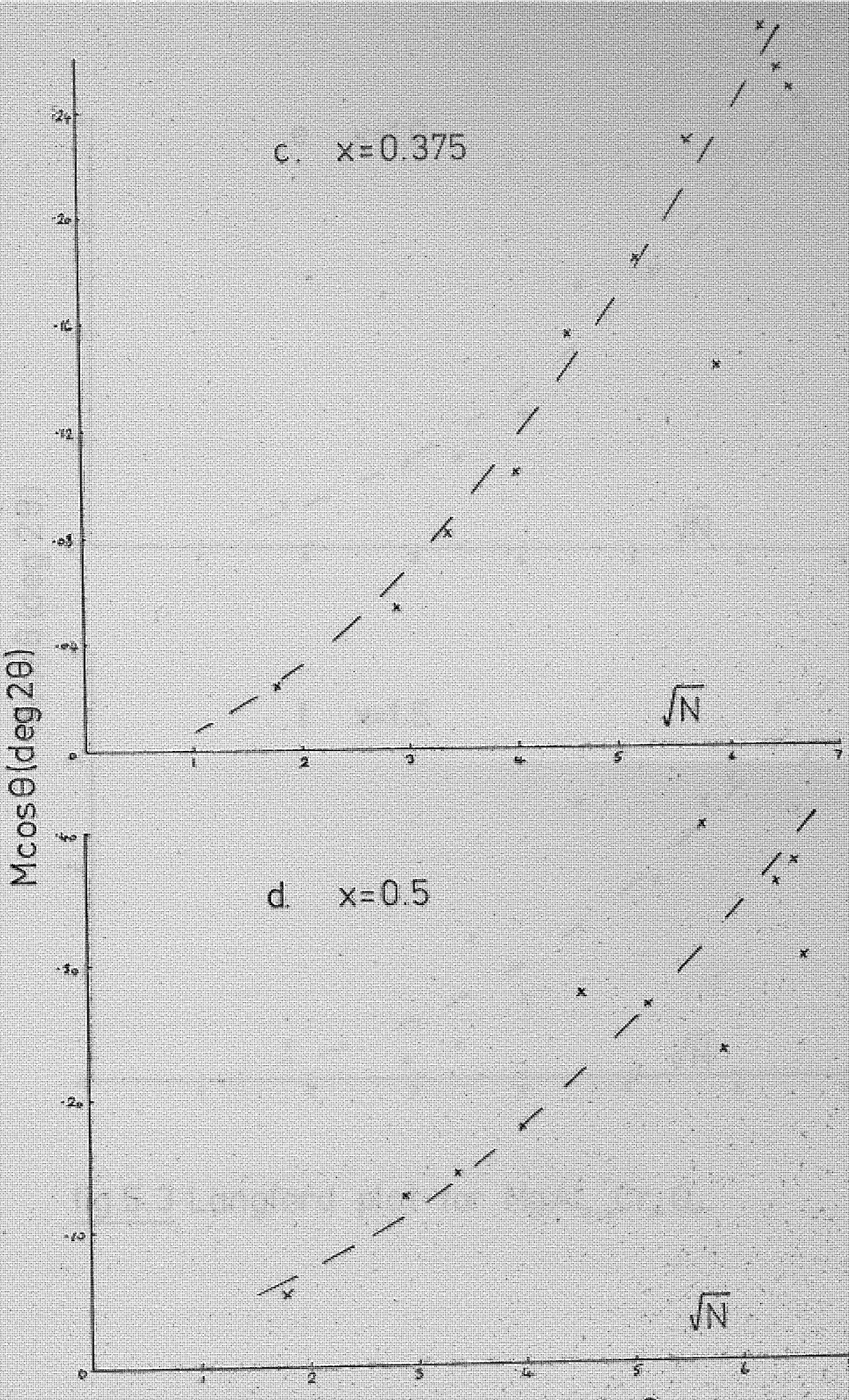

fig. 5.3 Langford plot for $MgAl_{2-x}Cr_xO_4$.

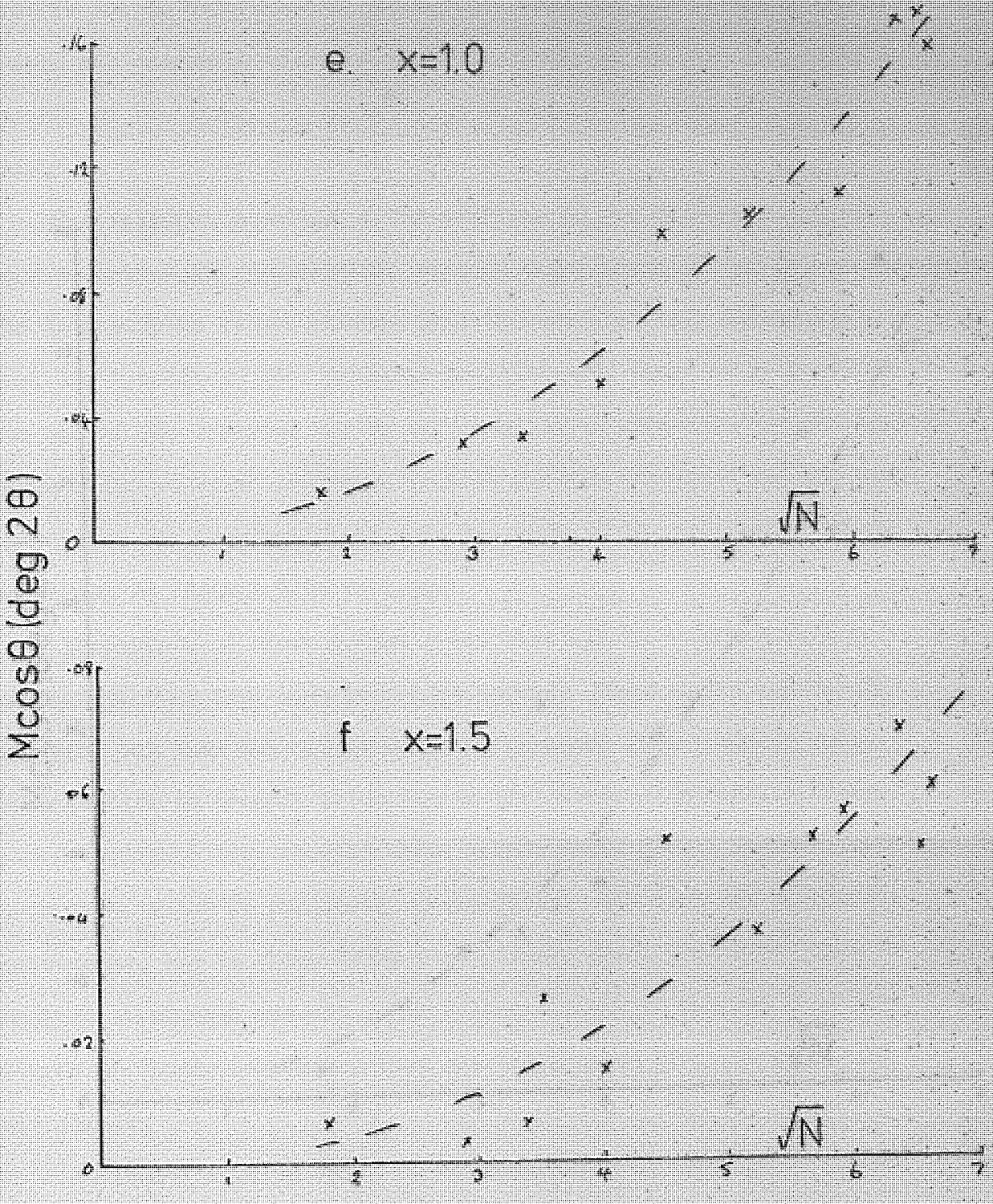

fig.5.3 Langford plot for $MgAl_{2-x}Cr_xO_4$.

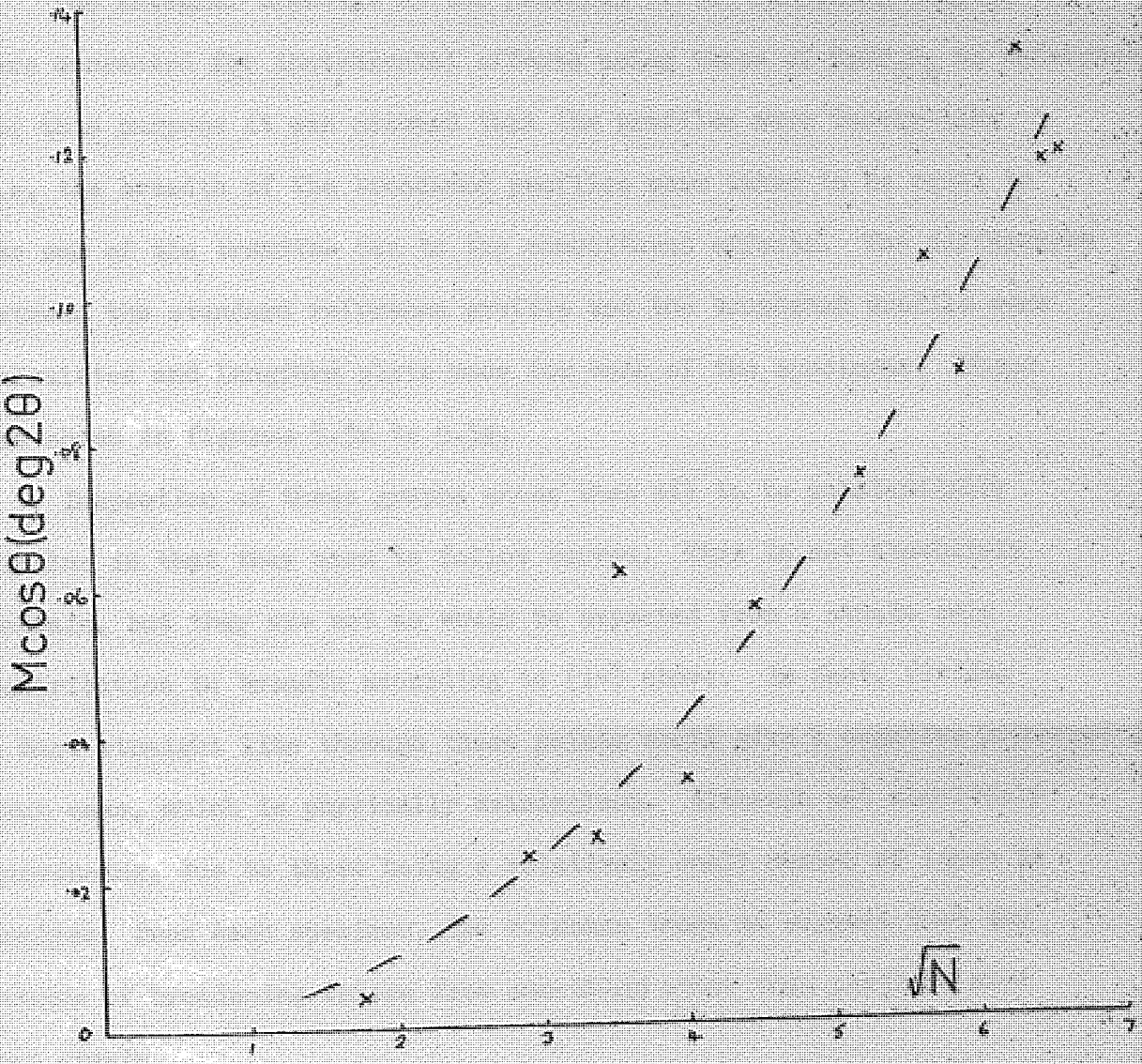

fig. 5.3 g. Langford plot for $MgAl_2O_4$.

effects due to non-spherical particles. However the profiles of this sample are extremely sharp as described above in section 5.1, thus the breadth of the lines is expected to be due to instrumental effects only.

The integral breadths of the profiles of the remaining samples were corrected for instrumental effects using those of $MgCr_2O_4$ as reference. For this purpose it was assumed that the profiles were Cauchy-like i.e. the breadth of the broadened profiles were taken to be equal to the sum of the breadths due to the constituent effects. The differences between the standard reference profile and the broadened profile were calculated and Langford plots made for each of the specimens. These are shown in figures 5.3a to 5.3g.

Inspection of these graphs shows them all to be substantially similar in that they seem to follow curves. This is not absolutely certain, but they are not as would be expected from a strain only contribution to breadth according to (iv) above. In fact, fitting a best straight line through these points would give a negative intercept in each case, which is physically meaningless. Although not absolutely convincing, due to there being a relatively small number of lines to analyse from each specimen, the evidence tends to suggest that the source of broadening arises from something other than particle size and strain.

Following on from this, it is interesting to note that Cervinka, Vogel and Hosemann (1970) have used similar plots in their analysis of distortions due to substitutions of impurity atoms in manganese ferrite. Vogel and Hosemann (1970) suggest that the breadth of a line subject to such distortions is made up of two parts, one due to particle size, the other due to the distortions, their expression being of the form

$$\beta_b = \frac{1}{L} + \frac{\pi^2}{a^3} \Delta^2 x_a h^2 \qquad \ldots\ldots\ldots 5.1$$

Where L is the mean linear crystallite size perpendicular to the reflecting plane,

a is the lattice parameter,

$\Delta^2 x_a$ is the standard deviation of the distance between crystal planes,

h^2 is the sum of the squares of the Miller indices of the reflection.

Thus a plot δb against h for a sample unaffected by such distortions should be a line parallel to the h axis as indicated in figure 5.1, the intercept on the δb axis giving a measure of the particle size.

Inspection of equation 5.1 suggests that a plot of δb against h should be parabolic; Such plots were in fact plotted and are shown in figures 5.3a to 5.3g and in each case the suggestion of the points lying on a curve is evident. Further plots of δb against h^2 were made (figures 5.4a to 5.4g). As the breadths have been corrected for instrumental effects using $MgCr_2O_4$ as a reference sample, these plots should, if Vogel and Hosemann's theory holds, be straight lines through the origin.

Inspection of figures 5.4a to 5.4g indicates a rough linear relationship but there is a large scatter about any straight line which may be drawn through them. Moreover, the intercepts from a straight line through these points for each sample would be small, of the order of zero, an indication perhaps that the particle size for each specimen was similar to that of the reference sample $MgCr_2O_4$.

Thus the integral breadth measurements seem to suggest that if particle size effects exist among the samples then they are probably very small and rather similar to those from picrochromite.

In an attempt to ascertain the particle size of the specimen, silhouettes of particles from all eight specimens were obtained by electron microscoy; These suggested a particle size of about 10^4 Å,

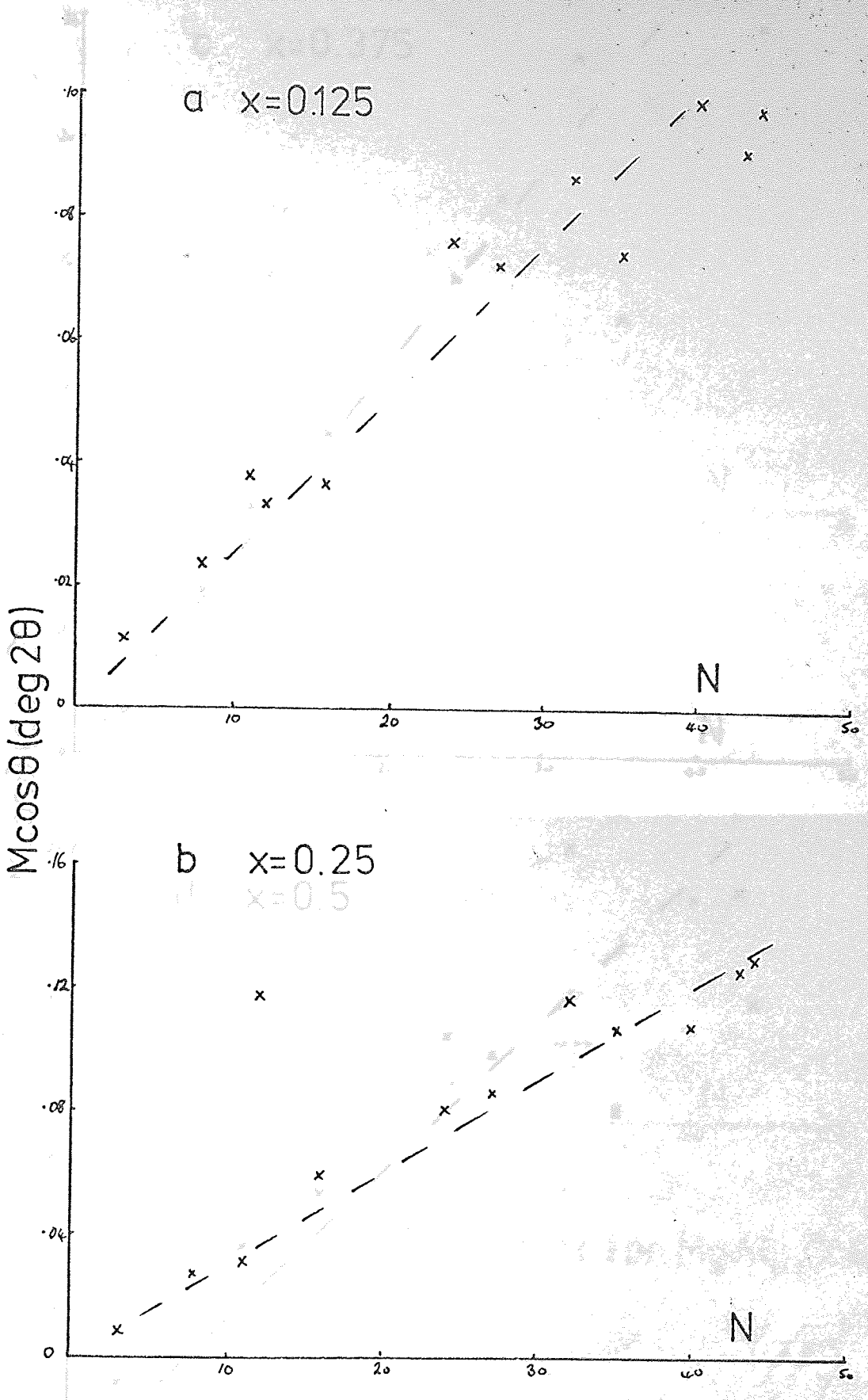

fig.5.4 Vogel & Hosemann plot for $MgAl_{2-x}Cr_xO_4$.

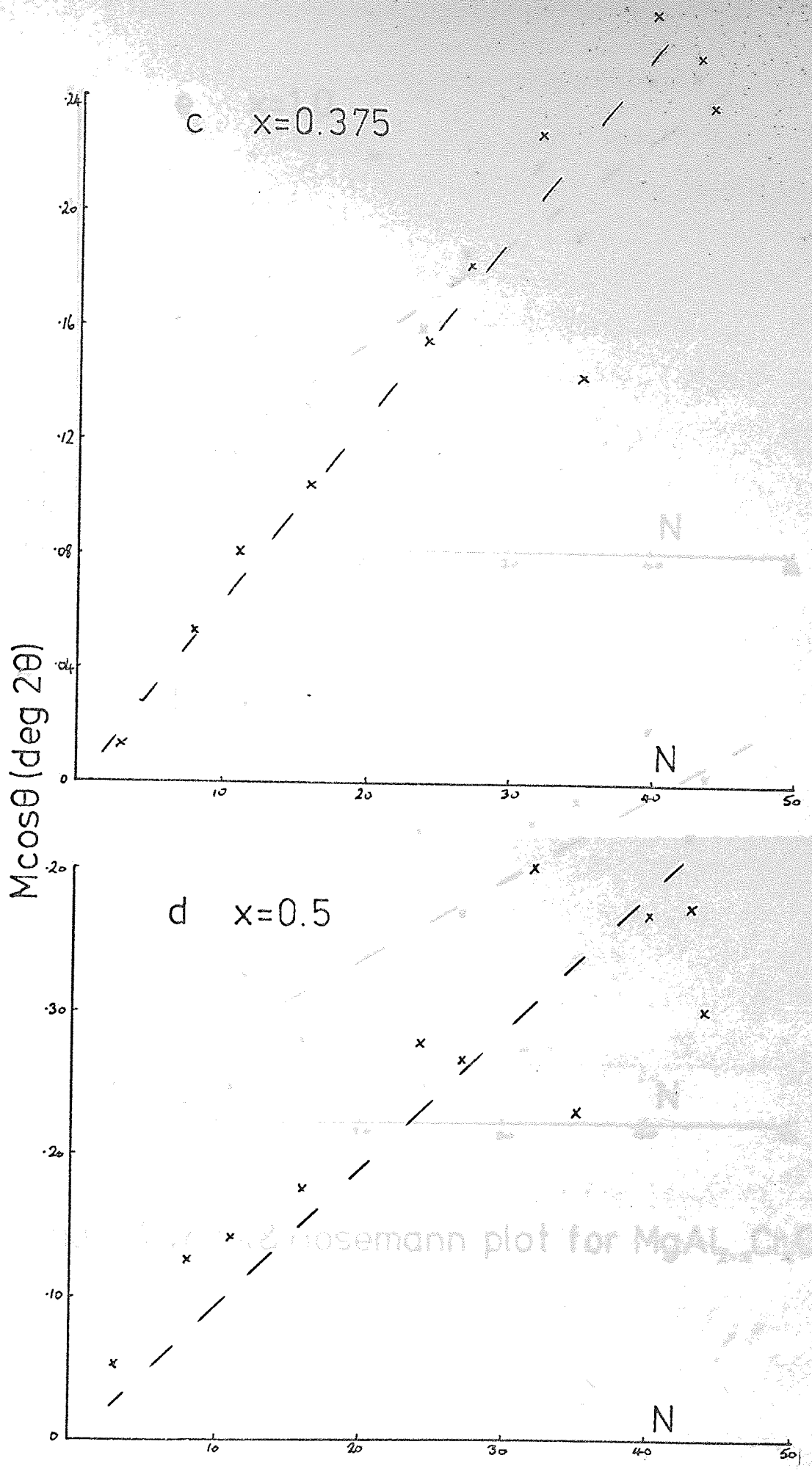

fig.5.4 Vogel & Hosemann plot for $MgAl_{2-x}Cr_xO_4$

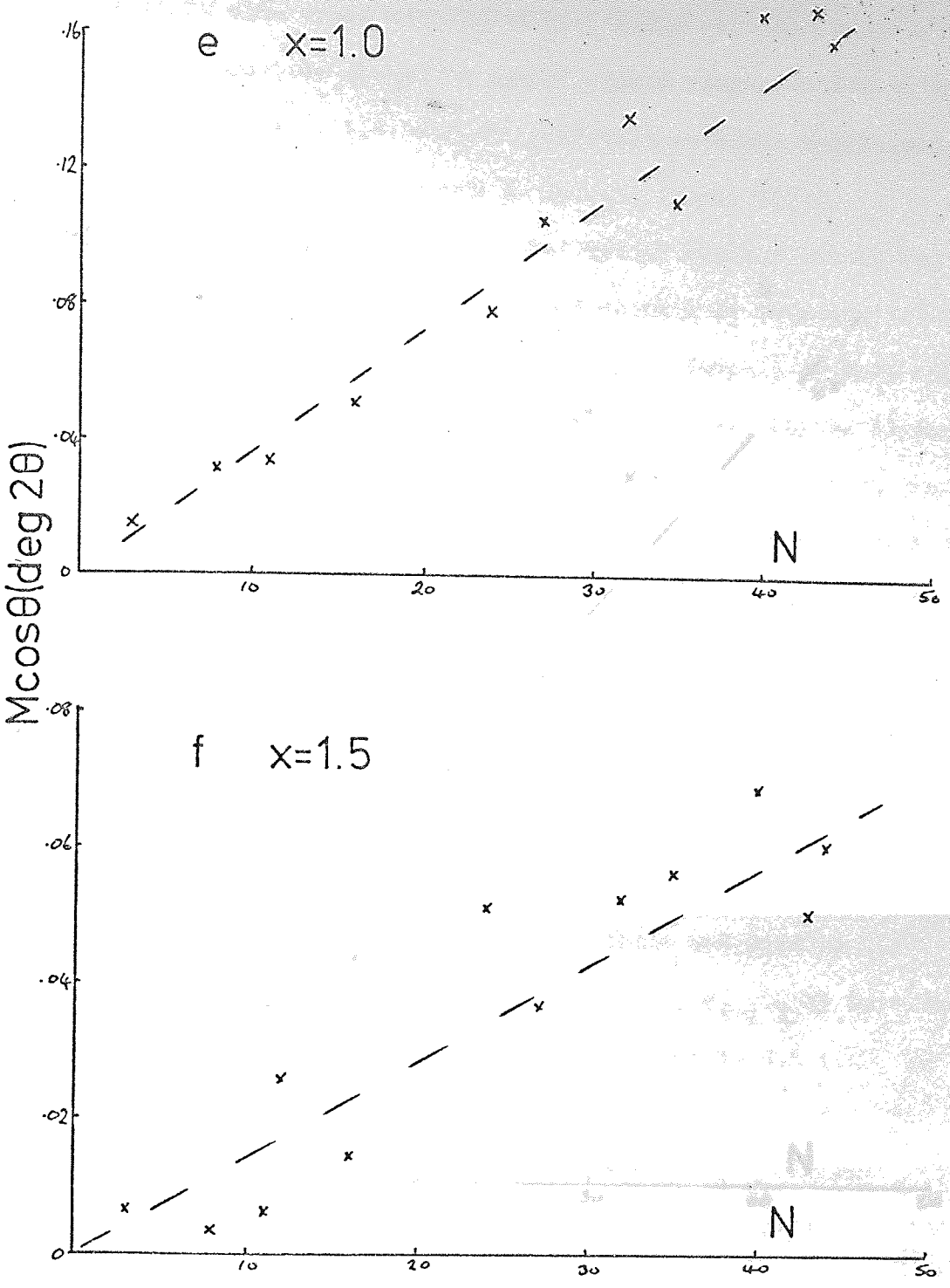

fig. 5.4 Vogel & Hosemann plot for $MgAl_{2-x}Cr_xO_4$

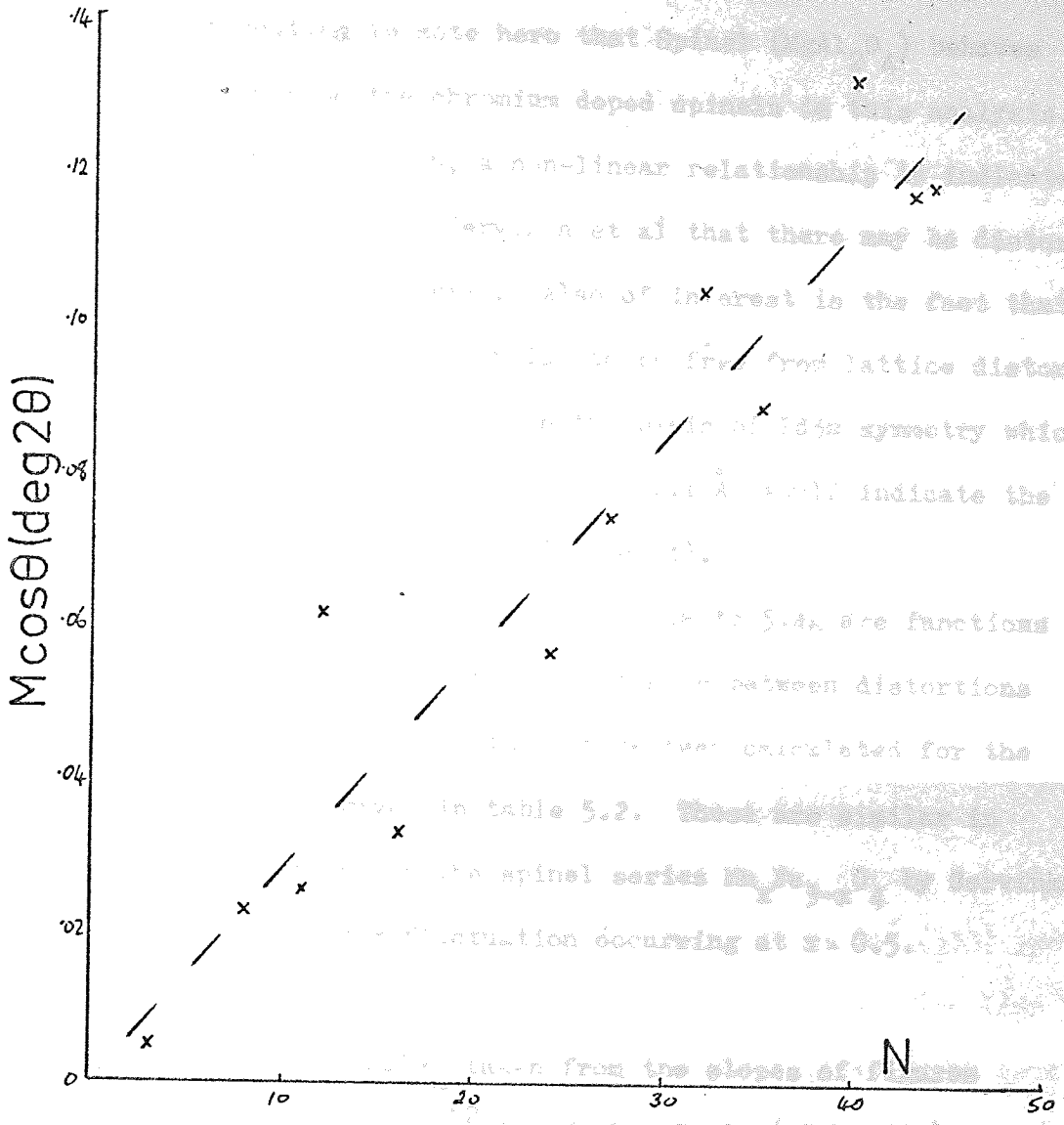

fig.5.4g Vogel&Hosemann plot for $MgAl_2O_4$

i.e. a particle size which would give negligible particle size broadening. The silhouettes showed an almost square cross-section with corners cut off at 45°, i.e. shapes consistent with the octahedral crystal shapes usually encountered in spinels (Bunn, 1961).

It is interesting to note here that Spinel ($MgAl_2O_4$) behaves in a similar manner to the chromium doped spinels in this analysis. In plotting Mcosθ against h, a non-linear relationship is indicated, this suggests, according to Cervinka et al that there may be distortions in the lattice of this material. Also of interest is the fact that $MgCr_2O_4$ appears, from this analysis, to be free from lattice distortions although structure determination on the basis of Fd3m symmetry which leads to the high Debye-Waller factor of 1.1 $\AA^2$ would indicate the presence of some distortions (see Chapter 4).

The slopes of the plots in figures 5.4a to 5.4g are functions of the statistical variation of the distances between distortions (Vogel and Hosemann, 1970) and these have been calculated for the seven samples and are given in table 5.2. These are similar in magnitude to those found in the spinel series $Mn_xFe_{3-x}O_4$ by Cervinka et al (1970), the maximum fluctuation occurring at $x = 0.5$.

Table 5.2 Values of $\Delta^2 x_a$ taken from the slopes of figures 5.4a to 5.4g in $\AA^2$ for $MgAl_{2-x}Cr_xO_4$ ($0 \leqslant x \leqslant 2$)

x	0	0.125	0.25	0.375	0.5	1.0	1.5
$\Delta^2 x_a$ ($\AA^2 \times 10^3$)	1.1	1.0	1.3	3.6	4.9	1.6	0.6

5.3 Variance analysis.

5.3.1 The data and its reduction.

As has been described earlier (Chapter 3) the data for this analysis

was gathered in the form of intensities (number of counts per 10 seconds) at intervals of $0.02^{\circ}2\theta$ across the profile. To give an indication of the extent of the broadening which did occur at the maximum breadth observed, the profiles for the two samples $MgCr_2O_4$ and $MgCr_{0.5}Al_{1.5}O_4$, are shown for the purpose of comparison in figures 3.2a to 3.2k, these being the results observed and fed into the computer for analysis. From these figures it can be seen that the broadening of the mixed spinel specimen lines is very extensive, also to be noted is the increase in general background of the profiles with increasing chromium content.

The computer program described by Hilleard and Webster (1969) was used to analyse this data and to calculate the variation of variance ($W_{2\theta}$) with range of calculation ($\Delta 2\theta$) across a profile and also the corresponding variation of centroid with range. The latter was also used in the lattice parameter calculations in Chapter 4. These variations were calculated assuming different background levels after the method of Langford and Wilson (1963). The optimum background gives a linear region on the $W_{2\theta}$ against $\Delta 2\theta$ plot. Figure 5.5 shows typical curves obtained for $MgAl_{2-x}Cr_xO_4$ ($x = 0.5$) for the (533) profile, of the variance-range plot calculated as outlined above. The line marked A is taken as the optimum background, those lines below show the effect of choosing the background too high, those above show the effect of background too low. In both cases higher order terms in $\Delta 2\theta$ are added to the variance (Langford and Wilson, 1963).

From these results, plots of W against $\Delta 2\theta$ were made and figures 5.6a to 5.6k show those corresponding to the profiles in figures 3.2a to 3.2k.

When these variance-range graphs were first plotted it was noticed that some showed a distinct step part-way along the straight portion, but the cause of this effect was not realised at the time. The

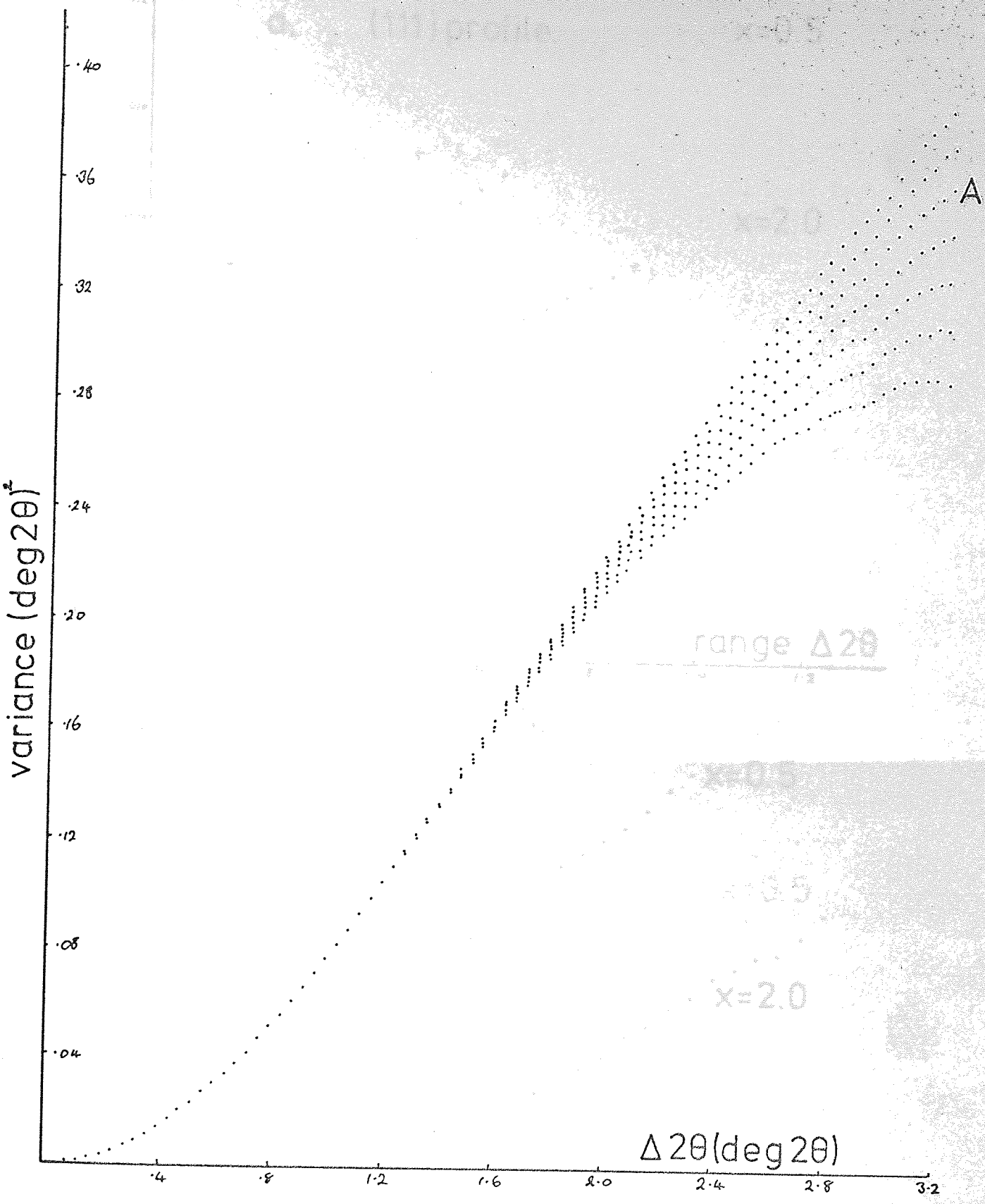

fig 5.5 Variance-range plot for (533) profile

$MgAl_{1.5}Cr_{0.5}O_4$

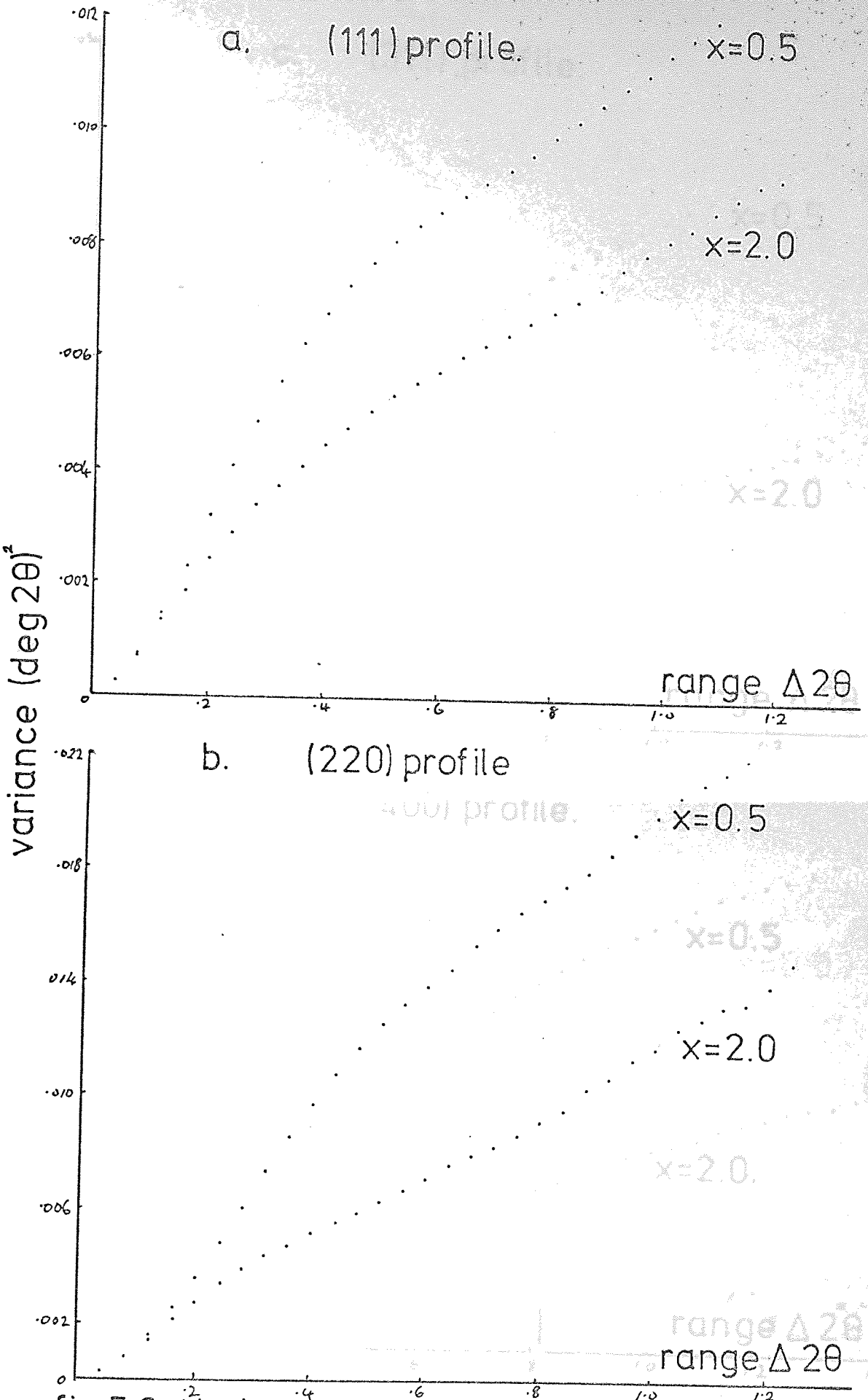

fig.5.6. Variance-range plot for $MgAl_{2-x}Cr_xO_4$.

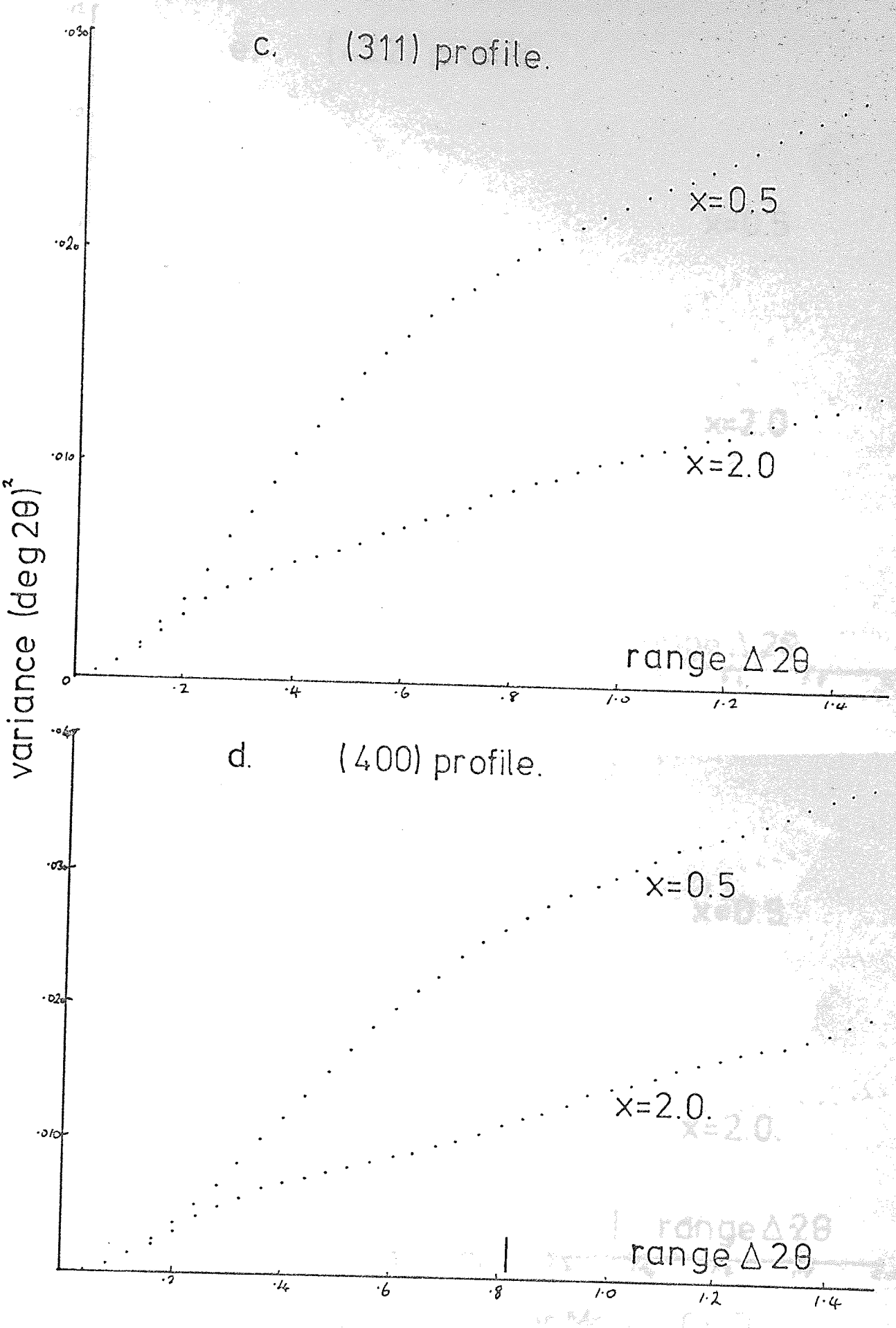

fig.5.6. Variance-range plot for $MgAl_{2-x}Cr_xO_4$.

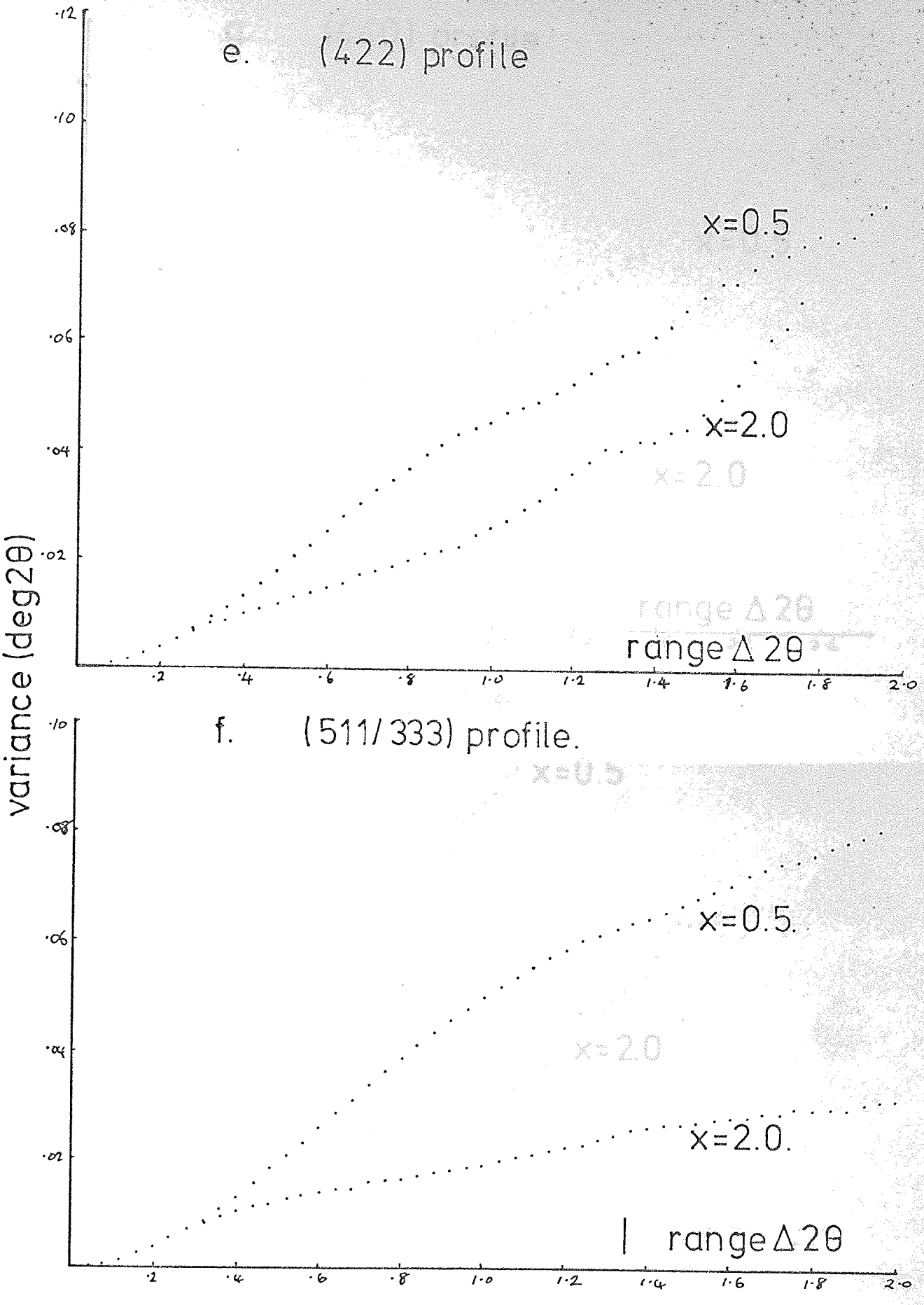

fig. 5.6. Variance-range plot for $MgAl_{2-x}Cr_xO_4$.

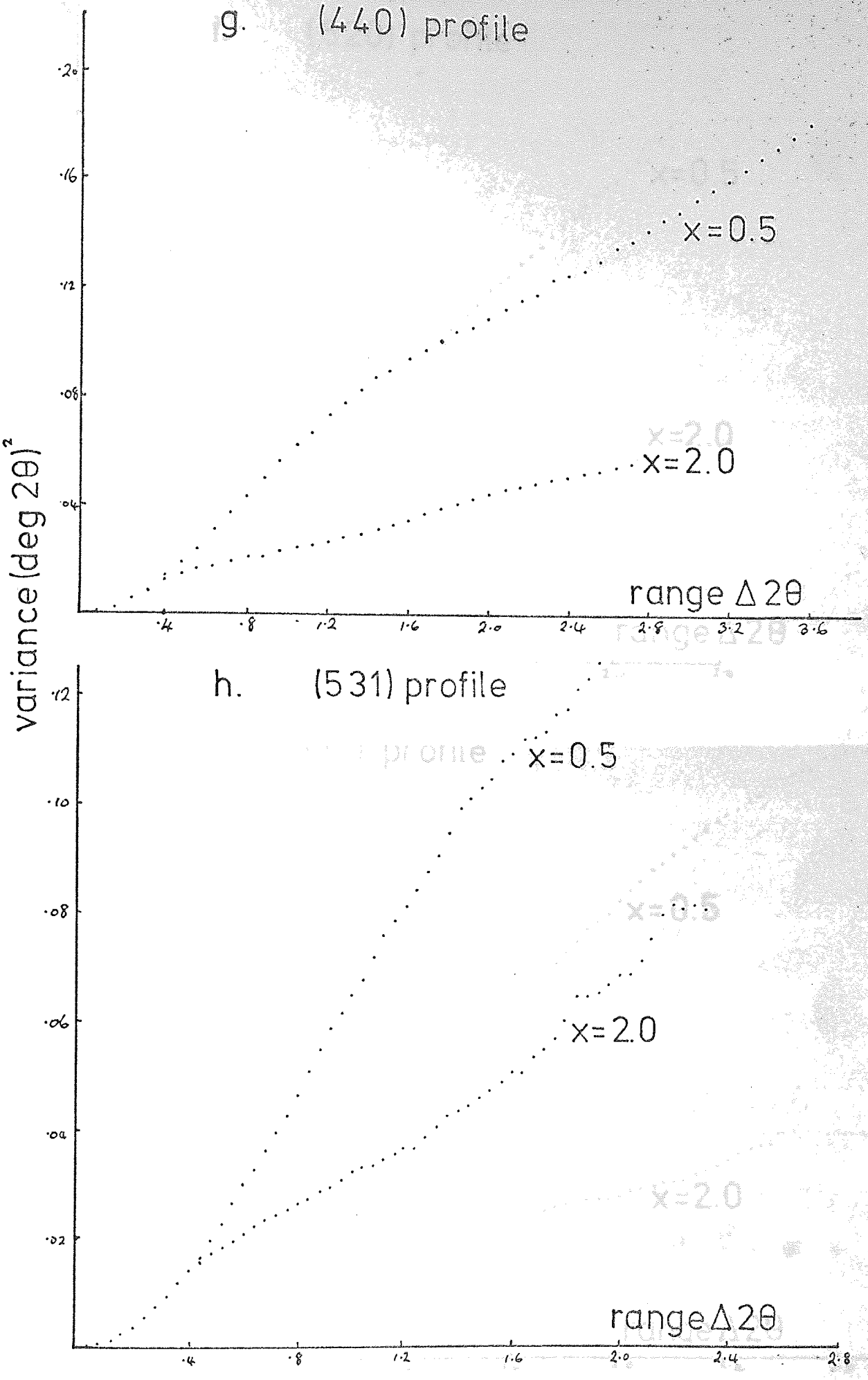

fig.5.6. Variance-range for $MgAl_{2-x}Cr_xO_4$.

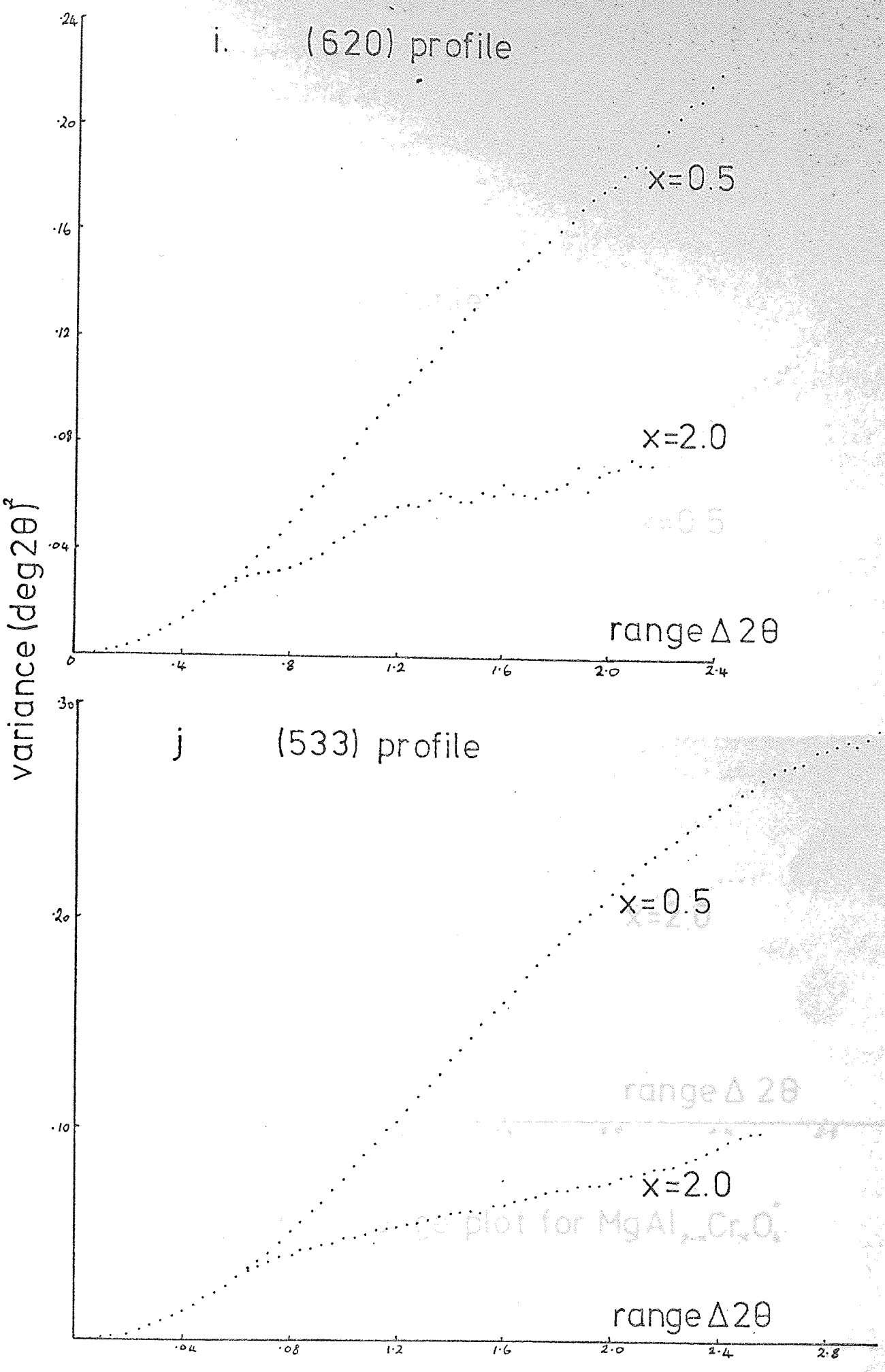

fig.5.6. Variance-range plot for $MgAl_{2-x}Cr_xO_4$.

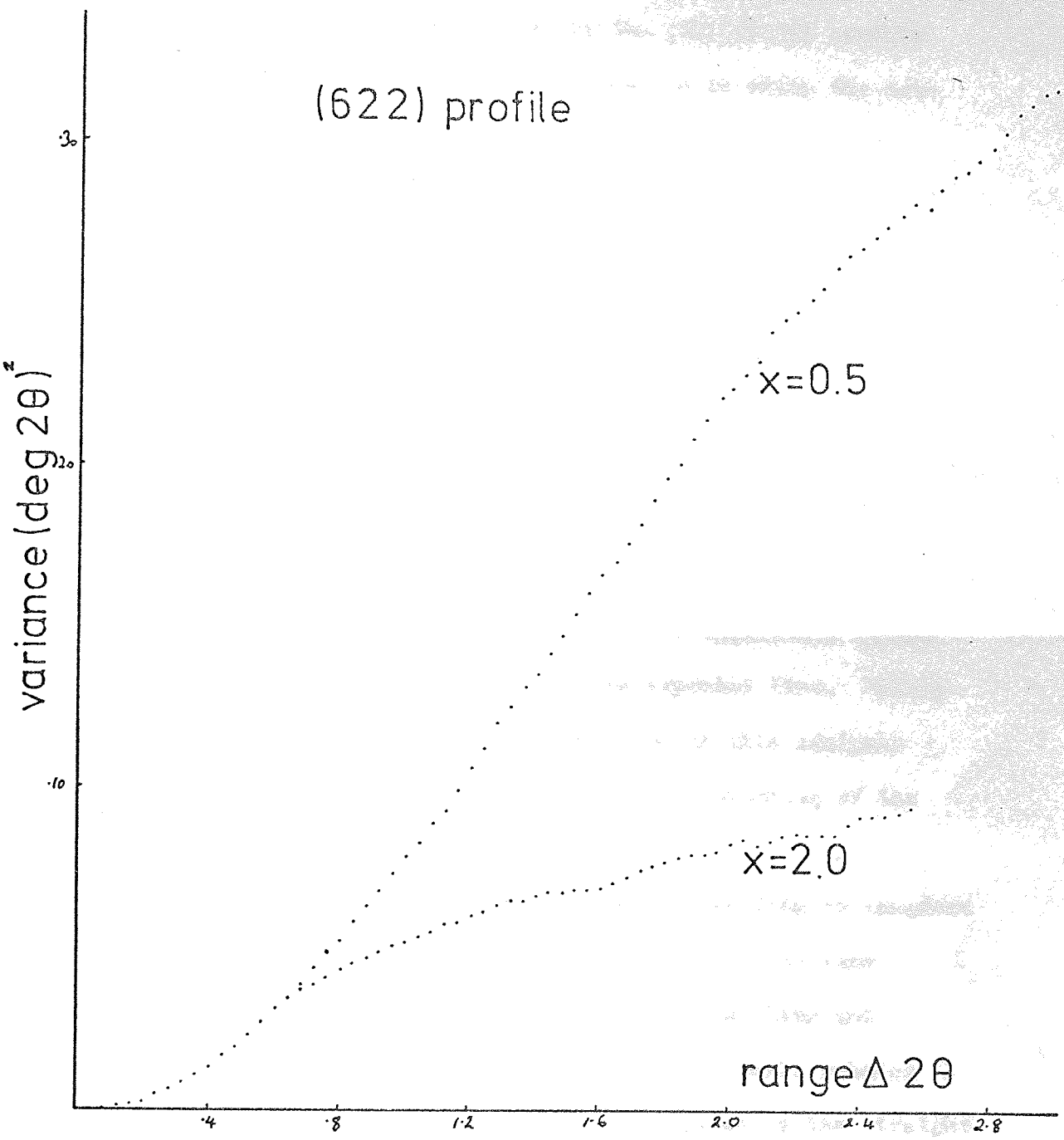

fig.5.6k. Variance-range plot for $MgAl_{2-x}Cr_xO_4$.

phenomenon was subsequently explained by Langford as arising from the presence of satellite lines on the low angle side of the K_α peak. A similar step effect has also been observed when the K_β contribution of a strong higher order line coincides with the tail region of the line under investigation. Figure 3.2f shows the (511)/(333) profile for $MgCr_2O_4$ and the enlarged low angle tail section in which the satellites occur is shown in figure 5.7.

5.3.2 Correction of the variance measurements.

Wilson's theory equating the variance of line profiles to the crystallographic properties of the substance (1961,1962 and 1963) suggests that the variance of the line profile is a linear function of the range over which the variance is calculated. However the variance slope and intercept of such a plot from a real profile have to be corrected for the effect of truncation of the profile. This is necessary in the calculation of the variance as it causes the apparently linear portion of the plot to become asymptotic to the expected line. Cheary (1971) has given a detailed theoretical discussion of this analysis and has indicated the effect of various degrees of broadening of the line profile on the variance slopes and intercepts.

For instance a variance-range plot calculated according to Langford and Wilson (1963) may have the appearance shown by the solid line in figure 5.8. The correct slope is given by the dotted line and the observed line becomes asymptotic to it and theoretically reaches it at infinite range. Now the slope and intercept given by the straight portion of the solid line would not be the true values, the slope would be too large and the intercept too low.

A further complication is introduced by the presence of the satellites as described above. A step is introduced into the linear portion of the characteristic and the line becomes asymptotic to a line whose

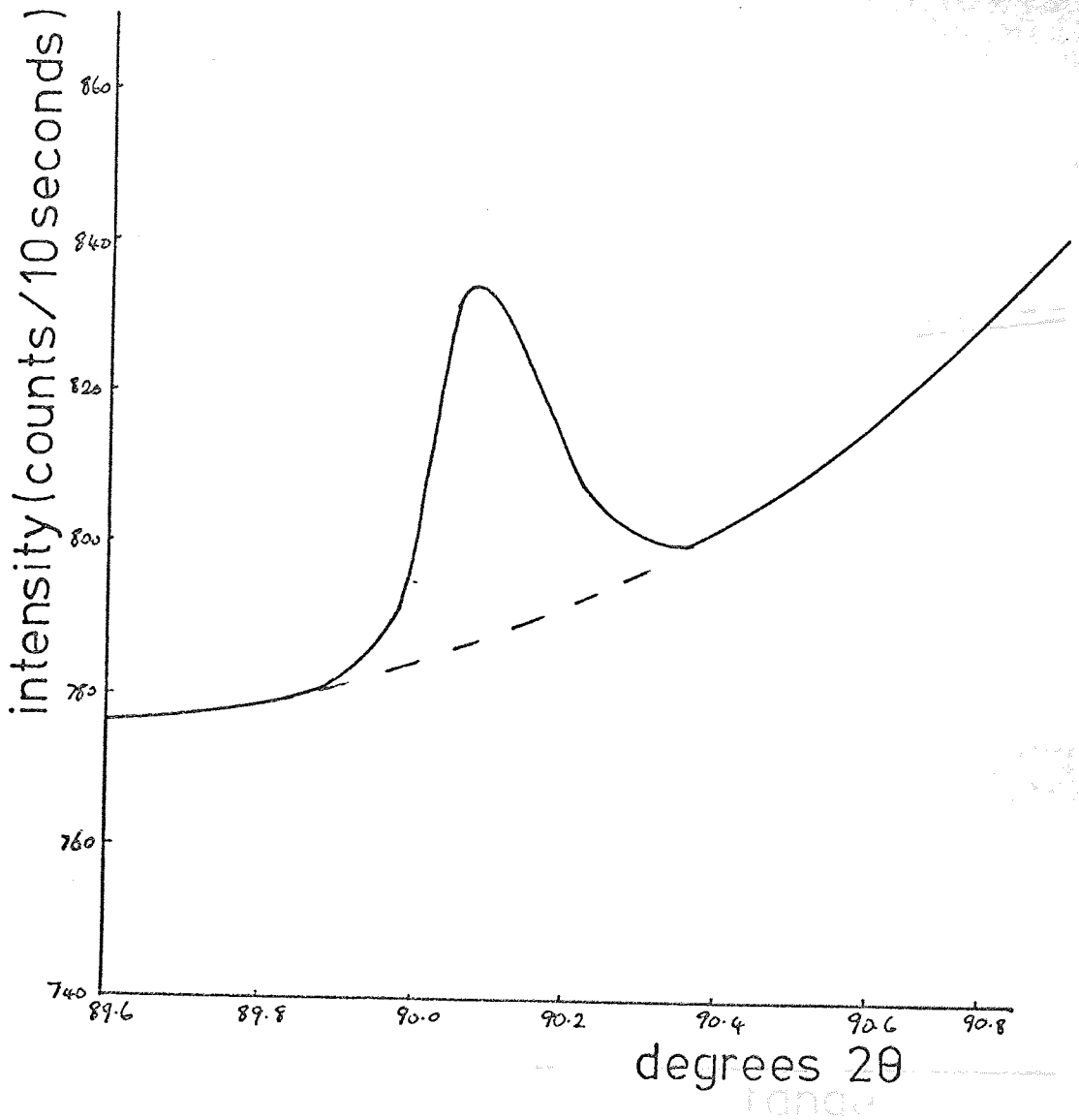

fig. 5.7 Low angle tail of the (511/333) profile of $MgCr_2O_4$ showing the presence of satellites.

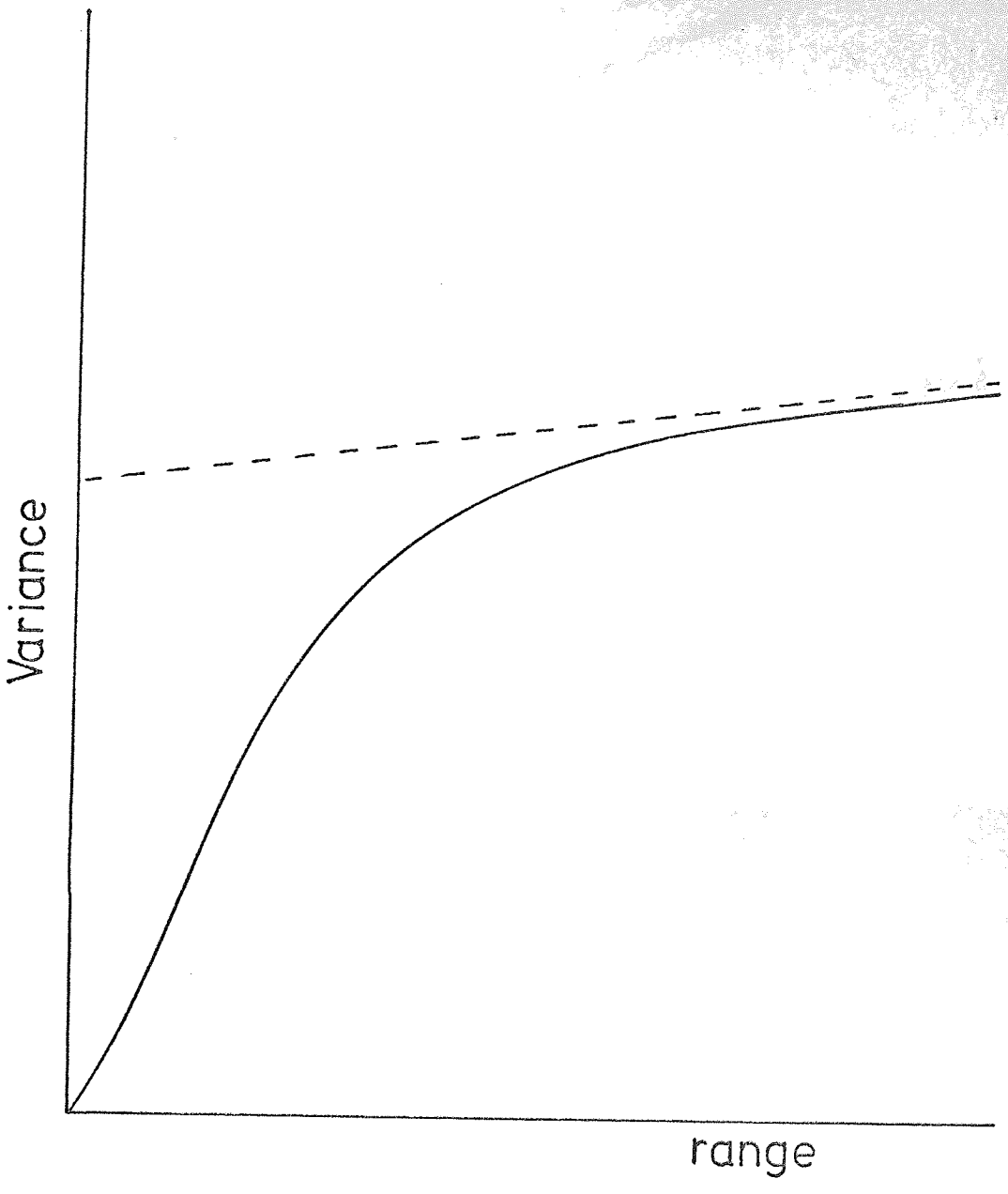

fig. 5.8. Indication of the effect of truncation on the variance calculation.

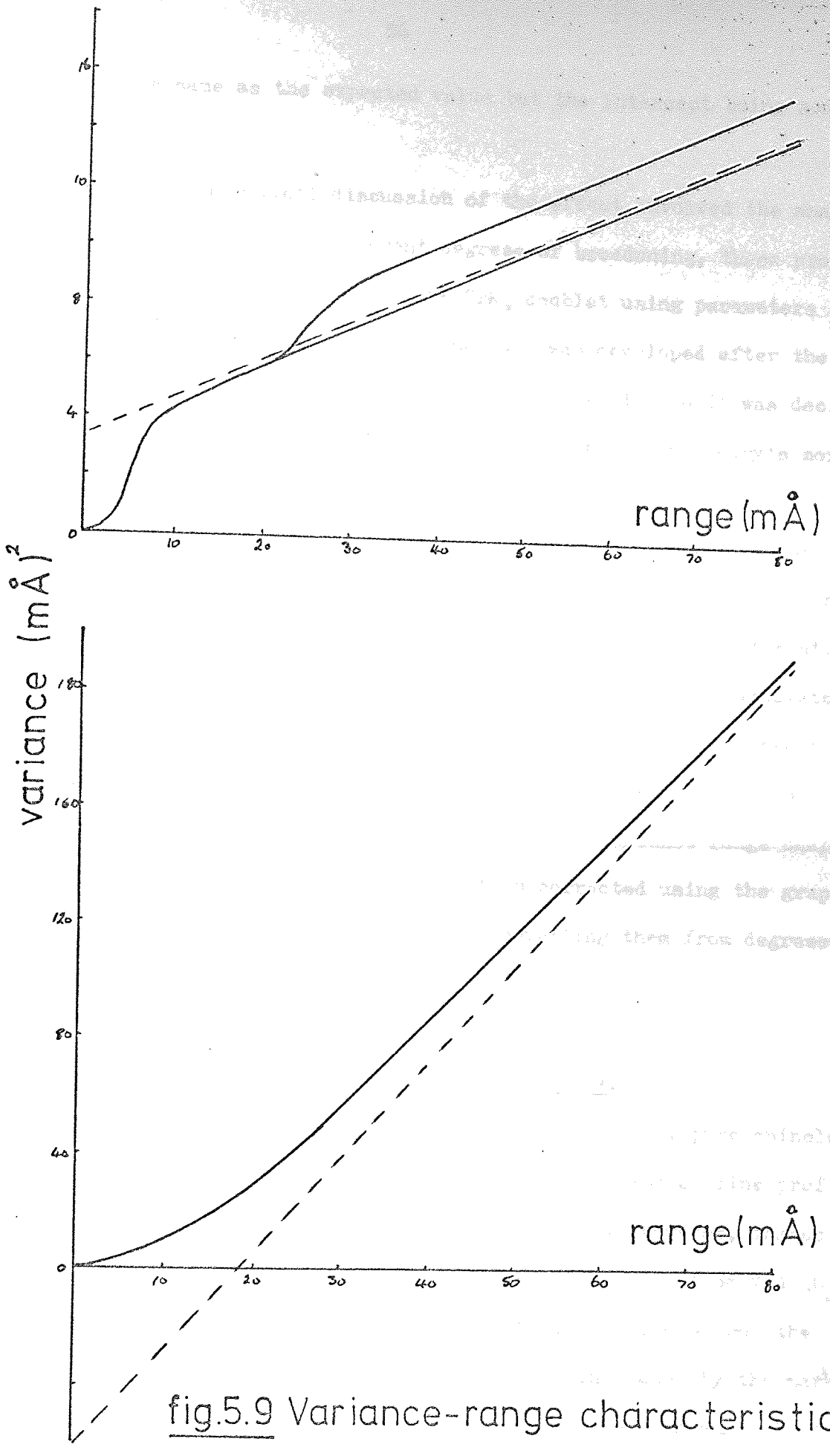

fig.5.9 Variance-range characteristics for profiles shown in fig.3.5.

slope is the same as the expected value but the intercept being somewhat higher.

Cheary's theoretical discussion of the effect involved the analysis of simulated profiles of different degrees of broadening, these profiles being simulated Cauchy curves of the CrK_α doublet using parameters described by Parratt (1936). This analysis was developed after the data for this study had been collected and analysed. So it was decided to correct these results by a graphical method based on Cheary's more rigorous calculations.

Figure 5.9a and b are the variance range plots calculated for the simulated profiles shown in figures 3.5a and b. The dotted lines indicate these calculated values. The straight portions of the characteristics indicate slopes and intercepts slightly different to those calculated. A graphical relationship was drawn up of the calculated value against the apparent value of slope and intercept from these simulated profiles. The values of slope and intercept taken from the variance-range characteristics of the spinel profiles were then corrected using the graphical relationship described above after converting them from degrees 2θ to mÅ.

5.3.3 Choice of reference sample and its analysis.

Of the eight specimens prepared, two were nominally pure spinels, i.e. $MgAl_2O_4$ and $MgCr_2O_4$, and would be expected to produce line profiles which were subject to instrumental broadening only. However, inspection of the profiles from the two materials showed that those from $MgAl_2O_4$ were substantially broader than those from $MgCr_2O_4$. Those from the latter material were in fact extremely sharp as indicated by the marked resolution of the $\alpha_1 - \alpha_2$ doublet in the medium to high angle lines. On the other hand, $MgAl_2O_4$ has been reported as partially inversed (Bacon, 1952),(Stoll et al,1964) and it seemed possible that this inversion could lead to extra breadth in its lines (however, see Chapter 6).

Wilson (1963a) has analysed the effects of instrumental broadening upon the variance and predicts that the slope and intercept contributions dependent on the angle of diffraction cause these values to increase regularly with increase of angle of diffraction. The angular variation of the intercept function has been confirmed by Langford (1968a) in an analysis of profiles from annealed nickel while Cheary (1971) found good agreement with the predicted angular variations of both slope and intercept using lithium ferrite.

The reference material for the present experiments was chosen to be $MgCr_2O_4$ because of the difficulties with $MgAl_2O_4$ described above. Additional evidence of its suitability was sought by plotting the slopes and intercepts of the variance-range characteristics against 2θ to test them against Wilson's theory. Figure 5.10 shows an angular variation similar to that predicted by the theory although these show some deviations from the smooth curves which may be attributed to experimental errors. The expected result being a smooth variation, the values of slope and intercept for the reference specimen profiles were taken from the smooth curves in figure 5.10. The profile data for $MgCr_2O_4$ and the values taken from the smooth variation with 2θ in figure 5.10 are listed in table 5.3

5.3.4 A note on the selection of background level.

The intensity data were analysed to produce variance-range curves for various assumed levels of background. Inspection of these curves indicated that over a range of background levels it was difficult to choose the correct background owing to the fact that the curves appeared equally linear over the required range from the 'knee', figure 5.9, to the step due to the presence of the satellite lines. To overcome this problem it was decided to take the data from each of the linear portions and perform a least squares analysis on these to calculate the slope

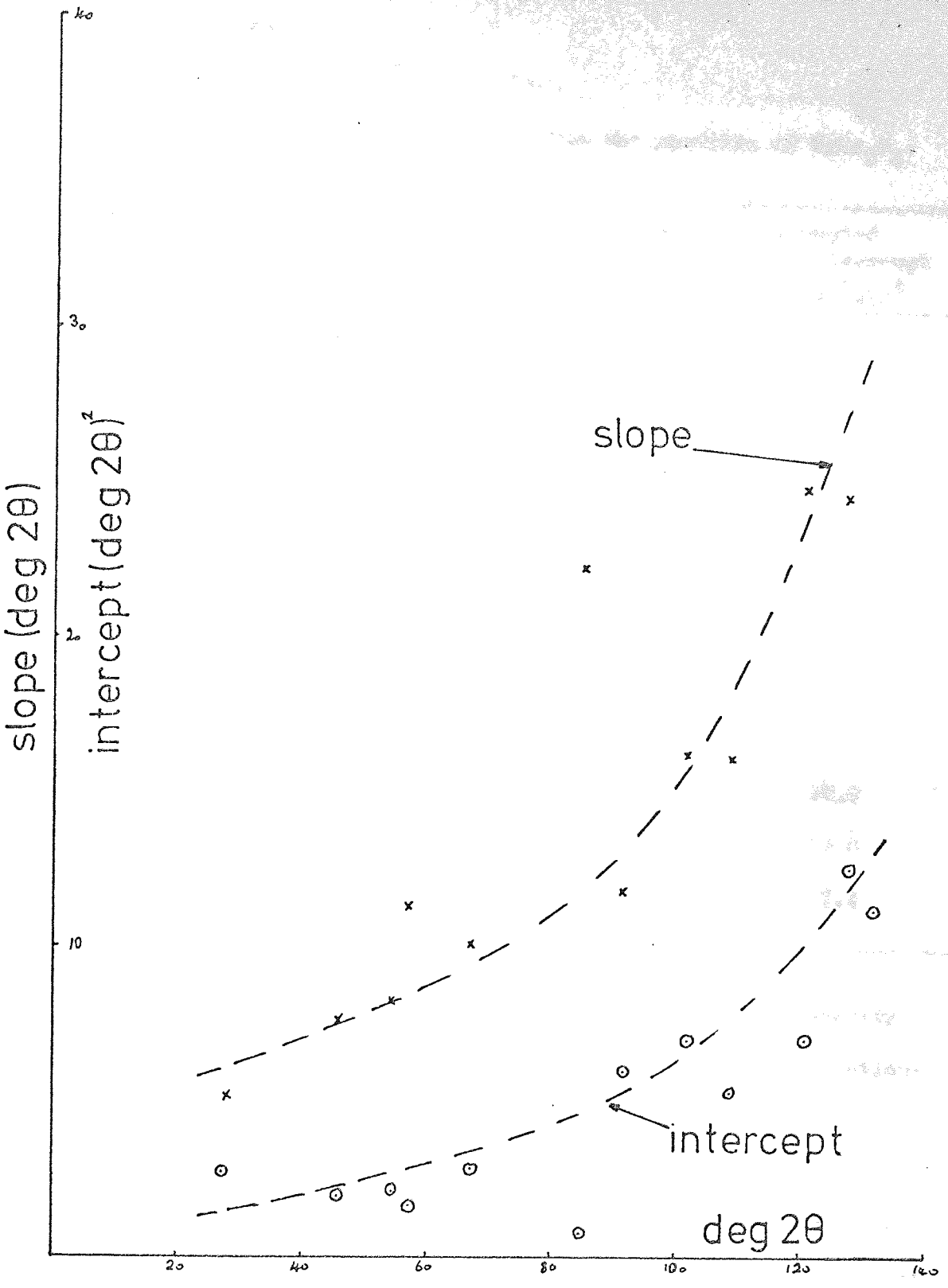

fig. 5.10. Variation of slope & intercept with Bragg angle for profiles of $MgCr_2O_4$

and intercept for each set of data and also to calculate the correlation coefficient in each case.

Table 5.3 Slopes and intercepts obtained from the profiles of $MgCr_2O_4$.

hkl	Slope $\Delta 2\theta \times 10^3$	Intercept $(\Delta 2\theta)^2 \times 10^3$	corrected slope $\Delta 2\theta \times 10^3$	corrected intercept $(\Delta 2\theta)^2 \times 10^3$
111	5.2	2.7	5.8	1.2
220	7.6	2.0	7.6	2.0
311	8.2	2.1	8.3	2.5
222	11.3	1.7	8.3	2.7
400	10.1	2.9	9.4	3.3
422	22.3	0.8	11.8	4.6
511/333	11.8	6.0	12.8	5.2
440	16.3	7.0	16.3	6.2
531	16.2	5.3	18.0	7.4
620	24.9	7.0	23.8	10.0
533	24.6	12.5	27.4	12.0
622	41.4	11.2	29.0	12.4

The correlation coefficient was used as a measure of the linearity of the data. This was considered valid in this analysis as the relationship being investigated, i.e. $W_{2\theta}$ against $\Delta 2\theta$, was a linear one over the range considered and the higher the value of r the better the linearity of the data. Thus for each profile analysed, for each assumed background level, a value of slope, intercept and correlation coefficient (r) was calculated.

A plot was made of the correlation coefficient against the background level used in the varianced calculation. Provided the background levels were chosen carefully, this plot gave a value of background at

which r was a maximum, typically r had a value of 0.999 and better. This value of background was taken as the optimum value. Plots of slope and intercept against background could be used to interpolate for those values corresponding to the optimum background level (see figure 5.11). This method of choice of background was similar to that used by Langford and Wilson (1963) in their analysis of profiles from aluminium and nickel samples.

5.3.5 Calculation of residual slopes and intercepts for the chromium doped spinels.

The intensity data for the remaining Cr^{3+} doped spinels were analysed in a similar manner to that decided for the reference sample.

Theoretically, the variance of a diffraction line is derived in terms of the reciprocal space vector s. Experimentally the variance is measured in degrees 2θ and then converted to the variance in s by multiplying by the angular factor $\cos^2\theta / \lambda^2$ (Wilson, 1963).

In the case of particle size analyses reported so far the reference specimens were chemically identical with the test specimens and the corresponding lines occur at the same Bragg angle, thus the conversion factor is the same for each sample, and the difference between the variances of the reference specimen and the broadened sample may be calculated before conversion. In this study however the reference and test specimens are chemically different and corresponding lines are displaced from each other owing to the differences in the lattice constants, i.e. 8.101 Å for the specimen in which x = 0.125 and 8.333 Å for $MgCr_2O_4$, the parameters for the remaining samples depending on the Cr^{3+} content. It was therefore necessary to convert both reference and broadened variances to 's' before the residual slopes and intercepts were calculated as the angular factor varied from sample to sample for corresponding profiles. These values are listed below in tables

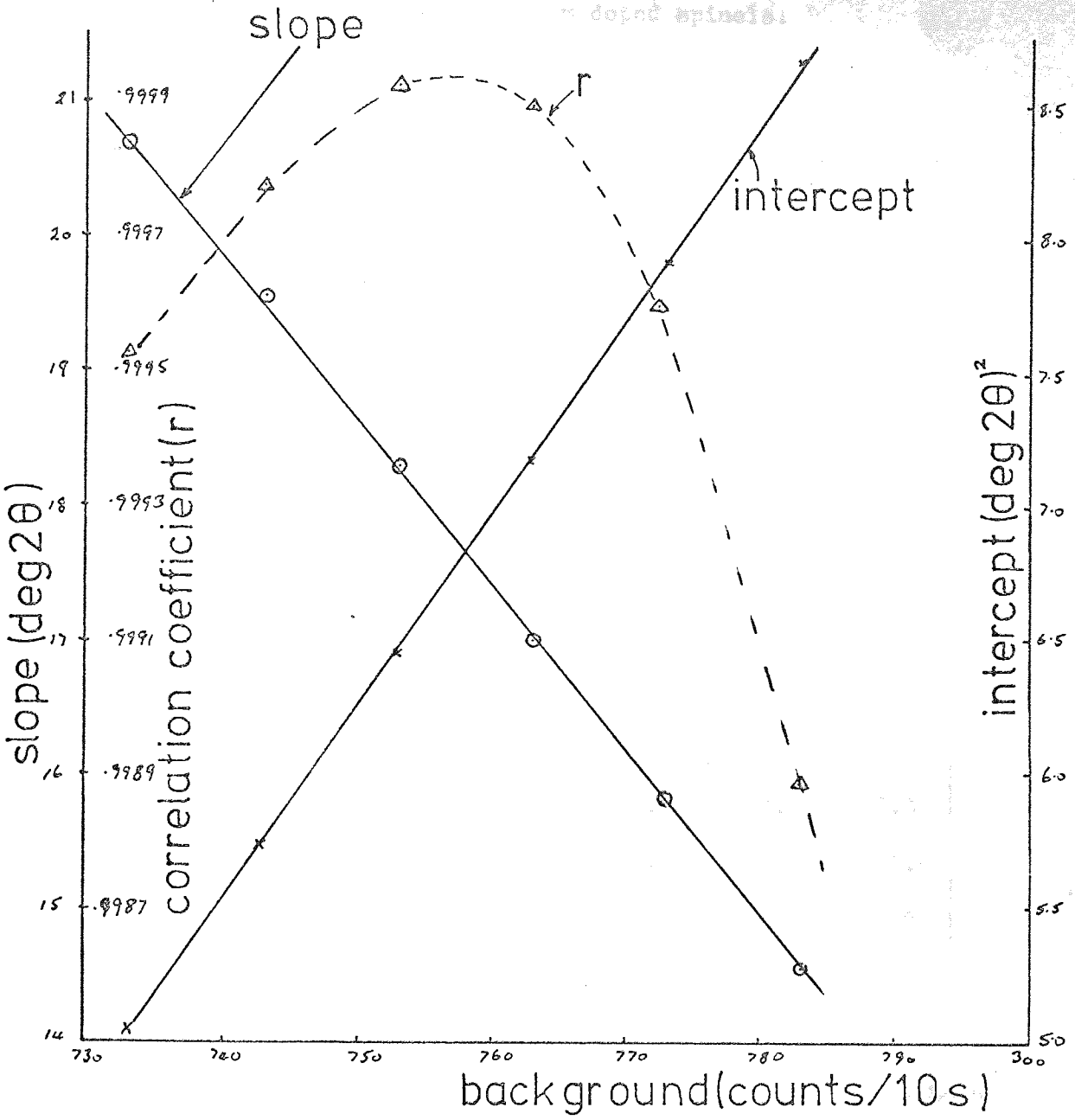

fig.5.11. Selection of optimum background level. (440 profile $MgAlCr_2O_4$).

5.4 and 5.5.

Table 5.4 Residual slopes of the chromium doped spinels.
units $\text{Å}^{-1}_{x10^4}$

hkl \ x	0.125	0.25	0.375	0.5	1.0	1.5
111	2.7	0.9	4.1	1.6	0.3	1.0
220	4.0	3.8	4.1	11.9	8.3	0.7
311	3.2	1.5	2.7	5.0	2.4	0.3
222	13.1	35.8	-	-	-	15.2
400	3.7	3.2	9.8	10.0	1.2	1.7
422	5.7	6.3	22.4	22.0	10.7	13.6
511/333	5.6	3.1	24.0	35.2	5.9	0.4
440	1.0	2.2	11.9	20.8	6.2	1.9
531	17.4	15.2	15.4	40.4	19.8	10.9
620	11.3	20.6	45.7	53.2	14.6	8.3
533	9.3	6.9	35.5	51.8	13.6	12.9
622	18.6	26.7	27.8	47.5	15.5	7.8

5.4 Discussion of the variance results.

The results given in table 5.5 show that the intercept takes both positive and negative values. This variation in sign eliminates particle size broadening effects as this is predicted by Wilson to produce negative values only.

Strain effects, when small, produce a contribution to the variance intercept only. Inspection of table 5.4 indicates the slope values for all specimens to change as well as the intercept. Thus the cause of broadening in these samples probably arises from effects other than strain only.

Table 5.5 Residual intercepts of Cr^{3+} doped spinels.
units $\mathring{A}^{-2} \times 10^{6}$

x / hkl	0.125	0.25	0.375	0.5	1.0	1.5
111	2.2	3.2	2.6	7.1	4.1	2.1
220	-0.7	-0.6	1.5	1.9	-2.1	-0.4
311	-1.9	0.8	7.3	12.0	0.6	-0.1
222	-3.8	-10.8	-	-	-	-3.8
400	-0.2	1.0	1.5	11.9	2.2	-0.5
422	0.3	1.4	-2.8	6.7	-0.3	-3.3
511/333	0.9	3.7	0.4	-3.8	2.0	1.6
440	4.2	4.0	4.1	14.0	2.6	1.4
531	-4.7	1.1	1.6	-11.9	-4.7	-1.8
620	-1.7	-4.8	-19.5	20.2	-1.5	-0.3
533	0.5	3.7	-12.3	-16.4	-0.2	-0.4
622	-3.5	-7.3	-6.0	-15.8	-3.5	0.6

The contribution due to strain only is a term which is proportional to the square of the tangent of the angle of diffraction, thus it becomes large at high angles. In the case of a specimen containing particle size plus strain, the contribution due to particle size changes as $\sec^2\theta$, which at the higher angles varies in a very similar manner to that of $\tan^2\theta$ but with opposite sign, thus with the presence of particle size and strain the intercept term contributions tend to cancel each other. The slope term increases as $\sec\theta$ i.e. a smooth variation with angle of diffraction. Inspection of table 5.4 shows that the slope values for all specimens do not show this smooth variation.

The conclusion to be drawn from these observations is that the origin of the broadening in these chromium doped spinels is not due

to particle size, strain or a combination of the two. The remaining source of broadening to be considered is mistakes.

Wilson (1963) has shown that the variance of a line profile, corrected for the various constants, from a sample containing a mistake structure is

$$W = \left[\frac{J_s - J_a}{TJ_s}\right] \Delta s + \left[\frac{2J_a - J_n - J_s}{TJ_s}\right] Q'(0) \quad \ldots.5.2$$

The symbols have already been defined in section 2.3.3.3. Equation 5.2 does not explicity give the mistake structure; in practice a model must be assumed, values of J_a, J_s and J_n calculated according to this model and substituted into the equation. This must then be compared with the results obtained from experiment. The difficulty in this study was that no clue was provided by the experimental results which could lead to possible models for the mistake structure, unlike other studies of this kind for instance in Cu_3Au in which superlattice lines occur, or stacking fault studies in Co in which lines of the type (001) are unaffected. In the case of mistakes occurring at random it can be shown (e.g. Grimes, 1968) that equation 5.2 reduces to

$$W = \left[\frac{J_s - J_a}{TJ_s}\right] \Delta s - \left[\frac{J_s - J_a}{TJ_s}\right]^2 \quad \ldots\ldots\ldots 5.3$$

Thus the intercepts given in this case are all negative. Further there is a direct relationship between the slope and intercept of this expression such that a plot of the slope against the square root of the intercept would give a straight line of unit slope through the origin. The values listed in tables 5.4 and 5.5 show the intercepts to take both positive and negative values, and although the slope has a similar value to $(\,|\text{intercept}|\,)^{\frac{1}{2}}$, a plot of these gives a very wide scatter of points about the expected 45° line. Figure 5.12 is a typical plot for $MgCrAlO_4$ showing in fact that in some instances

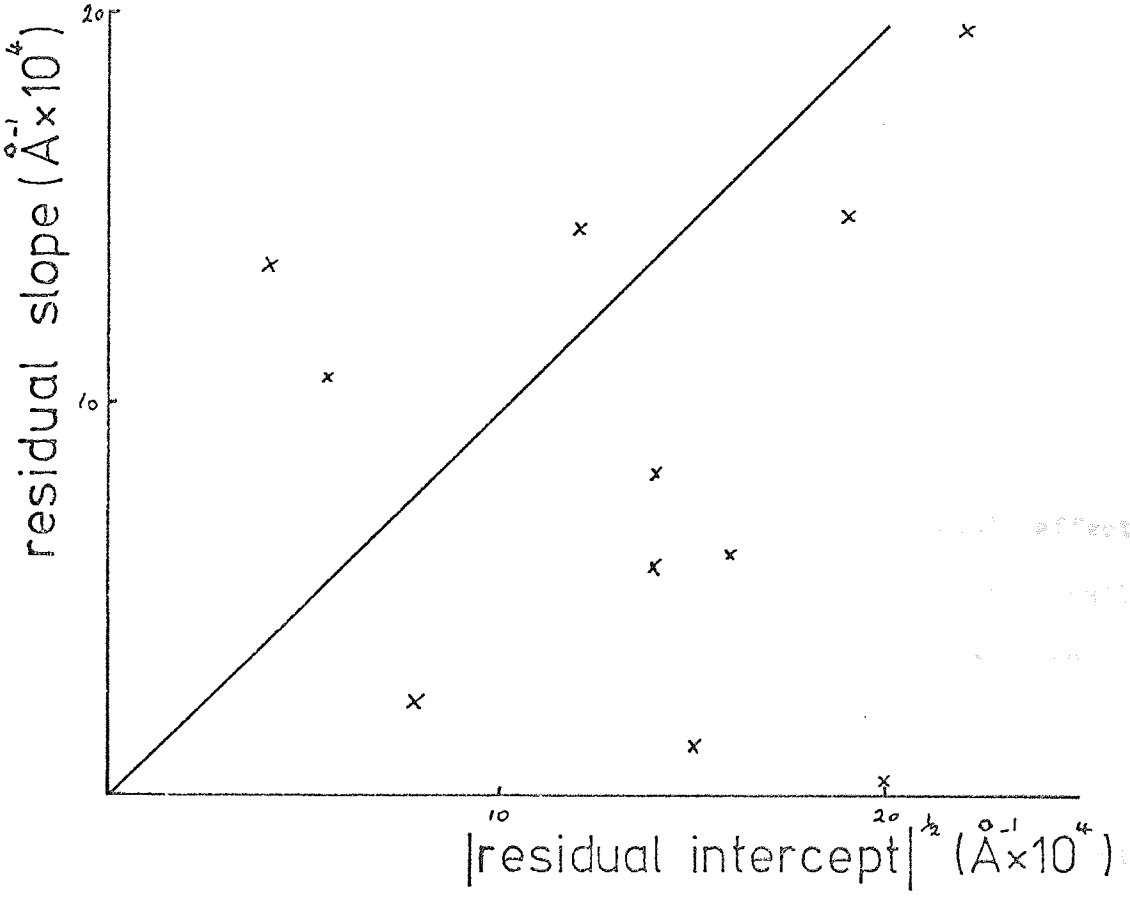

fig5.12. Slope vs $|\text{intercept}|^{1/2}$ - typical results for specimen $MgAlCrO_4$.

there is an order of magnitude or more difference between the two quantities.

Equation 5.2 may be rewritten in the form

$$W \simeq \left[\frac{J_s - J_a}{TJ_s}\right] \Delta s - \left[\frac{J_a - J_n}{TJ_s} - \frac{J_s - J_a}{TJ_s}\right] Q'(0)$$

Thus the intercept is of the form

$$(P - \text{slope}) \cdot Q'(0)$$

where $Q'(0)$ is always positive.

If P is positive and larger than the slope, which is also positive, the intercept will have a positive value. Because of the relationship between slope and intercept given above, the intercept will have a magnitude which will decrease as the slope increases and vice versa, i.e. the value of the intercept will reflect the variation of the slope in going from one profile to the next provided it can be assumed that P changes at a slower rate than the slope. Thus if the slope changes value from one diffraction line to the next, this change could affect the intercept value of that line. This effect may be shown graphically and figures 5.13a to 5.13f show these plots for the chromium doped spinels in this study.

The slope and intercept data are plotted on convenient scales to show the variation of slope and intercept as the order of 'reflection' increases. The 'mirror' effect occurs in all cases which tends to confirm that these materials possess a mistake structure of some kind.

The scales used in figures 5.13a to 5.13f to show the mirror effect are of different orders of magnitude, and it seems that this difference must be connected with the value of $Q'(0)$. In each case the difference in order of magnitude of the values of slope and intercept is of the order of 1/100. The magnitude of $\frac{J_a - J_n}{TJ_s}$ and $\frac{J_s - J_a}{TJ_s}$ are probably of the same order, the difference in the sizes of slopes and

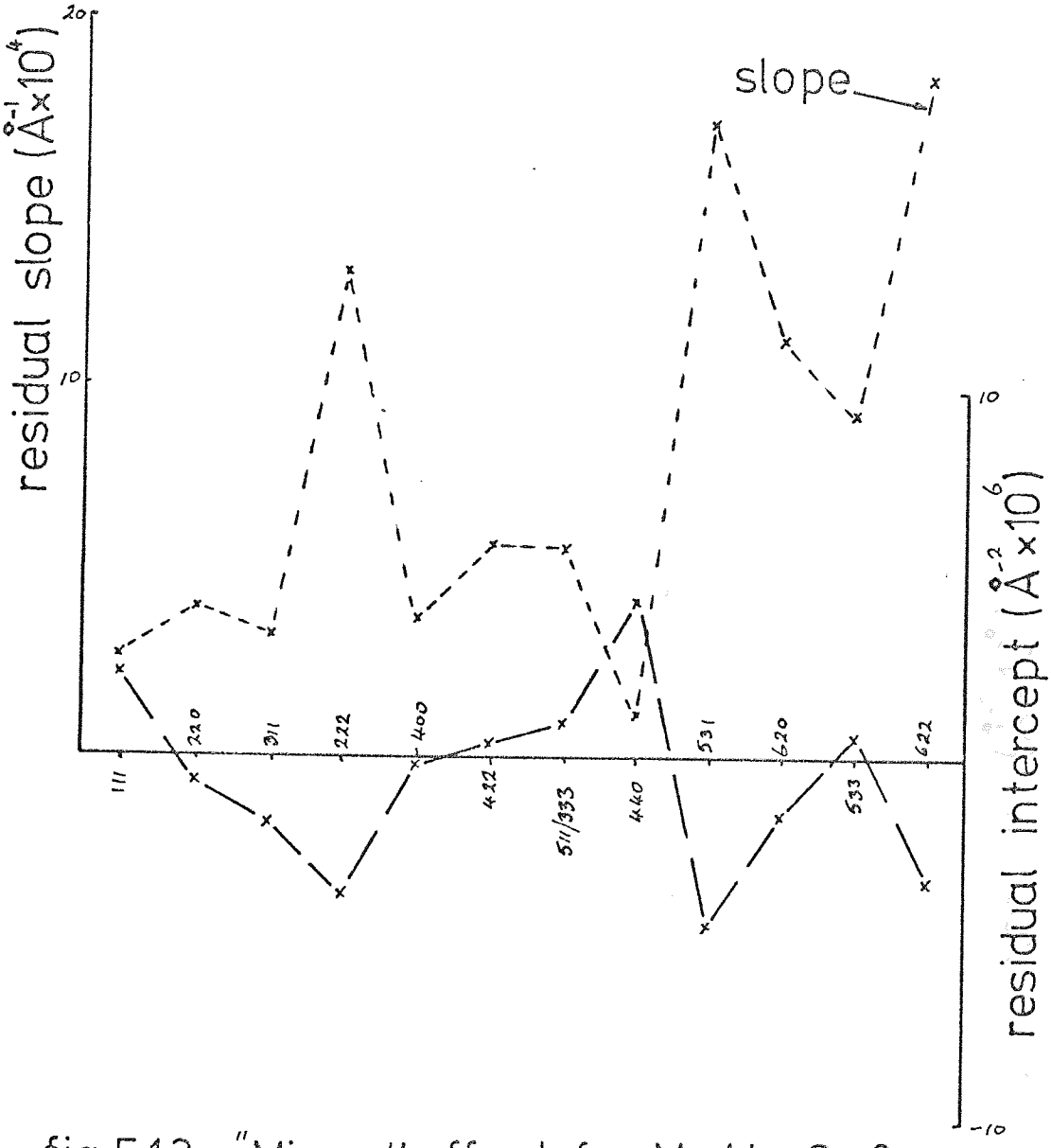

fig.5.13.a "Mirror" effect for $MgAl_{2-x}Cr_xO_4$
x=0.125.

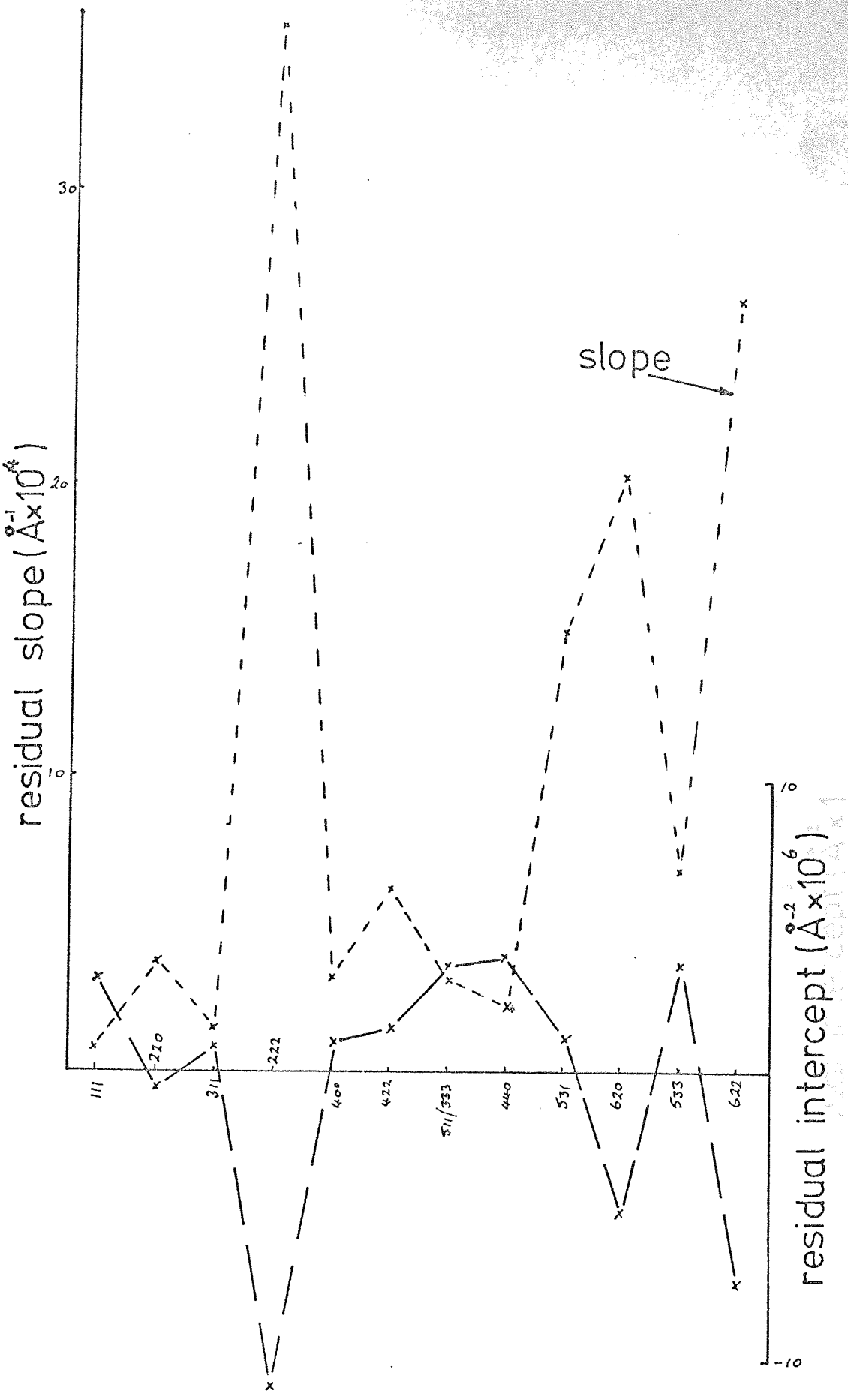

fig.5.13b "Mirror" effect for $MgAl_{2-x}Cr_xO_4$
$x = 0.25$.

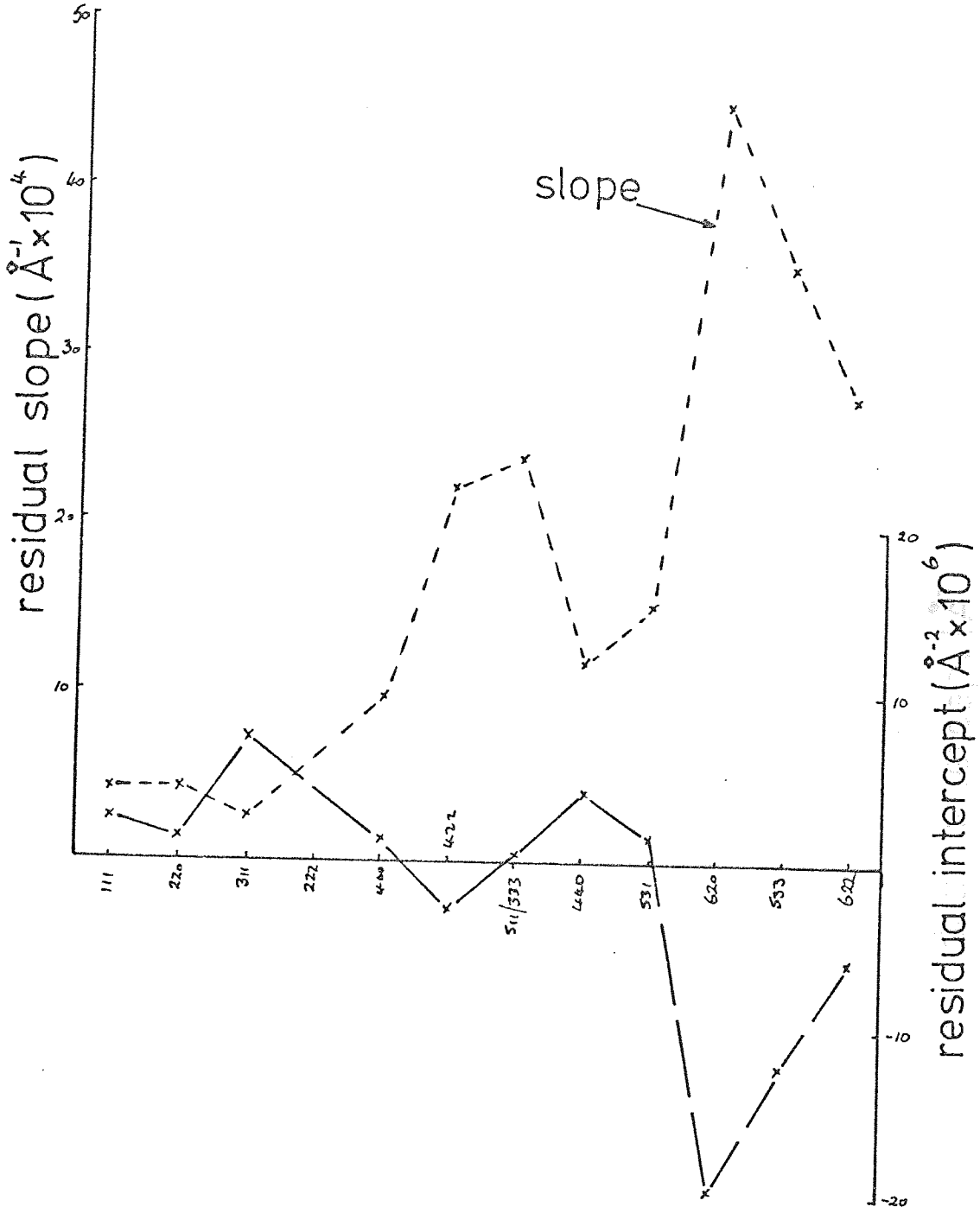

fig. 5.13c. Mirror'' effect for $MgAl_{2-x}Cr_xO_4$ x = 0.375.

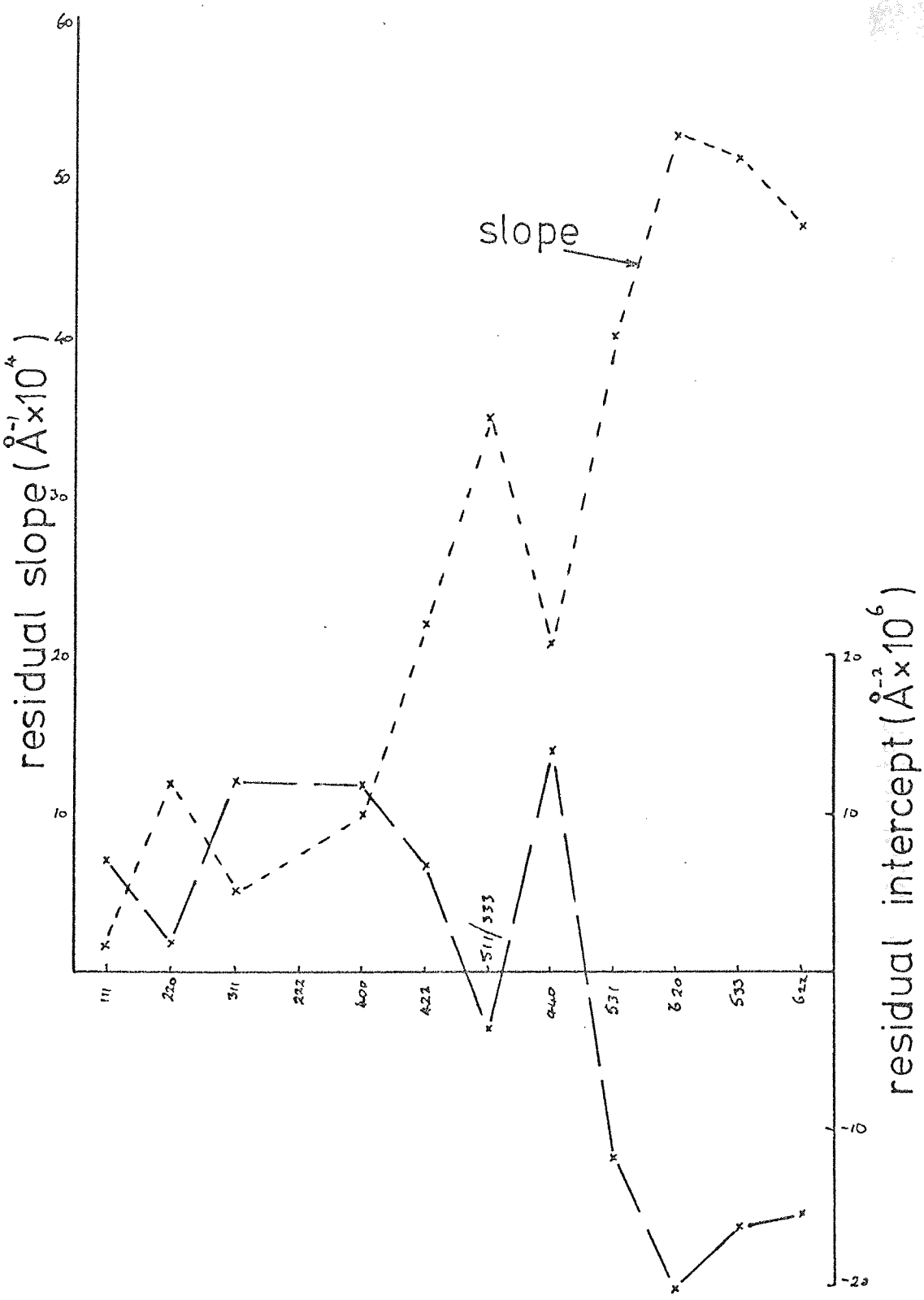

fig. 5.13d. "Mirror" effect for $MgAl_{2-x}Cr_xO_4$ x = 0.5.

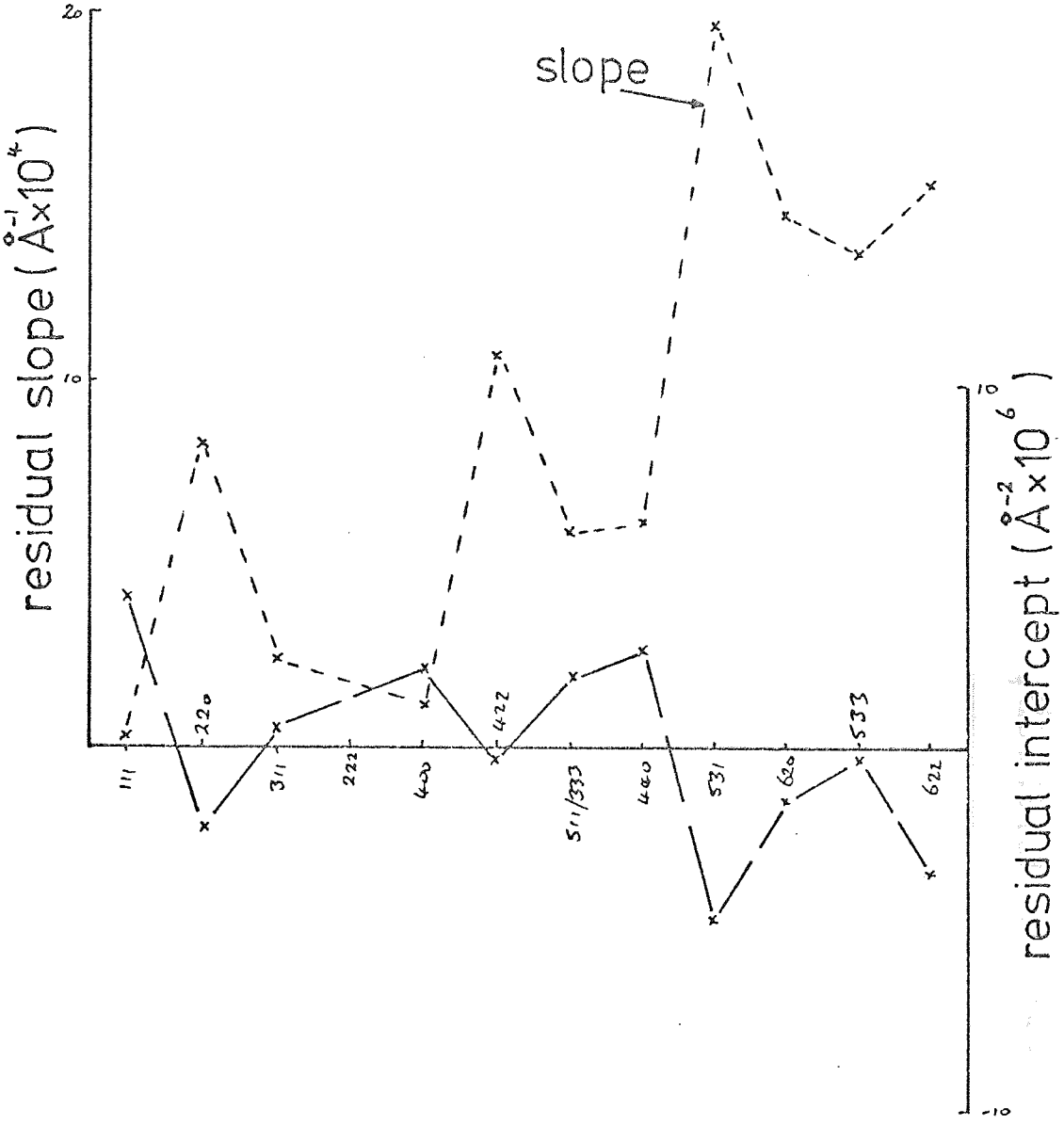

fig. 5.13e. Mirror" effect for $MgAl_{2-x}Cr_xO_4$ x=1.0.

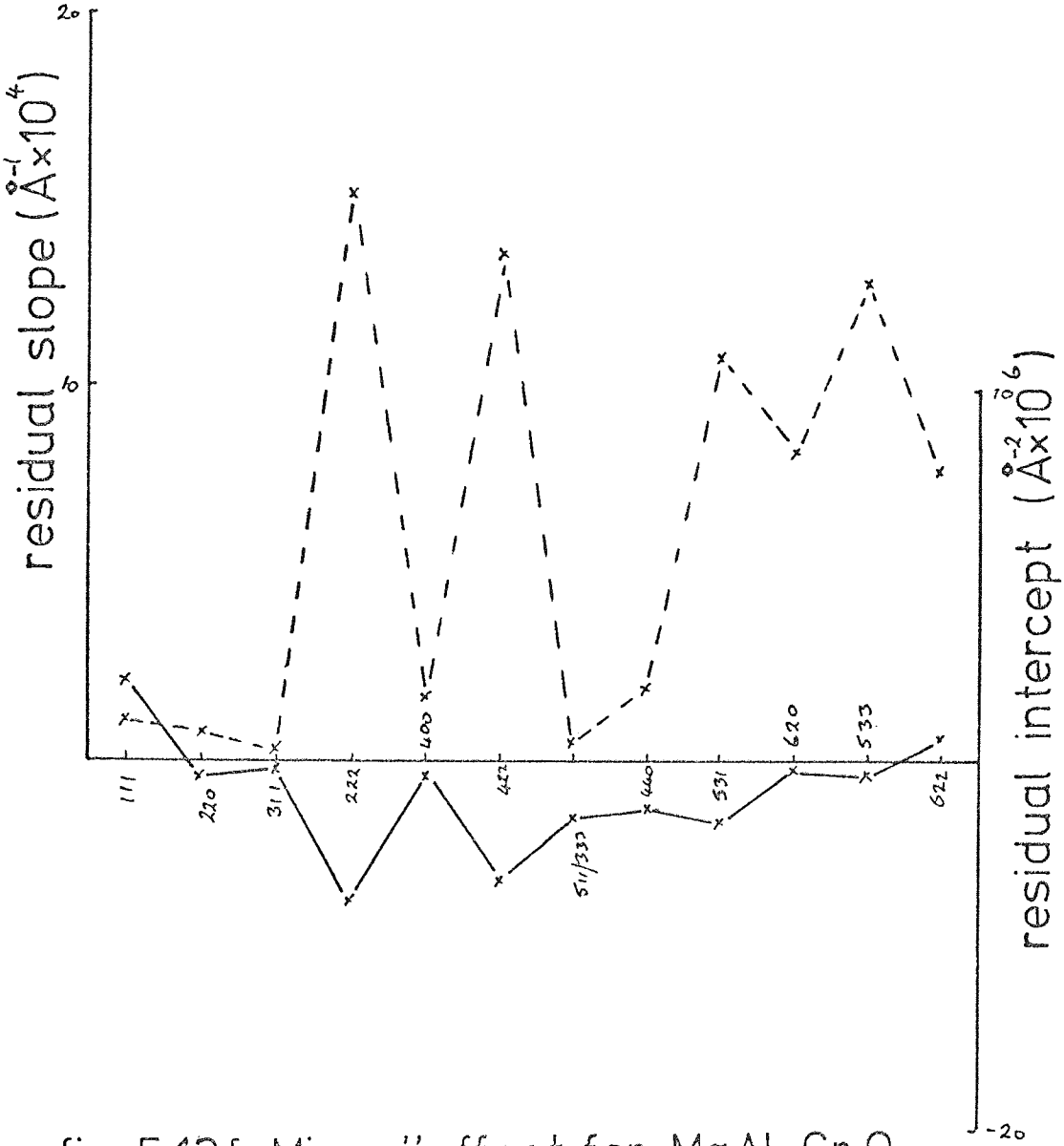

fig. 5.13f. Mirror'' effect for $MgAl_{2-x}Cr_xO_4$ x=1.5.

intercepts being accounted for by assigning a value of about 1/100 to $Q'(0)$. The actual value of $Q'(0)$ probably varies from profile to profile but also probably not to any great extent as the mirror effect appears so markedly for each sample.

A point to notice from the analysis is that a plot of residual slope against chromium concentration for all profiles shows in general terms that for small concentrations, the slope has small values which increases to a maximum at $x = 0.5$, thereafter fall drastically to values similar to the low concentration values at $x = 1.0$. This effect is indicated in figure 5.14a and 5.14b for all profiles.

A similar plot of residual intercept against concentration shows an opposite effect, i.e. the intercept decreases to a minimum value at $x = 0.5$ and increases to $x = 1.0$ as would be expected in view of the mirror effect described above. Figure 5.15 shows this effect for high angle profile residual intercepts.

Lewis (1966 and 1967) has observed through electron microscopy the presence of anti-phase domains in single crystals of $MgAl_2O_4$. Also Cheary (1971) has shown that chromium doped lithium ferrite also contains anti-phase domains in which the chromium ions accumulate at the domain boundaries. He found that the super-lattice lines were broadened to an extent which depended on the size of the anti-phase domains, i.e. the super-lattice lines exhibited a 'particle size' broadening where the particles concerned were the anti-phase domains. The variance slopes of these super-lattice lines were shown to be functions of the Miller indices and the domain thickness which depended on which planes the domain boundaries occurred.

However in this study of chromium doped spinels, there were no super-lattice lines observed and the usual spinel lattice lines were all broadened. Despite this complication, it was decided to attempt to fit the variance slopes observed with one or other of the models

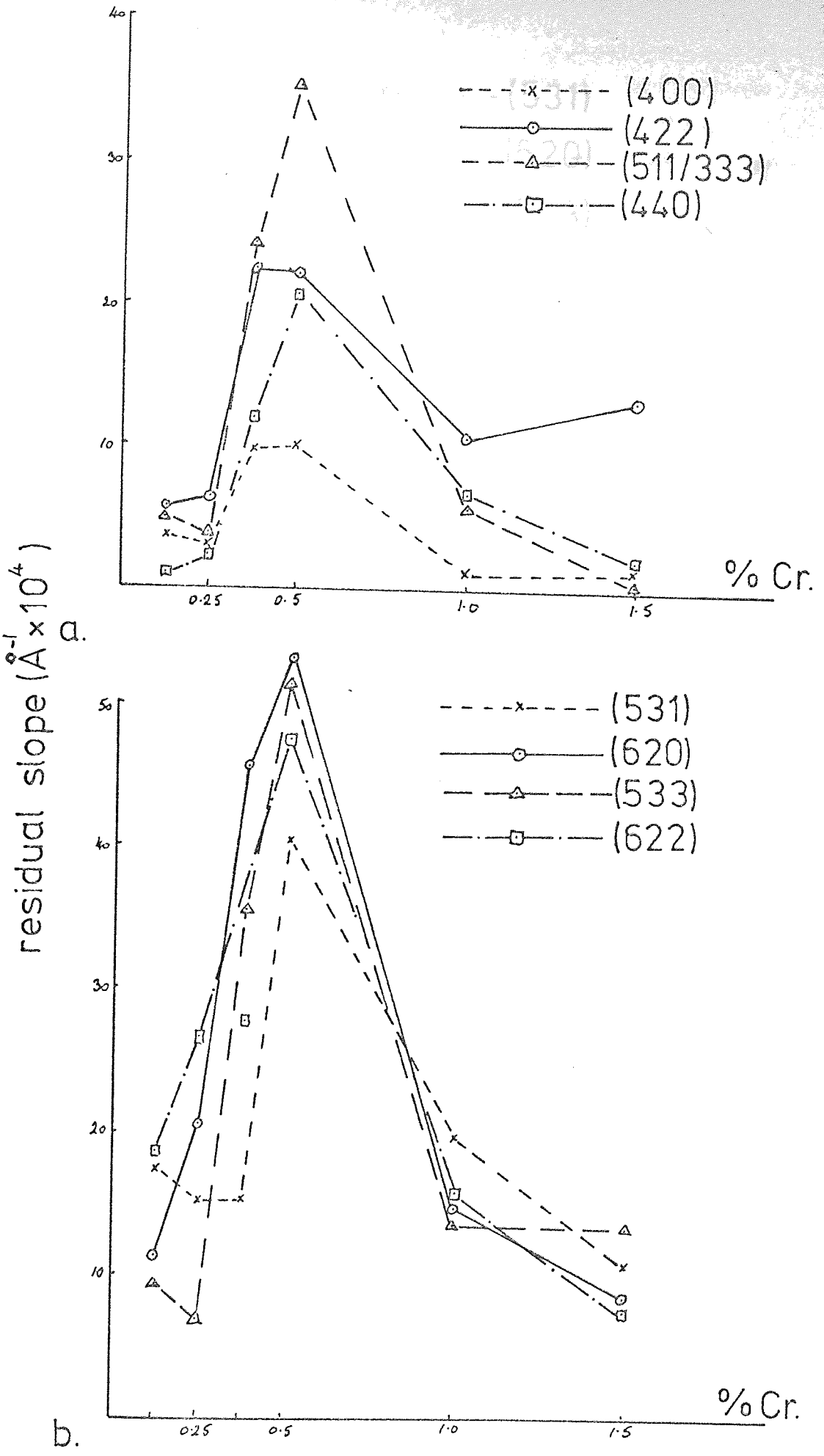

fig.5.14 Slope vs Chromium concentration.

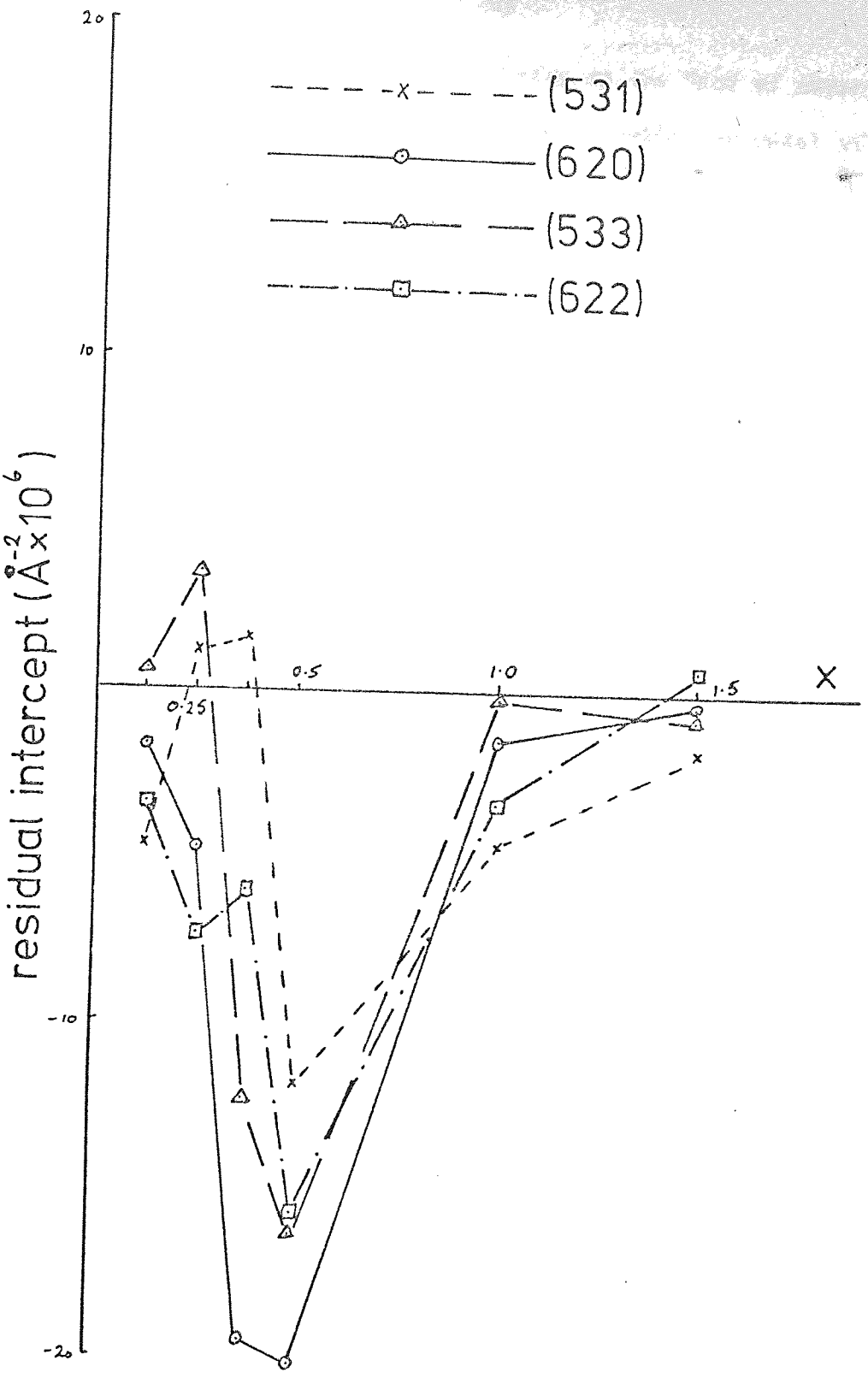

fig.5.15. Intercept vs Chromium concentration.

of domain structure suggested by Cheary as the lack of super-lattice lines made it very difficult to choose a particular model with any confidence.

Models which could be used were as follows:

(i) slope $\frac{4}{3} \frac{(h + k + l)}{\sqrt{N} \cdot T_{100}}$

for domain boundaries on (100) planes;

(ii) slope $\frac{8}{3} \frac{(2h + k)}{\sqrt{2N} \cdot T_{110}}$

for (110) boundary domains;

(iii) slope $\frac{16h}{3\sqrt{3N} \cdot T_{111}}$ if $h \geq k + l$

or slope $\frac{8}{3} \frac{(h + k + l)}{\sqrt{3N} \cdot T_{111}}$ if $h < k + l$

for (111) boundaries domains;

(iv) slope $\frac{4}{3T}$

when the domain thickness is independent of direction (Cheary, 1971)

T_{100}, T_{110}, T_{111} and T are the mean distances between domain boundaries.

Inspection of the functions of (hkl) above shows that some have similar characteristics as the variance slopes found in this study, i.e. they have values which behave in an irregular way as the order of reflection increases; in fact similar to the behaviour of the slopes indicated in figures 5.13a to 5.13f.

It was decided to test whether any of the models (i), (ii) and (iii) above would account for the results observed in these experiments. Values of T_{100}, T_{110} and T_{111} were determined for each of the profiles for each sample. A mean value of T_{hkl} was calculated for each sample

and using the relationship below to give the mean deviation (σ) of T_{hkl} from the mean, a measure of the validity of the model could be determined.

$$\sigma = \frac{100}{n\,\overline{T}_{hkl}} \sum \left| T_{hkl} - \overline{T}_{hkl} \right| \quad \%$$

where n is the number of profiles used in the calculation of the mean value $\overline{T}_{hkl}$.

T_{hkl} is the thickness calculated from the (hkl) profile.

The result of this analysis is tabulated in table 5.6 in which the values of σ are included.

Table 5.6 Results of the analysis of the variance slopes in terms of anti-phase domain models.

x	0.125	0.25	0.375	0.5	1.0	1.5
T_{100} / Å	480	600	240	250	1060	1440
σ_{100} %	70	88	76	99	110	109
T_{110} / Å	950	1110	480	450	1820	2850
σ_{110} %	68	80	76	116	114	104
T_{111} / Å	600	760	320	320	1380	1920
σ_{111} %	71	88	79	103	122	112

It can be seen from the the table that if the materials contain an anti-phase domain structure, the results follow a pattern which agree with the observed broadening i.e. the smallest domain thickness corresponds to the sample exhibiting the greatest broadening of profiles. However the values of σ are all extremely large indicating the models chosen do not account for the results extracted from the variance analysis.

5.5 Variance results for $MgAl_2O_4$.

Nominally $MgAl_2O_4$ is a pure spinel which until relatively recently was considered to be normal. However neutron diffraction studies (Bacon, 1952, Stoll et al, 1964) have shown this material to be partially inverse.

The profiles from a pure crystalline substance would be expected to have sharp diffraction lines provided particle size and strain effects were small. Inspection of the profiles from this material shows them to be broader than those of $MgCr_2O_4$, this observation being confirmed by the integral breadth analysis, and a variance analysis was carried out on this sample in an exactly similar manner to that used on the profiles from the chromium doped spinels.

Table 5.7 gives the results obtained from $MgAl_2O_4$ for the residual slopes and intercepts for all profiles. Comparison of these results and those from the chromium doped spinels shows them to be of the same form, i.e. that residual intercepts take both positive and negative values, and that there is a similar difference in magnitude of slopes and intercepts as in the doped spinel results and the mirror effect appears in these results also.

Figure 5.16 shows the results for $MgAl_2O_4$ in a graphical form which shows the similarity between these results and those from the doped spinels.

It may be inferred from these data that the source of broadening in $MgAl_2O_4$ is something other than particle size, strain or a combination of both. The broadening may be due to the effect of the partial inversion of the spinel associated with mistakes in the form of partial occupation of A and B sites by ions not expected to be found there, i.e. Al^{3+} ions in A sites and Mg^{2+} ions in B sites; this mixture is difficult to determine by X-ray measurements due to the similarity in scattering power of both these ions.

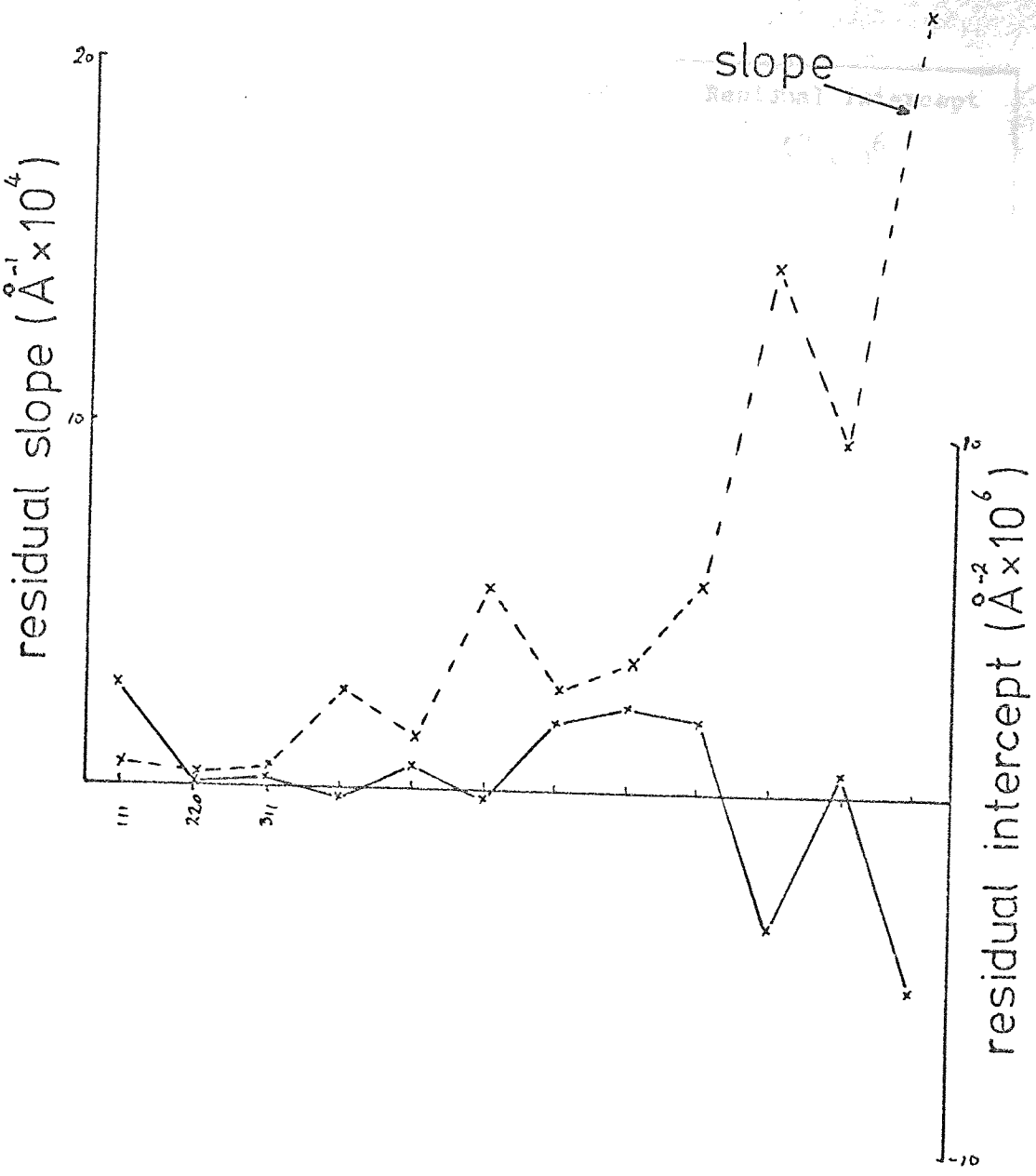

fig.5.16. Mirror''effect for $MgAl_2O_4$

Table 5.7 Residual slopes and intercepts for $MgAl_2O_4$

hkl	Residual slope $\AA \times 10^4$	Residual intercept $\AA^2 \times 10^6$
111	0.6	2.9
220	0.4	0.2
311	0.6	0.2
222	2.7	-0.2
400	1.4	0.6
422	5.6	-0.1
511/333	2.9	1.9
440	3.6	2.4
531	5.8	2.0
620	14.7	-3.8
533	9.8	0.6
622	21.8	-5.4

A further possible cause of broadening may be the presence of stacking faults which have been observed in single crystals of $MgAl_2O_4$ (Lewis, 1966) which can cause diffraction line broadening (Paterson, 1952). However these are tentative suggestions and more work is clearly necessary to determine the exact nature of the source of broadening.

CHAPTER 6

QUENCHING EXPERIMENTS

6.1 Introduction.

The analysis so far described relates to samples which had been slowly cooled after sintering at a high temperature. With this method of preparation, effects arising from excess vacancies, strain and inhomogeneity have time to anneal out and the final products are, as far as possible, well ordered. However, the nature of the sintering process is such that it is always possible that annealing is incomplete. For this reason it seemed desirable to subject certain selected samples to additional treatment in order to investigate further the stability of the structure giving rise to the line broadening and if possible to gain more information about this structure. This chapter describes results from these further experiments in which some specimens from the original samples were allowed to reach equilibrium at high temperature once again and then suddenly quenched.

The quenching apparatus was simply a vertical tubular furnace in which the sample was suspended in a metal basket in such a way that it was an easy task to cut the suspension to allow the basket and sample to fall directly into a dewar of liquid nitrogen without making contact with the walls of the furnace. In this way the material was quenched from the high furnace temperature to liquid nitrogen temperature in the shortest possible time. Equilibrium at the elevated temperature was achieved by keeping the sample at that temperature for six hours before quenching.

Liquid nitrogen was chosen as the quenching agent because:

(a) its low temperature gave as large a drop in temperature as was conveniently possible for each sample, and

(b) the sample would not be wetted by it. For instance, if water had been used, the problem of drying the material would have to be overcome, whereas with liquid nitrogen, once the sample had reached thermal equilibrium, it was a simple matter to remove it from the liquid which evaporated completely with no drying complications.

Any differences which may have occurred between the slow cooled samples and the hot sample were assumed to be 'locked in' the lattice during the quenching process and annealing out of these by aging was assumed to be very slow so X-ray diffraction measurements on these quenched samples, taken at room temperature, could be assumed to be of a sample at the elevated temperature, despite the length of time necessary to take these measurements. This is in contrast to the case in quenched metals which will quite quickly age anneal and changes in the structure that may have occurred will crystallise out in a very short time. In these oxide samples, the bonding between ions is much more stable and any faults introduced into the structure tend to remain.

Lattice parameter, structure determination and line broadening analyses were performed on the X-ray results from these quenched samples and were compared with those from the slow cooled samples described above.

6.2 Results from quenched sample with mixed composition.

The sample chosen for quenching was $MgAlCrO_4$, i.e. the specimen in which x = 1, as a representative example of the chromium doped spinels. The quenching temperature chosen was 1100°C.

A powder photograph of this quenched sample showed that only the spinel phase was present. A diffractometer specimen was prepared in an exactly similar fashion to that described in section 3.2.3 and

the X-ray line profiles obtained as before. The data collected were analysed as before to give for each profile at each selected background level, the total intensity of the line, the variation of the profile variance and centroid with range of calculation.

6.2.1 Lattice parameter determination.

Using the centroid versus range results extracted from the profile data, the profile centroid was selected in the fashion suggested by Pike and Wilson (1959) and described fully in section 4.2.1. This value of centroid was corrected for the various instrumental aberrations (Wilson, 1963) and figure 4.4 indicates how these vary with angle of diffraction.

The corrected centroids were then used to calculate the lattice parameter (a_{hkl}) for each reflection in the usual manner for a cubic material, then a plot of a_{hkl} against $\cot^2\theta$ extrapolated to $\cot^2\theta = 0$ was made to determine the intercept, this value being taken as the lattice parameter of the sample.

Table 6.1 lists the fully corrected centroids and lattice parameters calculated for each reflection, this latter quantity being calculated using the centroid wavelength as described before. Figure 6.1 shows these values plotted against $\cot^2\theta$; the extrapolated value a_o taken from this graph was 8.220 Å. This is to be compared to the value obtained for the unquenched sample i. e. 8.212 Å.

An expansion of the lattice is indicated by the results for a_o from the quenched and unquenched samples. If this were to be explained in terms of a linear expansion due to the temperature difference using the value of the coefficient of linear expansion for $MgCr_2O_4$, $\alpha = 7 \times 10^{-6}$ per degree (Beals and Cook, 1957), a change in lattice parameter seven times bigger than observed is expected. A possible reason for this expansion may be that at the elevated

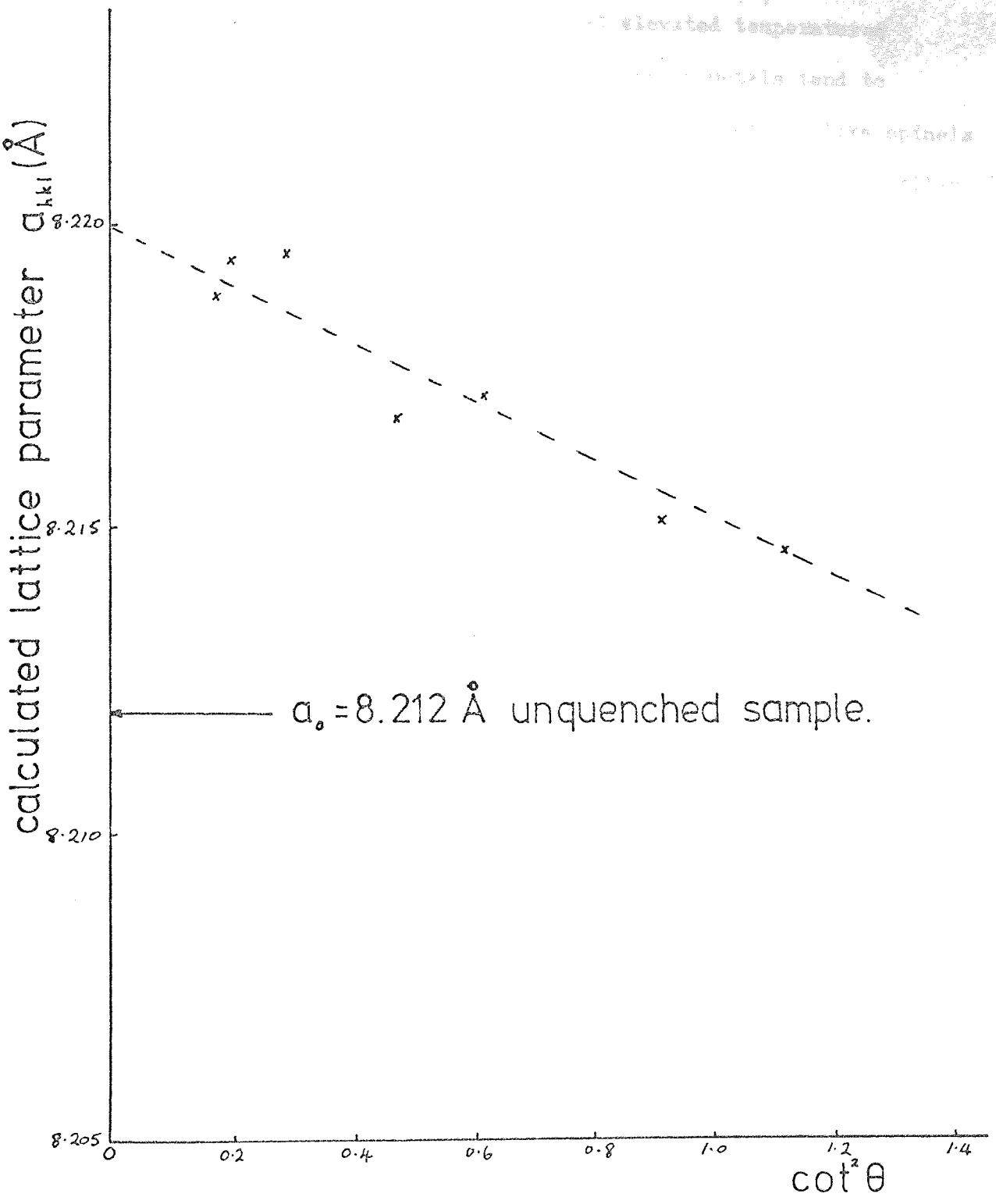

fig.6.1. a_{hkl} vs. $\cot^2\theta$ for $MgCrAlO_4$ (Q1100).

temperatures there may be vacancies occurring which are 'frozen' in by the quenching process, this is suggested by similar results from lattice parameter observations in metals at elevated temperatures (Simmons and Ballufi, 1960). However vacancies in metals tend to anneal out quickly at room temperature whereas in materials like spinels are unlikely to be very mobile . Migration energies of ions in similar substances as these spinels are cited by Grimes (1972) which suggests that the assumption taken above is a reasonable one.

Table 6.1 Corrected centroids and values of a_{hkl} for $MgAlCrO_4$ quenched from 1100°C.

hkl	corrected centroid deg. 2θ	a_{hkl} Å
111	28.344	8.107
220	46.613	8.189
311	55.196	8.201
400	67.852	8.210
422	86.180	8.215
511/333	92.861	8.215
440	104.109	8.217
531	111.131	8.217
620	123.630	8.220
533	132.099	8.219
622	135.194	8.219

Figures 6.2a to 6.2c show a few of the profiles obtained from both quenched and unquenched samples. Obvious differences are that the quenched peaks have shifted to lower angles, in accordance with the larger lattice parameter for this material, also the general back-

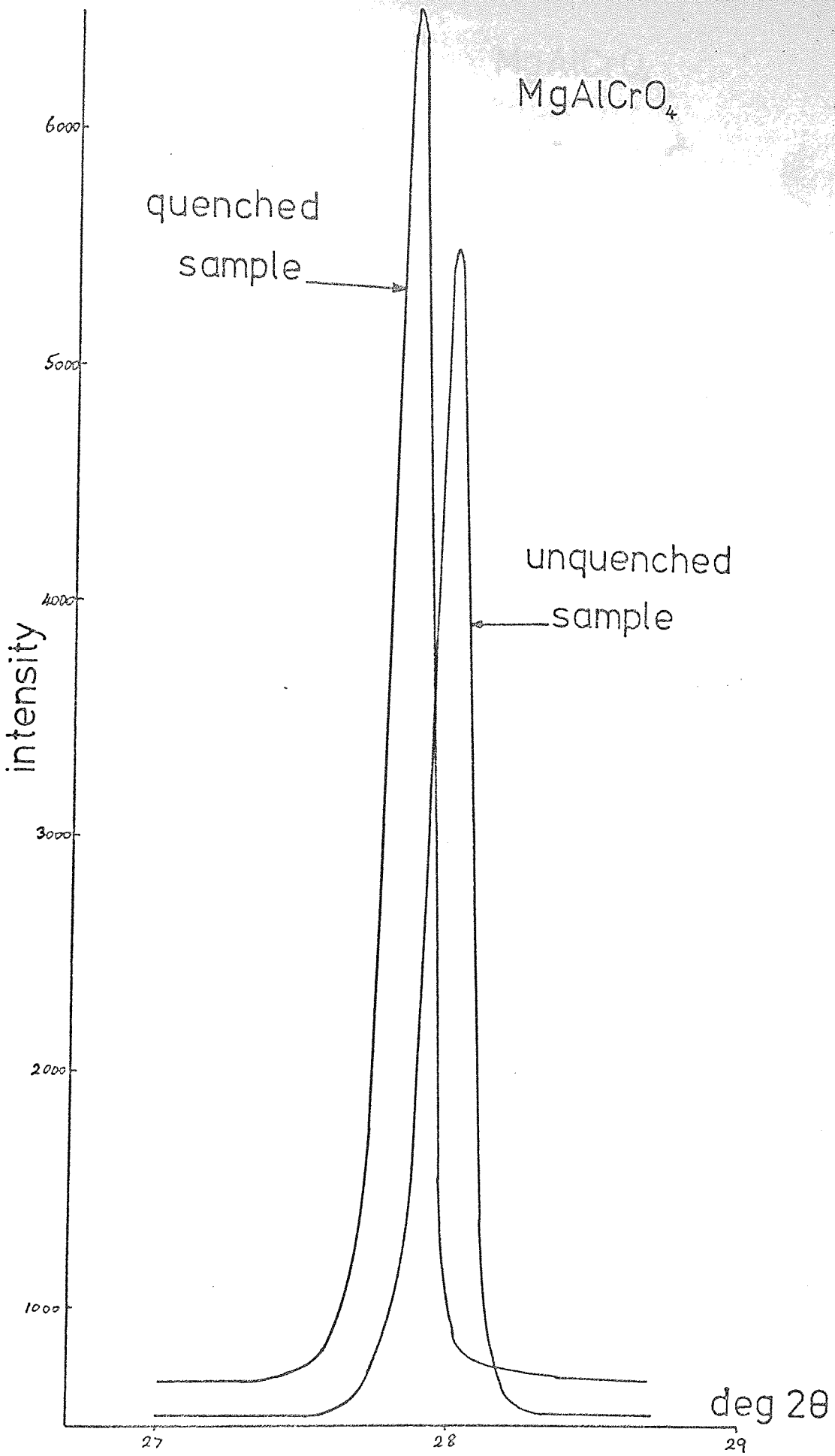

fig.6.2.a. Effect of quenching on (111) profile.

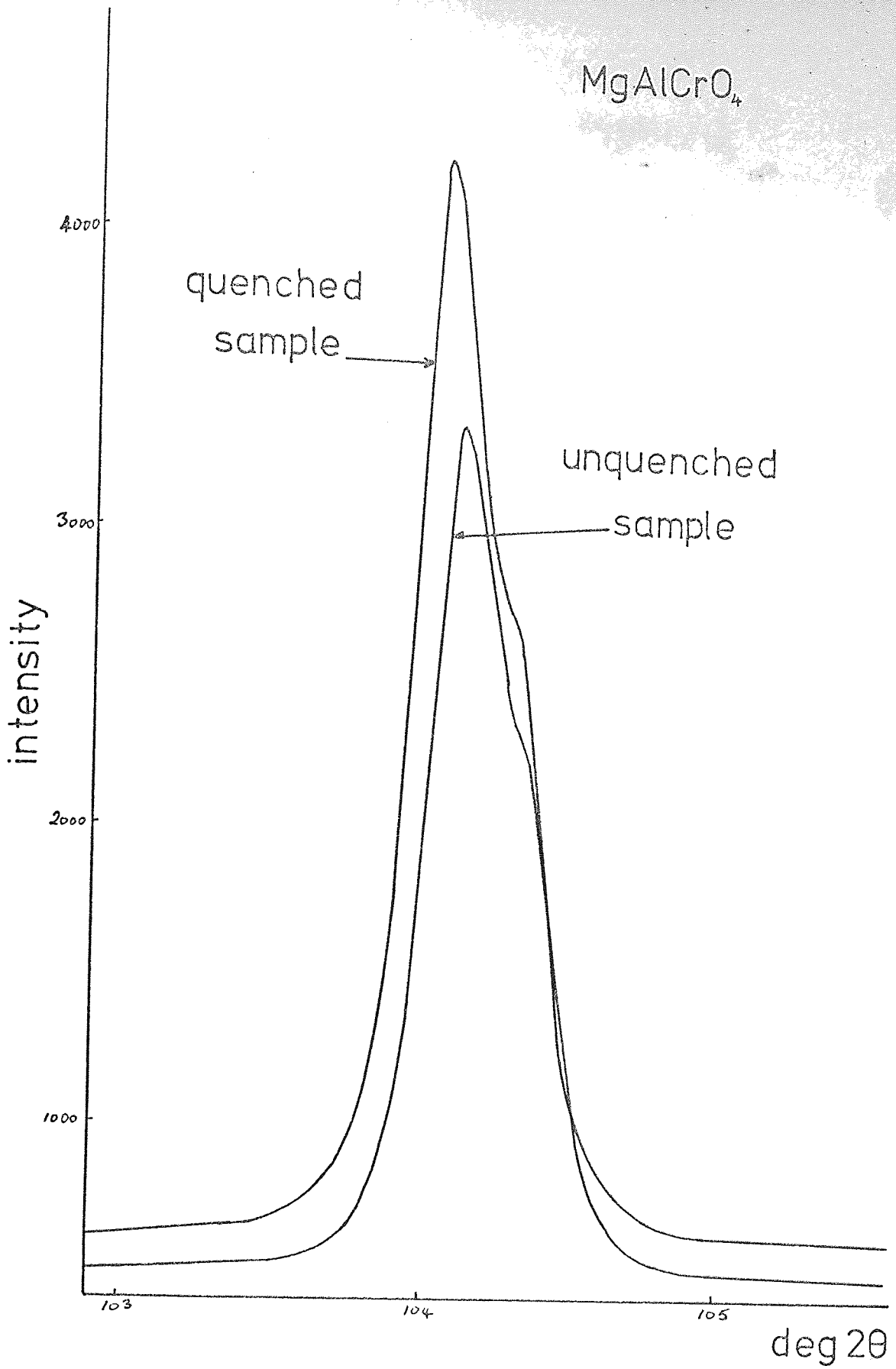

fig. 6.2.b. Effect of quenching on (440) profile.

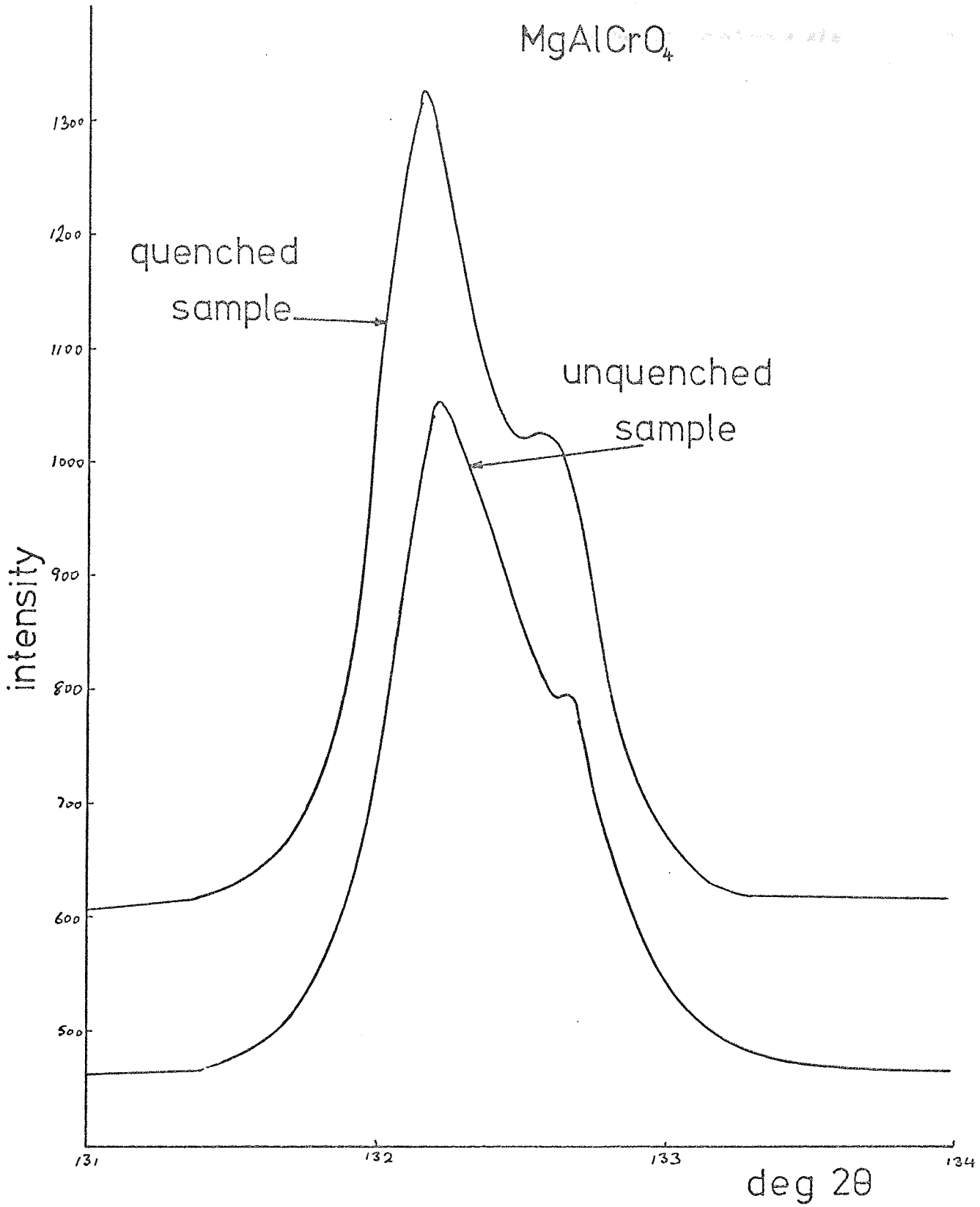

fig.6.2.c. Effect of quenching on (533) profile.

ground levels of the quenched specimens are higher, but absolute peak intensities remain substantially the same. These observations are of a general nature and hold for all the profiles measured.

6.2.2 Integrated intensity measurements.

For the purpose of comparing the quenched and unquenched structure, it was considered adequate to refer to Fd3m symmetry with Al^{3+} and Cr^{3+} ions distributed at random over the octahedral sites as described in Chapter 4. The final results obtained on this basis are given in table 6.2, the value of R being 2% which indicates a very good fit of the data for the model chosen

Table 6.2 Integrated intensities for quenched $MgAlCrO_4$

hkl	Observed intensity	Calculated intensity
111	7390	7420
220	6260	6550
311	20400	20400
400	73900	73900
422	3890	3460
440	104400	100100
531	2250	2480
620	2770	2010
533	10780	11000
622	3250	3060
R 2%	B 0.75 $Å^2$	

These results indicate that u = 0.387, as in the unquenched sample. The value of B quoted in the table was one used to correct the observed

intensities for the temperature effect in a computer program. The accuracy expected for B is of the order of ± 0.1 $\AA^2$ thus this value agrees, to within experimental error with that obtained for the unquenched sample i.e. 0.8 $\AA^2$.

These integrated intensity calculations indicate that the structure of the sample $MgAlCrO_4$ was substantially unchanged by heating. Thus an apparently negligible change was produced in the distribution over tetrahedral and octahedral sites. In several spinel materials, quenching is known to encourage inversion (see Chapter 1) but then Cr^{3+} has the highest known preference for the octahedral site (McClure, 1957). The present results add further confirmation to this conclusion.

6.2.3 Line breadth analysis.

A variance analysis was carried out on the profiles of the quenched specimen in a similar manner to that performed previously on the unquenched sample as described in section 5.3. The new results were compared with those obtained for $MgAlCrO_4$ (unquenched) and table 6.3 shows the fully corrected residual slopes and intercepts for both quenched and unquenched samples.

These results have been displayed graphically in figure 6.3. The slopes and intercepts have been plotted on appropriate scales against order of diffraction. When compared with the similar plot for the unquenched sample (figure 5.15f) it can be seen that the two plots show a marked similarity. The mirror effect is seen in each case. This again seems to indicate that the quenching process did not substantially alter the mistake structure in the material. This is unfortunate in some respects in that a more substantial change would have been more informative concerning the nature of the structure producing the broadening.

Table 6.3 Fully corrected residual slopes and intercepts for $MgAlCrO_4$

hkl	$MgAlCrO_4$ Quenched		$MgAlCrO_4$ Unquenched	
	Slope $Å^{-1} \times 10^4$	intercept $Å^{-2} \times 10^6$	Slope $Å^{-1} \times 10^4$	intercept $Å^{-2} \times 10^6$
111	2.5	2.2	0.3	4.1
220	6.2	-1.3	8.3	-2.1
311	3.2	2.7	2.4	0.5
400	6.8	-0.4	1.2	2.2
422	20.0	-6.3	10.7	-0.3
511/333	4.3	3.6	5.9	2.0
440	8.7	0.8	6.2	2.6
531	18.0	-4.4	19.8	-4.7
620	16.8	-3.5	14.6	-1.5
533	20.0	-4.8	13.6	-0.2
622	29.5	-9.8	15.5	-3.5

6.2.4 Discussion of the results from $MgAlCrO_4$(quenched).

As far as could be determined by the integrated intensity and variance analyses, the sample $MgAlCrO_4$ was structurally substantially the same whether quenched or not. The u parameter and the Debye-Waller factors in the two samples were found to be unchanged, the variance analysis gave a similar result for each although there were some changes in the slopes and intercepts of the variance-range plots. The overall impression however was that there was little change. This observation tends to confirm that broadening is not due to strain for quenching would probably increase this and consequently increase the line breadth.

Lattice parameter measurements indicated a slightly larger unit cell in the quenched material, the expansion possibly being due to the presence of vacancies.

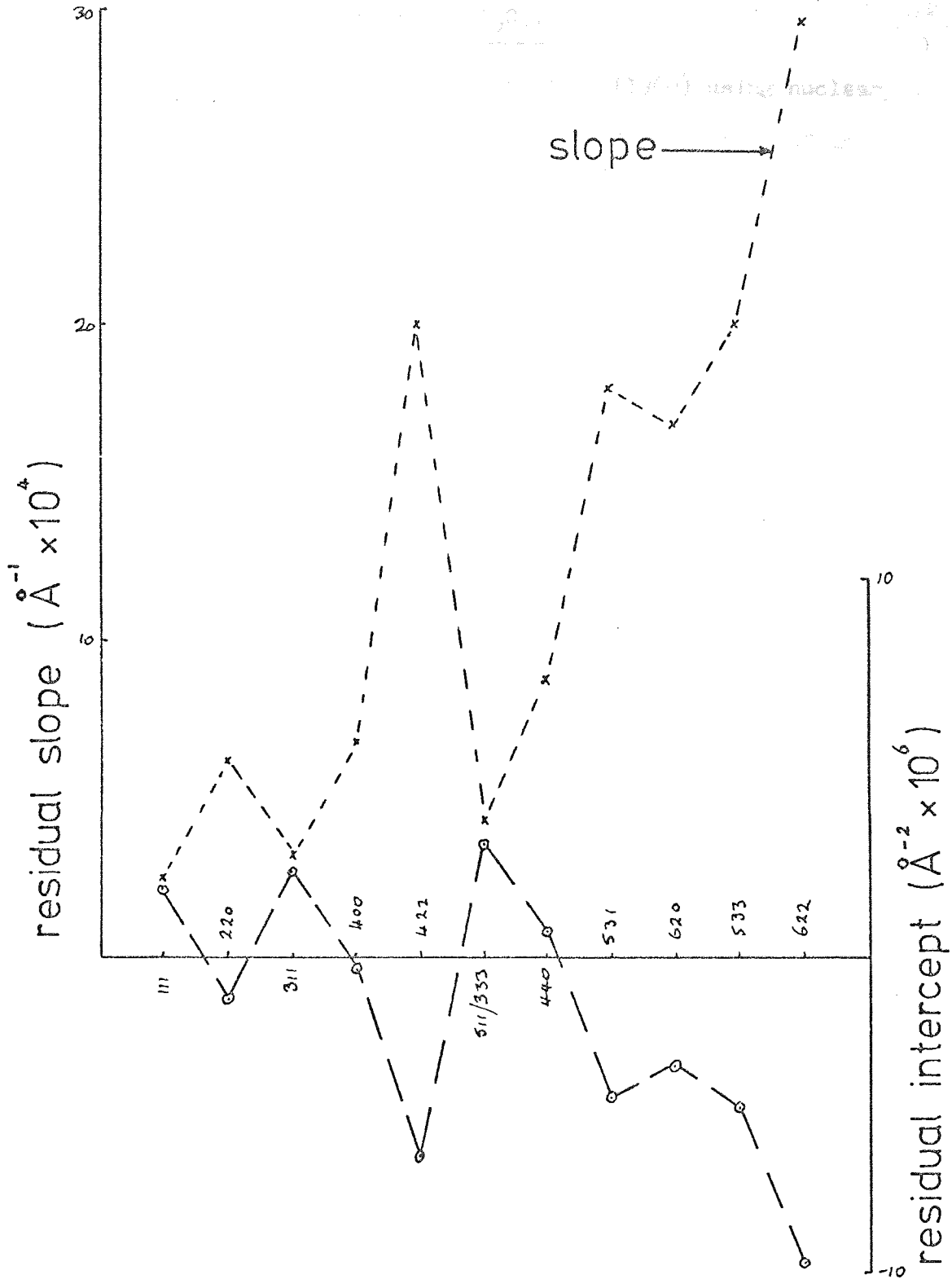

fig. 6.3. Slope and intercept vs order of diffraction for quenched $MgAlCrO_4$.

6.3 Results obtained from quenched $MgAl_2O_4$.

$MgAl_2O_4$ has been investigated by Brun et al (1960) using nuclear quadrupole resonance techniques to determine the distribution of the metal ions on the A and B sites within the lattice. Their results indicate that there is a change in the distribution above 800°C. It was decided to quench a sample at temperatures above this value in an attempt to change the structural properties and to check the result quoted by Brun et al.

The temperatures at which the material was quenched were 1100°C and 900°C, the method of quenching being that described above in section 6.1. Similar analyses were carried out and the results again compared with those obtained from the unquenched material.

6.3.1 Lattice parameters determination.

The lattice parameters for both quenched specimens were determined as before from the corrected centroids. Table 6.4 gives the fully corrected centroids and lattice parameters calculated in the usual manner for cubic materials for each diffraction line. Figures 6.4a and 6.4b show the result of plotting a_{hkl} against $\cot^2\theta$ to determine a_o.

A comparison of these two graphs with the similar one for $MgAl_2O_4$ unquenched, figure 4.5, indicates that the points are scattered more widely about the line in the quenched samples than in the unquenched material. However, the resultant lattice parameters are not significantly different from each other (both 8.080 A) or from the unquenched material for which an identical result had been obtained earlier.

An interesting feature emerges when the position of the diffraction lines are compared with those found in the unquenched sample. Figure 5.6a and 5.6b show the relative positions of the quenched lines and the unquenched ones. The expected line positions are indicated by vertical dotted lines, the actual positions of the quenched lines

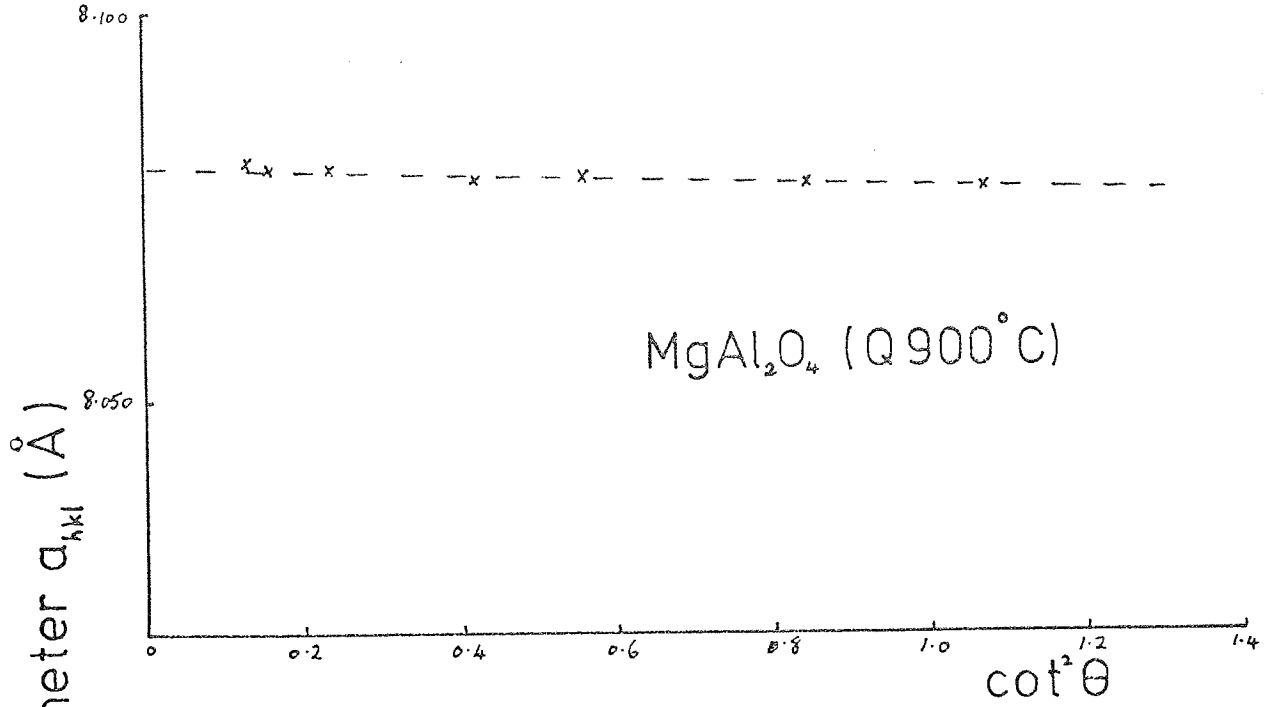

fig. 6.4.a.

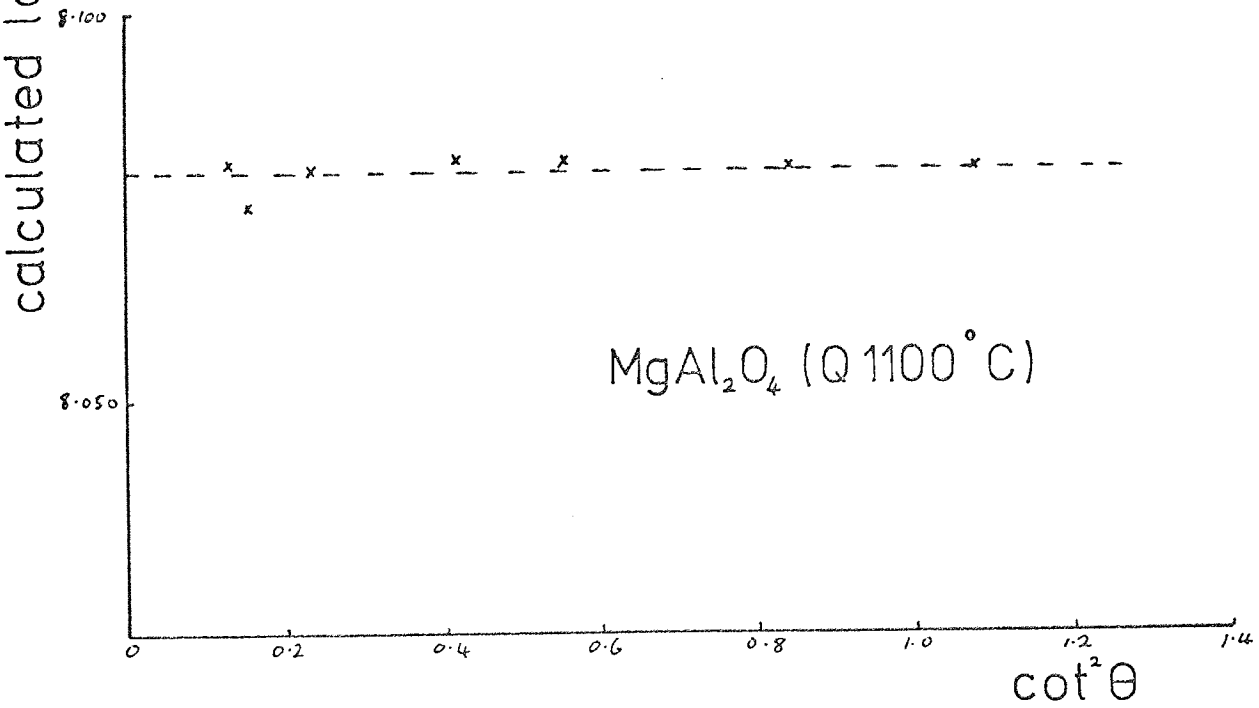

fig. 6.4.b. Lattice parameter determination for quenched Spinel.

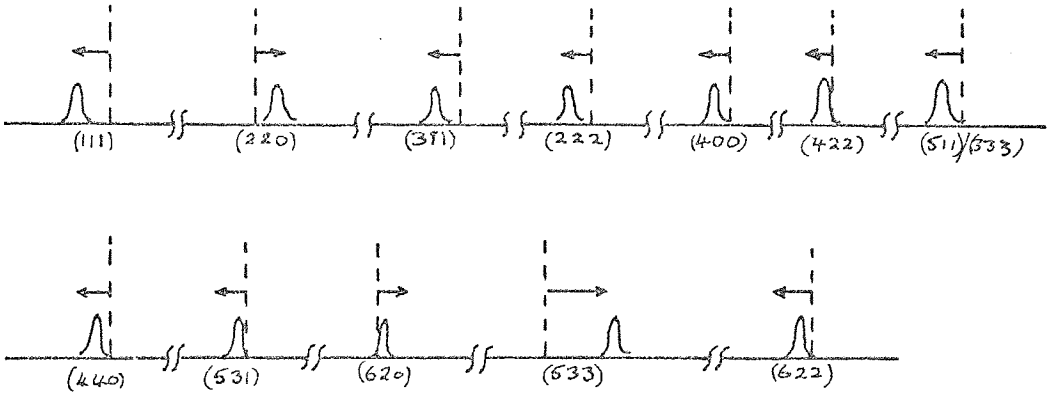

fig. 6.5.a

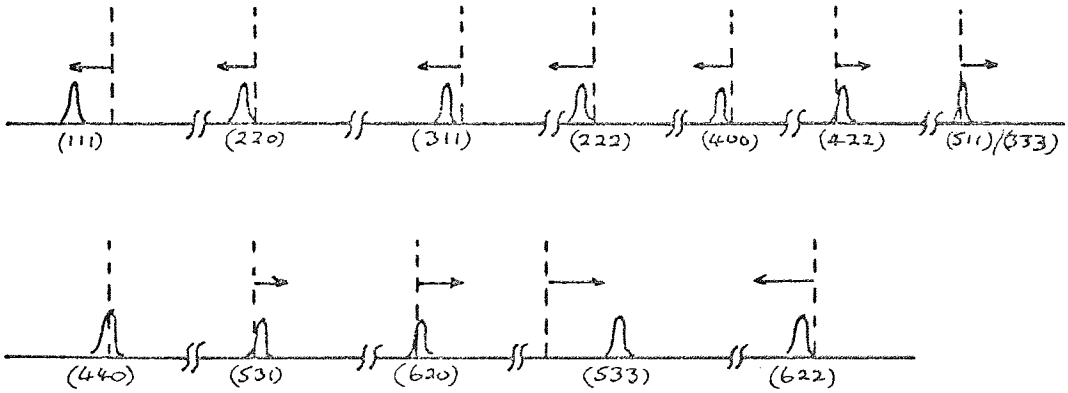

unquenched line centroids.

quenched line centroids.

fig. 6.5.b. Line shifts observed in the quenched samples of $MgAl_2O_4$.

are indicated as profiles. It can be seen that the lines are shifted in opposite senses, i.e. the (111) profile has been shifted towards the high angle. Similar shifts occur further along the spectrum. The magnitudes of the shifts are generally smaller in the sample quenched at the lower temperature.

Table 6.4 Fully corrected centroids and calculated lattice parameters for $MgAl_2O_4$ (quenched)

hkl	Q 1100°C		Q 900°C	
	Centroid deg 2θ	a_{hkl} Å	Centroid deg 2θ	a_{hkl} Å
111	28.437	8.064	28.469	8.069
220	47.399	8.061	47.311	8.075
311	56.099	8.079	56.127	8.076
222	58.832	8.079	58.863	8.076
400	69.107	8.079	69.124	8.079
422	87.989	8.079	88.020	8.077
511/333	94.899	8.080	94.928	8.078
440	106.629	8.081	106.663	8.079
531	113.972	8.081	114.054	8.078
620	127.445	8.080	127.447	8.080
533	136.958	8.075	136.786	8.079
622	140.235	8.080	140.233	8.080

Similar shifts have been observed in lines from cold worked metals (Barrett, 1952) and the phenomenon has been treated theoretically by Patterson (1952). The effect in metals has been shown to be due to the occurrence of stacking faults within the lattice (e.g. in cold worked aluminium and copper, Wagner, 1957a and b). The change of the position of the diffraction line has been expressed in terms of the

probability of the occurrence of stacking faults. In particular, with stacking faults on (111) planes in the face centred cubic system Warren (1959) has shown that for any given diffraction line, the expected shift is

$$2\theta^{\circ} = \frac{K\,90\sqrt{3}}{\pi^{2}}\,\alpha\,\tan\theta \qquad \text{.....6.1}$$

and α is the probability of the occurrence of a stacking fault,

θ is the Bragg angle for the line and

K is a parameter which is a function of the Miller indices and the multiplicity factor for the line as follows

$$K \quad \frac{\sum_{b} \pm L_{o}}{h_{o}^{2}\,(u + b)}$$

where $h_{o}^{2} = h^{2} + k^{2} + l^{2}$

$L_{o} = h + k + l$

u is the number of values of L_{o} equal to 3N

b is the number of values of L_{o} equal to 3N + 1 or 3N - 1

thus (u + b) is the multiplicity factor for the line.

The sign to be taken in the summation in the above expression being positive if $L_{o} = 3N + 1$ and

negative if $L_{o} = 3N - 1$ (N is an integer).

Values of K for the observed diffraction lines were calculated and these are given in column 2 of table 6.5.

A cursory inspection of the magnitudes of the shifts corresponding to $\Delta 2\theta$ in the present experiments showed that these were very small. Warren's suggestion that one should consider the change in separation of neighbouring lines instead of attempting to measure $\Delta 2\theta$ absolutely was therefore adopted in order to minimise the effects of experimental uncertainty. The line (311), which is particularly strong, was used as a primary reference position for the present results so that α was calculated from an expression of the form

$$\left[2\theta_2^\circ - 2\theta_1^\circ\right] = \frac{90\sqrt{3}}{2}\left[K_2 \tan\theta_2 - K_1 \tan\theta_1\right]\alpha \quad \ldots\ldots 6.2$$

The angular differences calculated from this analysis are given in table 6.5 which shows that in the sample quenched at 1100°C, all but two of the lines show a change in separation of the correct sign and all but four do the same for the sample quenched at 900°C. Using equation 6.2, values of α^{-1} were calculated for these lines showing the expected relative displacements and are also given in table 6.5. Mean values of α^{-1} were then calculated for both samples, these values being $\alpha^{-1} = 65$ for the sample quenched at 1100°C and $\alpha^{-1} = 115$ for that quenched at 900°C, (i.e. if the present analysis is based upon the correct model, then stacking faults must occur about once in every 65 planes or once in every 115 planes for these samples quenched at 1100°C and 900°C respectively.)

Although there is a large scatter in the individual values of α^{-1} they do compare reasonably well with those found by Wagner (1957) on a few lines studied in experiments on deformed metals.

These values of α may be used to estimate the stacking fault energy (γ) in each case using values of α reported for some face centred metals and corresponding values of stacking fault energies.

Table 6.6 shows values of α and γ extracted from various sources e.g. Amelinckx, 1964, Hirth and Lothe, 1968, Cockayne, Jenkins and Ray, 1971 and Bolling, Massalski and McHargue, 1961.

By comparing values obtained in these experiments for α^{-1} with those listed in table 6.6, estimates of stacking fault energies may be made. For instance values of about 20 and 50 ergs/cm^2 for the 1100°C and 900°C quenched samples respectively although this is very uncertain as Bolling et al have indicated that the value of α for a particular substance can depend on the amount of deformation suffered by the material.

Table 6.5 Expected and observed changes in separation of profiles for $MgAl_2O_4$ quenched samples.
(all changes quoted relative to the (311) profile)

hkl	K ø	Expected shift * $K_{hkl} \sim K_{311}$	Observed separation deg 2θ		α^{-1}	
			Q 1100°C	Q 900°C	Q 1100°C	Q 900°C
111	1/4	15/44	0.018	0.032	98	55
220	1/4	15/44	0.112	-0.004	22	-
311	-1/11	-	-	-	-	-
222	-1/8	3/88	0.002	-0.001	180	-
400	1/4	-15/44	-0.021	-0.010	160	330
422	0	- 1/11	-0.035	-0.038	22	20
511	-1/36	-25/396	-0.030	-0.031	10	10
333	0					
440	-1/8	3/88	-0.021	-0.025	-	-
531	2/35	-57/385	0.006	-0.048	-	39
620	-1/20	- 9/220	-0.060	-0.034	14	18
533	-5/43	12/473	0.556	-0.044	7	-
622	1/22	- 3/22	-0.038	-0.008	72	344

* negative sign indicates an increase in separation

ø here the positive sign indicates a shift towards the higher angle.

Table 6.6 Observed values of stacking fault energies and probabilities for a selection of metals.

Metal	α^{-1}	γ / ergs/cm^2
silver	60	16
aluminium	300	200
cobalt	10	20
copper	83	41
nickel	500	150

6.3.2 Integrated intensity calculations.

Integrated intensities of the quenched samples were compared with those obtained from the unquenched sample. Figure 6.6 indicates how the (533) profile, as a typical example, was affected by the quenching process at each temperature. The background intensity level remains at the same low level in each case but the intensity increases with increasing quenching temperature. The shapes of the profiles appear to be substantially the same, i.e. the $\alpha_1 - \alpha_2$ doublet is equally distinct in each and the half height width of each is also substantially the same. Also to be noted is the shift of the lines where the higher quenching temperature produces a larger shift towards the higher angle.

Using the intensity data for the quenched samples, values of B and u were determined for each in an exactly similar manner as before and described in section 4.3.2. Table 6.7 shows these results and those from the unquenched sample. It was found that the u parameter for both the quenched samples was 0.387 ± 0.001, i.e. the same value as was found for the unquenched spinel. The temperature factor, B, increased slightly with increasing quenching temperature, the values

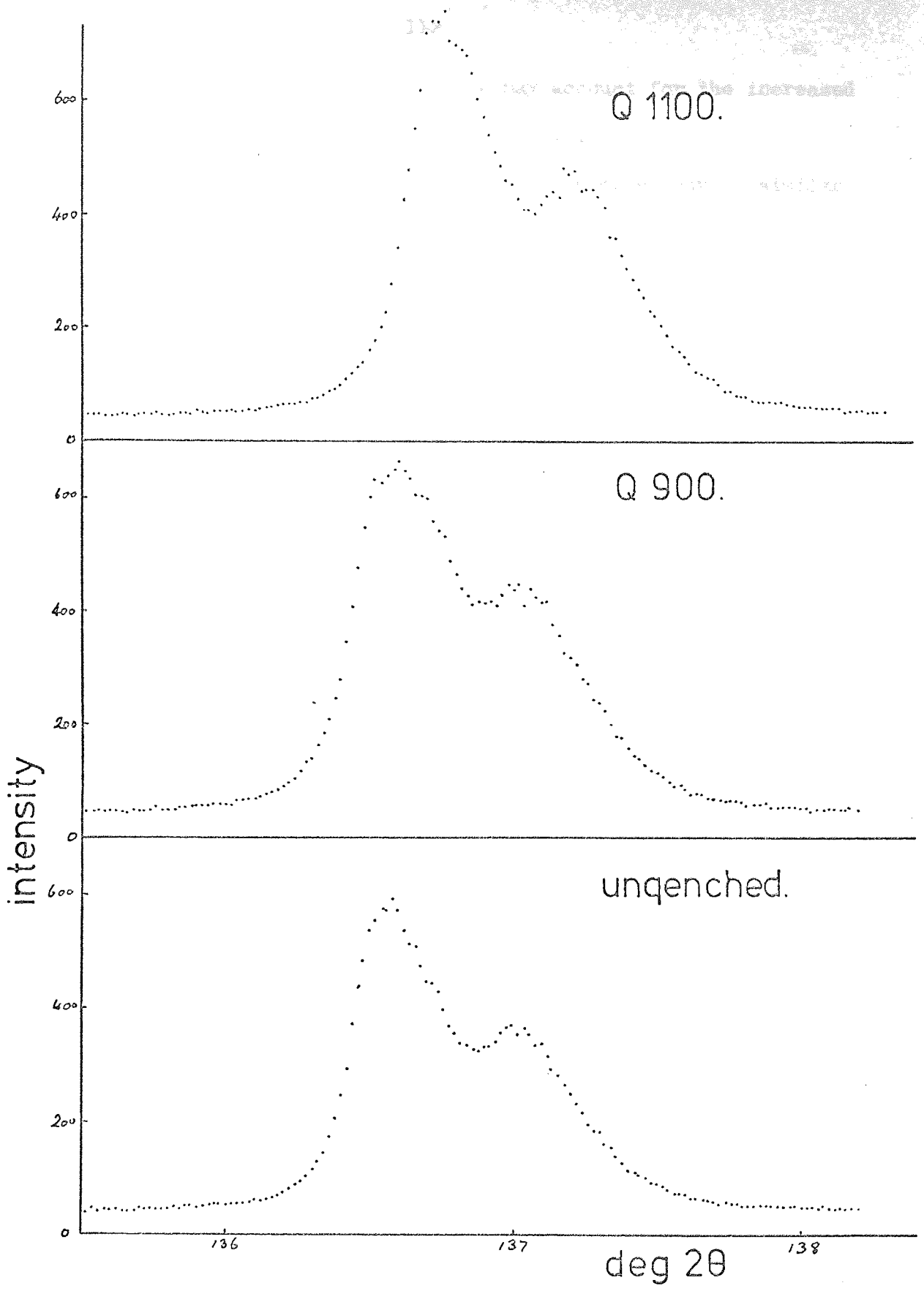

fig.6.6. Effect of quenching on the (533) profile $MgAl_2O_4$.

being given in the table; this increase may account for the increased intensity observed and indicated in figure 6.6.

These results indicate that the quenched samples have a similar structure to the unquenched spinel, namely that they are still normal spinels, thus the inversion observed by Brun et al (1960) above 800°C in their spinel specimen did not appear to occur here. This conclusion is supported by the value of u= 0.387 which suggests a normal structure (Verwey et al, 1947) and the fact that the relative intensities of the (111) and (220) profiles were unchanged by the quenching, this intensity ratio being an indicator of the inverse spinel in which the (220) line has a low intensity.

Table 6.7 Fully corrected observed integrated intensities compared with the calculated values for $MgAl_2O_4$, quenched and unquenched samples. (Intensities in absolute electron units)

hkl	I_{obs}(unquenched)	I_{obs}(Q 1100°C)	I_{obs} (Q 900°C)	I_{calc}
111	2900	2680	2580	2900
220	6450	6950	5950	6500
311	13650	12990	13240	13650
222	1050	980	1000	1600
400	52300	52100	53900	51200
422	4390	3450	3370	3460
440	79400	80000	79900	80100
531	960	1040	850	1100
620	2330	2200	2150	2010
533	8000	7770	7620	8170
622	950	867	910	700
u	0.387	0.387	0.387	
B / $Å^2$	0.4	0.5	0.45	
R %	2.5	2.0	3.0	

6.3.3 Line breadth analysis.

A variance analysis was performed on the intensity readings from the quenched samples as before and is described fully in section 5.3.

Table 6.8 shows the fully corrected residual slopes and intercepts for all the $MgAl_2O_4$ specimens. These results are also displayed in figure 6.7a and 6.7b; the corresponding chart for the unquenched sample is given in figure 5.16. The three graphs each show the 'mirror effect', i.e. a change in residual slope on going from one reflection to the next being reflected in the value of the residual intercept, indicating the structure of the three samples to be substantially the same.

Table 6.8 Fully corrected residual slopes and intercepts for all $MgAl_2O_4$ specimens.

hkl	Unquenched		Q 1100°C		Q 900°C	
	Slope $Å^{-1} \times 10^4$	Intercept $Å^{-2} \times 10^6$	Slope $Å^{-1} \times 10^4$	Intercept $Å^{-2} \times 10^6$	Slope $Å^{-1} \times 10^4$	Intercept $Å^{-2} \times 10^6$
111	0.6	2.9	2.4	2.6	2.4	6.0
220	0.4	0.2	1.7	-2.0	1.3	1.1
311	0.6	0.2	2.1	0.1	2.8	0.4
222	2.7	-0.2	5.5	-2.0	2.1	1.2
400	1.4	0.6	1.1	1.0	2.8	0.4
422	5.6	-0.1	4.6	0.8	1.4	3.5
511/ 333	2.9	1.9	2.1	2.7	4.0	2.2
440	3.6	2.4	1.4	3.3	0.4	4.2
531	5.8	2.0	6.8	-4.5	10.2	-0.5
620	14.7	-3.8	13.0	-2.2	12.0	-1.5
533	9.8	0.6	8.5	0.7	10.5	0.1
622	21.8	-5.4	15.8	-1.9	26.0	-12.8

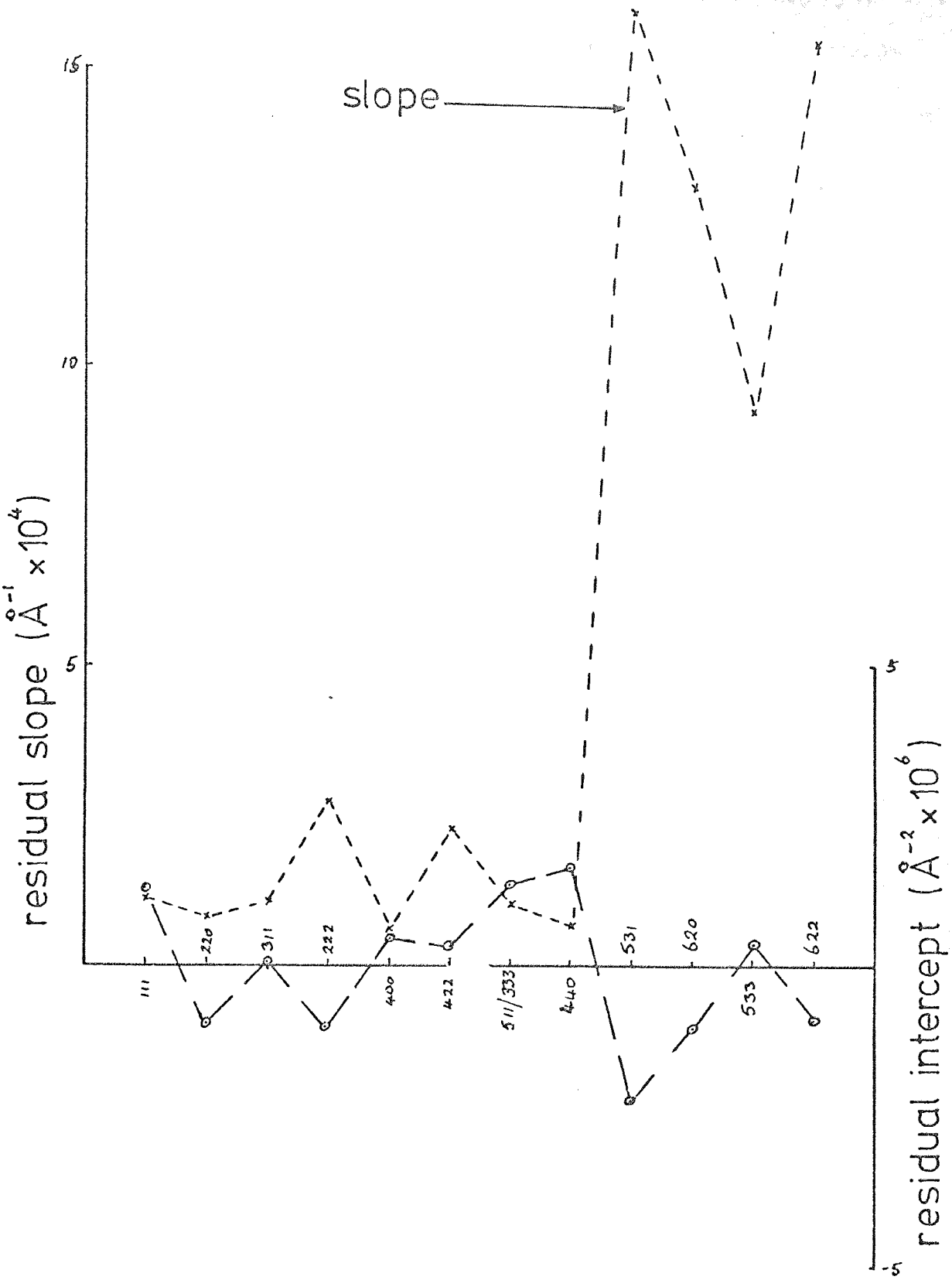

fig. 6.7.a. Slope and intercept vs order of diffraction for $MgAl_2O_4$ (Q 1100).

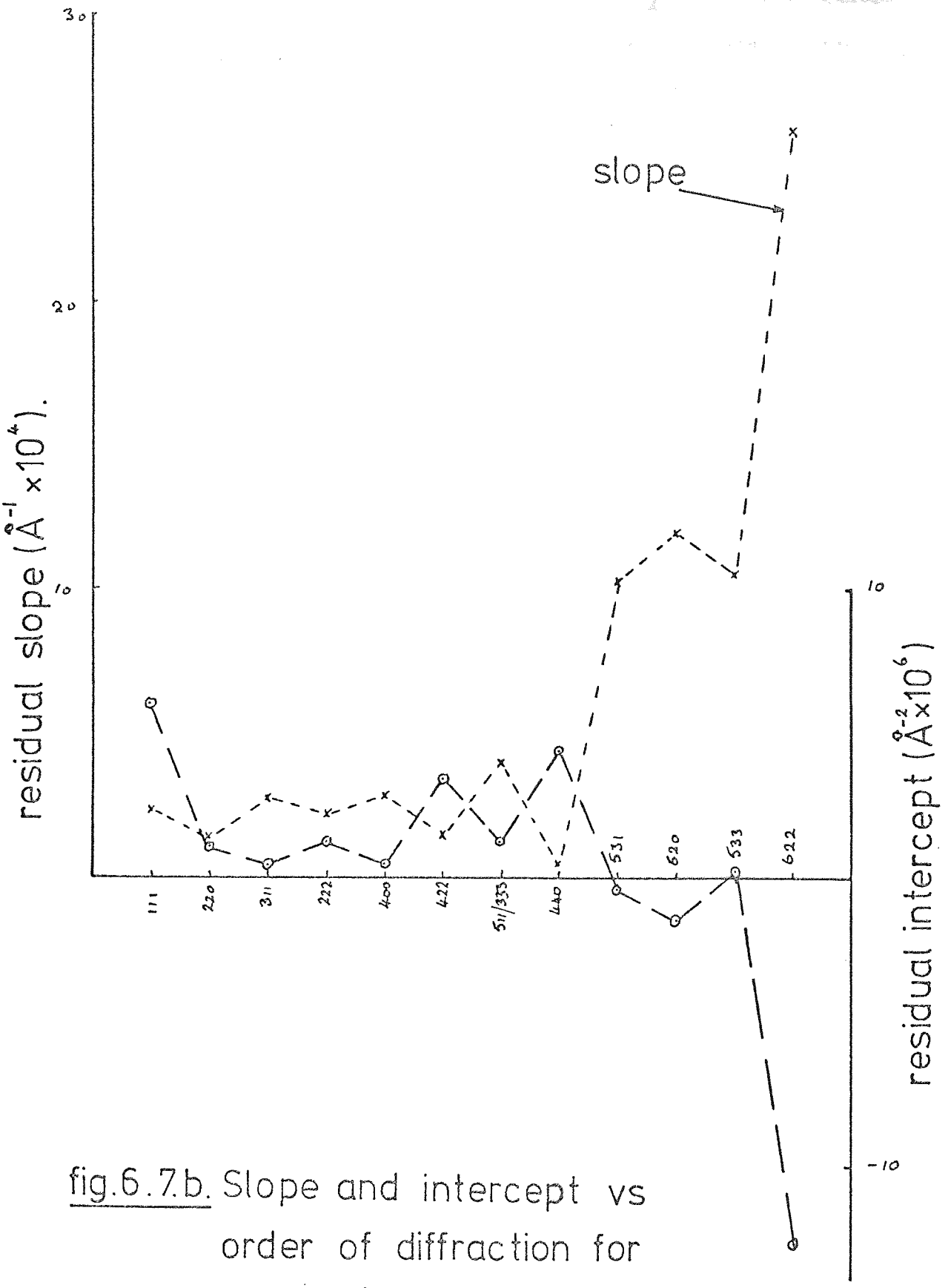

fig.6.7.b. Slope and intercept vs order of diffraction for $MgAl_2O_4$ (Q 900).

The breadth of the diffraction lines of $MgAl_2O_4$ has been commented upon in section 5.5 and the source causing this was suggested as the possible partial inversion of Spinel which has been reported (Brun et al, 1960). However stacking faults occur in this material which may themselves produce some inversion. In this context it is interesting that Lewis (1966 and 1967) has observed the presence of stacking faults by electron microscopical examination of thin crystal slices of $MgAl_2O_4$. However unfortunately no figures were given for stacking fault energy from this analysis.

6.4 Conclusions.

Comparison of the profiles from the quenched and unquenched samples of $MgAlCrO_4$ shows that the breadths of these profiles were substantially unchanged; this observation tends to confirm that the broadening occurring in the profiles from the chromites in this study arises from a mistake structure.

The background radiation to these profiles was generally much higher in the quenched material, this can be an indication of the presence of disorder in the crystal, and is probably due to vacancies occurring in the lattice as indicated by the increase of lattice parameter after quenching.

The behaviour of the profiles from $MgAl_2O_4$ after quenching suggests that the broadening observed in them is probably due to a form of stacking fault parallel to (111) planes though it is difficult to confirm this conclusion with Lewis's observations of faults in the single crystal material.

CHAPTER 7

SUMMARY AND CONCLUSIONS

7.1 Conclusions.

The principle conclusion to be drawn from this study is that the structure for $MgCr_2O_4$ is best described in terms of $F\bar{4}\,3m$ symmetry rather than the hithertoo accepted $Fd3m$.

The original integrated intensity measurements led through a refinement of the usually accepted $Fd3m$ symmetry model for cubic spinels to a result that the oxygen parameter $u = 0.387 \pm 0.001$, i.e. the same value for each specimen. However the Debye-Waller temperature factor (B) was anomalously high in those specimens containing chromium, its value increasing with increasing chromium content, the largest value being 1.1 $\AA^2$ in $MgCr_2O_4$ i.e. much larger than the usually accepted value associated with thermal vibrations of atoms in crystals such as 0.4 $\AA^2$ found in the case of $MgAl_2O_4$. The extra contribution to B can be accounted for by atomic displacements in the lattice.

This evidence, coupled with optical and infra-red data which indicated C_{3v} symmetry around the Cr^{3+} ion in chromites rather than D_{3d} as expected in $Fd3m$, led to a refinement of the intensity data, based on the $F\bar{4}\,3m$ symmetry, from $MgCr_2O_4$. The result of this refinement was that the oxygen ions were displaced by relatively larger distances from the equivalent $Fd3m$ positions described by $u = 0.387$ and the Cr^{3+} ions were slightly displaced from the centre of the octahedral site. The resultant Cr-O distances in the structure were found to be 1.97 $\AA$ and 1.94 $\AA$ which agree quite well with results observed in $NiCr_2O_4$ (1.98 $\AA$ and 1.97 $\AA$, Prince, 1961) and Cr_2O_3 (1.97 $\AA$ and 2.02 $\AA$, Newnham and Dehaan, 1962). Also emerging from this latter

refinement was a value of B of 0.4 $Å^2$, a value more reasonably associated with thermal vibrations.

The lattice parameters of these spinels were determined using the centroid as the measure of line position. The result of this analysis was that there was a positive deviation from Vegard's Law with a maximum deviation occurring at x = 0.5, a result which agreed fairly well with the results of Lou and Ballentyne (1968) who made similar measurements on single crystal materials. The lattice parameters for the two pure spinels, $MgAl_2O_4$ and $MgCr_2O_4$, were found to be 8.080 Å and 8.333 Å respectively.

A preliminary analysis of the breadths of the diffraction lines was made using integral breadths. The result of this was to indicate that the breadth of the profiles from $MgCr_2O_4$, the reference specimen, was substantially determined by instrumental factors, and diffraction broadening, if present at all, was negligible. Subsequent analysis of the remaining samples showed the broadening in their profiles to be inconsistent with particle size, strain or a combination of these two effects. However, there was a marked similarity to the behaviour reported by Cervinka et al (1970) shown by manganese ferrites.

A variance analysis was attempted to ascertain the cause of broadening in the diffraction lines. The variation of variance slopes and intercepts with order of diffraction was consistent with the results from the integral breadth analysis. Thus it was considered that broadening arose from the presence of a mistake structure. An analysis based on that of Cheary (1971) was made in an attempt to match the experimental results found here with possible models of anti-phase domains. However, none of the models tried were successful although an ultimate solution along these lines seems probable.

The result of the quenching experiment on $MgAlCrO_4$ showed the lattice parameter had increased by a small amount, this increase being attributed to the trapping of a vacancy concentration corresponding

to the higher temperature by the quenching process. This conclusion was supported by the observed increase in diffuse intensity which is consistent with this interpretation but also of interest is that negligible changes occurred in the line breadths.

The effect of quenching on $MgAl_2O_4$ showed the lines of both samples (quenched at 1100°C and 900°C) to have shifted in a way similar to that observed in face centred cubic metals subject to stacking faults. The stacking fault probabilities were calculated to be 1:65 and 1:115 respectively for the two quenched samples. These values are comparable with those previously observed in metals.

7.2 Suggestions for further work.

The cause of the extra breadth observed in these spinels was found to be due to a mistake structure, the exact nature of the structure not being established. Cheary (1971) in his study of chromium doped lithium ferrites had provided evidence that the Cr^{3+} ions accumulated on anti-phase domain boundaries which caused superlattice lines to exhibit broadening similar to particle size effects. In this study, Cr^{3+} doped $MgAl_2O_4$ was under investigation but the complexity of the problem in the $Mg(Al_{2-x}Cr_x)O_4$ series was increased by the lack of superlattice lines to facilitate the analysis, compared to the similar analyses of metallic alloys and the above mentioned lithium ferrite in which they do appear. Thus it would be desirable that further theoretical investigations should be pursued with the results obtained in this study in order that the mistake structure could be determined.

Following the analysis of the structure of $MgCr_2O_4$ which showed that the true space group for this compound must be $F\bar{4}3m$, it seems important that other compounds should be similarly examined. Apart from the present evidence, many other spinels containing chromium are known for which the Debye-Waller temperature factor (B) is substantially

higher than that estimated from infra-red measurements, (e.g. Grimes, 1972, cites some of these compounds).

Infra-red values of B should be consistent with the thermal vibrations of atoms within the crystals concerned and should correspond approximately with the Debye-Waller B, and structure refinements of the compounds mentioned above should be performed to account for these anomalously high values of B.

REFERENCES

Alexander, L, 1948, J. Appl. Phys., 19, 1068.

Alexander, L, 1950, J. Appl. Phys., 21, 126.

Amelinckx, S., 1964 Solid State Physics, Suppl. 6.

Anderson, P. W. 1956, Phys. Rev., 102, 1008.

Aqua, E. N., 1966, Acta Cryst., 20 560.

Arndt, U. W., 1955 X-ray Diffraction by Polycrystalline Materials eds. Peiser, H. H., Rooksby, H. P., Wilson, A. J. C. (Institute of Physics, London).

Azaroff, L. V., Buerger, M. J., 1958. The Powder Method in X-ray Crystallography, (McGraw-Hill, New York) p262.

Bacon, G. E., 1952, Acta Cryst., 5, 694.

Bacon, G. E., Roberts, F. F. 1953, Acta Cryst., 6, 57.

Baltzer, P. K., Wojtowicz, P. J., 1959 J. Appl. Phys., 30, 275.

Barrett, C. B., 1952, Imperfections in nearly perfect Crystals. (Wiley, New York), Chapter 3.

Barth, T. F. W., Posnjak, E., 1932, Z. F. Krist., 82, 325.

Barth, T. F. W., Posnjak, E., 1931, J. Wash. Acad. Sci., 21, 255.

Bearden, J. A., 1968, Rev. Mod. Phys., 39, 78.

Beals, R. J., Cook, R. L., 1957, J Amer. Ceram. Soc., 40, 279.

Bertaut, E. F., Delorme, C., 1954, Compt. Rendu, 238, 1829.

Blasse, G. 1963, J. Inorg. Nuc. Chem., 26, 1473.

Blasse, G., 1964, Phil. Res. Rep. Suppl. 3.

de Boer, F., van Santen, J. H., Verwey, E. J. W., 1950, J. Chem. Phys. 18, 1032.

Bolling, G. F., Massalski, T. B., McHargue, C. J., 1961, Phil. Mag., 6, 491.

Brabers, V. A. M., 1969, Phys.stat. sol., 33, 563.

Bragg, W. H., 1915, Phil. Mag., 30, 305.

Bragg, W. L., Claringball, G. F., 1965, Crystal Structures on Minerals, vol. 4, The Crystalline State, (Bell, London), pp. 102-7.

Braun, P. B., 1952, Nature, 170, 1123.

Brockhouse, B. N., Corliss, L. M., Hastings, J. M., 1955,
Phys. Rev., 98, 1721.

Brown, C. J., 1955, X-ray Diffraction of Polycrystalline materials.
eds. Peiser, H. S., Rooksby, H. P., Wilson, A. J. C.,
(Institute of Physics, London) p 399.

Brun, E., Hafner, S., Hartmann, P., Laver, F., 1960,
Naturwissenschaft (Germany), 47, 277.

Buerger, M. J., 1936, Z Krist., A95, 163.

Bunn, C. W., 1961, Chemical Crystallography, (O. U. P., Oxford).

Cervinka, L., 1965, Czech. J. Phys., B15, 747.

Cervinka, L., Hosemann, R., Vogel, W., 1970, Acta Cryst., A26, 277.

Cheary, R. W., 1971, Ph.D. Thesis, the University of Aston in
Birmingham.

Cheary, R. W., Grimes, N. W., 1972, J. Appl. Cryst., 5, 57.

Chipman, D., Paskin, D. R., 1959, J Appl. Phys., 30, 1992.

Cockayne, D. J. H., Jenkins, M. L., Ray, T. L. F., 1971, Phil. Mag., 24, 1383.

Corliss, L. M., Hastings, J. M., 1953, Phys. Rev., 90, 1013.

Delorme, C., 1955, Compt. Rendu, 241, 1588.

Dunitz, J. D., Orgel, L. E., 1957a, J. Phys. Chem. Solids, 3, 20.

Dunitz, J. D., Orgel, L. E., 1957b, J. Phys. Chem. Solids, 3, 318.

Edwards, H. J., Toman, K., 1970, J. Appl. Cryst., 3, 157.

Finch, G. I., Sinha, A. P. B., Sinha, K. P., Proc. Roy. Soc., A242, 28.

Fischer, P., 1967, Z. Kryst., 124, 275.

Ford, R. A., Hill, O. F., 1960, Spectrochim. Acta, 16, 1318.

Francombe, M. H., 1957, J. Phys. Chem. Solids, 3, 37.

Goodenough, J. B., 1963, Magnetism and the Chemical Bond,(Wiley, New York).

Goodenough, J. B., Loeb, A. L., 1955, Phys. Rev., 98, 391.

Gorter E. W., 1954, Phil. Res. Rep., 9, 295.

Graham, C. D., 1960, J. Phys. Chem. Solids, 17, 18.

Grimes, N. W., 1965, Private Communication.

Grimes, N. W., 1968, J. Phys. C,(Proc.Phys. Soc.) (2),1, 658.

Grimes, N. W., 1971, J. Phys. C, Solid State Physics, 4, L342.

Grimes, N. W., 1972a, Phil. Mag. 25, 67.

Grimes, N. W., 1972, Phil. Mag., 26, 1217.

Grimes, N. W., 1973, J. Phys. C, Solid State Physics, 6, L78.

Grimes, N. W., Collett, A. J., 1971, Phys. Stat. Sol.(b), 43, 591.

Grimes, N. W., Hilleard, R. J., 1970, J. Phys. C, Solid State Physics, 3, 866.

Grimes, N. W., Hilleard, R. J., Waters, J., Yerkess, J., 1968,
J. Phys. C, (Proc.Phys.Soc.) (2), 1, 663.

Hahn, H. 1951, Z. anorg. u. algem. Chem., 264, 184.

Hilleard, R. J., Webster, J. A., 1969, J. Appl. Cryst. 2, 193.

Hirth, J. P., Lothe, J., 1968, Theory of Dislocations, (McGraw-Hill, London).

Hulsher, W. S., van den Berg, K. G., Lodder, J. C., 1972,
Thin Solid Films, 9, 363.

Hwang, L., Heuer, A. H., Mitchell, T. E., 1973, Private communication.

International Tables of X-ray Crystallography, 1962, Kynoch Press Ltd.,

Jagodzinski, H., Saalfeld, H., 1958, Z. Kryst., 110, 197.

James, R. W., 1965, X-ray Crystallography, (Methuen, London).

Jones, F. W., 1938, Proc. Roy. Soc., A166, 16.

Jones, F. W., Sykes, C., 1938, Proc. Roy. Soc., A166, 376.

Kanomata, J., Ido, H., Kaneko, T., 1970, J. Phys. Soc. Japan, 29, 332.

Kataoki, M., Kanamari, J., 1972, J. Phys. Soc. Japan, 32, 113.

King, G. D. S., 1962, Acta Cryst., 15, 512.

Kino, Y., Lüthi, B., Mullen, M. E., 1972, J. Phys. Soc. Japan, 33, 687.

Klug, H. P., Alexander, L. E., 1954, X-ray Diffraction procedures for
polycrystalline materials, (Wiley, New York).

Ladell, J., Parrish, W., Taylor, J., 1959, Acta Cryst., 12, 561.

Langford, J. I., 1968a, J. Appl. Cryst., 1, 48.

Langford, J. I., 1968b, J. Appl. Cryst., 1, 131.

Langford, J. I., Wilson, A. J. C., 1963, Crystallography and Crystal Perfection, ed. Ramanchandran, G. N., (Academic Press, New York) p.207.

von Laue, M., 1926, Z. Krist., 64, 115.

Lewis, M. H., 1966, Phil. Mag., 14, 1003.

Lewis, M. H., 1967, Phil. Mag., 15, 481.

Lipson, H., Cochran, W., 1966, The Determination of Crystal Structures, (Bell, London).

Lipson, H., Steeple, H., 1970, Interpretation of X-ray Powder Diffraction Patterns, (MacMillan, London), p. 263.

Lotgering, F. K., 1956, Phil. Res. Rep., 11, 190.

Lotgering, F. K., 1962, J. Phys. Chem. Solids, 23, 1153.

Lotgering, F. K., 1966, J. Phys. Chem. Solids, 27, 139.

Lou, F. H., Ballentyne, D. W. G., 1968, J. Phys. C, (2) 1, 608.

Mazur, J., 1949, Nature, 164, 358.

McClure, D. S., 1957, J. Phys. Chem. Solids, 3, 311.

McClure, D. S., 1963, J. Chem. Phys., 38, 2289.

Miyahara, S., Ohnishi, H., 1956, J. Phys. Soc. Japan, 11, 1296.

Newnham, R. E., Dehaan, Y. M., 1962, Z. Krist. 117, 235.

Nicks, P. F., 1951, Ph. d. Thesis, University of London.

Nishikawa, S., 1915, Proc. Tokyo Math. Phys. Soc., 8, 199.

Ohnishi, H., Teranishi, T., 1961, J.Phys. Soc. Japan, 14, 106.

van Oosterhout, G. W., Rooymanns, C. J. M., 1958, Nature, 181, 44.

Parratt, L. G.,1936, Phys. Rev., 50, 1.

Paterson, A. L., 1939, Phys. Rev., 56, 978.

Patterson, M. S., 1952, J. Appl. Phys., 23, 805.

Pike, E. R., Wilson, A. J. C., 1959, Brit. J. Appl. Phys., 10, 57.

Pitts, E., Willetts, F. W., 1961, Acta Cryst., 14, 1302.

Poole, C. P. Jr., 1964 J. Phys. Chem. Solids, 25, 1169.

Poole, C. P. Jr., Itzell, J. F., 1963, J. Chem. Phys., 39, 3445.

Prince, E., 1957, Acta Cryst., 10, 554.

Prince, E., 1957, J. Appl. Phys., 32, Suppl. 3. 68.

Raccah, P. M., Bouchard, R. J., Wold, A., 1966, J. Appl. Phys., 37, 1436.

Rachinger, W. A., 1948, J. Sci. Instr., 25, 254.

Romejn, F. C., 1953, Phil. Res. Rep., 8, 304.

Roth, W. L., 1964a, J. de Physique, 25, 507.

Roth, W. L., 1964b, J. Phys Chem Solids, 25, 1.

Roy, D. M., Roy, R., Osborne, E. F., 1953, J. Amer. Soc., 36, 149.

Satomi, K., 1961, J. Phys Soc. Japan, 16, 258.

Scherrer, P., 1918, Nachr. Ges. Wiss. Gottingen, 26th. Sept. p.98.

Shannon, R. D., Prewitt, C. T., 1969, Acta Cryst., B25, 925.

Simmons, R. O., Ballufi, R. W., 1960, Phys. Rev., 117, 52.

Sinha, A. P. B., Sanjana, N. R., Biswas, A. B., 1957, J. Appl. Phys. 30, 1323.

Smit, J., Wijn, H. J. P., 1959, Ferrites, (Wiley, New York).

Spencer, R. C., 1931, Phys. Rev., 38, 618.

Stahl-Drada, R., Low, W., 1959, Phys. Rev., 116, 561.

Stokes, A. R., 1948, Proc. Roy. Soc., 61, 382.

Stoll, E., Fischer, P., Halg, W., Maier, G., 1964, J. Phys. France, 25, 5447.

Tanaka, M., Tokoro, T., Aiyama, Y., 1966, J. Phys. Soc. Japan, 21, 262.

Terauchi, H., Mori, M., Yamada, Y., 1972, J. Phys. Soc. Japan, 32 , 1049.

Thilo, W. E., Saur, R., 1955, Chemie der Erde, 17, 165.

Tournarie, M., 1956, Compt. Rendu, 242, 2016 and 2161.

Vegard, L., 1921, Z. Physik, 5, 17.

Verwey, E. J. W., de boer, F., van Santen, J. H., 1948, J. Phys. Chem., 16, 1019.

Verwey, E. J. W., Haaymann, P. W., 1941, Physica, 8, 979.

Verwey, E. J. W., Haaymann, P. W., Romeijn, F. C., 1947, J. Chem. Phys., 15, 181.

Verwey, E. J. W., Heilmann, E. L., 1947, J. Chem. Phys., 15, 174.

Villers, G., Lecerf, A., Raoult, M., 1965, Compt. Rendu. 260, 3017.

Vogel, W., Hosemann, R., 1970, Acta Cryst., A26, 272.

Wagner, C. N. J., 1957a, Acta Met., 5, 427.

Wagner, C. N. J., 1957b, Acta Met., 5, 477.

Wagner, C. N. J., 1966, Local Atomic Arrangements by X-ray Diffraction, (Gordon and Breach, New York) p. 219.

Wagner, C. N. J., Aqua, E. N., 1964, Advances in X-ray Analysis, 7, 46.

Walters, D. S., Wirtz, G. P., 1972, J. Amer. Ceram. Soc., 55, 59.

Warren, B. E., 1941, J. Appl. Phys., 12, 375.

Warren, B. E., 1959, Prog. in Metal Phys., 8, 147.

Warren, B. E., 1969, X-ray, Diffraction, (Addison Wesley, New York).

Warren, B. E., Averbach, B. L., 1950, J.Appl. Phys., 21, 595.

Warren, B. E., Biscoe, J., 1938, J. Amer. Ceram. Soc., 21, 49.

Warshaw, J., Kieth, M. L., 1954, J. Amer. Ceram. Soc. 37, 161.

Westrum, E. F.,Jr. Grimes, D. M., 1957, J. Phys. Chem Solids, 3, 44.

Westrum, E. F. Jr., Grimes, D. M., 1958, J. Phys. Chem., 61, 761.

Wickham, D. G., Croft, W. J., 1958, J. Phys. Chem. Solids, 7, 357.

Wilson, A. J. C., 1943, Proc. Roy. Soc. London, A181, 360.

Wilson, A. J. C., 1961, Proc. Phys. Soc. London, 78, 249.

Wilson, A. J. C., 1962, Proc. Phys. Soc. London, 80, 286 and 303.

Wilson, A. J. C., 1962a, Norelco Reporter, 9, No. 3.

Wilson, A. J. C., 1963, Proc. Phys. Soc. London, 81, 41.

Wilson, A. J. C., 1963a, Mathematical theory of X-ray Powder Diffractometry, (Philips Tech. Library).

Wilson, A. J. C., 1967, Acta Cryst., 23, 888.

Wyckoff, R. W. G., 1951, Crystal Structures (Interscience, New York).

ACKNOWLEDGEMENTS

This research was carried out at the University of Aston in Birmingham with financial assistance from the Polytechnic, Wolverhampton.

I would like to thank my supervisor, Dr. N. W. Grimes, for his advice, assistance and encouragement during the course of this work and for his enthusiasm for research which has sustained me throughout.

I would also like to thank Mr. G. V. Cochrane for his assistance in the collection of data.

Finally, I would like to thank my wife who has encouraged me throughout the course of this work.